COMBINATION OF TERRESTRIAL AND GPS DATA FOR EARTH DEFORMATION STUDIES

D. B. GRANT

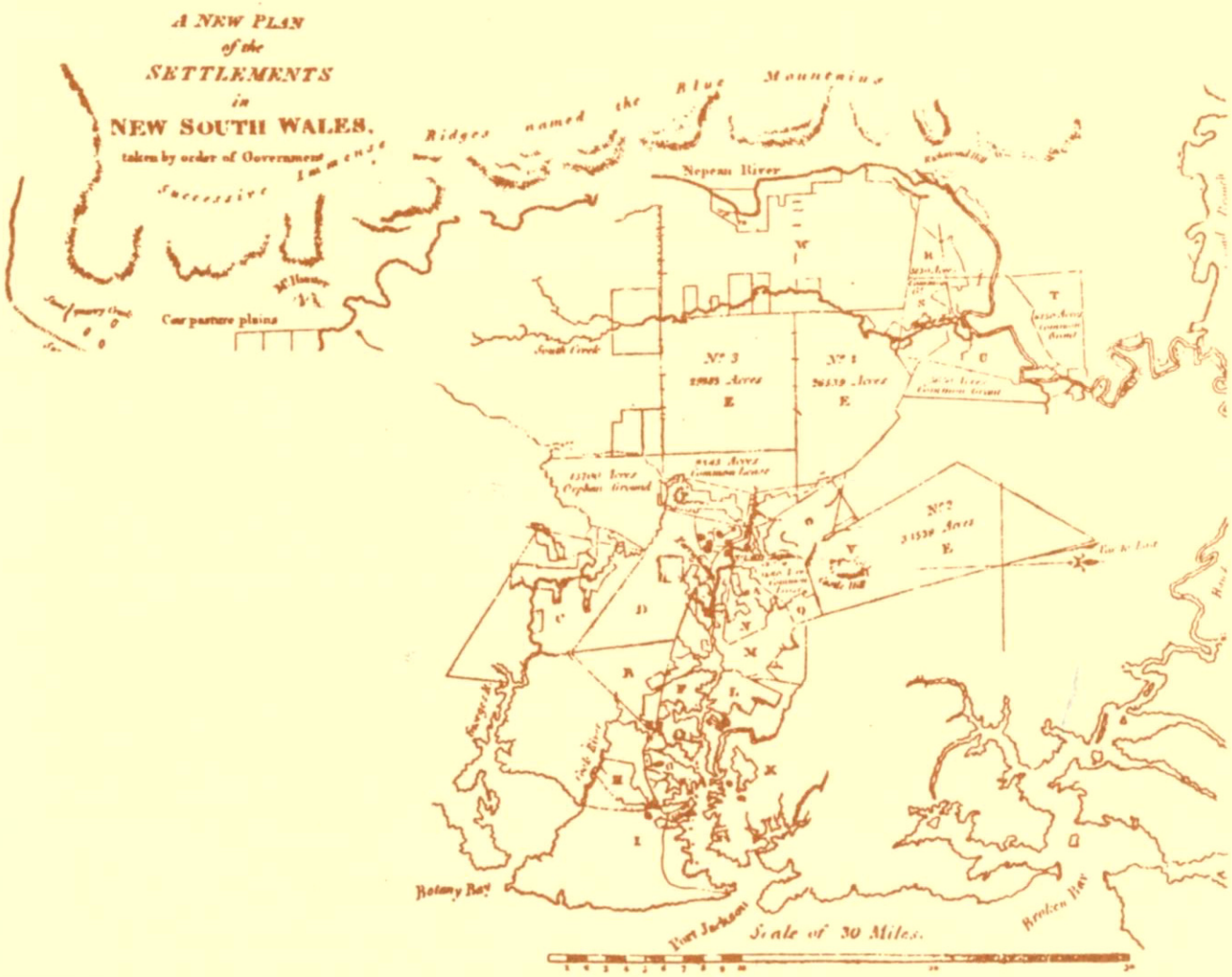

UNISURV S-32, 1990

Reports from

SCHOOL OF SURVEYING

THE UNIVERSITY OF NEW SOUTH WALES KENSINGTON, NSW AUSTRALIA 2033

UNISURV REPORT S-32, 1990

COMBINATION OF TERRESTRIAL AND GPS DATA FOR EARTH DEFORMATION STUDIES

D.B. Grant

Received: March, 1990

SCHOOL OF SURVEYING
UNIVERSITY OF NEW SOUTH WALES
P.O. BOX 1
KENSINGTON N.S.W. 2033
AUSTRALIA

National Library of Australia

Card No. and ISBN 0 85839 050 7

AUTHORS NOTE

This PhD thesis was completed and submitted in December 1988. In the 16 months between submission and publication there have been significant changes in the GPS world. The proposed constellation of !8 + 3 satellites has been changes to 21 + 3 satellites. New Zealand and Australia now have tracking stations as part of the Cooperative International GPS Network (CIGNET) and data from these stations is being used to generate precise ephemerides. Substantial improvement in the accuracy of tracking station coordinates and orbits will result. There have been improvements in receiver design. The Rogue receiver developed at the Jet Propulsion Laboratory, while not a field unit, allows such accurate pseudo range measurements that the difficulties of ambiguity resolution are greatly diminished. The Rogue antenna appears to reduce multipath to very low levels. When these advances become available in a field portable unit GPS will enter a new era. Thus, some of the values adopted for systematic errors in this thesis have proved to be pessimistic. On the other hand, ionospheric errors have increased and significant errors are found on lines as short as 2 - 3 km with single frequency observations during daytime.

I have no doubt that advances over the next few years will overcome most of the present difficulties of GPS. The main concerns of this thesis will soon seem out of date to GPS surveyors. Nevertheless deformation analysis is necessarily rooted in the past. The problems addressed here will still be of concern to those attempting to use "historical" GPS data to estimate deformation.

D.B. Grant
26 March 1990

ABSTRACT

Optimum procedures for detecting earth deformation from a combination of terrestrial and GPS geodetic observations are studied. This is directed towards the Earth Deformation Studies (EDS) programme in New Zealand. The terrestrial, GPS, and deformation adjustment models are investigated. It is found that the parameters of vertical homogeneous strain are not well determined and that their estimation leads to difficulty in the interpretation of other deformation parameters. It is demonstrated that a 2D adjustment of triangulation data is suitable for combination with GPS for the estimation of horizontal strain but that a 3D adjustment is required for best results when EDM distances are included in the terrestrial data set.

The GPS adjustment model is studied in detail, particularly some of the principal systematic errors (orbits, propagation delays and origin station coordinates). Simulations of GPS observation campaigns are used with errors rigorously propagated through to deformation parameters using the techniques of covariance analysis. The Kalman filter algorithm is employed as a means of dealing with dynamic variables and the equations of covariance analysis are developed in the Kalman filter setting. Strategies for selecting satellite and network geometry are compared using simulations. The effect of ambiguity resolution on deformation parameters is studied in detail. It is shown that the effect of tropospheric delay errors may be substantially reduced by estimation of residual zenith tropospheric delays. Where the tropospheric delay is time dependent, the Kalman filter algorithm gives optimum results. Orbit estimation is studied using a simulated regional tracking station network and is found to significantly improve the accuracy of deformation parameter estimates. With dual frequency observations, and the estimation of tropospheric delay and orbit parameters, the effect of GPS systematic errors is insignificant compared to that of terrestrial observation errors.

TABLE OF CONTENTS

ABSTRACT iii
LIST OF DIAGRAMS viii
LIST OF TABLES xi
LIST OF ACRONYMS xiii
ACKNOWLEDGEMENTS xiv

1 INTRODUCTION 1

2 GEODYNAMICS 7
2.1 PLATE TECTONICS IN NEW ZEALAND 7
2.2 EARTH DEFORMATION ANALYSIS 12
2.2.1 Datums, Transformation and Strain 12
2.2.2 Theory of Infinitesimal Deformation 14
2.2.3 Least Squares Estimation of Deformation 24
2.3 DEFORMATION ANALYSIS IN NEW ZEALAND 26
2.3.1 Geodetically Derived Strains 26
2.3.2 Comparison with Other Geodynamic Data 29
2.3.3 Assessment of Geodetic Data in Geodynamics 30

3 TERRESTRIAL GEODESY 31
3.1 INTRODUCTION 31
3.2 GEODETIC SURVEYING IN NEW ZEALAND 33
3.2.1 Early Surveys 33
3.2.2 New Zealand Geodetic Datum 1949 34
3.2.3 Transit 38
3.2.4 Earth Deformation Surveys 39
3.3 SYSTEMATIC ERRORS 41
3.3.1 Deflection of the Vertical 41
3.3.2 Height 43
3.3.3 Atmospheric Refraction and Propagation Delay 43
3.4 CASTLE POINT - NEW PLYMOUTH EDS 46
3.4.1 Observations 46
3.4.2 Adjustment Software 50
3.4.3 Choice of Strain Model 51
3.4.4 Network Adjustment Models 56
3.4.5 Geodetic Strain in Terrestrial Networks 62
3.4.6 Variance Component Estimation 69

4 **GEODESY WITH GPS** 71
4.1 THE GLOBAL POSITIONING SYSTEM 71
4.1.1 Satellite Constellation 71
4.1.2 Signals 72
4.1.3 Comparison with Terrestrial Geodesy 75
4.2 OBSERVATION EQUATIONS 77
4.2.1 Carrier Beat Phase 77
4.2.2 Observation Differencing 80
4.3 GPS PHASE ADJUSTMENT 84
4.3.1 Differenced and Undifferenced Models 84
4.3.2 Rank Defect in the Clock Bias Parameters 86
4.3.3 Kalman Filter Adjustment 88
4.3.4 Ambiguity Resolution 91
4.3.5 Dual Frequency 93
4.4 GPS DATUM DEFINITION 95
4.4.1 Multi-Station Adjustment with Fixed Orbits 96
4.4.2 Combined Orbit / Station Adjustment 97
4.5 GPS NETWORK AND DEFORMATION ADJUSTMENTS 99

5 **COVARIANCE ANALYSIS** 104
5.1 SIMULATIONS 104
5.2 COVARIANCE ANALYSIS IN LEAST SQUARES 106
5.3 COVARIANCE ANALYSIS IN THE KALMAN FILTER 113
5.3.1 Constant Systematic Errors 115
5.3.2 Dynamic Systematic Errors 117
5.4 DYNAMIC MODEL ERRORS 119
5.4.1 General Case:
Erroneous Dynamic Model for Adjusted Parameters 119
5.4.2 Special Case:
Dynamic Errors for Constant Adjusted Parameters 123
5.5 CHOICE OF GAIN MATRIX 125
5.6 COVARIANCE ANALYSIS AND DEFORMATION 127
5.6.1 The Covariance Analysis Equations 127
5.6.2 Derived 2D Strain Parameters 129
5.7 SUMMARY OF COVARIANCE ANALYSIS EQUATIONS 131

6 **GPS SYSTEMATIC ERRORS** 133
6.1 INTRODUCTION 133
6.2 STATION COORDINATE AND REFERENCE FRAME ERRORS 135
6.3 ORBIT ERRORS 137
6.4 TROPOSPHERIC DELAY 140
6.4.1 Constant Tropospheric Delay Error 142
6.4.2 Time Dependent Tropospheric Delay Error 147
6.4.3 Mapping Function Errors 148
6.5 IONOSPHERIC DELAY 149
6.6 CLOCK ERRORS 153
6.7 RECEIVER AND ANTENNA ERRORS 155
6.8 SUMMARY OF SYSTEMATIC ERRORS 156

7 **TERRESTRIAL / GPS COMBINATION** 157
7.1 SATELLITE GEOMETRY AND SELECTION 157
7.2 ACCURACY AND PRECISION 166
7.3 AMBIGUITY RESOLUTION 169
7.4 GPS NETWORK GEOMETRY 178
7.4.1 Principles of Network Design 178
7.4.2 Configuration of the Simulated Adjustment 179
7.4.3 Ambiguity Resolution 184
7.4.4 Dual Frequency 185
7.4.5 Results 187
7.4.6 Summary 196
7.5 TROPOSPHERIC DELAY 198
7.6 ORBIT ESTIMATION 206
7.7 TERRESTRIAL SYSTEMATIC ERRORS 214

8 **CONCLUSIONS AND RECOMMENDATIONS** 217

REFERENCES 226

APPENDICES

A LEAST SQUARES ADJUSTMENT

A.1 General Least Squares....243

A.2 Parametric Least Squares....245

B RANK DEFECT OF THE CLOCK BIASES

B.1 The Nature and Size of the Rank Defect....247

B.2 Overcoming the Clock Bias Rank Defect....250

C RELATIONSHIP BETWEEN LEAST SQUARES AND KALMAN FILTERING....255

D DYNAMIC MODELS

D.1 Dynamic Model Theory....258

D.2 Dynamic Models in GPS Adjustment....261

E BIAS DILUTION OF PRECISION (BDOP)....270

F SOFTWARE....275

G CONVERSION OF VCV MATRICES

G.1 Coordinate Conversions....282

G.2 Augmenting the VCV for the Origin Station(s)....284

LIST OF DIAGRAMS

Diagram 2.1.1 Crustal seismicity in New Zealand 8

Diagram 2.1.2 Tectonic setting of New Zealand 9

Diagram 2.1.3 Deep and intermediate earthquakes beneath the North Island, New Zealand 10

Diagram 2.1.4 Possible future tectonic development of New Zealand 11

Diagram 2.2.1 Topocentric reference system 17

Diagram 2.2.2 Relationship between vertical shear strain and rotation in near - planar geodetic networks 20

Diagram 2.2.3 Two interpretations of vertical shear strain e_{ev} as determined from displacements on a deformed cube 21

Diagram 2.3.1 Use of the fault line structure and the principal axis of compression to determine the nature of the strain 26

Diagram 2.3.2 Shear strain rates derived from geodetic data 28

Diagram 3.2.1a New Zealand Geodetic Datum 1949 (North Island) 36

Diagram 3.2.1b New Zealand Geodetic Datum 1949 (South Island) 37

Diagram 3.4.1 Terrestrial network: Castle Point – New Plymouth Earth Deformation Survey 47

Diagram 3.4.2 North-west sub-network being 9 stations of the Castle Point – New Plymouth EDS network 49

Diagram 3.4.3 Central sub-network being 10 stations of the Castle Point – New Plymouth EDS network 49

Diagram 3.4.4 South-east sub-network being 12 stations of the Castle Point – New Plymouth EDS network 50

Diagram 3.4.5 Strain between triangulation and trilateration 64

Diagram 3.4.6 Strain between trilateration adjustments 66

Diagram 4.1.1 Relative Geometry of Proposed Block II Satellites 72

Diagram 6.4.1 Zenith Tropospheric Delay Error 146

Diagram 6.5.1 Diurnal variation in zenith ionospheric delay at L1 frequency at latitude 39° N 149

Diagram 6.5.2 Correlation coefficient of ionospheric delay vs station separation in latitude and longitude 150

Diagram 7.1.1 Sky-plots of observing sessions used to evaluate BDOP1 159

Diagram 7.1.2 GDOP and BDOP1 for the period of simulated observations 160

Diagram 7.1.3 Sky-plots of simulated observing sessions with low BDOP1 165

Diagram 7.3.1 Progressive resolution of ambiguities and accuracy of remaining estimated ambiguities 170

Diagram 7.3.2 Accuracy of baseline as ambiguities are progressively resolved 172

Diagram 7.3.3 Errors in east baseline component with ambiguities progressively resolved 173

Diagram 7.3.4 Errors in height baseline component with ambiguities progressively resolved 175

Diagram 7.4.1 Simulated GPS network observations sessions 182

Diagram 7.4.2 Perturbation of **total shear strain** γ 188

Diagram 7.4.3 Precision and the perturbations in estimate of total shear strain γ for **ambiguity free** adjustments 189

Diagram 7.4.4 Precision and the perturbations in estimate of total shear strain γ for **ambiguity fixed** adjustments 190

Diagram 7.4.5 Perturbation of **2D scale** s_{2D} 193

Diagram 7.4.6 Perturbations in estimate of **total shear strain** γ and **2D scale** s_{2D} for **ambiguity free** and **ambiguity fixed** adjustments 194

Diagram 7.6.1 Orbit tracking network for simulated orbit / network adjustment. 207

Diagram 7.6.2 Total consider errors for initial satellite positions 210

Diagram 7.6.3 Simulated errors in satellite 6, day 7 211

Diagram B.2.1 Some choices of reference ambiguities 254

Diagram D.1 Comparison of Dynamic Models.....269

Diagram E.1 A comparison of GDOP and BDOP1 273

Diagram F.1 Programs and files used for simulation of GPS networks.....275

Diagram F.2 Programs and files used for adjustment and simulation of terrestrial networks.....276

LIST OF TABLES

Table 3.4.1 Estimates of strain between coordinates of different **3D** network adjustments 52

Table 3.4.2 Estimates of strain between coordinates of different **height fixed** network adjustments 54

Table 3.4.3 Geodetic strain estimates from different methods of height determination in combined adjustment 59

Table 3.4.4 Geodetic strain estimates from different methods of height determination in triangulation adjustment 60

Table 3.4.5 Geodetic strain estimates from different methods of height determination in trilateration adjustment 62

Table 7.1.1 Evaluation of BDOP1 as an indicator of good satellite geometry 161

Table 7.1.2 Baseline component errors for sessions A and B 163

Table 7.1.3 Simulated Observation Sessions 164

Table 7.2.1 Ratio of total error to precision for baseline components 167

Table 7.3.1 Total ambiguity error at time of resolution 171

Table 7.4.1 Simulated observation sessions for NW EDS network 181

Table 7.4.2 Simulated GPS network configurations to test the effect of different levels of redundancy 181

Table 7.4.3 Station re-occupations 181

Table 7.4.4 Systematic errors considered for covariance analysis 183

Table 7.4.5 Ambiguity resolution in simulated session adjustments 185

Table 7.4.6 Covariance analysis of the errors in deformation parameters from a 3D adjustment of **terrestrial data** and **GPS data** 195

Table 7.5.1 Maximum ambiguity errors (cycles) for session 7 with correlation times, T_{trop} of 1, 2, 4, 8, and 16 hours 201

Table 7.5.2 Height errors for a 90.1 km line 202

Table 7.5.3 Covariance analysis of the errors in deformation parameters from a 3D adjustment of **terrestrial data** and **GPS data** 203

Table 7.5.4 Covariance analysis of the errors in deformation parameters from **repeated GPS surveys** 204

Table 7.6.1 *A priori* uncertainties of observations, adjusted and unadjusted parameters 208

Table 7.6.2 Total errors in baseline components for selected representative baselines 209

Table 7.7.1 Covariance analysis of the errors in deformation parameters due to errors in the geoid height N and deflections of the vertical ξ and η 216

LIST OF ACRONYMS

BDOP	Bias Dilution of Precision
BIH	Bureau International de l'Heure
ECEF	Earth Centred - Earth Fixed
ECI	Earth Centred - Inertial
EF	Earth Fixed
EDM	Electronic Distance Measurement
EDS	Earth Deformation Studies
GDOP	Geometric Dilution of Precision
GPS	Global Positioning System
GPST	GPS Time
NZGD-49	New Zealand Geodetic Datum 1949
LLR	Lunar Laser Ranging
PDOP	Position Dilution of Precision
ppm	parts per million
PRN	Pseudo Random Noise
rms	root mean square
rss	root sum square
SLR	Satellite Laser Ranging
UTC	Universal Coordinated Time
VCE	Variance Component Estimation
VCV	Variance - Covariance (Matrix)
VLBI	Very Long Baseline Interferometry
WVR	Water Vapour Radiometer
ZD	Zenith Distance

ACKNOWLEDGEMENTS

Firstly, I wish to thank my supervisor, Professor Art Stolz for his help and guidance. During numerous discussions he provided encouragement for those ideas that had merit and a valuable restraint on those that were fruitless. His criticisms of my work were outstanding and assisted greatly in the composition of this thesis.

I am proud to have had the opportunity to work with a strong GPS research group at UNSW. The staff and fellow students have, by their assistance and good humour, made my stay both successful and enjoyable. Special thanks go to Dr Chris Rizos, Dr Ewan Masters Dr Bruce Harvey and Rod Eckels who provided especially valuable support in the early stages of my research; to Bernie Hirsch for his patient assistance with my software and to Professor Fritz Brunner and Dr Ritchard Coleman (Sydney University) for reviewing and advising on sections of my thesis.

During the period of my research I also benefited from visits to the School of Surveying by numerous experts in the field of geodesy. Special credit must go to Prof. Willi Caspary, who taught me much of what I know about least squares, and to Prof. Günter Hein for allowing the use of the integrated adjustment software, OPERA.

My research was made possible by a study award from the Department of Survey and Land Information, New Zealand. I am most grateful for this opportunity and for the extension of the original award which allowed me to upgrade the research to a PhD. I hope this thesis justifies the confidence they had in me. Particular thanks go to Dr John Hannah for his encouragement and for supplying me with data on the Castle Point - New Plymouth EDS survey.

My final and deepest thanks are for my family. My wife Linda encouraged me to apply for the study award, inspired me throughout the research, reviewed and corrected my writing and, during the final hectic months, sustained both me and our new daughter Katie.

1. INTRODUCTION

In 1973 the National Committee for Geological Sciences of the Royal Society of New Zealand published a report setting out a recommended 10 year programme for Earth Deformation Studies (EDS) in New Zealand (National Committee for Geological Sciences, 1973). The report stated that:

> *"The principal objectives of the programme are to discover the natural rates of earth deformation, and where it is taking place, in New Zealand."*

and amongst the detailed objectives:

> *"(3) knowledge of the relationship of earth deformation to earthquakes and volcanic activity as a preliminary necessity for*
> *(4) appraisal of the role of earth deformation studies in a future programme of earthquake and volcanic warning; ... "*

Earthquakes and volcanoes represent a significant threat to life and property in New Zealand. The study of earth deformation had been of interest to individual researchers for some time before 1973 but the impetus for the EDS programme came from the 1968 Inangahua earthquake which caused extensive damage and some loss of life, despite being in an area of relatively sparse settlement. Therefore, while earthquake and volcanic prediction were, realistically, not considered to be the primary aims of the programme, it was recognised that such predictions are possible long term goals. Suggate (1986) in reviewing progress in earth deformation studies, questions whether **imprecise** prediction of earthquakes is socially desirable, but notes that the more attainable goal of a spatial identification of risk is of great value in planning, especially for major developments.

The 1973 report lead to a planned and cooperative research programme by the government and academic organisations involved in geological, geodetic and geophysical research in New Zealand. The first 10 year review of the EDS programme (Royal Society of New Zealand, Earth Deformation Committee, 1985) noted that most of the objectives had been met and in some cases, particularly in the geodetic programme, had been exceeded. This review recommended that the EDS programme should continue, specifically recommending that:

> *"(8) The developments in satellite-based techniques for geodetic work should be closely monitored and investigated for future application."*

and noted:

> *"Developing space technology, in particular the proposed Global Positioning System (GPS) is expected to permit relative positions on the earth's surface to be measured to an accuracy of 0.1 ppm using interferometric techniques. It is clear that the next phase of the EDS programme should, if at all possible, be designed to investigate the capabilities of these and any other promising techniques.*
>
> *"At this stage it would not be wise to rely too much on the projected high accuracy satellite methods to replace conventional first order geodetic methods in the immediate future (i.e. next 10 years). Also these satellite techniques will need to be, initially at least, combined with conventional methods to ensure an adequate and known basis for verification of the technique and intercomparison of the different geodetic data sets."*

This thesis seeks, in part, to verify that GPS can be used to monitor earth deformation and to the address the issue of the intercomparison of GPS and terrestrial geodetic data.

GPS promises relative accuracy higher than is achievable by terrestrial methods on lines over 10 km and perhaps on lines shorter than this. Despite this, it is appropriate that this new and accurate geodetic tool be verified initially, against the less accurate but proven terrestrial methods. The study of earth deformation is a long term research project and a careful approach is required to new technology. Decisions made now will be assessed by researchers 100 years hence. New technologies such as GPS, while offering the possibility of faster detection of deformation, also present special problems. The systematic errors in GPS are different from those in horizontal directions or EDM distances and there are advantages in repeating observation schemes as closely as possible so that the effects of systematic errors tend to cancel. If, this principle is applied strictly however, the potential benefits of GPS are denied or, alternatively, the historical data is disregarded in favour of repeated GPS surveys. Deformation surveys are expensive and maximum use needs to be made of the available data. To regard the first GPS deformation survey as marking "year zero" in deformation studies would be to deny the valuable resource of more than 100 years of geodetic data. To maintain existing survey practices for fear of unknown new systematic errors would be a wasteful use of present resources. If the potential problem of different systematic errors in terrestrial and GPS observations is ignored, there

is a great danger that fictitious deformation will be detected and treated as if it had a geophysical cause. Thus the combination and intercomparison of terrestrial and GPS data sets is of prime importance.

When accurate EDM became available in the 1960s, the possibility of significant cost savings by replacing triangulation with trilateration was realised. This option was rejected for EDS surveys, in favour of combined triangulation / trilateration. This was a wise decision, especially in hindsight now that GPS threatens to supplant EDM for geodetic observations. The combined horizontal directions and EDM slope distances allow an assessment of the effect of systematic errors in the two observation types. Combined terrestrial / GPS surveys will be required for similar reasons to ensure both an accurate assessment of systematic errors and calibration of the techniques with respect to each other. Without a number of such combined surveys, the interpretation and comparison of estimates of deformation from terrestrial / terrestrial , terrestrial / GPS and GPS / GPS surveys will be difficult. Temporal changes in deformation rates are often studied as possible precursors to earthquakes and it will be important to ensure that any such changes detected, are due to a change in the nature of the deformation and not to a change in the type of geodetic observation used.

A careful assessment of systematic errors in terrestrial and GPS geodetic observations is required. This thesis concentrates more on the errors and characteristics of the new technique (GPS), than on the existing (terrestrial) techniques. The accuracy of terrestrial geodetic networks has been studied extensively in the past and a complete review is not given here. However a brief study is made of systematic errors in terrestrial data and the observations from one of the EDS survey networks are assessed. As GPS has not yet been used for deformation surveying in New Zealand the study of systematic errors in GPS is on a theoretical basis.

The problem of determining earth deformation is described in Chapter 2. A brief review is given of the tectonic setting of New Zealand. The theory of deformation analysis is given with an assessment of the estimability of deformation parameters from geodetic networks. The networks are approximately planar, limited as they are to the surface of the earth, and some of the possible deformation parameters are not well determined from such networks. This is analysed from a geometric viewpoint. A summary is given of

recent studies into earth deformation in New Zealand based on geodetic data. Comparisons between these studies and research from other disciplines (geology and geophysics) show surprising agreement and confirm the value of geodetic observations for earth deformation studies.

The present geodetic solution using terrestrial geodetic observations is described in Chapter 3. An outline is given of control and earth deformation surveys in New Zealand. Most of these were not designed for the detection of earth deformation but, nevertheless, provide a valuable data set for the study of deformation. This data has only been partly exploited so far. A brief review is given of the major systematic error sources in terrestrial observations. The Castle Point - New Plymouth EDS is used as a case study, to investigate different choices of deformation models. The studies of Chapter 2 on different deformation models from a geometric viewpoint, are complemented here with numerical studies. Different methods of combining the essentially 2D data set of a horizontal network with the 3D data set that will be provided by GPS are compared. Different subsets of the terrestrial observations are compared to determine their levels of systematic error. The possibility of estimating dilatation and differential rotation between regions from terrestrial and GPS observations is considered. A brief assessment is given of the use of variance component estimation to determine the relative accuracy of terrestrial and GPS observations.

The new geodetic solution of GPS is described in Chapter 4. A brief review of the system characteristics and a comparison with terrestrial geodesy is followed by a detailed description of the GPS adjustment model. The connection between the observations and the parameters of interest (the geometry of the network) is much less obvious with GPS than with terrestrial observations and so an understanding of the GPS adjustment model is essential to an assessment of the role and likely influence of systematic errors. Methods of dealing with singularities in the adjustment model are compared. A review is given of the Kalman filter adjustment algorithm which has proved useful for the adjustment of GPS data. The GPS datum definition problem is described for different adjustment models. This is more complex than the datum problem in terrestrial adjustment and an over-constraint of the datum can lead to fictitious estimates of deformation. Models for the combination of GPS and terrestrial data are considered and the model used in the analysis of this thesis is described.

The analytical theory used for simulations of GPS and terrestrial data is described in Chapter 5. Simulations are used because:

(a) GPS has not been used in New Zealand for deformation surveys.

(b) The optimum observation and adjustment strategies for GPS are still the subject of research and debate. Simulations offer an efficient way of testing strategies.

(c) The GPS satellite constellation will change significantly over the next few years and this may affect the accuracy of the system.

Simulations, in their simplest form are based on the assumption of normally distributed errors. This is inappropriate for GPS where the random errors are small and systematic errors play a major role. The techniques of covariance analysis are described in which systematic errors are also considered. These are put in the setting of the Kalman filter algorithm and the theory for analysing the effects of constant systematic errors, time dependent systematic errors, and errors in the dynamic model used for adjusted parameters is developed. The model for propagation of GPS systematic errors through to estimated deformation parameters is given.

The assumptions made about the magnitude and behaviour of GPS systematic errors are described in Chapter 6. The results of the covariance analysis depend on these assumptions so they are made after careful assessment. This is based on independent estimates of the major error sources and is backed up by an appraisal of the results actually achieved with GPS to ensure that unduly optimistic or pessimistic assumptions are not made. While these assumptions are to some extent arbitrary, they are much less so than the common assumptions that the errors are random, and that they cause errors of some specified number of parts per million in all coordinates. The systematic errors considered are station coordinates, reference frame definition, orbital elements, tropospheric delay, ionospheric delay, clock errors and receiver and antenna errors.

The results of the covariance analysis are presented in Chapter 7. These are given as errors in the parameters of a GPS adjustment and as errors in deformation parameters from a subsequent terrestrial / GPS deformation adjustment. Preliminary analysis is concerned with selection of the best satellite geometry for the GPS adjustment. The standard least squares technique of scaling *a posteriori* variance-covariance (VCV) matrices with the

a posteriori variance factor is assessed in the presence of significant systematic errors. The resolution of the integer carrier phase ambiguities is assessed, this being the key to accurate results with GPS. Some aspects of GPS network design are studied and the use of dual frequency receivers to eliminate ionospheric errors is considered. Different models for the estimation of tropospheric delay are compared and a combined orbit / network adjustment is simulated based on the use of receivers in Australia and New Zealand. Finally the covariance analysis software, designed principally for GPS, is applied to simulated terrestrial data to determine the effect of errors in the definition of the gravity field (geoid heights and deflections of the vertical) on combined terrestrial / GPS deformation adjustment.

2. GEODYNAMICS

2.1 PLATE TECTONICS IN NEW ZEALAND

New Zealand lies on the boundary between two tectonic plates and provides an interesting laboratory for research into plate tectonic theory. Seismic activity (see diagram 2.1.1) indicates substantial deformation over a zone 200-300 km wide, with an azimuth of 50° (Walcott, 1978a). The plate to the west of New Zealand is variously called the Indian, Indo-Australian or Australian plate. The name "Australian plate" is used in this thesis. The plate to the east of New Zealand is the Pacific plate.

While subduction zones are a feature of the Pacific basin and are studied extensively, New Zealand is unusual in having two reversed subduction zones linked by a transform fault (see diagram 2.1.2). In the north, the Australian plate is over-riding the Pacific plate while in the south the Pacific plate over-rides the Australian plate. The deformations caused by the convergence of these plates are rapid enough to be measurable over 10 years or less and there is a history of geodetic observation going back over 100 years which provides data suitable for deformation analysis.

To the east of the North Island is the Hikurangi Trough which marks the southern end of the Tonga-Kermadec-Hikurangi subduction zone. This zone is described by Kamp (1984). The geometry of the subducted Pacific plate may be deduced from the pattern of seismic foci which form a characteristic dipping plane known as a Benioff zone (see diagram 2.1.3). This is considered to be the plane of contact between the subducted and the over-riding plates (Scheidegger, 1982).

The deep seismic activity begins abruptly northwards of the point where the Hikurangi Trough meets the Chatham Rise. North of this area there is oblique oceanic-continent convergence while to the south there is oblique continent-continent convergence. Walcott (1978a) and Kamp (1984), suggest a progressive advancement of the subduction zone southwards through the North Island over the last 15 Myrs and a steady increase in the angle of dip. Walcott (1978a) suggests that this advance has been halted by the lighter continental lithosphere of the Chatham Rise and that the halt coincides with the start of rapid uplift of the Southern Alps 5 Myrs ago.

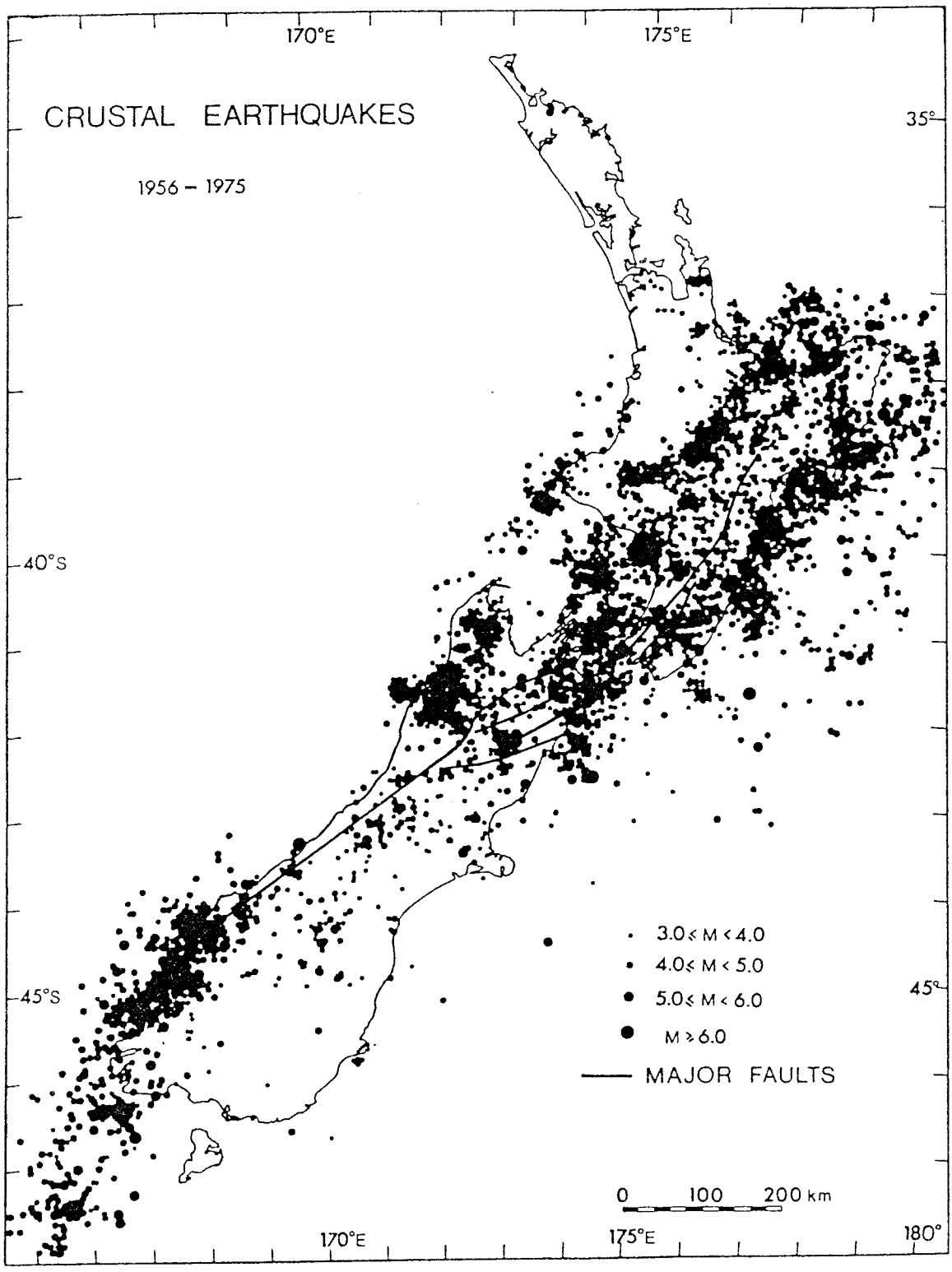

Diagram 2.1.1 Crustal seismicity in New Zealand. (After Hatherton, 1980)

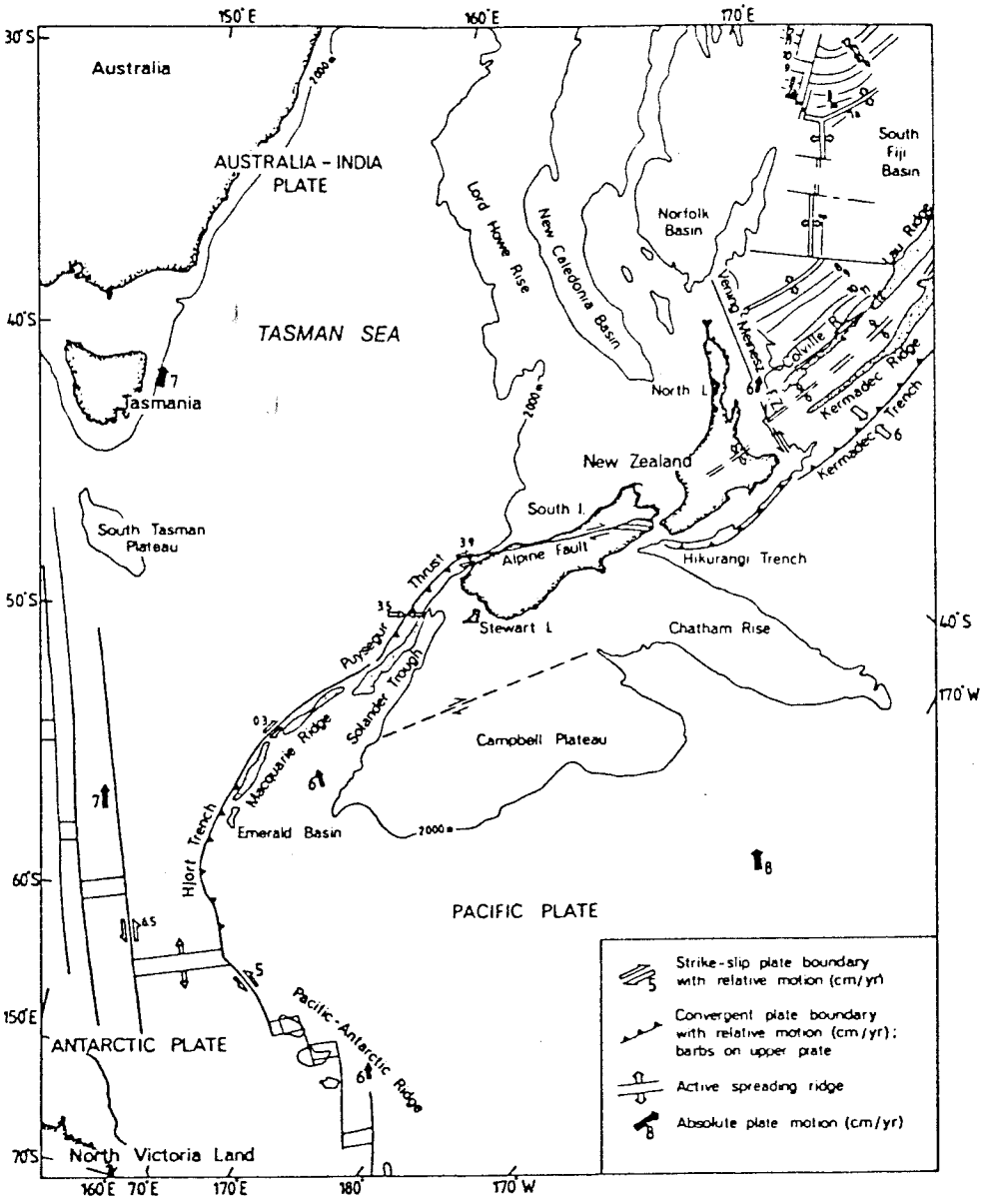

Diagram 2.1.2 Tectonic setting of New Zealand. (After Kamp, 1984)

To the north-west of the subduction zone, volcanic activity is found on the Australian plate, as is typical of subduction boundaries. There is also rifting in the Taupo volcanic zone which lies on the extension of the Havre Trough and may be considered as an example of back-arc spreading. Back-arc spreading is a feature often associated with subduction. It is a rift zone generally 150-250 km behind the volcanic arc on the over-riding plate. Hsui & Toksoz (1981) consider possible mechanisms for the appearance of such a zone of tension close to a convergent boundary.

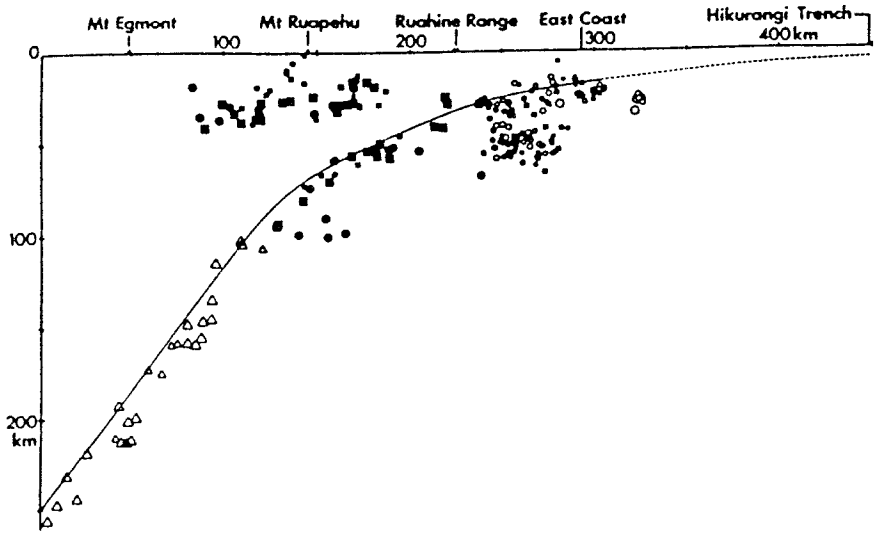

Diagram 2.1.3 Deep and intermediate earthquakes beneath the North Island, New Zealand. (After Reyners, 1980)

To the south of New Zealand is a subduction zone with the Pacific plate over-riding the Australian plate. Smith & Davey (1984) suggest a structure for this boundary with a section of the Australian Plate broken off and rotated into a near vertical position. There is some evidence of rifting to the east of the boundary in the Waiau valley but it is less active than the Taupo rifting.

Between the northern and southern subduction zones is the Alpine Fault which may be considered to be a transform boundary. However there is little change in the direction of the plate boundary between the subduction zones and the Alpine Fault. This gives a more complex picture than that of classical plate tectonics where subduction occurs at converging boundaries and the motion on transform boundaries is mostly parallel to the boundary. In this case oblique motion occurs on all boundaries. The different character of these boundaries may be due to the change between the continental lithosphere of the Chatham Rise and the oceanic lithosphere of the subduction zones (Walcott, 1978a). The central section of the boundary may thus be thought of as an example of continental collision rather than as a transform boundary. There is a strong component of compression across the Alpine Fault. Walcott (1979) gives the total amount of shortening perpendicular to the Alpine Fault as 70 km over the last 10 Myrs with most occurring over the last 5 Myrs. In the north and south of New Zealand the shortening is accommodated by subduction, while in the central region it results in substantial deformation and uplift. Despite this deformation, the area is notable for low seismicity compared

with the rest of New Zealand (see diagram 2.1.1). This seismic gap may be temporary but there is evidence that most of the motion along the fault is not by seismic slip. Walcott (1979) considers the slip on the Alpine Fault to be no more than one third of the total plate motion. It appears that most of the plate motion is accommodated by permanent anelastic, aseismic deformation.

The change, in Marlborough, from subduction to transform boundary zone is marked by a complex series of strike-slip faults. Karig (1969) suggests a tectonic development of the boundaries which would involve significant rotation of central New Zealand relative to the plate interiors (see diagram 2.1.4). Walcott (1979) gives palaeomagnetic evidence of rotation in Marlborough which is backed up by geodetic data (see section 2.3.2).

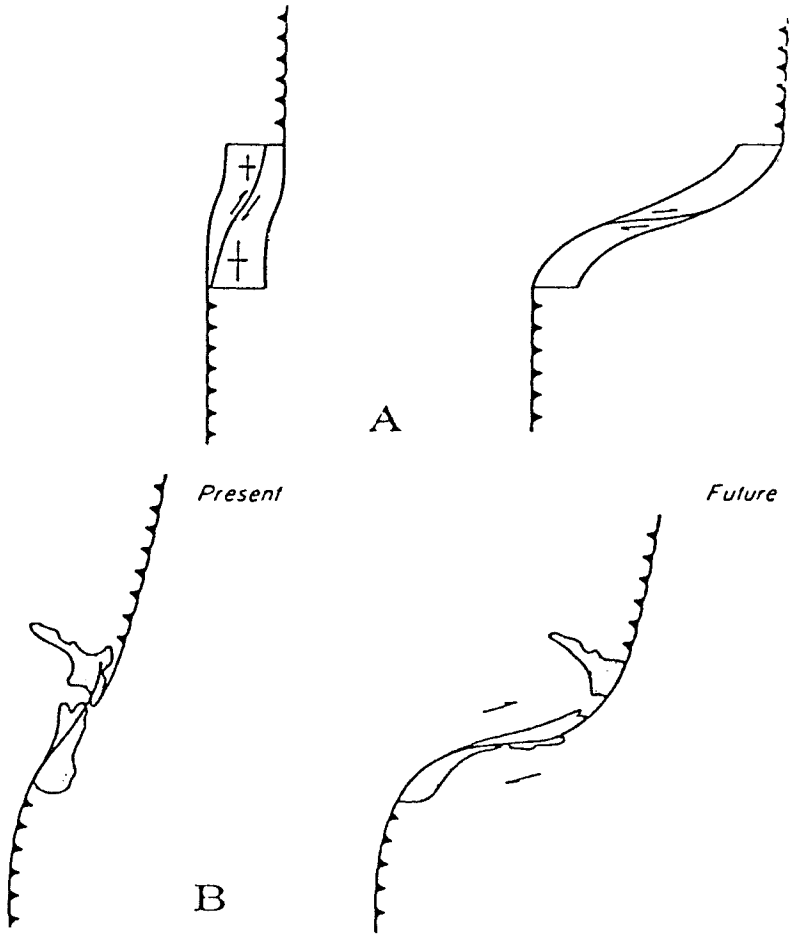

Diagram 2.1.4 Possible future tectonic development of New Zealand. (After Karig, 1969)

2.2 EARTH DEFORMATION ANALYSIS

2.2.1 DATUMS, TRANSFORMATION AND STRAIN

Geodetic observations may be used to generate coordinates in some reference system. This involves two steps.

1. Determine the relative geometry of points in the network (the inner geometry) from the observations.
2. Attach the network in some way to the reference system. This is the datum definition.

Given coordinates from two epochs, the displacement vectors may be derived. The interpretation of these is made difficult by their dependence on the datum definition at each epoch and by the possibility of changes in the reference system between epochs. The displacements may be used to derive the deformation parameters of **rigid body motion** (translation and rotation with respect to the reference frame) and **strain** (essentially the change in shape of the network). The strain parameters describe the change of inner geometry between epochs which is derived from the observations by step (1) above. The parameters of rigid body motion describe the change of datum definition in step (2) above.

For the datum definition problem, two types of network are considered.

Type A Those that use only observations independent of the datum such as horizontal directions.

Type B Those that also use observations of position and / or orientation relative to some reference system to define the datum such as astro-geodetic, TRANSIT, or GPS observations.

Datum Independent Networks.

The datum for networks of type A is usually defined by *a priori* coordinates of some of the points. The reference frame is then defined by, and fixed to, these points. If the same datum points are used in both epochs the reference frame moves with them. If the extent of significant deformation is less than the size of the network, **reference points** may be used which are outside the deformation zone. These provide a suitable datum for monitoring the movements of **object points** in the deformation zone. This technique is used to study deformations of man made structures such as dams, or areas of limited deformation such as landslips or glaciers. It can also be used to study the large and localised deformation that may be caused by earthquakes. For

examples of earthquake displacement surveys in New Zealand see Henderson (1937) and Boyes (1971). The new geodetic tools of VLBI, SLR and GPS allow high accuracy over long distances (>1000 km). It would be desirable, if possible, to have a set of relatively stable reference points in the interior of a tectonic plate (e.g., Australia) which could be used to define the motions of other points on the plate boundary (e.g., New Zealand).

If the extent of significant deformation is greater than the size of the network the choice of reference points becomes arbitrary. The displacements and the derived parameters of rigid body motion are then also arbitrary. A different choice of datum will give different, but equally valid, displacements and rigid body motions. In this case only the strain parameters are interpreted in the subsequent deformation analysis. The rigid body motions must be estimated but are treated as nuisance parameters. In fact it is not necessary to use coordinates to derive strain parameters. They may be derived directly from the observations without the need to define a datum (see Frank, 1966 and Bibby 1982).

Datum Dependent Networks.

In networks of type B the datum may be partly defined by the observations and the coordinates will then be in terms of the reference system of the datum observations. This is usually a global reference system such as an **earth centred - earth fixed** system (ECEF) or an **earth centred - inertial** system (ECI). ECEF reference frames are implicitly defined by the coordinates of points on the earth's surface such as astronomical observatories, radio telescopes or satellite tracking stations. ECI reference frames may be defined by the coordinates of stellar sources in a catalogue (either visible stars or radio sources) or by the motions of satellites (e.g., the moon, planets or artificial earth satellites). The rotations between ECEF and ECI systems are given by the equations of precession and nutation and by observed values of the earth rotation parameters (polar motion and UT1). The definitions and relationships between ECI and ECEF systems used in the study of geodynamics are covered in detail by papers in Gaposhkin & Kolaczek (1981).

2.2.2 THEORY OF INFINITESIMAL DEFORMATION

Before the results of strain analysis in New Zealand are presented, an introduction to the theory of deformation and the parameters commonly estimated from geodetic networks is given.

The deformation is assumed to be infinitesimal. This requires the change in the line element between two points to be much less than the distance between the points. This assumption is a reasonable one for earth deformation within the time scale of geodetic measurement (up to say 100 years). Harvey (1985) gives specific examples of the errors which may be caused by the assumption of infinitesimal deformation. In New Zealand, the strains observed are less than 1 part in 10^4 in 100 years (1 μstrain / year for 100 years) and if second order terms are ignored, the consequent errors are of the order of 10^{-4} μstrain / year. These are not significant when compared with those caused by other errors and assumptions.

Coordinates (x,y,z) in a right handed Cartesian system are assigned to points in the deformable body being studied. In the following equations, upper case bold characters (e.g., **A**) are used to represent matrices, and lower case bold characters (e.g., **a**) are used to represent vectors (single column matrices). If coordinates are available before and after deformation, a transformation of the coordinate system can be defined as

$$\mathbf{x}_2 = \mathbf{A}\,\mathbf{x}_1 + \mathbf{t} \qquad (2.2.1)$$

where $\mathbf{x}_1$, $\mathbf{x}_2$ are the vectors of coordinates being transformed, **A** is a matrix of transformation parameters and **t** is the translation vector.

For a general deformation model the elements of **A** are functions of position and time. This is **heterogeneous strain**. An assumption frequently made in deformation analysis is that of **homogeneous strain**. It is assumed that within a given region the elements of **A** may be considered to be constant. The validity of this assumption depends on the nature of the deformation, the size of the chosen region and on how accurately the deformation can be determined. When the strain is homogeneous, equation 2.2.1 is an example of an **affine transformation** (Harvey 1985). Under affine transformation straight lines remain straight and parallel lines remain parallel. The lengths and orientations of lines are generally changed by an affine transformation.

Even where the assumption of homogeneous strain is not valid for a complete network, it may be a reasonable assumption for part of the network. For example; strain may be homogeneous on either side of a major fault line with a discontinuity at the fault. An extreme example of dividing the network into sub-sections within which the strain is assumed to be homogeneous, is finite element analysis where the sub-sections consist of individual network triangles (e.g., Welsch, 1983).

Alternatively, a model of heterogeneous strain may be used where the elements of **A** are functions of position. For examples of heterogeneous strain models in theory and as applied in New Zealand, see Reilly (1986a, 1986b). In this thesis homogeneous strain is assumed and the limitations of the assumption are recognised. This will be discussed further in Section 2.3.1.

Equation (2.2.1) may now be rewritten (Harvey, 1985)

$$\mathbf{x}_2 = (\mathbf{S} + \mathbf{R})\mathbf{x}_1 + \mathbf{t} \tag{2.2.2}$$

The symmetric matrix **S** represents the strain tensor and **R** is the matrix of rigid body rotations. The elements of **S** and **R** are (Harvey, 1985)

$$\mathbf{S} = \begin{pmatrix} e_{xx} & e_{xy} & e_{xz} \\ e_{xy} & e_{yy} & e_{yz} \\ e_{xz} & e_{yz} & e_{zz} \end{pmatrix} \tag{2.2.3}$$

$$\mathbf{R} = \begin{pmatrix} 1 & \omega_z & -\omega_y \\ -\omega_z & 1 & \omega_x \\ \omega_y & -\omega_x & 1 \end{pmatrix} \tag{2.2.4}$$

where

$$e_{xx} = \frac{\partial u}{\partial x}$$

$$e_{yy} = \frac{\partial v}{\partial y}$$

$$e_{zz} = \frac{\partial w}{\partial z}$$

$$
\begin{aligned}
e_{xy} &= \frac{1}{2}\left(\frac{\partial u}{\partial y} + \frac{\partial v}{\partial x}\right) \\
e_{yz} &= \frac{1}{2}\left(\frac{\partial v}{\partial z} + \frac{\partial w}{\partial y}\right) \\
e_{xz} &= \frac{1}{2}\left(\frac{\partial u}{\partial z} + \frac{\partial w}{\partial x}\right) \\
\omega_x &= \frac{1}{2}\left(\frac{\partial v}{\partial z} - \frac{\partial w}{\partial y}\right) \\
\omega_y &= \frac{1}{2}\left(\frac{\partial w}{\partial x} - \frac{\partial u}{\partial z}\right) \\
\omega_z &= \frac{1}{2}\left(\frac{\partial u}{\partial y} - \frac{\partial v}{\partial x}\right)
\end{aligned}
\qquad (2.2.5)
$$

and where u , v , w are the displacements in x , y , z

$$
\begin{pmatrix} u \\ v \\ w \end{pmatrix} = \begin{pmatrix} x_2 \\ y_2 \\ z_2 \end{pmatrix} - \begin{pmatrix} x_1 \\ y_1 \\ z_1 \end{pmatrix} \qquad (2.2.6)
$$

The diagonal components of the strain tensor, e_{xx} , e_{yy} , e_{zz} are the **extensional strains** along the X , Y , and Z axes respectively. The off diagonal components e_{xy} , e_{xz} , e_{yz} are the **shear strains**. The components of the **R** matrix, ω_x , ω_y , ω_z given in equation 2.2.4 are equal to the **rotations** of the coordinate system axes about the X , Y , and Z axes respectively (assuming that the rotations are small which is part of the assumption of infinitesimal deformation).

The strain matrix **S** may be converted by rotation (or eigenvalue decomposition) to a diagonal form $\mathbf{S}_p$ in which all shears are zero and the diagonal terms are called the **principal strains** (e_1 , e_2 , e_3). These are the extensional strains in the **principal directions** which are given by the eigenvectors.

$$
\mathbf{S}_p = \begin{pmatrix} e_1 & 0 & 0 \\ 0 & e_2 & 0 \\ 0 & 0 & e_3 \end{pmatrix} \qquad (2.2.7)
$$

Topocentric Strain

The model used in this thesis is the topocentric strain model. The advantage of this model is that some of the parameters are virtually identical to those of the 2D or plane deformation model that has generally been used in practice. The features of the topocentric model and comparisons with other models are given in Harvey (1985). The axes of a topocentric coordinate system are E (east) , N (north) and V (vertical). The origin of the coordinate system is a point chosen near the centre of the network to be studied. It may be the centroid of the network as in Harvey (1985) but this is not necessary. A disadvantage of the centroid is that it changes if any stations in the network are deleted or if their relative positions are changed. The topocentric system has the vertical axis normal to the ellipsoid at the chosen origin point. The north axis N is orthogonal to the V axis and lies in the plane containing the V axis and the Z axis of the conventional terrestrial reference system (CTRS). The east axis is orthogonal to N and V such that the triplet E , N , V form a right handed system.

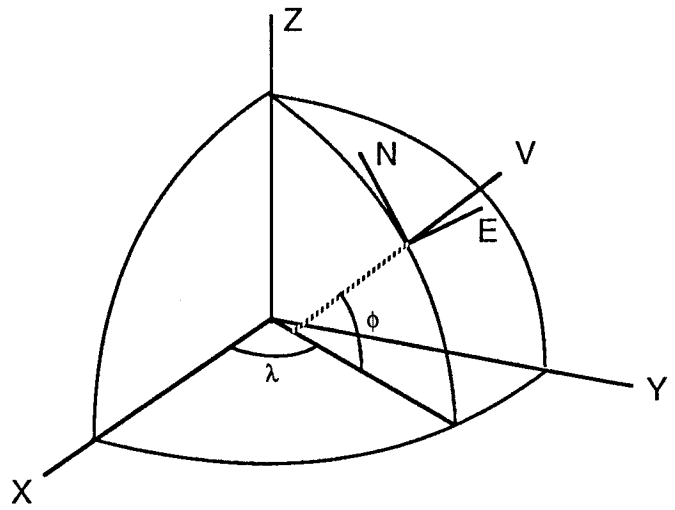

Diagram 2.2.1 Topocentric Reference System

The coordinates e , n , v are substituted for x , y , z in the strain equations above and thus

$$\mathbf{S} = \begin{pmatrix} e_{ee} & e_{en} & e_{ev} \\ e_{en} & e_{nn} & e_{nv} \\ e_{ev} & e_{nv} & e_{vv} \end{pmatrix} \qquad (2.2.8)$$

$$\mathbf{R} = \begin{pmatrix} 1 & \omega_v & -\omega_n \\ -\omega_v & 1 & \omega_e \\ \omega_n & -\omega_e & 1 \end{pmatrix} \qquad (2.2.9)$$

The assumption of homogeneous strain is only reasonable in New Zealand for networks of limited extent ; say 100 km or less as discussed in section 2.3.1. Over these distances the networks are approximately planar with all points close to the $E-N$ plane. The parameters of the topocentric model are easier to interpret for such networks, than the parameters of models with different axes. For example the rotation about the V axis is an azimuth rotation and the rotations about the E and N axes represent gradients north and east respectively between the two sets of coordinates which may be due, for example, to a linear change in uplift across the network. The strains in the east - north plane are more accurately determined than those in the vertical direction and the topocentric model allows the separation of the poorly determined parameters from the others. They may be held fixed and only 2D strain parameters estimated.

The topocentric strain model will be used with four different sets of parameters. The first is the **full 3D model** which contains 12 parameters. These are the 6 strain parameters in the matrix $\mathbf{S}$, the 3 rotations in the matrix $\mathbf{R}$ and the 3 translations in the vector $\mathbf{t}$ of equation 2.2.2. The second model is the **partial 3D model** or **11 parameter model**. This is the same as the full 3D model except that the vertical strain e_{vv} is not estimated. The third model is the **horizontal strain model**. This contains 9 estimated parameters with the vertical strains e_{ev} , e_{nv} , e_{vv} being held fixed. This model has 3D rotations, 3D translations and 2D strains. The fourth model is the **2D model**. This model has 6 parameters with the parameters ω_e , ω_n t_v also being held fixed. This model has 2D rotations, translations and strain.

Reilly (1979) considers the effect of network geometry and type of observation on the estimability of deformation parameters. In the past, the 2D model has been used in New Zealand but as GPS is a 3D system it is appropriate to consider whether one of the other models described above should be used. In Chapter 3, examples are presented of the estimation of the parameters of these four models from geodetic networks. Here this is discussed from a geometric viewpoint. If the network is completely planar, the vertical

extensional strain e_{vv} cannot be determined. Reilly (1979) shows that even with distance measurements on lines sloping at 30°, this parameter is not well determined. Lines with this gradient are possible using GPS in some mountainous areas between mountain top and valley floor but are unlikely in terrestrial geodetic nets because of problems with intervisibility.

Reilly (1979) notes that in a nearly planar geodetic network, the parameter combinations $(e_{ev} + \omega_n)$ and $(e_{nv} - \omega_e)$ can be determined directly from zenith distances or levelling data. Alternatively, coordinates from an adjustment using such data or from an adjustment of GPS may be used. However, $(e_{ev} - \omega_n)$ and $(e_{nv} + \omega_e)$ are not well determined and thus e_{ev} is not easily separated from ω_n, nor e_{nv} from $-\omega_e$. If the network lies completely on the east - north plane, e_{ev} and ω_n have identical signatures; namely an apparent rotation about the north axis. Similarly, e_{nv} and $-\omega_e$ have the signature of a rotation about the east axis. If the network has some vertical relief it will be possible to distinguish between these parameters but the results will be strongly dependent on small inhomogeneities in the horizontal coordinates. This is illustrated in diagram 2.2.2. An idealised network has been chosen which extends for 50 km across a mountain range 1000 metres high. This is projected onto the east - vertical plane. The effect of 10 ppm values for e_{ev} and ω_n are shown for 3 network stations (not to scale). The only difference in the effect of these 2 parameters is a small difference in horizontal displacement at the highest point. Thus the effect of $(e_{ev} - \omega_n)$ is a small systematic horizontal displacement at the highest point. In this example, a variation in horizontal displacement of 0.02 m per 1000 m in height can be interpreted as either 20 ppm deformation or as a small systematic departure of the horizontal strain from the assumption of homogeneity (0.02 m in 25 km or 0.8 ppm). The parameters e_{ev}, e_{nv}, ω_e, ω_n may therefore absorb the effects of inhomogeneities in the horizontal observations or adjustment, and their true values will tend to be swamped by noise.

It may be possible to estimate the vertical extensional and shear strains if *a priori* information is available from other sources. For example, conservation of mass and some knowledge of the compressibility of the crust could be used to constrain the magnitude of the 3D dilatation. However, the relationship between a 3D geophysical model of the lithosphere and surface deformation observed by geodesy may be uncertain and, if a geophysical model is used to constrain the geodetic adjustment, the estimated parameters may be biased.

Network Geometry

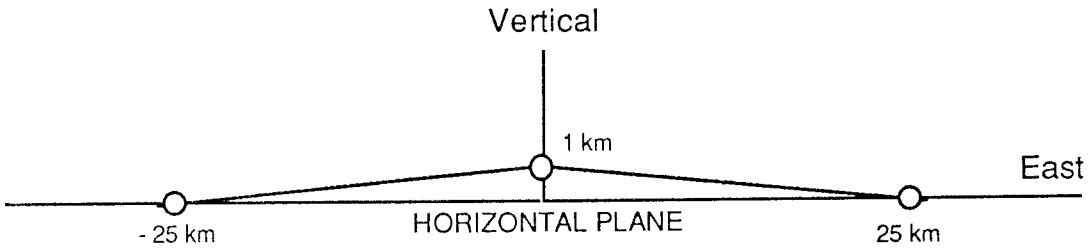

Effect on stations of rotation of ω_n = 10 ppm (2.06 arcsec)

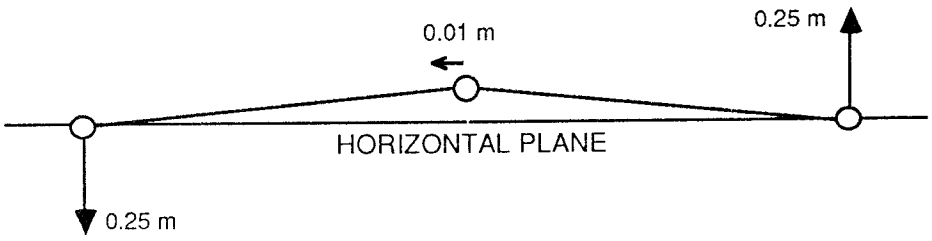

Effect on stations of strain e_{ev} = 10 ppm

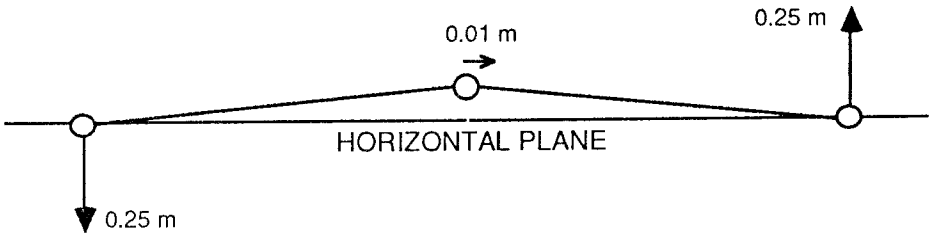

Effect on stations of combined ($e_{ev} - \omega_n$) = 20 ppm

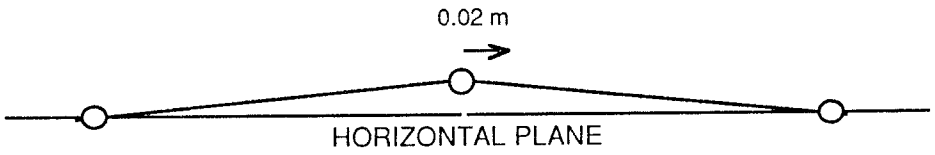

Diagram 2.2.2 Relationship between vertical shear strain and rotation in near - planar geodetic networks. (Not to scale)

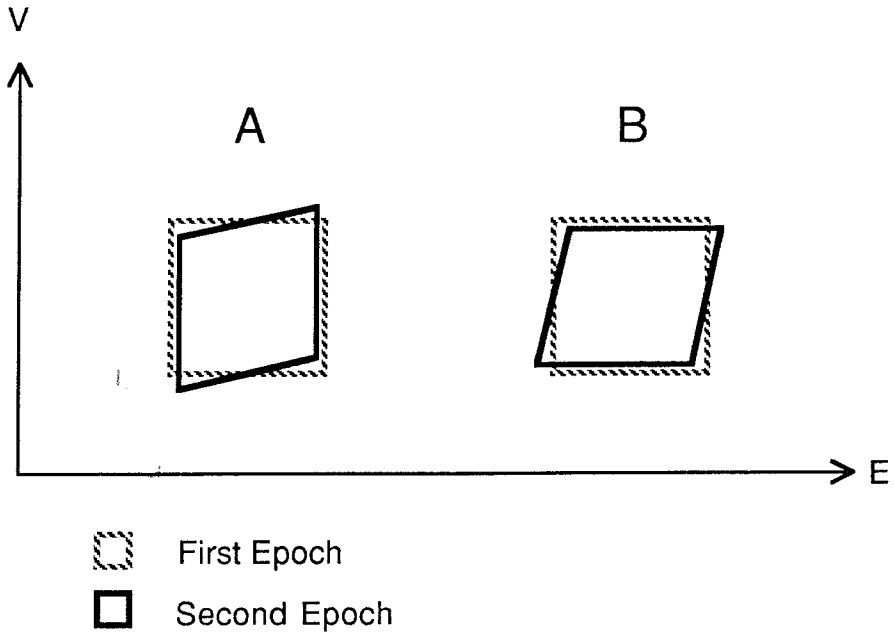

Diagram 2.2.3 Two interpretations of vertical shear strain e_{ev} as determined from displacements on a deformed cube.
A. Linear change in uplift with east coordinate.
B. Linear change in east displacement with height.
These interpretations differ only by a rotation about the north axis.

Even if the vertical shear strains could be accurately determined, the interpretation of their geophysical significance would be difficult. Diagram 2.2.3 shows two possible interpretations of a positive value for e_{ev}. The shear could be caused by a linear increase in uplift as the east coordinate increases or as a linear increase in displacement east as height increases (or some combination of the two). These two interpretations differ only by a rotation about the north axis. The estimate of this rotation is dependent on any changes in the definition of the reference system axes between epochs such as will be present if terrestrial observations are used in one epoch and GPS observations in the next. Thus it is seen that, from a geometric viewpoint, there are difficulties in interpreting the vertical shear strain parameters from combined terrestrial / GPS data. In Chapter 3 this topic is examined further to see if there are any advantages or disadvantages in holding these parameters fixed at zero.

Alternative 2D Strain Parameters

If only the 2D model is considered, the matrices **S** and **R** now become

$$\mathbf{S} = \begin{pmatrix} e_{ee} & e_{en} \\ e_{en} & e_{nn} \end{pmatrix} \qquad (2.2.10)$$

$$\mathbf{R} = \begin{pmatrix} 1 & \omega_v \\ -\omega_v & 1 \end{pmatrix} \qquad (2.2.11)$$

The set of three strain parameters in **S** are not the only way to describe the deformation and an alternative set is frequently used. These are (e.g., Frank, 1966; Bibby, 1975)

Pure Shear	$\gamma_1 = e_{ee} - e_{nn}$	
Engineering Shear	$\gamma_2 = 2e_{en}$	
Dilatation (2D scale change)	$s_{2D} = \frac{1}{2}(e_{ee} + e_{nn})$	(2.2.12)

There is a variety of definitions for shear and dilatation parameters in the literature. For example, Welsch (1982,1983,1986a) defines γ_1 with the opposite sign to that above. The definitions of equations 2.2.12 have been chosen because they have been used extensively in New Zealand (Bibby, 1973, 1975, 1981; Bibby & Walcott, 1977; Walcott, 1978a, 1978b, 1979, 1984 Blick, 1986. See also Wellman, 1981). The dilatation of equation 2.2.12 is the mean 2D extensional strain. Many other authors (e.g; Prescott et al 1979; Livieratos & Vlachos, 1981; Dermanis & Livieratos, 1983; Welsch, 1982,1983,1986a; Harvey, 1985) prefer the areal dilatation (change in area per unit area) which is the sum of the horizontal extensional strains and thus equal to twice the dilatation defined above.

Of the parameters in equations 2.2.12 , s_{2D} can only be estimated if the change of scale is accurately known and the rotation ω_v in **R** can only be estimated if the change of orientation is accurately known. However γ_1 and γ_2 are relatively independent of orientation and scale and may be estimated from triangulation data where scale and orientation are not well known. For example; an error in the scale definition of 10 ppm will only affect the estimation of γ_1 and γ_2 by the same proportion; i.e.; 1 part in 10^5. The dependence of γ_1 and γ_2 on the orientation is related to the definition of the axes E and N by which the strains are defined. An error of 1 minute in the definition of azimuth will affect γ_1 and γ_2 by a maximum of 3 parts in 10^4.

These are second order effects which are ignored under the assumption of infinitesimal deformation. Rotation and dilatation are affected directly (one to one) by uncertainties in the definition of orientation and scale respectively.

From the three parameters in equation 2.2.12 the following may also be derived using the equations in Bibby & Walcott (1977) or Harvey (1985) and remembering the difference in the definition of dilatation.

Total Shear	$\gamma = (\gamma_1^2 + \gamma_2^2)^{1/2}$
Maximum Principal Strain	$e_1 = s_{2D} + \frac{\gamma}{2}$
Minimum Principal Strain	$e_2 = s_{2D} - \frac{\gamma}{2}$
Azimuth of e_1	$\theta = \frac{1}{2}\arctan\left(\frac{\gamma_2}{-\gamma_1}\right)$
Azimuth of e_2	$\varphi = \frac{1}{2}\arctan\left(\frac{-\gamma_2}{\gamma_1}\right) = \theta \pm \frac{\pi}{2}$
Azimuth of γ	$\psi = \frac{1}{2}\arctan\left(\frac{-\gamma_1}{-\gamma_2}\right) = \theta + \frac{\pi}{4}$ (2.2.13)

The direction of e_1 (θ) is the direction of maximum extension or tension and the direction of e_2 (φ) is the direction of minimum extension or maximum compression. Therefore φ is also called the direction of the **principal axis of compression**. The direction of maximum right lateral shear is given by ψ and the direction of maximum left lateral shear is $\psi \pm \frac{\pi}{2}$. As the deformation environment in New Zealand is generally compressive, the direction of the principal axis of compression φ is the most useful of the three directions θ , φ , ψ given above. The direction of maximum shear ψ may be the most appropriate for an environment with simple shear across a plate boundary or fault line (e.g., in California). These directions are based on the surveying convention that azimuth is measured clockwise from north towards east. Welsch (1982,1983,1986a) uses the mathematical convention that angles are counted positive anti-clockwise from east towards north. Note the ambiguity in the expressions for θ , φ and ψ if care is not taken to put the result of the arctan function into the correct quadrant. This potential ambiguity is often overlooked in the literature. For example, Walcott (1984) uses

$$\varphi = \frac{1}{2}\arctan\left(-\frac{\gamma_2}{\gamma_1}\right) \qquad (2.2.14)$$

which does not differentiate between θ and φ. Savage & Burford (1970) use the pair of equations

$$\sin 2\theta = \left(\frac{\gamma_2}{\gamma}\right) \quad , \quad \cos 2\theta = \left(\frac{-\gamma_1}{\gamma}\right) \qquad (2.2.15)$$

and these equations, taken together, define θ unambiguously.

2.2.3 LEAST SQUARES ESTIMATION OF DEFORMATION

The methods used to estimate deformation parameters may be categorised as the observation difference method, the coordinate difference method and the method of simultaneous reduction.

Observation Differences

Where observations have been repeated in different epochs, the strain parameters may be estimated directly from differences in the observations without the need for a network adjustment. This is the basis of the method used by Frank (1966), and others since then, to estimate the shear strains γ_1 and γ_2 from repeated triangulation. This method is of most value when the observation schemes for each epoch are identical. If some observations appear only in one epoch they cannot be used, and in such cases this method does not make full use of the available data. This model is not applicable to the case where terrestrial observations are available in one epoch and GPS observations in another epoch.

Simultaneous Reduction

Bibby (1982) describes how observations from different epochs can be used in a single adjustment to estimate station coordinates at some reference epoch and the deformation parameters between that epoch and other epochs. This method does not require identical observation schemes in each epoch to make the best use of the observations. It could be used to combine terrestrial data from one epoch with GPS baseline or multi-station figures from another epoch. It could also, in theory, be used with terrestrial observations and GPS phase observations in a combined multi-session / deformation adjustment but,

given the complexity of the GPS adjustment it is unlikely that such a model would be contemplated in practice.

Coordinate Differences

The geodetic observations from each epoch can be adjusted separately to generate coordinates, with these coordinates then being used as observations in a deformation adjustment. If the datum is minimally constrained in each epoch adjustment and if the coordinates and VCV matrices of these adjustments are used, without alteration, in the deformation adjustment, this method will give the same results as the method of simultaneous reduction. Brunner et al (1981) describe the inner coordinate technique in which the singular normal matrix of a free net adjustment is formed and the pseudo-inverse used in the adjustment. This is also called the minimum norm or minimum trace solution (Caspary, 1987) and ensures that the datum is defined with minimum constraints.

The coordinate difference method has the advantage that the observations can be checked for outliers and systematic errors at the network adjustment stage before being used to estimate deformation parameters. The deformation adjustment is based on a number of assumptions which need to be checked, such as the assumption that the deformation is homogeneous or that heterogeneous deformation can be completely described by the chosen parameters. Some stations may have been subject to localised deformation or disturbance. It will be easier to detect these anomalous single point movements at the deformation adjustment stage, if it is known that the observations associated with these points showed no inconsistency at the network adjustment stage. If the network and deformation adjustments are combined, as in the method of simultaneous reduction, it may be difficult to distinguish between instrument or target eccentricity and single point movements.

The method of simultaneous reduction and the coordinate difference method are equivalent if there are no gross or systematic errors in the observations. In general, such errors are to be expected and the coordinate difference method offers more flexibility in detecting and dealing with them.

2.3. DEFORMATION ANALYSIS IN NEW ZEALAND

2.3.1 GEODETICALLY DERIVED STRAINS.

The geodetic surveys used by Bibby and Walcott in their papers on strain in New Zealand (Bibby, 1975, 1981; Bibby & Walcott, 1977; Walcott, 1978a, 1978b, 1979, 1984), are horizontal triangulation surveys dating back over 100 years. The earliest surveys are not of high accuracy but in some areas the deformation rates are sufficient to cause changes in angles of 12" per century. Errors of this magnitude, when systematic, are detectable by the early triangulation surveys.

Strain rates as calculated by Bibby and Walcott, allow data from different epoch pairs to be directly compared with each other. If the strain rate is constant the data from several epochs may be combined in one calculation of the strain rates with resultant increase in redundancy and precision. The deformation parameters are calculated directly from horizontal direction observations in the two epochs (the method of simultaneous reduction) rather than from coordinates. Accurate scale and orientation are generally not available for more than one epoch so only $\dot{\gamma}_1$, $\dot{\gamma}_2$ or $\dot{\gamma}$, φ are used in the deformation analysis. Because the dilatation rate is not available from the observations, the interpretation of the strain relies on knowledge of the pattern of fault lines in the area. If the principal axis of compression is 90° to fault lines then the deformation is interpreted as compressive; if it is parallel to the fault lines then the deformation is considered to be tensional and if it is at 45° to the fault then there is simple shear across the fault line. This is illustrated in diagram 2.3.1.

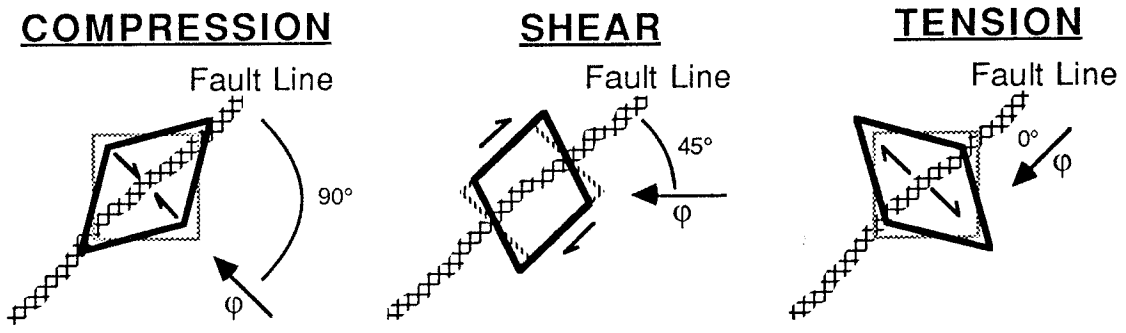

Diagram 2.3.1 Use of the fault line structure and the principal axis of compression to determine the nature of the strain.

For a detailed analysis of strain rates in New Zealand, region by region, the reader is referred to the above listed papers by Bibby and Walcott. Some of the general features of strain in New Zealand are presented here.

The assumption of homogeneity has been found to be valid provided the region of study is sufficiently small. This may be either because the strains are homogeneous or because the observations are not sufficient to identify the inhomogeneities. The triangulation surveys of last century were on a small scale with lines of 10 km or less. This density of data allows strain rates to be calculated for small networks for which the assumption of homogeneity appears to be valid and then tested against neighbouring networks. Bibby & Walcott (1977) found in Marlborough that there is a systematic change in strain over 80 km but that the change in a network covering 20 km is so small as to be negligible. In calculating strain rates the assumption is made that the rate is invariant with time. In the Marlborough shear zone this assumption appears to be valid. The rates derived from different epoch pairs are not significantly different from each other (Bibby 1981).

In the east of the North Island adjacent to the subduction zone, changes of strain with time have been identified. Prior to the 1931 Hawkes Bay earthquake (magnitude 7.9) the principal axis of compression was normal to the direction of the plate boundary indicating compression across the boundary (Walcott 1978b). Since the earthquake the axis of compression has been parallel to the boundary which indicates extension across the boundary. This is interpreted by Walcott (1978b) as either post-seismic relaxation or gravitational sliding towards the trench. In the south of the North Island a complementary picture emerges. Before 1920 the estimated strain indicates an extensional component across the boundary. This extension may have been occurring since an earthquake in 1855 (magnitude of about 8). Since 1920 there has been a compressional component across the boundary which suggests that the subduction locked about 1920 (Walcott 1978b). The stress has been accumulating since that date and when the failure point is reached a major earthquake may be expected. However part of the compression up to now will be recovery of the earlier extension and part may lead to permanent anelastic deformation.

An analysis of strain adjacent to the Alpine Fault in the South Island indicates inhomogeneous strain across the fault. Walcott (1979) describes strain

analysis at Okarito where a network crossing the fault gives a shear strain rate of 0.67 ± 0.1 μstrain/yr. An analysis of that part of the network which does not cross the fault gives a shear strain rate of 0.24 ± 0.07 μstrain/yr. The strain across the fault is thus strongly heterogeneous.

Walcott (1984) gives strain rates for several areas of approximately 40 km x 40 km throughout New Zealand. These have been calculated using a set of axes which are parallel to and normal to the plate boundary. Two different sets of axes have been used to allow for the different orientation of the boundary in the North and South Islands. This data has then been used to produce contours of strain rates over the country. These are shown in diagram 2.3.2 below. Positive $\dot{\gamma}_1'$ indicates relative compression across the boundary and negative $\dot{\gamma}_1'$ indicates relative extension. The shear across the boundary is given by $\dot{\gamma}_2'$.

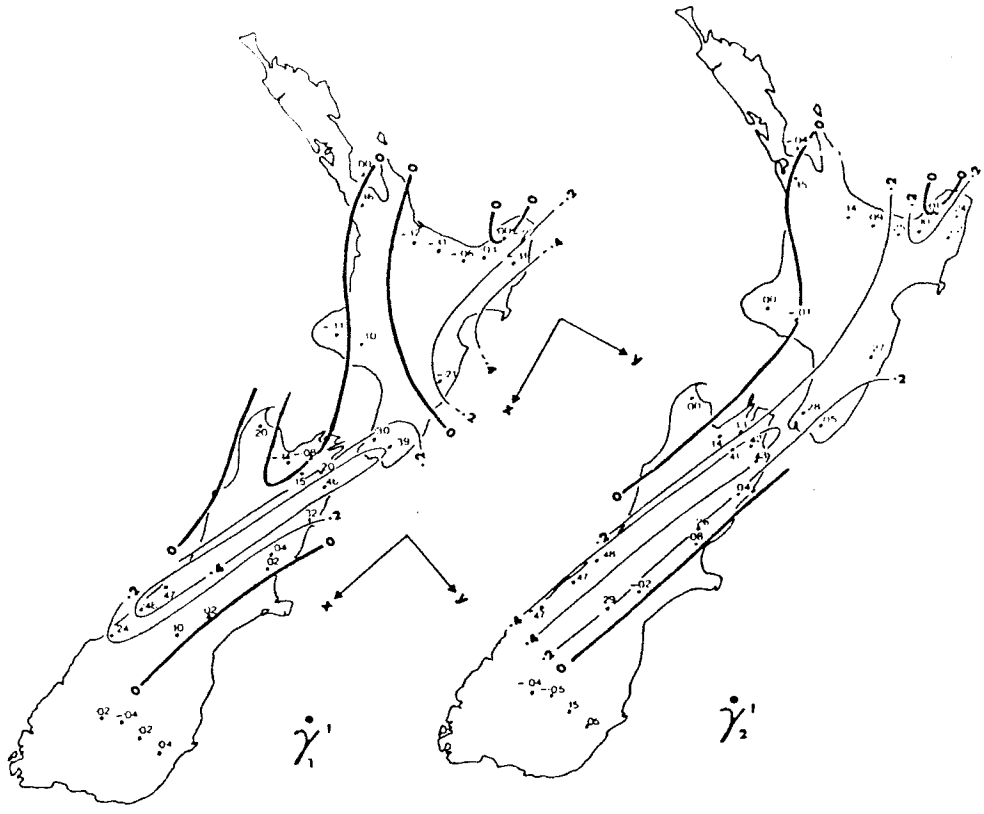

Diagram 2.3.2 Shear strain rates derived from geodetic data. The axes used to derive the strain values in the North and South Islands are shown. (After Walcott, 1984)

2.3.2 COMPARISON WITH OTHER GEODYNAMIC DATA.

The information provided by derived strains may in some cases be compared with data from other earth sciences. This allows independent checks to be made on different data sets and from the comparisons, hypotheses can be refined.

The velocity across the plate boundary has been calculated by integration of geodetically determined strains across the northern part of the South Island (Bibby, 1981). The result is 54 ± 9 mm/yr with an azimuth of 264° ± 10°. This is not significantly different from the value of 47 ± 5 mm/yr at 270° ± 5° for the same region calculated by Walcott (1984) from relative plate motions which were derived from sea floor spreading data. The agreement between these two results is surprising considering that the first is derived from 100 years of data while the second is based on magnetic anomalies 3 Myrs old. In comparing these two results the assumption is made that almost all of the deformation caused by the relative plate motion is within the deformation zone. The data does not contradict this assumption which is a fundamental tenet of the plate tectonic theory. It also appears that the deformation, in this region at least, is surprisingly uniform in time.

Walcott (1984) assumes that the sum of the extensional strains ($e_{ee} + e_{nn} + e_{vv}$) is zero due to conservation of mass and thus relates compression across the boundary ($\dot{\gamma}_1'$) to dilatation and thence to uplift or subsidence. The short term $\dot{\gamma}_1'$ derived from geodetic data can then be compared with long term estimates based on rates of uplift and rates of erosion. He finds a close correspondence despite a number of assumptions made in the comparison. He deduces long term dilatation rates in the Southern Alps of the order of 0.1 ppm/yr.

The rate of rotation of central New Zealand relative to the Australian plate derived from geodetic values of $\dot{\gamma}_2'$ by Walcott (1984) is 8°/Myr (0.029"/yr). This can be compared with an estimate of 6°/Myr derived from palaeomagnetism as an average over the last 5 Myr. There is an indication that the rotation is increasing and this may help to reconcile the two values.

The direction of the principal axis of compression as obtained from geodetic data may, in many cases, be compared with that derived from study of micro-earthquakes and from geological data. Bibby (1981) compares values for the north east of the South Island. The geodetic value is 90° ± 7°. The direction from micro-earthquake studies over a wider area is 105° ± 10° and the direction from geological evidence covering 20,000 years is 110°-115°.

Walcott (1979) has found that the shear strain across the plate boundary in the South Island is substantially less than the estimate of slip on the fault. He reconciles these differences by noting that the structure of rocks adjacent to the Alpine Fault indicates a rotation in line with the fault and that the shear may be absorbed over a wide area by permanent anelastic deformation.

2.3.3 ASSESSMENT OF GEODETIC DATA IN GEODYNAMICS

The strain parameters derived in New Zealand from geodetic data do not represent the complete state of deformation. The parameters are dependent on assumptions of homogeneity in space and time. Of the parameters of 3D rigid body motion and homogeneous strain only two, γ_1 and γ_2, have been used in the deformation analysis. Despite these limitations, the two parameters derived have proved particularly useful in deformation analysis. The papers by Bibby and Walcott listed at the start of section 2.3 provide good examples of the application of strain data to problems in the structure and local dynamics of the earth. This data has proved useful in several ways. It fills gaps in knowledge left by the other techniques of geology and geophysics. It quantifies processes which are otherwise only qualitative. It assists the analyst in choosing between alternative hypotheses where other data is ambiguous and it provides an independent check on that data. The additional information which can be expected from space techniques will help further in resolving many present problems in geodynamics.

3. TERRESTRIAL GEODESY

3.1 INTRODUCTION

The principles and practice of terrestrial geodesy are well defined in texts such as Bomford (1980) or Vanicek & Krakiwsky (1986) to which the reader is referred. This Chapter deals with some aspects of terrestrial geodetic surveys in New Zealand that are relevant to the study of earth deformation. A summary is given of surveys in New Zealand which, by design or good fortune, are of value in deformation analysis. The principal systematic errors in terrestrial geodetic observations are briefly discussed. Data from the Castle Point - New Plymouth Earth Deformation Studies (EDS) survey has been adjusted in a number of different configurations. The sets of coordinates obtained from these adjustments are then used in deformation adjustment software to determine the strain between data sets. It is reasonable to assume that there was no significant earth deformation during the 3 months of this observation campaign, and thus the **geophysical strain** is zero. The estimates of strain obtained are thus due solely to variations in the method of adjustment and choice of observations. The term **geodetic strain** is used here to describe the strain caused by systematic errors in the geodetic observations or adjustment model. From these estimates of geodetic strain, conclusions can be drawn about:

- the optimum method of adjusting the terrestrial data available in New Zealand for deformation analysis,
- the deformation model with the greatest potential value for the interpretation of deformation,
- the strengths and limitations of the terrestrial data that affect its combination with GPS data.

One possible use of combined terrestrial / GPS data is the estimation of relative uplift or subsidence. The principal difficulty lies in the comparison of orthometric heights from precise levelling and ellipsoidal heights from GPS. At present, the errors in relative geoid height determination are often larger than the systematic errors in either the precise levelling or the GPS heights. The results of Kearsley (1986) suggest that the error in relative geoid height can be reduced to the level of 2 to 3 ppm of the baseline length which is of the order of errors in the GPS ellipsoidal heights. Kearsley's method makes use of observed gravity in an inner zone having a radius of 1° to 2° (110 km to 220

km). Outside this zone a high order geopotential model is used. The greatest distance of any point in New Zealand from the sea is about 1° and marine gravity data is sparse with uncertainties in this area of the order of 20 mgal (Wessel & Watts, 1988). Thus there may be difficulties in applying this method to New Zealand data.

An assessment of the methods used to estimate accurate relative geoid heights is beyond the scope of this thesis. Nevertheless, without such an analysis it is difficult to draw useful conclusions about the estimation of uplift or subsidence from combined terrestrial / GPS data. Therefore this study is confined to the analysis of horizontal triangulation or trilateration networks for strain. The orthometric heights in these networks are mostly determined from trigonometric levelling with uncertainties of the order of 0.2 m to 1.0 m depending on the care taken in the observation of the vertical angles. Our main interest in these heights arises from the need to ensure that height errors do not corrupt the estimates of horizontal deformation.

3.2. GEODETIC SURVEYING IN NEW ZEALAND

The history of the definition of the New Zealand Geodetic Datum 1949 (NZGD-49) is given in Lee (1978) together with a history of the early control surveys in New Zealand. Bevin (1981) and Bevin et al (1984) describe the history of earth deformation surveying in New Zealand. Some of the key points are summarised in this section.

3.2.1 EARLY SURVEYS

Between settlement in 1840 and the abolition of the provincial governments in 1876 there were few surveys of a standard sufficient to be of use for deformation analysis. Triangulation was uncommon and generally of low accuracy. From 1877 to 1900 minor triangulation was extended over all settled areas. This consisted mostly of chains of polygons with few cross rays and with sides of about 5 km. By the mid 1880s a continuous chain of triangles ran the length of New Zealand. These surveys were not intended to provide a primary geodetic datum, as had been recommended in a report to the Government in 1855. They were an interim measure to link the settlement surveys that had been undertaken in a piecemeal and haphazard fashion. Accuracy was low by the standards of geodetic survey and triangle miscloses of 20" or more are not uncommon (Blick, 1986). The extra accuracy and redundancy that could have been provided by the observation of additional cross rays was deliberately avoided, presumably to simplify the calculations and reduce costs (Lee, 1978). Where observations were made of astronomical azimuth the techniques were not sufficiently accurate to allow rotations relative to a global reference system to be determined. The measurement of baseline lengths was also not accurate enough for dilatation to be determined from these surveys. Given a dilatation rate of 0.1 ppm/yr and a rotation rate of 0.03" /yr (Walcott, 1984; see section 2.3.2) accuracies of 5 ppm in scale and 1.5" in azimuth in these 100 year old surveys would be required for dilatation and rotation to be detected at the 95% confidence level.

This early New Zealand triangulation contained serious deficiencies for the maintenance of a national survey system. However, the time that has elapsed since these surveys were made and the rates of deformation typical in New Zealand are such that the earth deformation "signal" is above the high observation noise. The value of these triangulation schemes also stems from the fact that the field books of raw observations have been kept. This is

important, as the coordinates, bearings and lengths of lines calculated from these surveys were not derived by rigorous adjustment and have no value for deformation analysis. While the surveys do not cover the whole country, the density of the information is high with distances between stations typically 5 km. In areas of heterogeneous strain the networks may therefore be broken up into small regions where the assumption of homogeneity is reasonably valid (e.g., Bibby & Walcott, 1977). In most of New Zealand, the triangulation surveys of the 1870s and 1880s are the first epoch of data for strain analysis.

3.2.2 NEW ZEALAND GEODETIC DATUM 1949

Observations for 1st order geodetic triangulation began in 1923 and continued with interruptions until 1949. The result was New Zealand Geodetic Datum 1949 (NZGD-49). The lengths of triangle sides was initially 30 km and was later increased to 50 km due to slow progress. The majority of triangle miscloses were less than 1" although occasionally up to 5". From 1929, Wild T3 theodolites were used and observations were made to lamps at night. The triangle miscloses improved, seldom exceeding 2". At least 12 sets of horizontal observations were observed at each station, in most cases derived from more than one nights observation. Vertical angle observations generally consisted of 2 or more sets observed near midday or midnight to minimise the effects of refraction. In 1931 the work was halted by a large earthquake near the city of Napier. The fire which followed the earthquake destroyed survey records for the province. Work was halted on the 1st order triangulation to re-introduce cadastral survey control in the province. When the primary triangulation restarted and the area was re-observed, comparisons indicated shifts of up to 0.4 m during or immediately after the earthquake.

Eight baselines were measured: 5 in the North Island, measured between 1909 and 1913, and 3 baselines in the South Island measured in 1947. The lengths of these ranged from 8.4 km to 18.3 km. Two of the North Island baselines were re-measured in 1947 and the differences were 12 ppm and 7 ppm. The mean of these values was applied to the other North Island baselines. Bevin & Forster (1973) describe the re-measurement of some of the baselines by laser geodimeter. Differences of a few ppm were obtained depending on the metre - foot ratio used. The S.I. ratio adopted on metrication in 1972 differs by 2.5 ppm from the ratio valid when the invar tape used in 1947 was calibrated. It also differs by 1.7 ppm from the ratio used to derive imperial units for the International (Hayford) Spheroid 1924 used in the

geodetic adjustment. The differences in baseline lengths derived by Bevin and Forster are of the order of the systematic errors in the measurements and no conclusions can be drawn as to the effect of earth deformation on these lines. For the purposes of deformation analysis, scale is considered to be undefined by surveys conducted before the advent of EDM.

Astronomic observations for latitude were made at 67 stations being 1 in 3 first order stations in the North Island and 1 in 6 first order stations in the South Island. Astronomic azimuth was observed at 40 stations being 1 in 7 stations in both islands and at 12 Laplace stations astronomic longitude was also observed. These observations were generally carried out using the same theodolites as the triangulation (Troughton & Simms transit theodolites before 1929 and Wild T3 theodolites from 1929). A fundamental longitude was also observed as part of a world wide programme in 1933 and this was incorporated in the network. The astro-azimuth observations began in 1927 in the North Island and continued to the end of the triangulation observations in the South Island in 1942. A variety of star catalogues including the Nautical Almanac and the American Ephemeris were used until 1941 when the FK3 became available and was used for the remaining reductions. No account was taken of possible systematic differences between these catalogues as the errors were considered to be less than the errors in the observations. The effects of polar motion were not included in the calculations for the same reason. The internal precisions (1σ) of the azimuths, derived from the repeatability of the 12 sets observed, are an average of 0.46" and a maximum of 0.71" (Lee 1978). There is no mention by Lee, of the azimuth observations being spread over more than one night so it is presumed that they are single night observations only. The internal precisions are therefore likely to be optimistic if used as a measure of external precision or accuracy. If these azimuths are to be used to estimate rotations, the original observations should be re-calculated using a consistent catalogue and ILS polar motion values. In the approximately 50 years since these observations were made the expected rotation of central New Zealand relative to the Australian plate, based on the figures of Walcott (1984) is 1.5". (See section 2.3.2). This is discussed further in section 3.4.5.

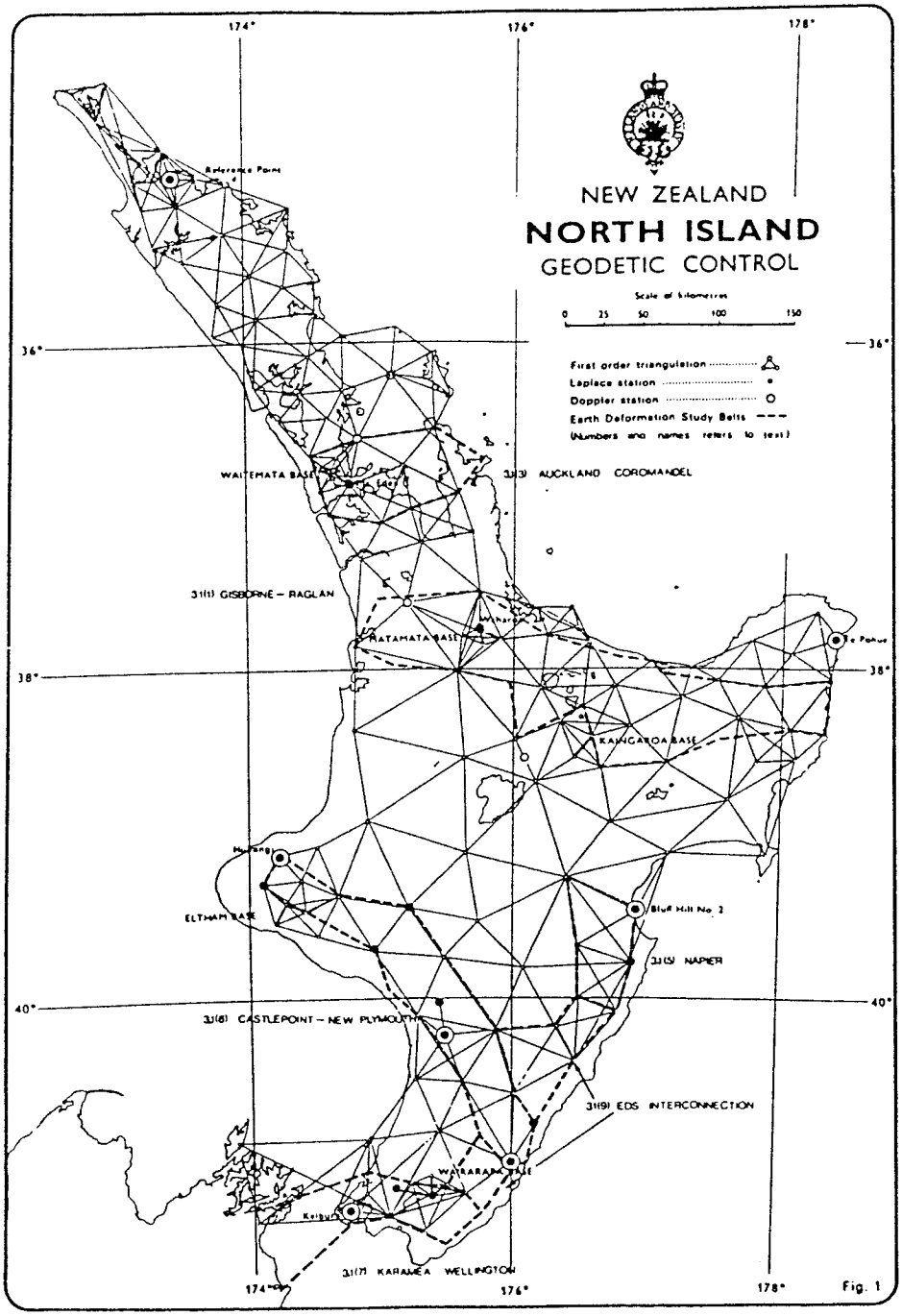

Diagram 3.2.1(a) New Zealand Geodetic Datum 1949 (North Island) after Bevin et al (1984)

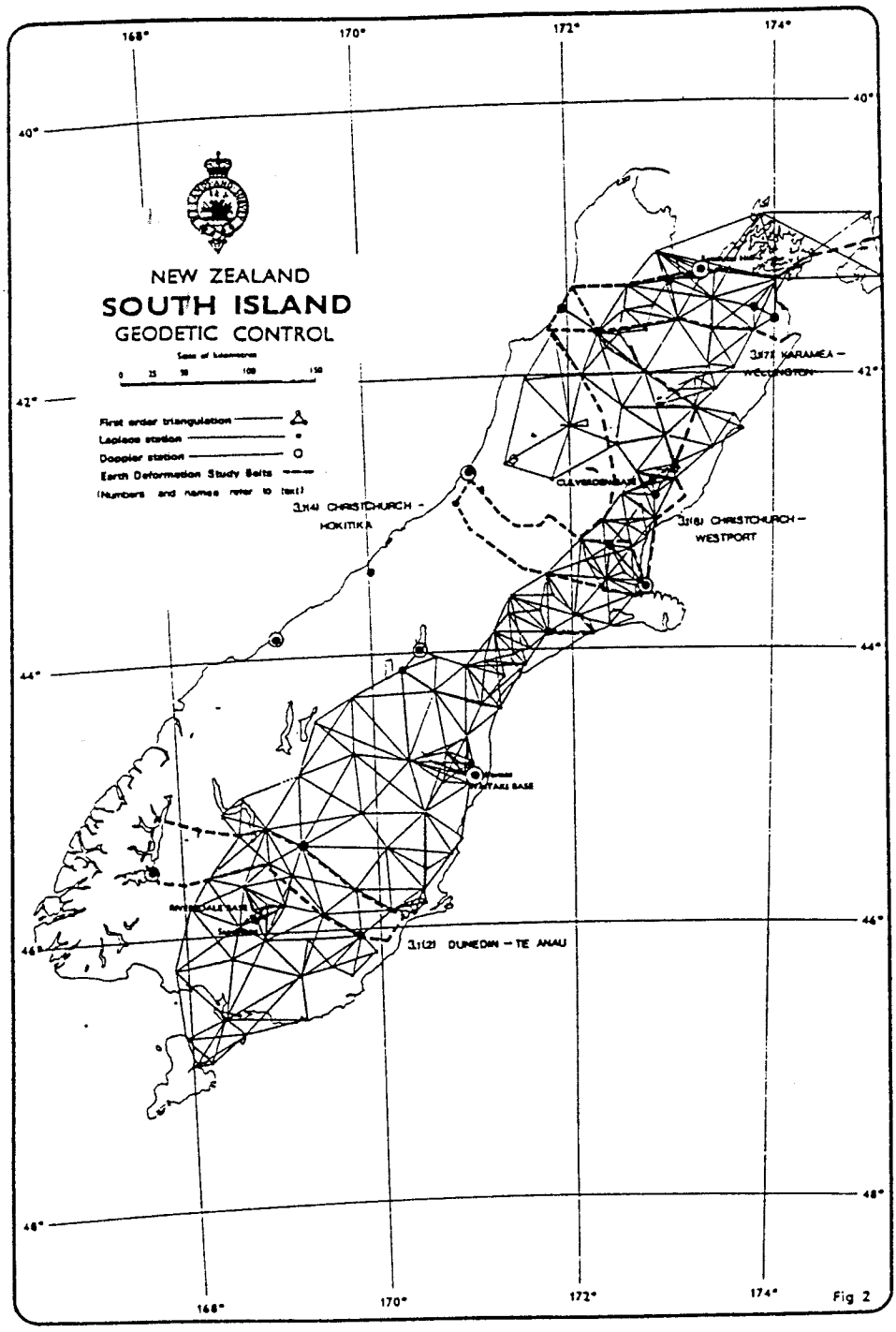

Diagram 3.2.1(b) New Zealand Geodetic Datum 1949 (South Island) after Bevin et al (1984)

The triangulation of the North Island was completed in 1938, 15 years after commencement. The observation of triangulation in the South Island was completed between 1938 and 1942. The mountainous country of the Southern Alps and the west coast of the South Island was avoided. The two main islands were linked by a braced quadrilateral with sides up to 120 km which allowed scale to be carried through between the islands.

The adjustment of NZGD-49 is of little consequence in the context of deformation analysis, as the original observations are available. It appears that orthometric heights were used in the reduction of observations as if they were ellipsoidal heights. Similarly, although astro latitude and longitude were observed at a number of stations, it appears that the horizontal and vertical angles were not corrected for deflection of the vertical (Lee, 1978; Reilly, 1980). A number of other compromises were made as the calculations were performed laboriously on calculating machines.

Since the definition of NZGD-49 there have been extensive 2nd and 3rd order triangulation schemes. These have been adjusted into the datum by holding the 1st order stations fixed. This does not account for any deformation that may have occurred between the surveys. Once again, the original observations are available and should be used in preference to the coordinates. The microwave Tellurometer, introduced to New Zealand in 1959, and the laser Geodimeters introduced in the 1960s, allowed EDM traverses to extend control into those areas of the South Island that had been left out of the primary triangulation.

3.2.3 TRANSIT

Between 1975 and 1977, 18 sites in the North and South Islands were occupied with TRANSIT Doppler receivers. The expected accuracy of these position fixes ranges from 1.5 metres in each axis to 5 metres (Rowe, 1981). The Doppler position determinations were used by Mackie (1982, 1983) to estimate the translations along the x, y and z axes between NZGD-49 and WGS-72. Because of the uncertainties in the TRANSIT data and the inconsistencies in the adjustment of NZGD-49, the orientation and scale between NZGD-49 and WGS-72 is expected to change significantly from region to region.

The TRANSIT data is not considered to have any value in estimating deformation when combined with earlier terrestrial data as it is too sparse, too

inaccurate and based on a different reference system. Similarly it is of little value for estimating deformation subsequent to 1977. The main value of these observations is in providing *a priori* station coordinates with respect to the geocentre for tracking GPS satellites.

3.2.4 EARTH DEFORMATION SURVEYS

The measurement of earth deformation in New Zealand was initially concerned with large movements across fault lines at the time of major earthquakes. In the 1929 Murchison earthquake, uplift of 4.9 m and horizontal movements of 3.5 to 4 m were observed by re-measurement of surveys. Subsequent earthquakes in Napier (1931), Wairoa (1932) and Inangahua (1968) caused movements across fault lines at the several metre level (Bevin et al, 1984). These movements were detected by surveys that had not been intended to monitor earth deformation, including the primary triangulation at Napier and Wairoa. Following the 1929 Murchison earthquake, small survey patterns were placed across active faults and at present 28 fault monitoring patterns have been established. None have shown discrete fault movement although significant shear strain has been detected (Blick, 1986).

In more recent times the emphasis in geodetic measurement of earth deformation has been extended to include larger scale surveys to detect regional strain. It has become apparent that deformation is occurring continuously over a broad zone which covers most of the country. Wellman (1955) was the first in New Zealand to report strain from geodetic observations without there being any known causative earthquake. Since then a number of authors have reported extensive aseismic strain from geodetic observations. These are summarised in section 2.3.

In 1973 the Earth Deformation Committee was set up by the Royal Society of New Zealand to coordinate activity for the investigation of earth deformation in New Zealand. A number of programs were initiated or stepped up under the auspices of this committee. A description of these and the progress after 10 years is given in the report by the Royal Society of New Zealand, Earth Deformation Committee (1985). The major geodetic projects are:

- major 1st order geodetic surveys
- regional monitoring patterns
- fault monitoring patterns
- strain monitoring patterns

- tilt monitoring patterns
- precise levelling
- astro-geodetic observations
- TRANSIT doppler observations and
- gravity measurements.

The fault monitoring patterns and strain monitoring patterns are small networks of 4 to 8 stations. The stations are separated by distances of approximately 1 km. The tilt monitoring patterns are groups of bench marks extending up to 1 km from a central point. These three types of network use precise terrestrial observations and over these distances it is unlikely that GPS can provide the accuracy necessary to replace the terrestrial techniques.

3.3. SYSTEMATIC ERRORS

The principal difficulty in using terrestrial data from one epoch and GPS data from another epoch to monitor earth deformation, is that of the different character of the systematic errors associated with each technique. Where the same observation type is used for both epochs, the effect of many of the systematic errors can be minimised by repeating observation schemes as closely as possible. The propagation of errors is then nearly the same in both epochs and there will be a tendency for the errors to cancel when deformation is estimated. The principal error sources in terrestrial observations are different from those of GPS observations and the errors will propagate through the networks in different ways. Therefore, these errors will tend not to cancel when terrestrial observations from one epoch and GPS observations from another are used. The systematic errors of terrestrial observations that may have been ignored in the past need to be studied. The most insidious errors are those that are small but which affect many of the observations. Although the effect on individual observations may be small compared to the observation variance, the net result is that the residuals are not normally distributed (the assumption on which the optimality of least squares adjustment depends) and the common assumption of zero correlations between observations is false. The cumulative effect on the adjusted parameters may be significant.

3.3.1 DEFLECTION OF THE VERTICAL

Errors in the *a priori* astronomic coordinates or deflections of the vertical may cause systematic errors. The deflections may be determined by astro-geodetic observation but such observations are usually made only at a few stations, if any, in geodetic networks. Gravimetric deflections may also be derived from observed gravity, normal gravity or a high order geopotential model. If topographic data is available in a convenient form, such as a digital terrain model, then corrections for the effect of local masses may be applied.

It is often assumed that the deflection is zero (this assumption was made in the adjustment of NZGD-49). Thomson et al (1974) give examples of the network distortion that results from neglect of the deflections of the vertical. It is reasonable to assume, in most cases, that the deflection does not change significantly from one epoch to the next. If nearly identical triangulation networks are observed in two epochs and if the deflections are modelled the same way in both epochs (for example, if they are neglected in both epochs),

the effect of the deflection error will tend to cancel. Coleman & Lambeck (1983) demonstrate the spurious deformation that may be estimated if the observations are corrected in one epoch and not in the other. Similarly, if terrestrial methods are used in one epoch and space techniques such as GPS in the next, the effect of deflection errors will not cancel.

The Laplace equation gives the difference between an observed astronomic azimuth and the reduced geodetic azimuth. The correction $\Delta\alpha_{ij}$ to an astronomic azimuth α_{ij} from station i to station j is (Vanicek & Krakiwsky, 1986)

$$\Delta\alpha_{ij} = -\eta_i \tan\phi_i - (\xi_i \sin\alpha_{ij} - \eta_i \cos\alpha_{ij}) \cot z_{ij} \qquad (3.3.1)$$

where z_{ij} is the zenith distance from i to j, ξ_i and η_i are the components of the deflection of the vertical at i and ϕ_i is the latitude of i. The first term may be neglected in reducing direction observations as it is the same for all directions from a point and is thus indistinguishable from the unknown orientation error. It is required in reducing azimuth observations. As equation 3.3.1 is used for reducing observations, it may also be used to determine the effect of errors in the *a priori* values of ξ_i and η_i used in the reduction. For horizontal lines the effect of the deflection on direction observations is zero. For a line with a zenith distance of 95° the effect has a maximum value of 0.087 d_i where

$$d_i = \sqrt{\xi_i^2 + \eta_i^2} \qquad (3.3.2)$$

is the total deflection. The maximum effect occurs on lines at right angles to the direction of total deflection d_i. This is a small error if the deflections used are correct to within a few arcsec. If gravimetric deflections are used, the deflection errors will tend to be larger in mountainous terrain than in flat terrain (Kearsley et al, 1985). The observed lines will also tend to be steeper in mountainous terrain and thus the effect on the horizontal directions of deflection errors will be greater.

The deflection errors have effects which are not isotropic (being azimuth dependent). Nor are they necessarily homogeneous (being dependent on the gradient of the line). Therefore, even though the effect of these errors may be small compared with the observation uncertainty, the signature of the error is

similar to that of strain and the effect on a deformation adjustment may be significant.

3.3.2 HEIGHT

Errors in the *a priori* ellipsoidal heights of stations can affect the reduction of EDM distances significantly. This error may be split into two components: the effect of an error in the height difference between stations and the effect of a height error common to both stations. As with errors in the deflection of the vertical, the effect of height difference errors is greatest for steep lines. For example, an error in the height difference of 1 m on a line having zenith distance of 95° will result in an error of 0.087 in the reduced distance. An error of 6 m in the elevation of both stations will cause approximately 1 ppm error in the reduced distance on the ellipsoid. The effect of a height error will be the same whether the distances are explicitly reduced to the ellipsoid before processing in a 2D adjustment or whether this occurs implicitly in a 3D adjustment where the heights are held fixed. The heights used in the reduction of distances to the ellipsoid are, of course, ellipsoidal heights. For terrestrial surveys a major source of error in these heights will be the error in the geoid height N.

The reduction to the ellipsoid of azimuths and horizontal directions also depends on height due to the skew normal correction. This is a small correction and where it is applied, it is unlikely to be affected by realistic height errors. For example; a height error of 10 m at a latitude of 40° has an effect of less than 1 milli-arcsecond. If the correction is ignored then the error will be 0.13" at 2000 metres elevation on an azimuth of 45° and latitude 40°. This is a small error but, being azimuth dependent and height dependent, the effect on the network will not be isotropic or homogeneous and could introduce slight geodetic strain.

3.3.3 ATMOSPHERIC REFRACTION AND PROPAGATION DELAY

In terrestrial techniques, as in space techniques, a major source of error is unmodelled atmospheric effects; refraction for direction observations and propagation delay for distance observations. This is a limitation on the estimation of strain from repeated terrestrial surveys as well as for terrestrial / GPS combination. One method often used to deal with atmospheric errors is to inflate the observation variances to cover the error. This implicitly assumes that the errors are normally distributed which will often not be the case. For that

part of the error that cannot be eliminated by using atmospheric models or by estimating refraction / delay coefficients, this method of assuming normally distributed errors may be the only alternative. If the observations are repeated under a wide variety of atmospheric conditions the assumption of normally distributed errors may be reasonable.

The triangle miscloses may be used to estimate the accuracy of horizontal direction observations. For the surveys of last century, instrumental errors will usually be larger than refraction errors. Since the advent of modern optical theodolites such as the Wild T3, refraction errors are of a similar magnitude to instrumental errors or observer bias. Grazing rays across sloping ground are likely candidates for horizontal refraction where the stratification is parallel to the ground and not horizontal. Hannah (1986) has investigated the observations of earth deformation surveys in New Zealand to determine whether day observations are more affected by horizontal refraction than night observations. He found the *a posteriori* variance factor of the direction observations to be the same for day and night observed directions. However the estimation of a single factor for all observations could mask systematic azimuth or station dependent differences in the horizontal directions that cause geodetic strain.

For observations of zenith distance, refraction is usually the largest error and this is the reason for the poor determination of orthometric heights in geodetic networks. The error may be reduced by the observation of simultaneous reciprocal vertical angles. Even if orthometric height was well determined from zenith distance observations, the problem of geoid height determination for combining terrestrial and GPS observations would still remain. This is briefly discussed in section 3.1 above.

The corrections for propagation delay usually applied to EDM observations in New Zealand, depend on meteorological observations at the end points of the line. These observations are strongly influenced by local and surface effects and are often not representative of the atmosphere along the line. Two colour EDM or a combination of infa-red and microwave frequencies can be used to achieve accuracies of 0.1 ppm (Slater et al, 1983) but these instruments have not been used in New Zealand. The line ratio method (or its equivalent, the estimation of a common scale factor for EDM observations taken in quick succession at a point) is also promising. EDM observations may then be used

to determine relative geometry with low systematic error (e.g. Robertson, 1972; Vincenty 1975). Slater (1979) used multi-wavelength EDM to evaluate the accuracy of line ratios calculated from single frequency EDM and found the accuracy was about 0.5 ppm. Angus-Leppan (1979) suggests a combination of the line ratio technique and atmospheric modelling as described by Brunner & Fraser (1978). Van den Berg (1979) and Denys (1987) describe the estimation of common scale factors in control surveys in New Zealand. The line ratio method, for best results, depends on the rapid observation of a number of lines from a point and it may not be appropriate to apply this method retrospectively to EDM data that has not been observed in this manner. The use of atmospheric models to improve the reduction of EDM observations (Brunner & Fraser, 1978) should be investigated further for New Zealand conditions.

3.4. CASTLE POINT - NEW PLYMOUTH EDS

3.4.1 OBSERVATIONS

The observations of the Castle Point - New Plymouth EDS are described by Hannah (1986). This network was virtually observed twice during the observation campaign: once during the day and once at night. The data set used in this study consists of the day observed horizontal directions, the day and night observed EDM slope distances, the day and night observed zenith distances and the astronomic observations of azimuth, latitude and longitude. The night observed horizontal directions were not available for this analysis. Hannah (1986) found no significant difference between the *a posteriori* variance factor for day and night direction observations but, as noted in section 3.3.3, there could still be significant geodetic strain between triangulation adjustments based on these two sets of observations. This merits further study.

The network, shown in diagram 3.4.1, consists of 25 stations in a triangulation chain running across the lower North Island from north-west to south-east. The chain is 250 km long and 35 km wide on average. The heights of the stations range from 145 m to 1155 m and the steepest line has a slope of 2° 15' . The distance between adjacent stations is typically 25 km.

There are 174 direction observations, each being the mean of at least eight sets. The observation weights used are based partly on the standard deviation of the mean of these sets and partly on the *a priori* variance scaling factor which gives an *a posteriori* variance factor $\hat{\sigma}_o^2$ of unity. The *a priori* uncertainty of a direction observation is typically 0.74". There are reciprocal zenith distance observations on 77 lines (day) and 80 lines (night). These are means of at least 3 sets and are generally not simultaneously observed. An *a priori* uncertainty of 2.0" was initially assigned to these observations but, following an examination of the residuals, this was revised to 5.0" .

There are night observed EDM slope distance observations on 81 lines, 74 of which were also measured during the day. The instrument used was the Model 8 Geodimeter and *a priori* uncertainties of 0.005 m. +1.3 ppm were used. A scale difference between the day and night observations was found with the day observations being generally longer. This scale difference ranges from –1.33 ppm to +6.42 ppm with a mean of +2.18 ppm and a standard deviation of 1.38 ppm. This standard deviation of the scale differences is

consistent with an internal precision of 0.98 ppm for the observations in each of the data sets. This day / night scale difference has also been reported by Jones (1971) and in New Zealand by Bevin & Forster (1973).

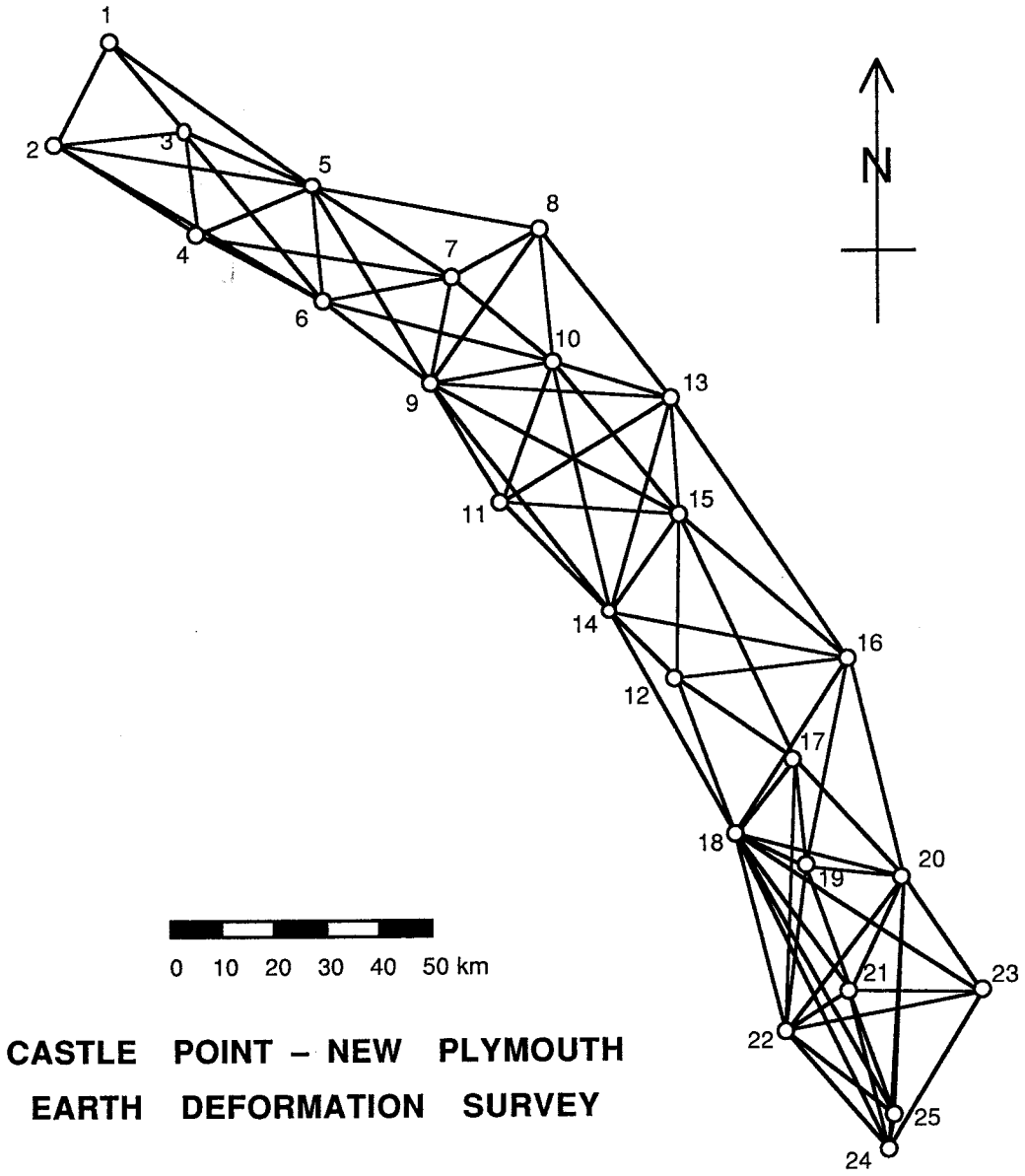

Diagram 3.4.1 Terrestrial network: Castle Point – New Plymouth Earth Deformation Survey.

There are 8 astro-azimuth observations, each being the mean of at least 16 sets over 2 or more nights. These are reciprocal observations on 4 lines and have *a priori* uncertainties of 0.5". Astro-latitudes and longitudes were observed on at least 2 nights at these 8 stations. Latitudes and longitudes were also observed at 4 other network stations and 4 non-network stations in the general area. The mean *a priori* uncertainties of the observed latitude and

longitude are 0.25" and 0.30" respectively. These figures are based on the internal precision of the repeated observations. The data supplied by the Department of Survey & Land Information (New Zealand) includes deflections of the vertical, derived by astro-geodetic interpolation, for the 13 network stations that have no observed latitude or longitude. The details of this interpolation are not known and *a priori* uncertainties of 2.0" have been assigned to these values. This is approximately twice the error that could be expected from a careful gravimetric estimation of deflections (Kearsley et al, 1985).

Sub-networks

The complete network, being 250 km long, is too large for the assumption of homogeneous strain to be valid. It has been divided into 3 sub-networks shown in diagrams 3.4.2, 3.4.3 and 3.4.4. These are the north-west, central and south-east networks and they consist of 9, 10 and 12 stations respectively. The network divisions were chosen, somewhat arbitrarily, so that there is an overlap of 3 stations between adjacent networks and each network has observed reciprocal astro-azimuths on 2 lines. This allows an investigation into the effect of multiple azimuth observations on the estimation of strain. The observations were partitioned into a set for each sub-network and were adjusted separately. No significant difference was found between the results of the 3 sub-network adjustments and an adjustment of the complete network.

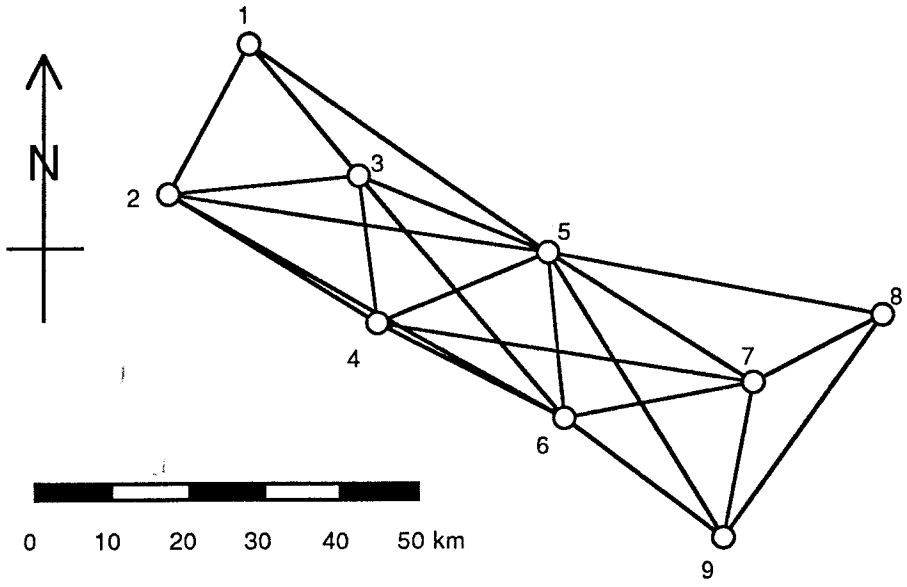

NORTH WEST NETWORK

Diagram 3.4.2 North-west sub-network being 9 stations of the Castle Point – New Plymouth EDS network

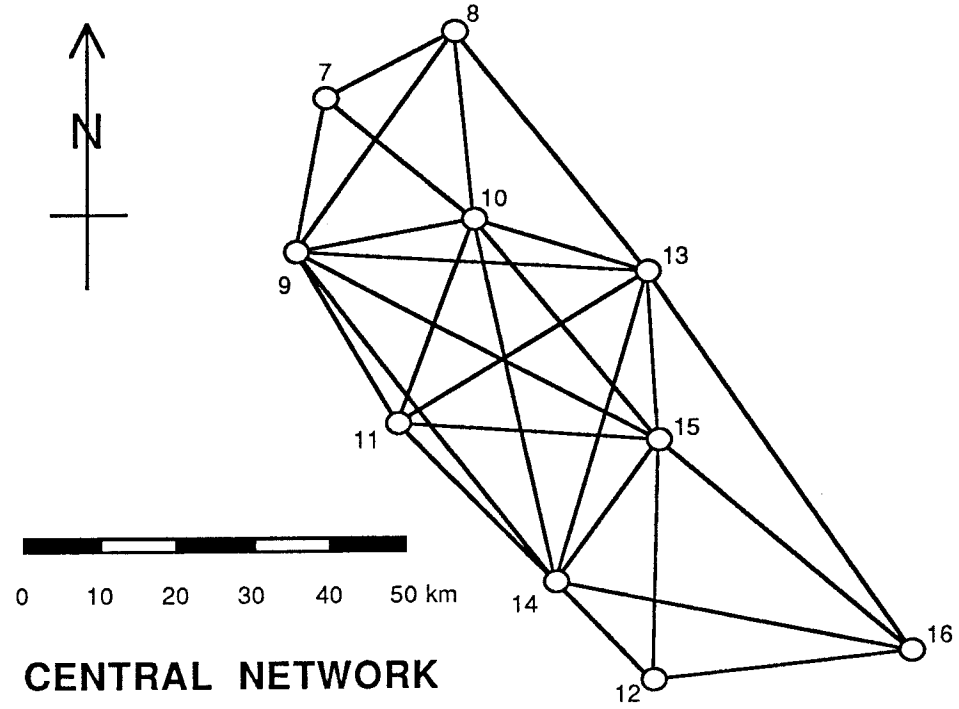

CENTRAL NETWORK

Diagram 3.4.3 Central sub-network being 10 stations of the Castle Point – New Plymouth EDS network

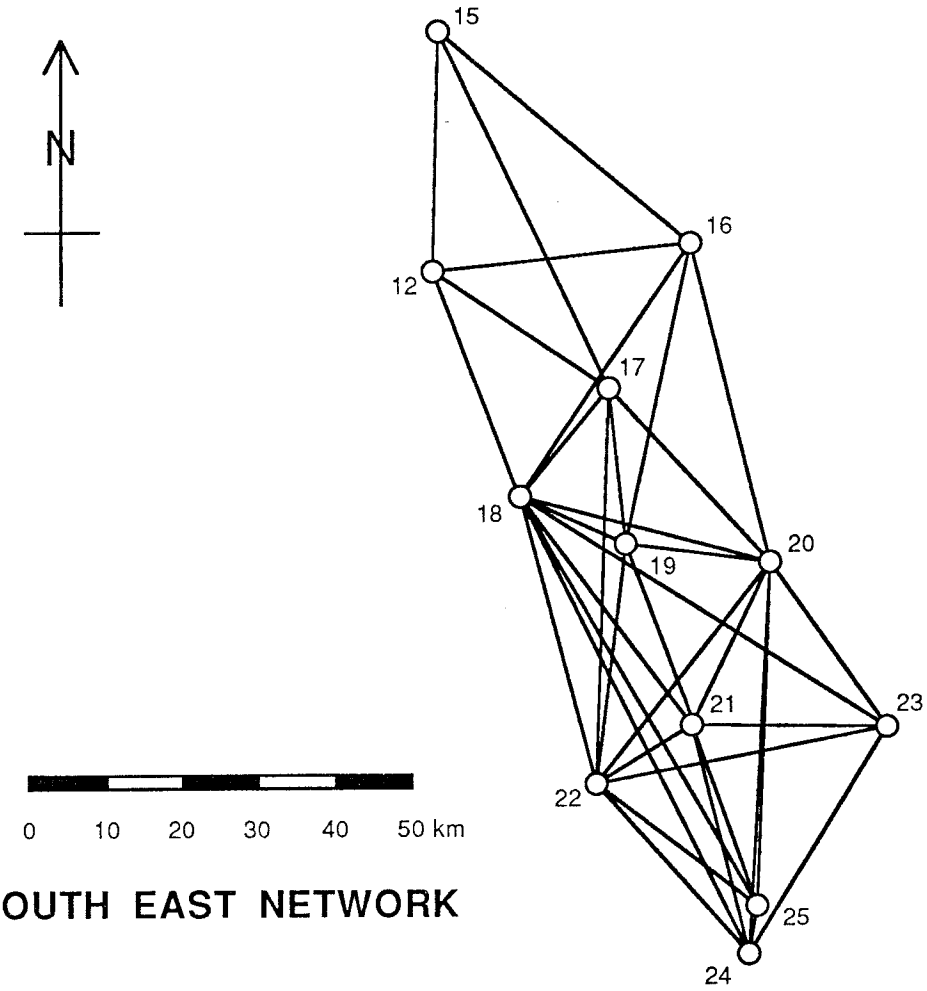

Diagram 3.4.4 South-east sub-network being 12 stations of the Castle Point – New Plymouth EDS network

3.4.2 ADJUSTMENT SOFTWARE

The integrated adjustment software OPERA 2.3 was used for the terrestrial network adjustments. The features and operation of this software are described by Hein (1982a, 1982b); Hein & Landau (1983); Eissfeller & Hein (1986) and Landau et al (1987). It allows the adjustment of a wide variety of observations including horizontal directions, slope distances, astro-latitude, longitude and azimuth, gravity, potential differences (levelling), and GPS baselines or networks. These are adjusted by least squares collocation as described by Moritz (1980a). The concept of **integrated geodesy** was developed by Krarup in 1973 and appears in Eeg & Krarup (1973). The principle of integrated geodesy is that the station coordinates and the gravity field are determined in a single adjustment that uses all observations. There is no need to apply "corrections" to the observations for geoid height, deflections

of the vertical, etc., as these are implicit in the adjustment model. The full features of this model have not been used here as gravity data, levelling observations and GPS data were not available and so it was used in the 3D adjustment mode. A refraction coefficient was estimated for each line that had reciprocal zenith distance observations. Deflections of the vertical were estimated for all stations and the coordinates of one station were held fixed.

The theory developed by Harvey (1985), was used for the estimation of strain between coordinates of different adjustments of the networks. The topocentric strain option was used which allows comparative testing of the different deformation models given in section 2.2.2.

3.4.3 CHOICE OF STRAIN MODEL

The following analysis is based on data sets that are subsets of the Castle Point - New Plymouth EDS observations. The first data set has day observed zenith distances and EDM distances The second data set has night observed zenith distances and EDM distances. The significance of the discrepancy between the day and night EDM observations is discussed in section 3.4.5. In this section the data is used purely to assess the 4 models of homogeneous topocentric strain introduced in section 2.2.2. These are the full 3D strain model ; the 11 parameter model in which the vertical extensional strain (e_{vv}) is held fixed at zero; the horizontal strain model in which the vertical shear strains (e_{ev} , e_{nv}) are also fixed at zero; and the 2D model where the vertical strains, rotations about the horizontal axes (ω_e , ω_n) and the vertical translation (t_v) are fixed at zero. The change in the estimates of strain for the different models is of interest here: not the actual strain itself. The analysis was applied to the north-western, central and south-eastern networks described in section 3.4.1. Similar results were obtained for all networks and only the results for the north-western network are presented here.

The geodetic strain between the coordinates of 3D network adjustments of these data sets was considered first. The differences in horizontal coordinates range from –0.113 to +0.107 m. The differences in height range from –1.046 to +1.845 m.

Table 3.4.1 Estimates of strain between coordinates of different **3D** network adjustments. Different EDM and ZD observations (day vs night) were used and all other observations were the same for both adjustments.

Param	Units	3D Strain	11 Parameter	Horizontal Strain	2D
e_{ee}	ppm	−2.00 ± 0.61	−2.03 ± 0.61	−2.20 ± 0.60	−2.21 ± 0.60
e_{nn}	ppm	−1.95 ± 0.81	−2.00 ± 0.80	−2.47 ± 0.77	−2.46 ± 0.77
e_{vv}	ppm	−196.7 ± 375.1			
e_{en}	ppm	−0.09 ± 0.56	−0.12 ± 0.56	−0.45 ± 0.53	−0.46 ± 0.53
e_{ev}	ppm	13.33 ± 17.24	14.61 ±17.06		
e_{nv}	ppm	29.80 ± 17.86	32.21 ±17.26		
ω_e	arcsec	4.02 ± 3.98	4.35 ± 3.93	−2.18 ± 1.77	
ω_n	arcsec	−5.90 ± 3.74	−6.06 ± 3.73	−3.08 ± 1.46	
ω_v	arcsec	0.04 ± 0.36	0.05 ± 0.36	0.06 ± 0.35	0.01 ± 0.35
s_{2D}	ppm	−1.98 ± 0.46	−2.01 ± 0.46	−2.34 ± 0.43	−2.34 ± 0.43
γ_1	ppm	−0.06 ± 1.09	−0.04 ± 1.09	0.28 ± 1.08	0.25 ± 1.08
γ_2	ppm	−0.19 ± 1.12	−0.23 ± 1.12	−0.89 ± 1.07	−0.91 ± 1.07
γ	ppm	0.20 ± 1.14	0.23 ± 1.13	0.94 ± 1.04	0.95 ± 1.04
$(e_{ev} + \omega_n)$	ppm	−15.27 ± 7.14	−14.78 ± 7.08		
$(e_{nv} - \omega_e)$	ppm	10.32 ± 8.73	11.13 ± 8.60		

The estimates of strain for the 4 strain models are summarised in table 3.4.1. Note that while the vertical extensional strain e_{vv} in the 3D strain model is large, its uncertainty is even larger. This parameter is not well determined from nearly planar geodetic networks as discussed in section 2.2.2. When e_{vv} was fixed to zero in the 11 parameter strain model the estimates of the other parameters changed only slightly. Thus, even in the presence of large height differences, the parameter e_{vv} can be held fixed without significantly affecting the estimation of the other deformation parameters. This may not be true for networks with steep lines but it is true for nearly planar terrestrial networks of which this EDS network is a typical example. Therefore, **it is recommended that e_{vv} need not be estimated** and thus that the 3D strain model not be used. To summarise, the reasons for not estimating e_{vv} are that:

(i) it is not well determined from nearly planar geodetic networks,

(ii) it is highly sensitive to systematic errors in the heights,

(iii) it therefore provides no useful information on deformation and,

(iv) no significant bias is introduced to the estimates of the other parameters when it is held fixed to zero.

In the horizontal strain model, the rotations about the horizontal axes, ω_e and ω_n, are significant but when these were fixed to zero in the 2D strain model, the remaining parameters were not altered significantly. The greatest difference between models was that between the 11 parameter strain model and the horizontal strain or 2D strain models. A decision must be made whether to estimate e_{ev} and e_{nv} and this decision affects estimates of the other parameters. The estimate of shear strain γ obtained when e_{ev} and e_{nv} were estimated is 0.6 - 0.7 ppm different from that obtained when they were fixed.

To further investigate the difference between the 11 parameter and horizontal strain models, calculations are presented from network adjustments in which the heights were effectively held fixed and the zenith distances were not used. These two adjustments differ only in the choice of day or night observed EDM distances. This was achieved by using pseudo observations of ellipsoidal height with *a priori* uncertainties of 0.001 m. and so these network adjustments may be referred to as **3D height fixed**. This model is similar to the 3D height fixed model of Vincenty & Bowring (1978) and Vincenty (1980). The horizontal coordinates obtained are the same as those of a 2D network adjustment where *a priori* heights are used to reduce the observations to the ellipsoid.

The strain between these two 3D height fixed network adjustments was then estimated. As the heights are identical in both data sets, e_{vv} is zero and results are only presented for the 11 parameter, horizontal strain and 2D models. These are summarised in table 3.4.2.

If the parameters, ω_e and ω_n, are interpreted as being the same quantities that are estimated in a 3D transformation adjustment (the rotations between reference frame axes), zero rotations will be expected as the height differences are zero. In the 11 parameter model, these rotations are large and statistically significant and their interpretation depends on the estimates of the vertical shear strains e_{ev} and e_{nv}. In this case, the values obtained for e_{ev}, e_{nv}, ω_e and ω_n in the 11 parameter model are due entirely to small systematic variations in the horizontal displacement with station height. Note that the estimates of $(e_{ev} + \omega_n)$ and $(e_{nv} - \omega_e)$ are close to zero and that the rotations ω_e and ω_n are zero in the horizontal strain model as expected. In section 2.2.2 the estimation of vertical shear strains was discussed and it was

noted that small but systematic variations in the horizontal coordinate displacements with height could result in large values for the estimates of e_{ev}, e_{nv}, ω_e and ω_n. Therefore the estimates of these 4 parameters are highly sensitive to systematic errors in the horizontal coordinates and their interpretation for earth deformation is difficult.

Table 3.4.2 Estimates of strain between coordinates of different **height fixed** network adjustments Fixed heights were the same in both network adjustments. Different EDM observations (day vs night) were used and all other observations were the same.

Param	Units	11 Parameter	Horizontal Strain	2 D
e_{ee}	ppm	−2.00 ± 0.60	−2.17 ± 0.59	−2.15 ± 0.58
e_{nn}	ppm	−2.00 ± 0.80	−2.46 ± 0.76	−2.48 ± 0.76
e_{vv}	ppm			
e_{en}	ppm	−0.15 ± 0.55	−0.48 ± 0.53	−0.48 ± 0.53
e_{ev}	ppm	18.50 ±16.96		
e_{nv}	ppm	−28.96 ±17.21		
ω_e	arcsec	5.97 ± 3.55	0.00 ± 0.00	
ω_n	arcsec	−3.82 ± 3.50	0.00 ± 0.00	
ω_v	arcsec	0.03 ± 0.36	0.02 ± 0.34	−0.01 ± 0.33
s_{2D}	ppm	2.00 ± 0.45	−2.31 ± 0.43	−2.32 ± 0.43
γ_1	ppm	−0.00 ± 1.08	0.28 ± 1.07	0.33 ± 1.05
γ_2	ppm	−0.29 ± 1.11	−0.97 ± 1.06	−0.96 ± 1.05
γ	ppm	0.29 ± 1.11	1.01 ± 1.04	1.01 ± 1.03
$(e_{ev} + \omega_n)$	ppm	0.00 ± 0.02		
$(e_{nv} - \omega_e)$	ppm	0.01 ± 0.03		

The estimation of 2D strain (in particular the estimation of γ_1 and γ_2 or γ and φ) from horizontal terrestrial data, using heights assumed to be without error, has been successfully applied in the past in New Zealand. The estimates of strain derived in this way have proved very useful in interpreting earth deformation. They have been found to be consistent with studies of earth deformation from other disciplines such as Geophysics and Geology. In using GPS for strain analysis there are obvious advantages in estimating strain parameters consistent with those that have proved useful in the past.

The simultaneous reduction model used in New Zealand to estimate 2D strain directly from the geodetic observations is equivalent to using the 2D strain

model on coordinates from an 2D (or 3D height fixed) adjustment as in the third column of table 3.4.2. Estimates of strain within 10% of this are obtained, if the horizontal strain or 2D strain models are used with 3D adjustment data sets (third and fourth columns of table 3.4.1). If e_{ev} , e_{nv} are estimated, a change is required in the interpretation of the estimates of horizontal strain.

Therefore, **it is recommended that the parameters e_{ev} and e_{nv} should not be estimated** and thus that the 11 parameter strain model not be used. The reasons for not estimating e_{ev} and e_{nv} are that:

(i) they are highly sensitive to small systematic errors in the horizontal coordinates,

(ii) the interpretation of the other parameters is difficult when they are estimated and,

(iii) when they are fixed, the estimates of the other parameters are close to those that have proved useful in the past for interpreting earth deformation.

Note that it is recommended that e_{vv} **need not** be estimated and that e_{ev} and e_{nv} **should not** be estimated.

There is no significant difference between the parameter estimates in the horizontal strain and 2D strain models even where the fixed rotation parameters are significant as in table 3.4.1. In adjustments between terrestrial and GPS networks the rotations ω_e , ω_n and the vertical translation t_v will be significant due mainly to differences in the reference frame definition. These parameters provide useful information on the reference frames even though their use in interpreting deformation is limited. **It is recommended that the parameters ω_e and ω_n should be estimated and therefore that the 9 parameter, horizontal strain model be used.**

These conclusions are based on the use of terrestrial data for the estimation of deformation parameters. The data from the first GPS deformation surveys will not only be used with terrestrial data, but also with GPS data from future surveys. The use of repeated GPS survey data to determine earth deformation is beyond the scope of this thesis, but the question of whether the conclusions above will apply in such cases is briefly addressed.

To determine e_{vv} to an accuracy of 1 ppm, height differences accurate to 2 mm between stations separated in height by 2000 m are required. For lines with a gradient of 1 in 10 (5.7° elevation angle), proportional errors of the order of 0.1 ppm or better and sub-millimetre constant errors (including the determination of the position of the antenna phase centre) are required. Even for very steep lines with gradients of 1 in 2 (elevation angle of 30°) between mountain top and valley floor it is unlikely that GPS could provide the 2 mm accuracy required in the foreseeable future.

The vertical shear strains may be interpreted as either due to a systematic variation in uplift with horizontal position or as a systematic variation in horizontal displacement with height (two quite different phenomena) or some combination of the two (see section 2.2.2). This difficulty in the interpretation of the vertical shear strains is due mainly to the limitation in the geometry of geodetic networks. Therefore, unless small very high precision networks with steep lines (say >30° elevation angle) are observed with GPS, it appears that the conclusions above, that e_{ev} , e_{nv} and e_{vv} not be estimated, will also apply to repeated GPS surveys in the future.

3.4.4 3D NETWORK ADJUSTMENT MODELS

The horizontal strain model has been chosen for the combination of terrestrial and GPS data and now a set of 3D coordinates and variance - covariance (VCV) matrix for the terrestrial data must be generated. There are a number of ways of doing this.

A A 3D adjustment of the terrestrial data including observed zenith distances. A data set of this type has been generated using the day observed EDM distances and zenith distances together with the horizontal directions and astronomic observations.

B If observed zenith distances are not available (e.g. for early surveys in New Zealand), pseudo-observations of ellipsoidal heights with realistic variances could be used in a 3D adjustment. This is equivalent to Bayesian estimation with *a priori* variances on the height parameters. A data set of this type has been generated using pseudo observations of ellipsoidal height with *a priori* uncertainties of 0.5 metres and no zenith distance observations.

C If only 2D network adjustment software is available, the following procedure could be adopted.

(i) use the *a priori* heights to reduce the observations to the ellipsoid.

(ii) adjust the observations on the ellipsoid in a 2D adjustment.

(iii) create a 3D set of coordinates using the *a priori* heights.

(iv) create a 3D VCV matrix with realistic variances on the heights.

A data set that is the equivalent of this has been generated by performing a 3D adjustment with observed heights as in **B** except that *a priori* uncertainties of 0.001 metres were assigned to the heights to effectively give a 2D adjustment. The variances of the heights were then changed *a posteriori* to $(0.500 \text{ metres})^2$.

D Adopt the same procedure as in **C** except that in step (iii), the heights used to create the 3D coordinate set are different from those used to reduce the observations to the ellipsoid. This is clearly undesirable but there are a number of reasons why such a change in the heights may occur. Orthometric heights may be used to reduce the observations and ellipsoidal heights may be used in the final coordinate data set. If the network adjustment is not well documented and if the strain is estimated some time later by different people or organisations, there may be confusion as to which heights were used in the data reduction. A data set that is the equivalent of this has been generated by performing a 3D height fixed adjustment as in **C,** changing the height variances to $(0.500 \text{ metres})^2$ and changing the heights to equal those of the 3D adjustment in **A**.

In data sets **A** and **B** the coordinates and VCV used in the strain adjustment have not been changed from those generated in the network adjustment. In the others a change has been made to the VCV (sets **C** and **D**), and heights (set **D**). The differences between the 3D adjusted heights used in **A** and **D** and the pseudo observed *a priori* heights of **B** and **C** range from –0.467 to +1.819 m. The *a priori* heights were generated from orthometric heights obtained from trigonometric levelling and geoid heights calculated using the OSU81 180x180 geopotential model (Rapp, 1981). The adjusted heights in the 3D model **A** depend on the day observed zenith distance observations (reciprocal but generally not simultaneous) and the estimates of the deflection of the vertical. Thus the large differences in height above are expected.

The VCV matrix of a simulated GPS observation campaign of the north-western network was generated using the simulation software described in Appendix F. It was assumed, for simplicity, that all 9 stations were occupied for a 2 hour observing session and that tropospheric zenith delay parameters were estimated in the adjustment (see section 7.5). It was also assumed that the ambiguities were all resolved to their correct integer values and fixed in the adjustment. It is well known that the VCV of the adjusted parameters from a GPS adjustment is often very optimistic. In the simulated adjustment, the precision of baselines between adjacent stations is of the order of 0.002 m, 0.003 m, and 0.013 m in east, north and height components respectively. The high precision indicated by these values would not be matched in practice by high accuracy because of the presence of significant systematic errors, e.g., orbital errors. In Chapter 7, results of studies into the effect of systematic errors in GPS adjustment are presented. Here, a VCV matrix similar to the one that would be obtained from an adjustment of real GPS data is all that is required.

The coordinates used in conjunction with this simulated GPS VCV matrix were those of the full 3D adjustment in data set **A**. The deformation between the GPS data set and the reference data set **A** was in this way arbitrarily set to zero. The 9 parameter horizontal strain model was used to estimate the deformation between the GPS data and data sets **B**, **C** and **D**. Any differences between these estimates of strain and zero (the strain obtained using the reference data set **A**) are due solely to the method used to generate heights and height variances, and are therefore geodetic strain.

The results of the strain analysis from these data sets is summarised in table 3.4.3. Only the estimates of rotation about the vertical axis, the dilatation and the total shear strain are shown. The results shown are only for the north-western network.

Table 3.4.3 Geodetic strain estimates from different methods of height determination in combined adjustment of horizontal direction and EDM distances.

Data Sets	Rotation ω_v	Dilatation s_{2D}	Total Shear γ
GPS / A	0 ± 0.24	0 ± 0.31	0 ± 0.77
GPS / B	−0.02 ± 0.24	0.00 ± 0.31	0.02 ± 0.77
GPS / C	−0.03 ± 0.24	0.15 ± 0.32	0.37 ± 0.76
GPS / D	−0.04 ± 0.24	0.45 ± 0.32	0.79 ± 0.75

Key to Data Sets

A 3D adjustment using zenith distances. Reference data set.

B 3D adjustment using pseudo observed heights. σ_{height} = 0.5 m.

C 3D height fixed adjustment using pseudo observed heights. σ_{height} = 0.001 m.. σ_{height} changed *a posteriori* to 0.5 m.

D 3D height fixed adjustment as in **C**. Heights changed *a posteriori* to those of **A**. σ_{height} changed *a posteriori* to 0.5 m.

GPS Simulated GPS VCV and coordinates of data set **A**.

The parameter estimates for data sets **GPS / B** are insignificant. Thus, for this network at least, the different methods of determining heights in **A** and **B** (zenith distances and pseudo observed ellipsoidal heights) have little effect on the horizontal strain parameters. If the height differences between **A** and **B** were substantially larger than the 1 to 2 metre differences here, or if the network had steeper lines (maximum elevation angle here of 2° 15') , this conclusion might not be applicable. In data set **C**, the effective fixing of the heights causes geodetic strain at the 0.5σ level. If the terrestrial heights are changed after the network adjustment, as in data set **D**, geodetic strain above the 1σ level is introduced. As expected, the rotation about the vertical axis is not affected significantly by the method of height determination.

Therefore, the conclusion drawn from these results is that the adjustment of a terrestrial geodetic network incorporating horizontal directions and EDM distances, should be a 3D adjustment. If zenith distance or levelling observations are not available in the same epoch as the horizontal data, pseudo observed ellipsoidal heights can be used. One possible source of these heights, if no others are available, is the GPS network itself, although it

should be noted that the estimated rotations about the horizontal axes then have no significance. It is not advisable to assign heights to the terrestrial stations other than those used in the 2D or 3D height fixed adjustment. The decision on how the heights are to be determined and what variances they should have, should be made **before** a 3D network adjustment and not **after** a 2D network adjustment.

EDM slope distances are dependent on station height but horizontal directions have only have a small dependence through the skew normal correction. Therefore, the above analysis was repeated for triangulation and trilateration adjustments to see if there was any difference in the dependence of the geodetic strain on the method of height determination. Data sets **A** to **D** were generated for triangulation adjustments using the same horizontal directions, zenith distances, ellipsoidal heights and astronomic observations as were used above for the combined terrestrial adjustments. One arbitrarily chosen distance was included to define the scale. The dilatation is thus arbitrary and has not been shown in the results.

Table 3.4.4 Geodetic strain estimates from different methods of height determination in triangulation adjustment of horizontal directions.

Data Sets	Rotation ω_v	Total Shear γ
GPS / A	0 ± 0.29	0 ± 1.81
GPS / B	−0.02 ± 0.29	0.11 ± 1.67
GPS / C	−0.02 ± 0.29	0.11 ± 1.67
GPS / D	0.00 ± 0.29	0.01 ± 1.85

Key to Data Sets

A 3D adjustment using zenith distances. Reference data set.

B 3D adjustment using pseudo observed heights. σ_{height} = 0.5 m.

C 3D height fixed adjustment using pseudo observed heights. σ_{height} = 0.001 m.. σ_{height} changed *a posteriori* to 0.5 m.

D 3D height fixed adjustment as in **C**. Heights changed *a posteriori* to those of **A**. σ_{height} changed *a posteriori* to 0.5 m.

GPS Simulated GPS VCV and coordinates of data set **A.**

The coordinates of the 3D adjustment using zenith distances (data set **A**) were again defined as a reference and used together with the simulated GPS VCV to provide the GPS data set. The differences between the 3D adjusted heights used in **A** and **D** and the pseudo observed heights of **B** and **C** range from −1.222 to +0.980 m. The estimates of rotation and total shear from the deformation adjustments are given in table 3.4.4. The geodetic strain is insignificant for all data sets. The deformation adjustment is generally insensitive to the method of height determination and this reflects the fact that the horizontal direction observations are relatively insensitive to the station heights.

Data sets **A** to **D** were next generated for trilateration adjustments using the same EDM distances, zenith distances, ellipsoidal heights and astronomic observations as were used above for the combined terrestrial adjustments. The coordinates of the GPS data set were obtained from data set **A** as above. The differences between the 3D adjusted heights used in **A** and **D** and the pseudo observed heights of **B** and **C** range from −1.166 to +0.989 m. The estimates of rotation, dilatation and total shear from the deformation adjustments are given in table 3.4.5. The results are similar to those of the combined adjustment presented in table 3.4.3. The different heights in data set **B** do not introduce significant strain but geodetic strain is introduced if either of the other data sets are used.

In conclusion, a distinction is made between those terrestrial adjustments that use distance observations and those that don't. If EDM distances are used, a 3D terrestrial network adjustment is required for the best results. The heights of this adjustment should be used, without alteration, in the deformation adjustment. In the network studied here, the estimates of strain are quite insensitive to metre level variations in the heights used provided that realistic variances are used for either the zenith distances or the pseudo observed heights. For smaller networks with steeper lines, the results would probably be more sensitive to height errors. Brunner & Coleman (1988) note significant effects of height errors in a trilateration network of short steep lines used to monitor deformation in California.

Table 3.4.5 Geodetic strain estimates from different methods of height determination in trilateration adjustment of EDM distances.

Data Sets	Rotation ω_v	Dilatation s_{2D}	Total Shear γ
GPS / A	0 ± 0.25	0 ± 0.32	0 ± 0.86
GPS / B	−0.01 ± 0.25	−0.00 ± 0.32	0.02 ± 0.82
GPS / C	−0.03 ± 0.25	0.14 ± 0.33	0.37 ± 0.84
GPS / D	−0.04 ± 0.25	0.45 ± 0.33	0.92 ± 0.84

Key to Data Sets

A 3D adjustment using zenith distances. Reference data set.

B 3D adjustment using pseudo observed heights. σ_{height} = 0.5 m.

C 3D height fixed adjustment using pseudo observed heights. σ_{height} = 0.001 m.. σ_{height} changed *a posteriori* to 0.5 m.

D 3D height fixed adjustment as in **C**. Heights changed *a posteriori* to those of **A**. σ_{height} changed *a posteriori* to 0.5 m.

GPS Simulated GPS VCV and coordinates of data set **A**.

For triangulation networks, the method of height determination is less important. This is fortunate as many early triangulation surveys have little or no height information. It appears that a 2D adjustment of the network may be used and a 3D data set constructed using ellipsoidal heights and realistic variances as in data sets **C** or **D**.

3.4.5 GEODETIC STRAIN IN TERRESTRIAL NETWORKS

In the manner of the previous sections, strain was estimated between different subsets of the observations so that some idea of the magnitude of geodetic strain could be obtained. For each of the 3 sub-networks of the Castle Point - New Plymouth EDS network, 3 adjustments were carried out. These were:

1 A triangulation adjustment using horizontal directions, pseudo observations of ellipsoidal height, astro-latitude, longitude and azimuth and one arbitrary distance to define the scale.

2 A trilateration adjustment using day observed EDM slope distances, ellipsoidal heights and astro-azimuth.

3 As for **2** except using night observed EDM slope distances.

The three adjustments are essentially independent except for the common astro-azimuth observations and ellipsoidal heights. The total shear strain γ and the direction of the principal axis of compression φ between the triangulation adjustment and the two trilateration adjustments are illustrated in diagram 3.4.5. The total shear strain ranges from 1.4σ to 1.9σ and is quite systematic being similar for all 3 sub-networks. Horizontal directions and EDM distances have different systematic errors which propagate differently through triangulation and trilateration networks so these significant strain values are not unexpected. Similar problems are expected in estimating strain from terrestrial and GPS data.

These results demonstrate that caution is required when determining the significance of strain estimates based on data sets with different types of observation in each epoch. The observation weights in the network adjustments were chosen to give estimated variance factors $\hat{\sigma}_o^2$ close to 1.0 for the combined data sets. The variance factors in the strain adjustments were mostly less than 1.0 with the largest being 1.13. Thus there is nothing in the least squares adjustments to indicate that the *a priori* observation uncertainties are too small. Only a small data set has been analysed here, but these results suggest that an additional *ad hoc* variance factor of about 4 could be used prior to significance tests for strain. The standard deviations of the estimated parameters would then be increased by a factor of 2.

Most of the work in earth deformation analysis in New Zealand until now has been based purely on triangulation data but EDS and other control surveys over the last 20 years have also used EDM and in the future GPS will be used. The estimates of strain from different regions or different epochs may be based on different types of observations. Any attempted comparison of these values will be difficult if the uncertainties are too optimistic. A number of combined terrestrial / GPS surveys will be required to determine an *ad hoc* variance factor similar to that determined above for triangulation vs trilateration.

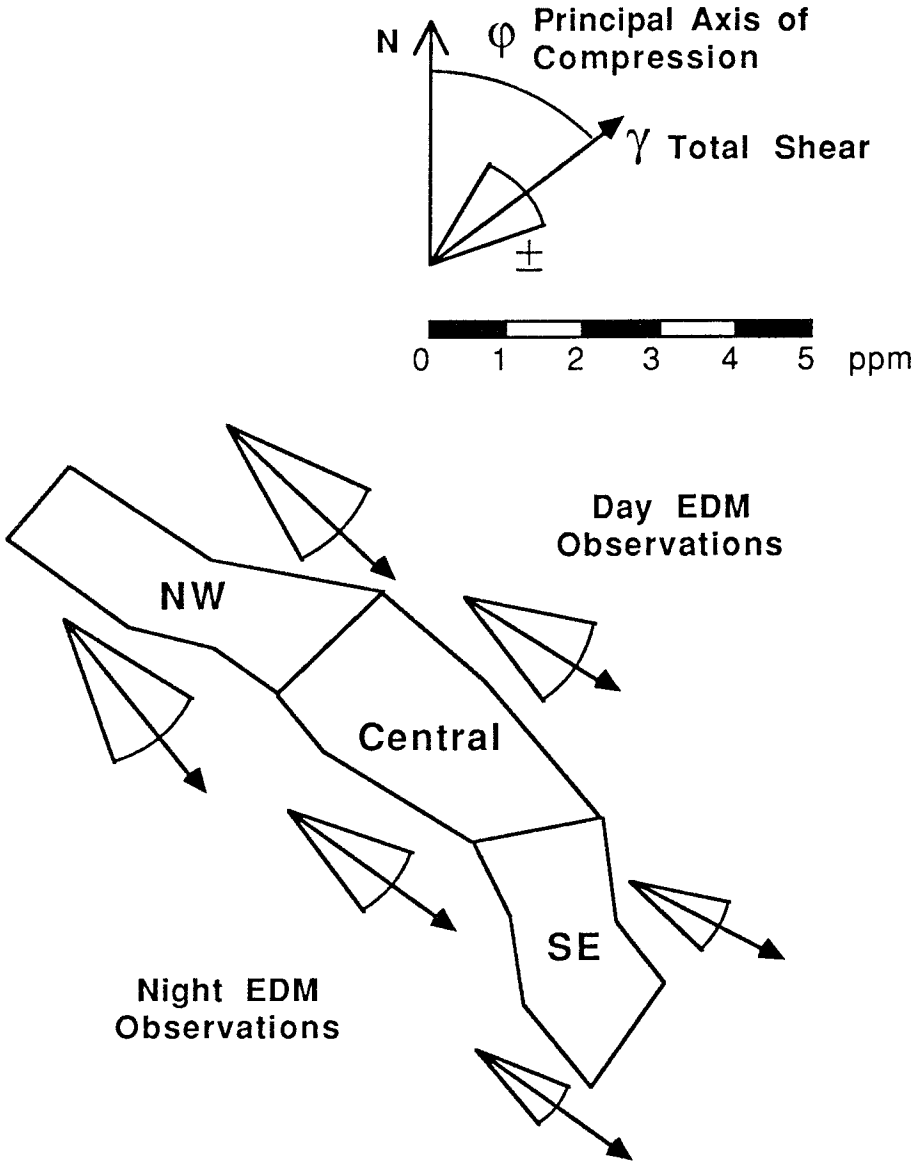

Diagram 3.4.5 Strain between triangulation and trilateration. Calculated from adjustments of the NW , Central and SE Networks. Day and Night EDM observations used in trilateration adjustments.

EDM and Dilatation

The results of the deformation adjustment between the trilateration adjustments, shown in diagram 3.4.6, demonstrate the effect of the mean scale change between night and day EDM observations of more than 2 ppm, noted in section 3.4.1. Jones (1971) reported night / day scale differences of about 4 ppm from 200 lines measured in Canada and attributes these to ground proximity effects on the meteorological observations. Bevin & Forster (1973)

reported similar results in New Zealand and noted that the scale difference does not appear to be significant on lines which have very low ground clearance for most of their length. The mean of night and day observations may be used as a more accurate definition of scale where both have been observed on most of the lines in a network but in many cases only day or only night observations are available. In some cases a network may have a combination of day and night EDM observations and significant distortion could be introduced if these were adjusted together without making allowance for a scale difference between them. Day and night scale factors could be determined but it unlikely that this simple categorisation of "night" and "day" is sufficient to fully describe the scale difference. If it is due to ground proximity effects as suggested by Jones (1971) then presumably, the effect varies with different weather conditions (overcast or clear, calm or windy); different locations (exposed mountaintops or sheltered valleys) and, as noted by Bevin & Forster (1973), different lines depending on ground clearance.

The precision of the dilatation estimate is based on the assumption that the errors in the EDM observations are normally distributed. This is not true if only night or day EDM observations are available and the precision of the dilatation will be optimistic. As well as the random errors in EDM measurements of the order of 1 - 2 ppm, these is a systematic uncertainty in the mean definition of scale of about the same magnitude. Walcott (1984) gives the rate of dilatation in New Zealand as approximately 0.1 ppm/yr or less (see section 2.3.2). Thus it will take about 20 years for geophysical dilatation to approach the level of systematic errors in the EDM data and considerably longer before it can be detected with confidence. In areas of low dilatation it may be a century or more before dilatation can be detected using this EDM data. If dilatation is to be estimated using EDM and GPS data, improved atmospheric modelling such as that of Brunner & Fraser (1978) will be required.

From the estimate of shear strain γ between trilateration adjustments, shown in diagram 3.4.6, it can be seen that the night / day scale difference is not uniform. The shear strain is close to the 1σ level and this is presumably due to variations in the scale difference for reason such as those noted above. However the direction of the principal axis of compression φ appears to be more random than that estimated between triangulation and trilateration.

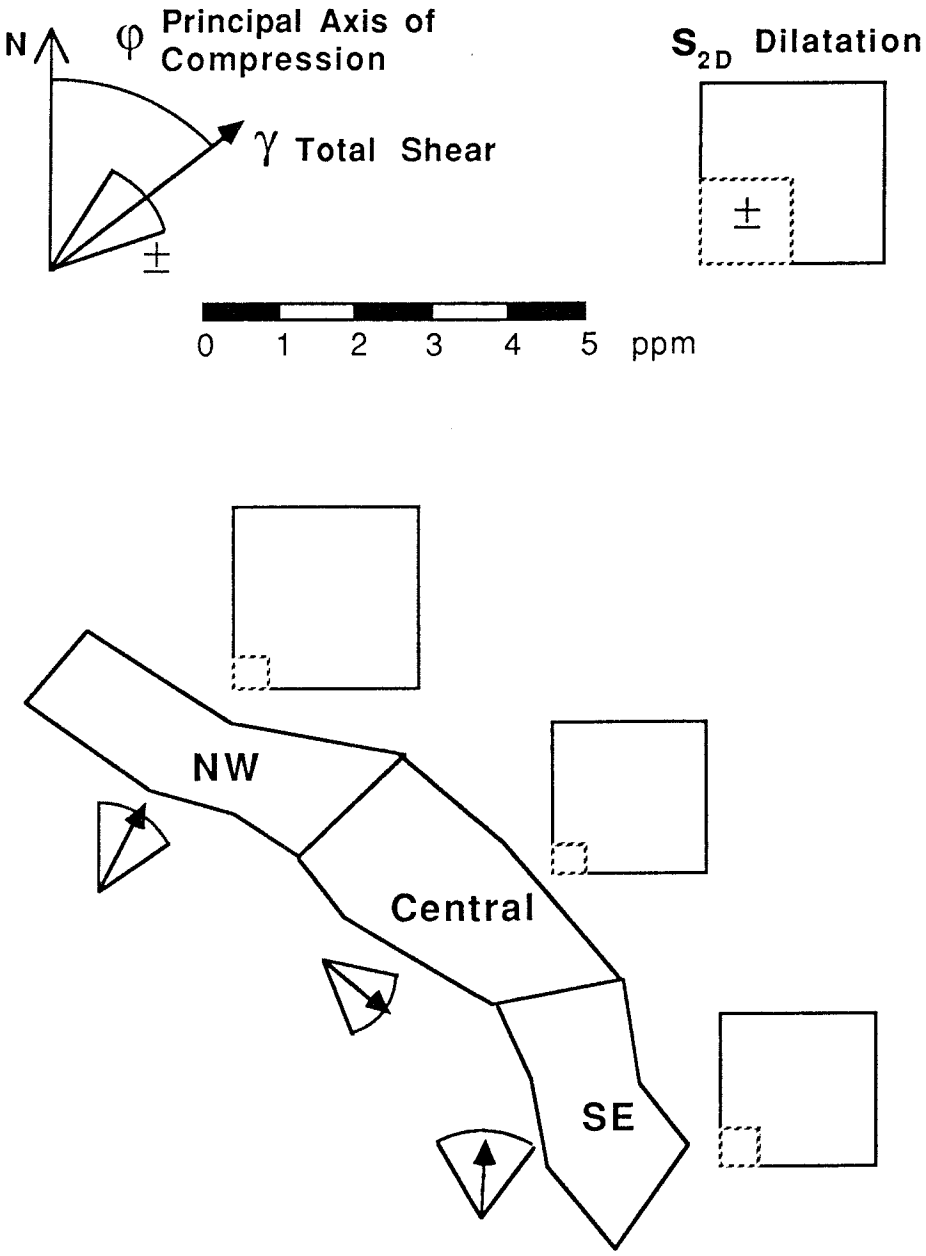

Diagram 3.4.6 Strain between trilateration adjustments (day vs night EDM observations)

Astronomical Azimuth and Rotation

Torge (1980) recommends that astronomic azimuth observations be at least 200 km apart to avoid distortion of the network due to systematic errors in the azimuth observations. Harvey (1985) using this recommendation, suggests that networks extending up to 400 km should have only one observed azimuth so that systematic errors will only cause a rotation of the network. The distortion that could be introduced by the use of several azimuth observations

would be due to an error in the observed **relative orientation** of azimuth lines. An error in the **mean orientation** would only introduce a rotation of the whole network about the vertical axis. However, if the azimuth observation weights are chosen appropriately, the azimuth observations should be no more likely to introduce distortion than direction observations which are also observations of relative orientation and which can also be affected by systematic errors. Any observation that can be used to **detect geophysical strain** has the potential to **cause geodetic strain** and should not be rejected *a priori* on the grounds of this potential alone. If the azimuth observations are known to be of poor quality then the decision may be made to reject them as with any observation. Alternatively, they may be given such high *a priori* variances that they cannot distort the network adjustment. Otherwise they should be used and be subjected to the same outlier detection tests used for the direction observations. If they introduce significant distortion to the adjustment this can be detected at the network adjustment stage.

The principal difference between errors in azimuth observations and errors in direction observations is that an error in the longitude deflection of the vertical has a much greater effect on the reduced geodetic azimuths than on the directions for which the major effect is absorbed by the orientation parameter. From equation 3.3.1, it is seen that an error of 1" in astro-longitude results in an error of 0.84" in azimuth at latitude ±40°. The *a priori* uncertainty assigned to the azimuth observation should account for the uncertainty in the longitude deflection.

There are 4 observed astro-azimuths (reciprocal azimuths on 2 lines) in each of the networks analysed here which extend for approximately 100 km. To check that these multiple azimuth observations do not cause geodetic strain, adjustments using directions, distances, latitudes, longitudes and 4 azimuth observations were compared with adjustments using the same directions, distances latitudes and longitudes, but having only 1 azimuth observation as recommended by Torge (1980) and Harvey (1985). In the resulting deformation adjustments the only significant parameter was the rotation ω_v as expected. The maximum estimate of ω_v was 0.90 ± 0.55 arcsec and the maximum estimate of shear strain γ was 0.06 ± 1.05 ppm. The variation between the azimuth observations is therefore significant (as shown by the significant rotation) but (in this case) does not result in significant shear strain.

If rotation is estimated from astro-azimuth observations and GPS determined azimuth, the result will be biased by the error in the longitude deflection of the vertical. If rotation were determined from repeated astro-azimuths, the rotation would be biased only by the **change** in this deflection between epochs which can be assumed to be relatively small. Can astro-azimuth observations and GPS can be used to estimate the rotation of parts of New Zealand relative to each other? The procedure would be:

(i) Use GPS to determine azimuths on lines that have had astro-azimuth observations.

(ii) Determine the rotations between the GPS and astro-azimuth observations at each point.

(iii) Compare the rotations from different regions to see if any differential rotation can be detected.

The assumption is made that the astro-azimuth observations are in terms of a consistent reference system and that any differential rotations are then due only to observation errors and local or regional tectonic rotation. The azimuth observations of NZGD-49 would need to be re-calculated using polar motion and a single stellar catalogue before this assumption could be considered to be reasonable (see section 3.2.2).

The **internal precisions** of the NZGD-49 astro-azimuths are an average of 0.46" and a maximum of 0.71" (Lee, 1978). The upper value is taken as an optimistic estimate of the **external precision** or accuracy. The astro-longitudes at the Laplace stations have internal precision of 0.30" to 0.45" (Lee, 1978) and again, the upper value is taken as an optimistic estimate of accuracy. If the GPS azimuths are accurate to 1 ppm (0.2") then the GPS / terrestrial rotations will have uncertainty of 0.86" and the differential rotation between two azimuth lines will thus have an uncertainty of 1.2". The expected rotation of central New Zealand relative to other regions since the observations for NZGD-49, is 1.5" (0.03"/yr for 50 years; see section 2.3.2). Therefore, even with the optimistic accuracies chosen and the assumption that there is no uncertainty or change in the reference systems, the rotations will only just be significant at the 1σ level. There are only 12 Laplace azimuths in the observations for NZGD-49 and thus the relative rotation of different regions will be determined from only one or two pairs of Laplace azimuths. With such low redundancy it will be difficult to distinguish between systematic errors and rotation with a tectonic cause. The other 28 astro-azimuths observed for NZGD-49 have no observed astro-longitude and if gravimetric deflections of

the vertical are used, errors greater than the optimistic value of 0.45" used above can be expected (Kearsley et al 1985). The azimuth observations of the EDS surveys, beginning in 1980 are more accurate (0.5" as an estimate of the accuracy of an astro-azimuth) but the maximum tectonic rotation between different regions in New Zealand in the 5 to 8 years since they were observed is only expected to be 0.15" to 0.25". Therefore, it is concluded that terrestrial and GPS observations cannot be used in New Zealand in the near future to determine tectonic rotations with confidence.

3.4.6 VARIANCE COMPONENT ESTIMATION

The theory of variance component estimation (VCE) is described, for example, by Welsch (1981) and Caspary (1987) and is applied to combined terrestrial / GPS networks by Welsch & Oswald (1985); Welsch (1986b). VCE may be used when networks are observed by terrestrial methods and GPS, and allows the determination of the relative uncertainties of the different types of observation. The terrestrial and GPS observations should be simultaneous or near simultaneous to ensure no appreciable earth deformation.

The relative *a priori* uncertainties of directions and distances in the Castle Point - New Plymouth EDS were determined by Hannah (1986) using a method which is an approximation of VCE. The directions were used in a triangulation adjustment and the *a priori* weights scaled to give an *a posteriori* variance $\hat{\sigma}_o^2$ of unity. The distances were then added to the adjustment and their weights scaled to give $\hat{\sigma}_o^2$ of unity again. The result of this analysis is *a priori* uncertainties of 0.005 m + 1.3 ppm for the distances and around 0.74 arcsec or 3.6 ppm for directions. This analysis is not the same as VCE but is based on a similar principle. It is likely that the result would be different if the distances had been adjusted first in a trilateration adjustment with the directions then added in. In the method used, any inconsistency between the directions and distances is accommodated entirely by an increase in the *a priori* distance uncertainties. In VCE it would be accommodated by a change in the uncertainties of **both** distances and directions. Thus the estimated uncertainties of the distances are probably larger from the above method than if VCE had been used.

In view of the significant shear strains between the 2 trilateration adjustments, it would seem that the *a priori* uncertainties of the distance observations are too optimistic. If VCE had been used they would probably have been even

more optimistic for the reasons noted above. This highlights the limitations of VCE, or similar methods, when used in isolation. They are based on the assumption that all significant errors are randomly represented in the data set and it is often assumed that a single variance scale factor is sufficient to account for the errors in one observation type. Observations may form a self consistent set, as the day or night EDM observations do when taken separately, and still be affected by undetected systematic errors, such as the day / night scale factor. VCE, if applied automatically without caution, will then give undue weight to these observations.

Combined terrestrial / GPS surveys will not be observed at all points of interest for earth deformation. The technique that is more likely can be thought of as a calibration of GPS in terms of terrestrial observations. This calibration will be functional (estimation of translation, scale difference and rotation) and stochastic (estimation of variance components). These calibrations will then be used for other surveys where GPS and terrestrial observations are from different epochs and where earth deformation is to be estimated. Strictly, this will only be applicable where the nets used in the calibration process are almost identical to those where the calibrations are applied. This will not be possible in practice. The early triangulation surveys were slow and thus conducted under a wide variety of conditions and seasons. One of the principal advantages claimed for GPS is speed and networks may be completed in a few days under a limited range of conditions and with a limited sample of errors.

It is recommended that methods such as VCE be accompanied by attempts to evaluate the effect of systematic errors. The estimation of strain from subsets of combined observation schemes, as used in section 3.4.5 for directions and distances, provides valuable information on the relative accuracy of different observations and on systematic errors that may have gone undetected otherwise. A high level of redundancy is required for such analysis. The techniques of covariance analysis, developed in Chapter 5 and applied in Chapter 7, will also assist by:

(i) warning of possible under-estimation of errors by VCE and
(ii) determining the relative accuracy of the nets used in the calibration process and those where the calibration is applied.

4. GEODESY WITH GPS

4.1. THE GLOBAL POSITIONING SYSTEM

The characteristics of the Global Positioning System may be found in a large number of publications. For background material the reader is referred to Remondi (1984), King et al (1987) and Eckels (1987). Only a brief review of the characteristics of the system is given here but the GPS observation and adjustment models are described in some detail. These will be used to study the effects of systematic errors on estimated coordinates and deformation parameters. This will help in distinguishing between geophysical strain and geodetic strain. The validity of this analysis depends on both the method of adjustment and assumptions made about the magnitude and behaviour of the systematic errors. The systematic errors are studied in Chapter 6.

4.1.1 SATELLITE CONSTELLATION

The systematic error analysis for GPS, is based on the proposed 18 satellite constellation. The geometry of the constellation is illustrated in diagram 4.1.1. The simulated satellites are in 6 orbital planes inclined at 55° to the equator and separated in right ascension by 60°. In each plane there are 3 satellites separated by 120° in argument of latitude (true anomaly plus argument of perigee). Going from one orbital plane to the next (increasing right ascension) the argument of latitude of the 3 satellites increases by 40°. The radius of the nearly circular orbits is approximately 26,500 km (altitude above the earth of approximately 20,200 km). The satellites complete 2 orbits per sidereal day (23 hours 56 minutes) during which time the earth completes one rotation about its spin axis. Thus, relative to the earth, the satellites return to the same point in the sky after one sidereal day. Due to the symmetry of the 18 satellite constellation, the satellite geometry relative to the earth is duplicated twice a day but with different satellites. Satellites 12, 10, 11, 15, 13, 14, 18, 16, 17 (on diagram 4.1.1) have the same ground tracks as satellites 1, 2, 3, 4, 5, 6, 7, 8, 9 respectively with a time offset of 11 hours 58 minutes. (Note that the satellite numbers used here for the Block II constellation are not necessarily those that will be valid when the satellites become operational.)

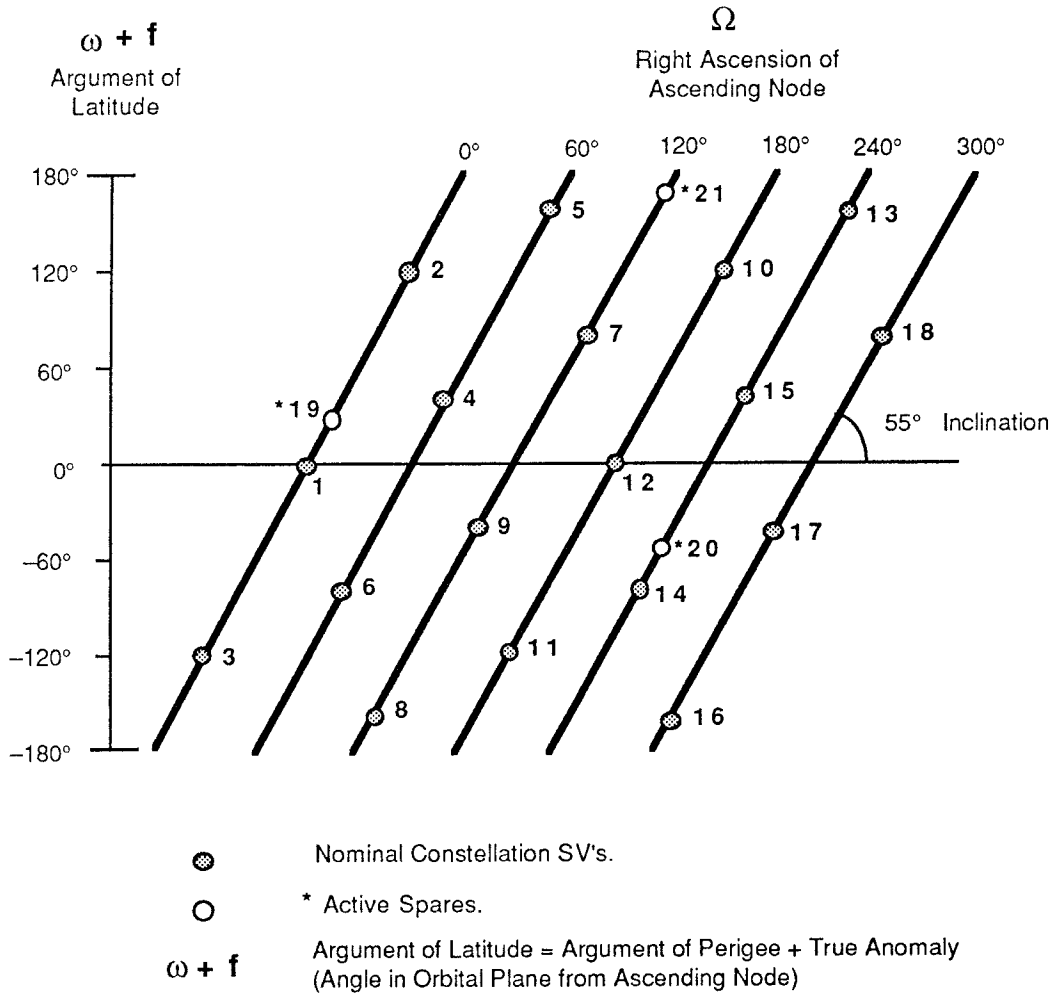

Diagram 4.1.1 Relative Geometry of Proposed Block II Satellites

In addition to these 18 satellites it is planned to have 3 spare satellites which will be active (broadcasting). These are also shown on diagram 4.1.1. These spares will be used to replace satellites that fail. However, their availability is uncertain and thus only the 18 nominal satellites are considered. The original proposal for GPS called for 24 satellites and this is still a possibility, depending on additional funding being made available by the U.S. Congress.

4.1.2 SIGNALS

Codes

The GPS signals are broadcast on 2 carrier waves; L1 and L2, having frequencies of 1575.42 MHz (wavelength of approximately 19 cm) and 1227.60 MHz (wavelength of approximately 24 cm) respectively. The carriers are modulated with 1 or 2 pseudo random noise (PRN) sequences known as the P code and the C/A code. The chipping frequencies of these signals are 10.23 MHz (P code) and 1.023 MHz (C/A code) which correspond to

wavelengths of 30 metres and 300 metres respectively. The P and C/A codes are timing signals that allow the time of transmission of the signal to be determined. Given an identical code sequence in the receiver, the time shift required to correlate the two signals can be measured. This time shift, scaled by the speed of light, is the **pseudo-range**. It is the satellite - receiver range biased by the difference in clock errors between satellite and receiver. If the time shift can be resolved to, say, 1% of the wavelength, the nominal precision of the pseudo-range is 0.3 metres for P code and 3 metres for C/A code.

The P code is modulated on both L1 and L2 frequencies and thus the P code pseudo-ranges can be measured on both frequencies. As the effect of the ionosphere on the transmitted signals is dispersive, the P code pseudo-ranges can be corrected for the effects of the ionospheric delay. The C/A code is only modulated on the L1 frequency and thus the effect of the ionosphere on C/A code pseudo-ranges must be determined in some other way or ignored. Both P and C/A codes are available to all users in the Block I satellites but it is intended that the P code will not be available for general civilian use with the Block II satellites.

Given pseudo-ranges to 4 satellites at any instant, it is possible to solve for the 4D coordinates of the receiver position: 3 spatial parameters x, y, z and the receiver clock error. This assumes that the 4D coordinates (position and clock error) of the satellites are known and are correct. The specified positioning accuracy for the Block II system at the 95% confidence level is ± 20 metres using the P code and ± 100 metres using the C/A code (Stein, 1986). If observations from 2 receivers to the same 4 satellites are available each epoch, the effect of the satellite clock errors and much of the satellite position errors cancel in the calculation of the baseline. Accuracies at the 2 to 3 metre level are possible with this method (Chisholm, 1987). These accuracies are not generally sufficient for geodetic surveying. For navigation the pseudo-ranges play a primary role but in geodetic surveying they play a secondary role, providing extra information for the elimination or estimation of errors. For example, the pseudo-range observations are often used to synchronise the receiver clocks at the μsec level. The principal observation for GPS geodesy is integrated carrier beat phase.

Carrier Beat Phase

If the receiver can duplicate the P or C/A codes it is possible to remove the code from the signal and reconstruct the original carrier phase signal. Receivers with the P code, such as the Texas Instruments TI 4100, can do this on both frequencies (with the Block I satellites). For those that only have the C/A code, such as the Trimble 4000SX or the Wild Magnavox WM101, this is only possible for the L1 carrier phase. Another technique is to square the received signal thus generating a "codeless" signal with twice the frequency of the original carrier wave (King et al, 1987). This technique is used by the Macrometer V1000 and may be used on both L1 and L2 (e.g. the Macrometer II and Mini Mac).

The **carrier beat phase** observation is the difference between the phase of the received carrier phase and the phase of a signal generated by the local receiver oscillator at the same nominal frequency. If both receiver and satellite frequencies are the same and if there are no changes in the atmospheric propagation delays, the carrier beat phase changes by 1 cycle as the satellite - receiver range changes by 1 wavelength (approximately 19 cm for L1 and 24 cm for L2). If this phase can be measured with an accuracy of 1% of a cycle the measurement precision is approximately 2 mm which is 2 orders of magnitude better than P code and 3 orders of magnitude better than C/A code. The carrier beat phase may be thought of as an ambiguous pseudo-range. It is biased by errors in the satellite and receiver oscillators as pseudo-ranges are, but there is an additional bias called the **integer ambiguity**. This bias arises because the total integer number of cycles in the difference between received and local oscillator phase is indeterminate. These biases are discussed further in section 4.2 in relation to the GPS observation equations and in section 4.3.4 on GPS processing.

Navigation Message

The navigation message is a 50 bps signal modulated on both L1 and L2 carriers. It contains the broadcast ephemeris, an almanac (approximate ephemeris) of all other satellites, clock correction parameters, ionospheric correction parameters, satellite health and timing information which assists the receiver in locking onto the P and C/A codes. The **broadcast ephemeris** is a predicted or extrapolated ephemeris based on measurements from a set of monitor stations that continuously track the GPS satellites. The method of generation of the broadcast ephemeris is described by King et al (1987). Clock

error parameters are also generated which give the relationship between the satellite clock and **GPS Time** (GPST). GPST has the same rate as UTC and, in theory, differs from it by an integer number of seconds as the leap seconds applied to UTC are not applied to GPST. In practice GPST is maintained by 3 cesium clocks at the Master Control Station which are "steered" to within 1 μsec of UTC as defined by the U. S. Naval Observatory (Percival, 1987). Satellite manoeuvres may be required from time to time as satellites drift out of position or as some satellites fail and others are moved to replace them. Any ephemeris (broadcast or otherwise) will probably be less accurate during and immediately after such manoeuvres.

4.1.3 COMPARISON WITH TERRESTRIAL GEODESY

GPS observations are independent of the local gravity field at the observation point. They are dependent on the global gravity field as this affects the motion of the satellites but at an altitude of over 20,000 km the satellites are only affected by large scale variations in the gravity field. A geopotential model of degree and order 8 is considered sufficient for modelling GPS orbits (Rizos & Stolz, 1985). Station intervisibility is not a requirement of GPS. Network stations may be chosen on the basis of logistics, geometry or at sites of special interest for deformation. They may be located in valleys where transport is cheaper and where the weather conditions are less extreme. This does not mean that the mountain top trig stations can be completely abandoned for deformation surveys. They have the longest record of geodetic observation and should be included, to some extent, in future observation schemes. GPS is a 3D system and thus the separation of horizontal and vertical control is eliminated. However the ellipsoidal heights obtained from GPS cannot be compared directly with orthometric or normal heights derived from levelling. GPS can theoretically be used in all weather but there may be reduced accuracy during bad weather, particularly thunderstorms (Ware et al 1985). Overall GPS has been shown to require much shorter field observation times than terrestrial techniques although in the early stages of implementation the extra time required for data processing may partly offset this.

GPS surveys have a number of disadvantages compared with terrestrial surveys. Firstly, the adjustment models are generally more complex. The theories of triangulation, trilateration or levelling are well established and the consequences of assumptions made in setting up the model can usually be readily understood. This is not the case for GPS carrier phase adjustment. The

models used to process the data are complex and there is still much to be learned. The data collection and pre-processing stages for terrestrial observations are more open to scrutiny and analysis than those of GPS. The observations that are output by a GPS receiver are the result of substantial internal pre-processing. While the general principles of this pre-processing may be understood, the details are often not available to the user where this is proprietary information. Even in a receiver manufacturing company there may be few that completely understand all the subtleties of the receiver processing.

The number of observations in a terrestrial geodetic network is much lower than in a GPS network. The problems of data collection, storage and processing are not as severe for terrestrial techniques. Archiving GPS data in a secure, permanent and accessible form will be a significant problem. This raw data needs to be kept for 100 years or more to allow the use of improved processing methods and improved tracking station coordinates in the future. The large number of observations in a GPS survey campaign may also impose limitations on the quality of the data editing and data processing procedures that are practicable. Short cuts may be required to avoid extensive processing backlogs and these may bias the results. The complexity of the GPS model is such that the effects of such short cuts may not be readily apparent.

4.2. OBSERVATION EQUATIONS

4.2.1 CARRIER BEAT PHASE

In developing the observation equations for carrier beat phase it is useful to suppose that every clock / oscillator can be compared directly with a "perfect" oscillator having a known and constant frequency f_0 in the chosen reference time scale (e.g GPS Time). The phase of the "perfect" oscillator at time T is represented by $\Phi(T)$. The behaviour of phase with time in general obeys the relation

$$\Phi(T) = \Phi(T_0) + \int_{T_0}^{T} f(T)\, dT \qquad (4.2.1)$$

where $f(T)$ is the time dependent frequency of the oscillator and T_0 is the time of a reference epoch. Because the frequency of the "perfect" oscillator is constant at f_0

$$\Phi(T) = \Phi(T_0) + f_0 (T - T_0) \qquad (4.2.2)$$

The oscillators in the satellites and receivers are used to generate timed signals such as the P code, C/A code and observation time tags. It is common therefore, to think of them as clocks and to think of the errors caused by the variation of frequency as clock errors. This nomenclature makes it difficult to distinguish between the carrier phase error caused by variations in the receiver oscillator frequency, and the error in the observation time tag which is also affected by these frequency variations. The term **clock phase error** is used for the former and **time tag error** is used for the latter. Although the carrier phase and observation time tags are generated by the same oscillator, they are generally treated as if they were independent in GPS processing. For example, the time tags are often corrected according to the clock error estimates obtained from a pseudo range point position. These corrections will generally not be accompanied by an equivalent correction to the observed carrier phase.

The phase of the imperfect satellite or receiver oscillator at time T is represented by $\phi(T)$ and the clock phase error $c(T)$ is defined in terms of the phase error $\left(\phi(T) - \Phi(T)\right)$. I.e.,

$$c(T) = \frac{1}{f_0}\left(\phi(T) - \Phi(T)\right) \qquad (4.2.3)$$

or

$$\phi(T) = \Phi(T) + f_0\, c(T) \qquad (4.2.4)$$

In using equations 4.2.3 or 4.2.4 to relate phase to clock phase errors, it is necessary to account for both the integral and fractional parts of the phase. This point is important when considering how the phase is actually measured.

Now consider the transmission of a signal from a satellite i to a receiver j. The time of reception of a signal at receiver j is T_j. The time of transmission of that signal from satellite i is T_j^i. The transit time of the signal from i to j is $\tau_j^i(T_j)$ and is defined by

$$\tau_j^i(T_j) = T_j - T_j^i \qquad (4.2.5)$$

The beat phase formed as an observation in the receiver is the difference between the phase of the received signal and the phase of the local receiver oscillator. The phase of the received signal at the time of **reception** T_j is equal to the phase of the transmitted signal at the time of **transmission** T_j^i. Therefore,

$$\begin{aligned}\phi_{bj}^i(T_j) &= \phi_{rj}^i(T_j) - \phi_{loj}(T_j) \\ &= \phi^{ti}(T_j^i) - \phi_{loj}(T_j)\end{aligned} \qquad (4.2.6)$$

where :

$\phi_{bj}^i(T_j)$ = the carrier beat phase for receiver j , satellite i , at reception time T_j

$\phi_{rj}^i(T_j)$ = the received signal phase from satellite i at receiver j at time T_j

$\phi_{loj}(T_j)$ = the local oscillator phase of receiver j at time T_j

$\phi^{ti}(T_j^i)$ = the transmitted signal phase from satellite i at transmission time T_j^i

From equation 4.2.4

$$\phi_{loj}(T_j) = \Phi(T_j) + f_0\, c_j(T_j) \qquad (4.2.7)$$

where $c_j(T)$ is the clock phase error of receiver j. Using equations 4.2.2, 4.2.4 and 4.2.5,

$$\begin{aligned}\phi^{ti}(T_j^i) &= \Phi(T_j^i) + f_0\, c^i(T_j^i) \\ &= \Phi(T_j) - f_0\, \tau_j^i(T_j) + f_0\, c^i(T_j^i)\end{aligned} \qquad (4.2.8)$$

where $c^i(T)$ is the clock phase error of satellite i. Combining equations 4.2.6, 4.2.7 and 4.2.8

$$\phi_{bj}^i(T_j) = -f_0 \left(\tau_j^i(T_j) - c^i(T_j^i) + c_j(T_j)\right) \qquad (4.2.9)$$

The transit time is made up of two parts. The main part is derived from the true geometric range ρ_j^i between the satellite at the time of transmission and the receiver at the time of reception. This is determined by the position vectors of the satellite and the receiver in the chosen reference system. Given the speed of the signals (c, the speed of light) the time taken for the signal to travel this distance can be calculated. It is because of the information on satellite and receiver position vectors contained in the geometric range, that GPS can be used for positioning. The value used for the speed of light c is the speed in a vacuum. The second part of the transit time accounts for the extra time taken for the signal to travel through the earth's atmosphere. This is caused by a change in velocity but can also be modelled as a time delay, a phase delay or as an increase in range. This is written here as a phase correction ϕ_{atmos}. It may be further broken down into terms for different parts of the atmospheric delay (ϕ_{ion} for the ionosphere, ϕ_{trop} for the troposphere).

$$f_0\, \tau_j^i(T_j) = (f_0 / c)\, \rho_j^i(T_j) + \phi_{atmos} \qquad (4.2.10)$$

There will also be a random noise associated with the phase measurement process which can be described by the term ϕ_{noise}. Combining equations 4.2.9 and 4.2.10 and including the noise gives the equation

$$\begin{aligned}\phi_{bj}^i(T_j) = &-(f_0/c)\, \rho_j^i(T_j) + f_0\,(c^i(T_j^i) - c_j(T_j)) \\ &- \phi_{atmos} + \phi_{noise}\end{aligned} \qquad (4.2.11)$$

The measured carrier beat phase differs from this model in one important respect. The definition of clock phase error in equation 4.2.3 depends on the integral and fractional part of the carrier phase. When the carrier beat phase is measured in the receiver the measurement is ambiguous as to the number of

integer cycles. This integer is set to some arbitrary value when the satellite signal is first acquired (e.g. zero). There is an unknown integer number of cycles n_j^i difference between the measured carrier beat phase and the model of equation 4.2.11. This will be a unique number for each satellite-receiver pair. It will be constant in time if the receiver tracks the integer number of cycles after the satellite signal has been acquired. This observation is then called **integrated carrier beat phase**. If the receiver fails to track the signal correctly and the ambiguity changes between epochs then a **cycle slip** has been introduced. If there was no atmospheric delay, n_j^i would be equal to the number of integer wavelengths in the satellite-receiver range at the time of signal acquisition. In general it also includes the number of whole cycles in the atmospheric delay at that time.

The model of the measured carrier beat phase must include this integer ambiguity term. This is given in equation 4.2.12 below.

$$\phi_{bj}^i(T_j) = -\left(f_0/c \right) \rho_j^i(T_j) + f_0 \left(c^i(T_j^i) - c_j(T_j) \right) + n_j^i - \phi_{atmos} + \phi_{noise} \qquad (4.2.12)$$

This is the basic observation equation for integrated carrier beat phase. The dependence of ϕ_{noise} and ϕ_{atmos} on the receiver, satellite and epoch is not explicitly noted in the equation but it should be remembered that these terms will be slightly different for every observation. The change in observed carrier beat phase with time is equal to the change in the following quantities:

satellite - receiver geometric range;
satellite - receiver clock phase difference;
net number of cycle slips;
atmospheric delay and;
measurement noise.

4.2.2 OBSERVATION DIFFERENCING

The largest unknown terms in equation 4.2.12 are usually the satellite and receiver clock phase errors and the integer ambiguity. These are known collectively as the **clock biases**. An error of only 3 picoseconds in the clock phase difference between satellite and receiver will affect the GPS L1 carrier

beat phase by 1 mm (0.005 cycles). A common technique in GPS adjustment is to form differences between observations to eliminate the unwanted clock biases, particularly the receiver and satellite clock phase errors.

Between - Satellite Differences

Receiver clock phase errors may be eliminated by forming the difference between observations from one receiver to two satellites at the same time. The operator ∇ is used to indicate a **between - satellites difference**. Using equation 4.2.12 with satellites 1 and 2 and receiver j

$$\nabla\phi_j^{12}(T_j) = \phi_{bj}^{1}(T_j) - \phi_{bj}^{2}(T_j) \qquad (4.2.13)$$

where the two observations have been made at exactly the same time T_j. The differenced observation may be written as

$$\begin{aligned}\nabla\phi_j^{12}(T_j) = &- (f_0/c)\,(\,\rho_j^{1}(T_j) - \rho_j^{2}(T_j)\,) \\ &+ f_0\,(\,c^{1}(T_j^{1}) - c^{2}(T_j^{2})\,) \\ &+ n_j^{1} - n_j^{2} - \nabla\phi_{atmos} + \nabla\phi_{noise}\end{aligned} \qquad (4.2.14)$$

Note that the receiver clock phase error has been eliminated.

Between - Station Differences

The satellite clock phase errors may be almost eliminated by forming the difference between observations from two receivers to one satellite at the same time. The operator Δ is used to indicate a **between - stations difference** also sometimes referred to, ambiguously, as a single difference. The observation times are given by the receiver clocks and include receiver time tag errors, written $te_j(T_j)$. Therefore, although the nominal observation or reception times of the two measurements may be the same, the actual time of measurement will differ from one receiver to the next. If the nominal reception time is t (lower case indicating **receiver clock time**) and is the same for both receivers then the true time of reception T_i at receiver i is given by

$$T_i = t - te_i(T_i) \qquad (4.2.15)$$

and therefore the difference in observation times is

$$T_1 - T_2 = te_2(T_2) - te_1(T_1) \qquad (4.2.16)$$

Using Equation 4.2.12 with receivers 1 and 2 and satellite i

$$\Delta\phi_{12}^{i}(t) = \phi_{b1}^{i}(T_1) - \phi_{b2}^{i}(T_2) \qquad (4.2.17)$$

and thus

$$\begin{aligned}\Delta\phi_{12}^{i}(t) = &- (f_0/c)\,(\,\rho_1^{i}(T_1) - \rho_2^{i}(T_2)\,) \\ &+ f_0\,(\,c^{i}(T_1^{i}) - c^{i}(T_2^{i})\,) \\ &- f_0\,(\,c_1(T_1) - c_2(T_2)\,) \\ &+ n_1^{i} - n_2^{i} - \Delta\phi_{atmos} + \Delta\phi_{noise}\end{aligned} \qquad (4.2.18)$$

The satellite clock phase errors do not completely cancel because they refer to different times. For C/A code receivers the receiver clocks can be synchronised to GPS time and thus to each other from the pseudo-range navigation solution. A position error of 300 metres in this solution corresponds to a time error of 1 μsec. For codeless receivers such as the Macrometer V1000 the clocks are synchronised directly before the observation session (King et al, 1987). The transit times to the satellite are different because of the different satellite - receiver ranges. This difference may be up to 1 millisecond for a 300 km baseline. The total difference in transmission times from the satellite is

$$\begin{aligned}T_1^{i} - T_2^{i} &= T_1 - T_2 + \tau_2^{i}(T_2) - \tau_1^{i}(T_1) \\ &= te_2(T_2) - te_1(T_1) + \tau_2^{i}(T_2) - \tau_1^{i}(T_1)\end{aligned} \qquad (4.2\ 19)$$

Assuming that the cesium satellite clocks have a short term stability of at least 1 part in 10^{10}, a difference in the satellite transmission times of 1 millisecond will result in a difference in the satellite clock phase errors of 0.1 picosecond or 0.03 mm which is insignificant. It is usual to assume that the satellite clock phase errors at the two transmission times are identical and thus cancel when the between - receivers difference is formed. Thus,

$$\begin{aligned}\Delta\phi_{12}^{i}(t) = &- (f_0/c)\,(\,\rho_1^{i}(T_1) - \rho_2^{i}(T_2)\,) \\ &- f_0\,(\,c_1(T_1) - c_2(T_2)\,) \\ &+ n_1^{i} - n_2^{i} - \Delta\phi_{atmos} + \Delta\phi_{noise}\end{aligned} \qquad (4.2.20)$$

Double Differences

This is the term applied to the observation which has been formed by differencing between satellites **and** receivers. This double difference phase may be created by forming the between-satellite difference phase and then

differencing between stations or by first forming the between-station difference and then differencing between satellites.

$$\begin{aligned}\phi_{DD}(t) &= \nabla\phi_1{}^{12}(T_1) - \nabla\phi_2{}^{12}(T_2) \\ &= \Delta\phi_{12}{}^1(t) - \Delta\phi_{12}{}^2(t)\end{aligned} \qquad (4.2.21)$$

Assuming that satellite clock phase errors cancel in a between stations difference, equation 4.2.20 can be used to derive the double difference observation equation.

$$\begin{aligned}\phi_{DD}(t) = &-(f_0/c)\left(\rho_1{}^1(T_1) - \rho_1{}^2(T_1) - \rho_2{}^1(T_2) + \rho_2{}^2(T_2)\right) \\ &+ n_1{}^1 - n_1{}^2 - n_2{}^1 + n_2{}^2 - \Delta\nabla\phi_{atmos} + \Delta\nabla\phi_{noise}\end{aligned} \qquad (4.2.22)$$

The only clock biases remaining in this equation are the integer ambiguities.

Triple Differences

Parameters which are constant with time may be eliminated by forming the **between-epochs difference**. The operator δ is used to represent this difference. If it is applied to double difference observations the **triple difference** observation results. Equation 4.2.22 may be used, together with the assumption that the integer ambiguities are constant in time, to derive the triple difference observation equation. The nominal reception times, in receiver clock time, are t_a and t_b.

$$\begin{aligned}\phi_{TD}(t_{ab}) &= \delta\Delta\nabla\phi_{12}{}^{12}(t_{ab}) \\ &= \phi_{DD}(t_a) - \phi_{DD}(t_b) \\ &= -(f_0/c)\left(\rho_1{}^1(Ta_1) - \rho_1{}^2(Ta_1) - \rho_2{}^1(Ta_2) + \rho_2{}^2(Ta_2)\right) \\ &\quad + (f_0/c)\left(\rho_1{}^1(Tb_1) - \rho_1{}^2(Tb_1) - \rho_2{}^1(Tb_2) + \rho_2{}^2(Tb_2)\right) \\ &\quad - \delta\Delta\nabla\phi_{atmos} + \delta\Delta\nabla\phi_{noise}\end{aligned} \qquad (4.2.23)$$

Note that all the clock bias terms, including the integer ambiguities, have been eliminated. If the assumption that the integer ambiguity is constant in time is false, as in the presence of a cycle slip, an extra term will be required. The triple difference observation is especially useful for cycle slip detection. Not only have the unknown clock biases been removed, but also the effect of errors in the other terms such as atmospheric delay, ephemeris error, receiver coordinate error, are substantially reduced by triple differencing, especially if the epochs are only a few seconds or minutes apart. Hence cycle slips may be distinguished from other errors.

4.3. GPS PHASE ADJUSTMENT

4.3.1 DIFFERENCED AND UNDIFFERENCED MODELS

In simulating GPS phase adjustment, the carrier beat phase observation of equation 4.2.12 will be used. This is called "one way phase" or "undifferenced phase" to distinguish it from the more commonly used single, double or triple differenced phase observations. The name undifferenced phase is, strictly speaking, a misnomer because it is formed by differencing the received and the receiver oscillator phases. Nevertheless it is a commonly used name and will be used in this thesis.

The use of undifferenced phase observations is described by, for example, Goad (1985), Lindlohr & Wells (1985) and King et al (1987). Lindlohr & Wells (1985) have studied the fundamental differencing theorem as it applies to GPS. This theorem may be written as:

> *"Linear biases can be accounted for either by reducing the number of observations so that the biases cancel , or by adding an equal number of unknowns to model the biases. Both approaches give identical results."* (Lindlohr & Wells, 1985)

Thus the effect of the clock phase errors may be eliminated either by double differencing or by estimating them at each epoch. This statement is based on the assumption that the double difference adjustment uses a weight matrix that accounts for the correlations introduced by differencing. Given a matrix operator $\mathbf{D}$ that creates a vector of linearly independent double difference observations ϕ_{DD} from a vector of undifferenced phases ϕ_{UD}

$$\phi_{DD} = \mathbf{D}\,\phi_{UD} \tag{4.3.1}$$

and a VCV matrix of the undifferenced phases $\mathbf{Q}_{UD}$, the VCV matrix of the double differences $\mathbf{Q}_{DD}$ is

$$\mathbf{Q}_{DD} = \mathbf{D}\,\mathbf{Q}_{UD}\,\mathbf{D}^{T} \tag{4.3.2}$$

If $\mathbf{Q}_{DD}$, as defined by equation 4.3.2 is used in an adjustment of the double difference observations ϕ_{DD} , the result will be the same as if $\mathbf{Q}_{UD}$ had been used in an adjustment of the observations ϕ_{UD} with the clock phase parameters being estimated for each epoch.

The number of clock phase parameters to be estimated in the undifferenced model is large but these parameters may be eliminated from the solution at each epoch (Goad, 1985). This may be achieved by partitioning and **reducing the normal equations** as described for GPS in King et al (1987) or, for more general applications, by Meissl (1982) and Cross (1983). A Kalman filter adjustment of the phase observations (see section 4.3.3) will be used in this study and in such an adjustment, the normal matrix does not appear. The same effect as that of reducing the normal equations can be achieved by partitioning and **reducing the observation equations** at each epoch. The procedure for reducing the observation equations is given by Meissl (1982). If the parameter vector is partitioned into common parameters $\mathbf{x}_c$ (e.g., station positions) and epoch parameters (e.g., clock phase errors) $\mathbf{x}_e$ then the design matrix $\mathbf{A}$ is partitioned similarly. Partitioning the observation equations for epoch i (see Appendix A for the least squares equations)

$$\left(\mathbf{A}_c\ \mathbf{A}_e\right)_i \begin{pmatrix}\delta\mathbf{x}_c\\ \delta\mathbf{x}_e\end{pmatrix} = \mathbf{w}_i + \mathbf{v}_i \tag{4.3.3}$$

gives the reduced observation equations

$$\bar{\mathbf{A}}_{c_i}\,\delta\mathbf{x}_c = \bar{\mathbf{w}}_i + \mathbf{v}_i \tag{4.3.4}$$

where

$$\bar{\mathbf{A}}_{c_i} = \left(\mathbf{I} - \mathbf{A}_{e_i}(\mathbf{A}_{e_i}{}^T\mathbf{P}_i\ \mathbf{A}_{e_i})^{-1}\mathbf{A}_{e_i}{}^T\mathbf{P}_i\ \right)\mathbf{A}_{c_i} \tag{4.3.5}$$

and

$$\bar{\mathbf{w}}_i = \left(\mathbf{I} - \mathbf{A}_{e_i}(\mathbf{A}_{e_i}{}^T\mathbf{P}_i\ \mathbf{A}_{e_i})^{-1}\mathbf{A}_{e_i}{}^T\mathbf{P}_i\ \right)\mathbf{w}_i \tag{4.3.6}$$

It is easily demonstrated (e.g. Meissl, 1982) that the reduced **normal equations** of Cross (1983) and King et al (1987) can be generated from these reduced **observation equations**. King et al (1987) refer to the method of eliminating clock phase errors by partitioning as **implicit differencing** to emphasise that the result is the same as the explicit observation differencing of section 4.2.2 and equation 4.3.1.

The reduction of the observation equations given, by equations 4.3.5 and 4.3.6, is an extra computational burden not required when the double difference model is used. It may be argued therefore, that the double

difference model is preferable, particularly as both methods give identical results. However, the matrix $\mathbf{DQ}_{UD}\mathbf{D}^T$ must be formed and inverted for a rigorous double difference adjustment and this balances the computational requirements of the two methods. Beutler et al (1987a) discuss the efficient computation of this VCV matrix for differenced observations. Double differencing has clear advantages when the observation scheme is simple (e.g. a single baseline adjustment using data from 2 receivers). When the observation scheme becomes more complex with a larger number of receivers, with missing observations, with receivers starting and finishing observation at different times and with satellites rising at slightly different times (e.g., when receivers are widely spaced or have different sky visibility), the undifferenced phase model has advantages. The automatic matrix operations in equations 4.3.5 and 4.3.6 replace the decision making required to determine which observation differences should be formed. Bock et al, (1986) discuss this decision making in the presence of missing observations. They also demonstrate that double differenced observations may be weighted according to baseline length to account for propagation and orbit errors. Their *a priori* VCV matrix is derived by applying the differencing operator to a VCV matrix of undifferenced phases $\mathbf{Q}_{UD}$ according to equation 4.3.2. This $\mathbf{Q}_{UD}$ is formed by considering undifferenced observations to be correlated according to baseline length. This can be achieved directly in the undifferenced case simply by using the $\mathbf{Q}_{UD}$ of Bock et al (1986) as the *a priori* observation VCV.

The undifferenced model is preferred because it offers the flexibility of alternative methods of modelling the clock phase errors while still allowing adjustment of the observations in a manner equivalent to double differencing if desired. Possible alternative clock phase error models include the use of clock polynomials or the use of a Kalman filter with an appropriate dynamic model for the clock phase errors. If the observations are differenced to eliminate clock phase errors then these alternative models cannot be applied. A study of clock phase error models is beyond the scope of this thesis but the software DASH developed here has wider applications than the use of GPS data for earth deformation studies, and the undifferenced phase model was adopted for greater flexibility.

4.3.2 RANK DEFECT IN THE CLOCK BIAS PARAMETERS

If the estimation of all the clock biases in the undifferenced model (the satellite and receiver clock phase errors plus the ambiguities), or in the double

difference model (the ambiguities) is attempted, the normal matrix will be singular. The rank defect in that part of the design matrix that is associated with the clock bias parameters is noted in Remondi (1985) and discussed in detail by Lindlohr & Wells (1985). The size of the rank defect and the reason for its existence are covered in Appendix B.1. Given R receivers observing S satellites for T epochs, the total number of clock biases is: RT receiver clock phase errors, ST satellite clock phase errors and RS ambiguities. If the normal matrix is formed with all of these clock biases, it has a rank defect of R+S+T−1. In the double difference adjustment model the clock phase errors have been eliminated and the RS ambiguities are the only clock biases to be estimated. If the normal matrix is formed with these RS ambiguities, the rank defect is R+S−1. One method of overcoming the rank defect, is to hold R+S−1 ambiguities fixed for both undifferenced or double differenced adjustments and to also hold T clock phase errors fixed in undifferenced adjustments. It is demonstrated in Appendix B.2, that the ambiguities estimated using this strategy have integer expectation values.

In the undifferenced model, the T clock phase errors of a reference oscillator may be fixed as noted in Appendix B.1. This may be thought of as a definition of the **phase datum** of the adjustment. R+S−1 reference ambiguities are then chosen to eliminate the remaining rank defect. These are chosen so that they provide a phase link between the reference oscillator and every other oscillator. In Appendix B.1 it is noted that it is the lack of an unambiguous phase difference between the reference oscillator and the other R+S−1 oscillators that caused the rank defect. A common method of achieving this phase link, is to hold the ambiguities between a **base receiver** and all satellites fixed and the ambiguities between a **base satellite** and all receivers fixed. The remaining estimated ambiguities are between non-base receivers and non-base satellites. This, and other more complex choices of reference ambiguities, are illustrated in diagram B.2.1 of Appendix B.2.

It has been noted by Lindlohr & Wells (1985), and confirmed numerically in this study (section 7.4.3), that the choice of reference clock bias parameters does not affect the estimates of non-bias parameters if the rank defect is exactly eliminated by the fixed reference parameters (i.e., if the number and choice of reference clock biases is both necessary and sufficient to eliminate the rank defect). The method used to eliminate the rank defect is therefore arbitrary if estimates of the remaining clock biases are of no interest. If,

however, estimates close to integers are required for the ambiguities so that they can be fixed to integers in a second adjustment, the choice of reference clock biases is no longer arbitrary. Using the base receiver / base satellite concept for undifferenced or double differenced phase adjustment, the ambiguities from stations close to the base receiver are more accurately determined than those from stations further away. The choice of base receiver is therefore important. It should be chosen near the centre of the network to minimise the distances from it to other receivers. This increases the likelihood that the ambiguities can be resolved and fixed to integer values. It is not necessary that the base receiver be at the station with fixed coordinates. Nor is it necessary that the reference oscillator be that of the base receiver or base satellite. These points are discussed further in section 7.4.3 where different choices of base station and base satellite are made in simulated GPS phase adjustments.

For implicit double differencing, where the clock phase errors of a reference oscillator also need to be fixed, the choice of reference oscillator is arbitrary unless the clock phase errors are of interest (unlikely as they are generally eliminated from the solution). It is not even necessary for it to be the most stable oscillator, because the clock phase errors are considered to be independent from epoch to epoch and thus the adjustment does not depend on the stability, between epochs, of any oscillator.

4.3.3 KALMAN FILTER ADJUSTMENT

The Kalman filter adjustment algorithm is used for the simulations of GPS phase adjustment. The Kalman filter equations are presented in a notation consistent with that used for least squares in Appendix A.

The most common application for the Kalman filter in GPS is kinematic positioning where the receiver is moving. For this study the receivers are static but there are a number of other parameters that change with time, namely the clock phase errors, the tropospheric delay, the ionospheric delay and the satellite positions. The Kalman filter allows a great deal of flexibility in dealing with these, either as parameters to be estimated or as unmodelled error sources. One of the processing options available with the Kalman filter algorithm is that of sequential least squares which in turn is equivalent to a standard least squares adjustment. In other words, least squares adjustment is a special case of a Kalman filter adjustment where special conditions have

been implicitly imposed on the behaviour of the parameters in time. This is discussed in Appendix C.

The Kalman filter equations may be found in a number of publications. They are given in a notation familiar to geodesists in Krakiwsky (1981) and Cross (1983). Suppose that observations are available at epochs t_1 , t_2 , t_3 , ..., t_i , ..., t_n and that the parameters are to be estimated at each epoch. There are two functional models. The **primary or observation model** for epoch t_i is

$$\mathbf{w}_i + \mathbf{v}_i = \mathbf{A}_i \, \delta\mathbf{x}_i \tag{4.3.7}$$

where the parametric model of Appendix A has been adopted. The **secondary or dynamic model** describes the behaviour of the parameters in time. The recursive equation

$$\mathbf{x}_i = \Phi_i \ \mathbf{x}_{i-1} + \mathbf{y}_i \tag{4.3.8}$$

is used where Φ_i is the transition matrix from epoch t_{i-1} to epoch t_i and $\mathbf{y}_i$ is the vector of errors in the dynamic model as embodied in the transition matrix Φ_i . The dynamic model errors are assumed to have zero mean, to be uncorrelated between epochs and it is assumed that $\mathbf{y}_i$ and $\mathbf{x}_{i-1}$ are uncorrelated. The $\mathbf{y}_i$ have the same role in the secondary or dynamic model as the residuals $\mathbf{v}_i$ have in the primary or observation model. The observations $\boldsymbol{l}_i$ and thus the misclose vectors $\mathbf{w}_i$ are also assumed to be zero mean, uncorrelated between epochs and uncorrelated with $\mathbf{x}_{i-1}$. Equation 4.3.8 can be expanded in terms of the *a priori* parameter estimates $\mathbf{x}^o_i$ for epoch t_i and the parameter corrections $\delta\mathbf{x}_i$.

$$\mathbf{x}^o_i + \delta\mathbf{x}_i = \Phi_i \, (\mathbf{x}^o_{i-1} + \delta\mathbf{x}_{i-1}) + \mathbf{y}_i \tag{4.3.9}$$

and propagating the *a priori* parameters according to

$$\mathbf{x}^o_i = \Phi_i \, \mathbf{x}^o_{i-1} \tag{4.3.10}$$

gives

$$\delta\mathbf{x}_i = \Phi_i \, \delta\mathbf{x}_{i-1} + \mathbf{y}_i \tag{4.3.11}$$

The Kalman filter estimation procedure has two steps based on the observation and dynamic models. Given a least squares estimate $\delta\hat{\mathbf{x}}_{i-1}$ for the parameters at epoch t_{i-1} , the dynamic model is used to predict values for the

parameters at epoch t_i . This is the **prediction step**. The predicted parameter correction vector is written $\delta\tilde{\mathbf{x}}_i$ where the symbol $\tilde{}$ denotes a prediction based on a least squares estimate. The second step is to use the observations and the predicted parameters to produce a least squares estimate $\delta\hat{\mathbf{x}}_i$. This is the **filtering step**. A third step may also be employed called the **smoothing step**. This involves the recalculation of earlier estimates $\delta\hat{\mathbf{x}}_1$ to $\delta\hat{\mathbf{x}}_{i-1}$ using the new information contained in the observations of epoch t_i . For a given epoch t_i , the predicted parameters $\delta\tilde{\mathbf{x}}_i$ are derived from observations up to and including t_{i-1} ; the filtered estimates $\delta\hat{\mathbf{x}}_i$ are derived from observations up to and including epoch t_i, and the **final** smoothed estimates are derived from observations up to and including the final epoch t_n . Smoothing will not be considered further in this thesis. The interested reader is referred to Merminod & Rizos (1988).

The VCV matrix of the parameters is also propagated forward at the prediction and filtering steps. The equations for the prediction step are

$$\delta\tilde{\mathbf{x}}_i = \Phi_i \, \delta\hat{\mathbf{x}}_{i-1} \tag{4.3.12}$$

$$\tilde{\mathbf{Q}}_{x_i} = \Phi_i \, \hat{\mathbf{Q}}_{x_{i-1}} \, \Phi_i^T + \mathbf{Q}_{y_i} \tag{4.3.13}$$

For the Kalman filter equations, the notation of Bierman (1977) is adopted, where the predicted and filtered VCV matrices are written $\tilde{\mathbf{Q}}_x$ and $\hat{\mathbf{Q}}_x$ rather than as $\mathbf{Q}_{\tilde{x}}$ or $\mathbf{Q}_{\hat{x}}$ as is used for least squares in this thesis. This notation reflects the fact that the VCV matrices are passed through the prediction and filter steps in a similar manner to the parameters.

The filtering step begins with the calculation of the **gain matrix**

$$\mathbf{G}_i = \tilde{\mathbf{Q}}_{x_i} \mathbf{A}_i^T \, (\mathbf{Q}_i + \mathbf{A}_i \, \tilde{\mathbf{Q}}_{x_i} \mathbf{A}_i^T \,)^{-1} \tag{4.3.14}$$

Next the filtered estimate of the parameters is calculated according to

$$\delta\hat{\mathbf{x}}_i = (\mathbf{I} - \mathbf{G}_i \, \mathbf{A}_i) \, \delta\tilde{\mathbf{x}}_i + \mathbf{G}_i \, \mathbf{w}_i \tag{4.3.15}$$

and by propagation of variances

$$\hat{\mathbf{Q}}_{x_i} = (\mathbf{I} - \mathbf{G}_i \, \mathbf{A}_i) \, \tilde{\mathbf{Q}}_{x_i} \, (\mathbf{I} - \mathbf{G}_i \, \mathbf{A}_i)^T + \mathbf{G}_i \, \mathbf{Q}_i \, \mathbf{G}_i^T \tag{4.3.16}$$

which can be shown (e.g. Krakiwsky, 1981; Cross 1983) to simplify to

$$\hat{\mathbf{Q}}_{x_i} = (\mathbf{I} - \mathbf{G}_i \mathbf{A}_i)\, \tilde{\mathbf{Q}}_{x_i} \qquad (4.3.17)$$

The five equations 4.3.12 - 16 or 17 are the Kalman filter equations and are applied at every epoch for which observations are available. Only one matrix inversion is required (in equation 4.3.14) and the order of this matrix is the number of observations in that epoch. Equation 4.3.16, while requiring greater computational effort than the commonly used 4.3.17, is more numerically stable (Bucy & Joseph, 1968) and has been implemented in the software DASH developed for this thesis. See Bierman (1977) for a detailed discussion on numerical stability in the Kalman filter algorithm.

The Kalman filter estimation procedure needs to be started with an initial estimate and VCV matrix of the parameters. For example, given pseudo observed values of the parameters $\boldsymbol{l}_x$ (see Appendix A on least squares adjustment) and a VCV matrix $\mathbf{Q}_x$, these could be used as the predicted estimates for epoch t_1 . The misclose vector of the pseudo observed parameters is

$$\mathbf{w}_x = \boldsymbol{l}_x - \mathbf{x}^o_1 \qquad (4.3.18)$$

and will be zero if the *a priori* parameters $\mathbf{x}^o_1$ are set equal to the pseudo observed values. For epoch t_1

$$\delta\tilde{\mathbf{x}}_1 = \mathbf{w}_x \qquad (4.3.19)$$

$$\tilde{\mathbf{Q}}_{x_1} = \mathbf{Q}_x \qquad (4.3.20)$$

The Kalman filter equations 4.3.14 - 16 or 17 are then used to calculate the filtered estimate for epoch t_1 and so on.

4.3.4 AMBIGUITY RESOLUTION

Ambiguity resolution is generally considered to be the key to accurate horizontal positioning with GPS. If the ambiguities are well determined in the phase adjustment it may be possible to hold them fixed at integer values in a new adjustment. This is often called "bias fixing" although the name itself is ambiguous as the integer ambiguities are only some of the biases found in GPS observations. The horizontal coordinates of the **"ambiguity fixed"**

solution, particularly the east component, are generally more accurate than those of the **"ambiguity free" solution** provided the ambiguities have been fixed to the correct integer values. It is demonstrated in the simulations of section 7.3, that the heights are not greatly improved by resolving the ambiguities.

The ability to resolve the ambiguities depends on the change in satellite geometry and thus on the length of the observation period. The ambiguities estimated are, in effect, double differenced with respect to the reference ambiguities of the base receiver and base satellite (see Appendix B.2). Thus their estimation is affected by those errors that are not eliminated by double differencing. The largest of these are tropospheric delay, ionospheric delay, orbit errors and errors in the origin station coordinates. The effect of these errors on double differences, and thus on the estimated ambiguities, increases with an increase in the distance from the base receiver to the receiver associated with the ambiguities to be estimated. (In a 2 station or baseline solution it is simply dependent on the length of the baseline.) The distance at which ambiguity resolution becomes difficult depends on the magnitude of these errors and is therefore quite variable. Using standard processing techniques it is generally accepted that the ambiguities can usually be resolved for baselines up to 20 - 30 km and that it becomes increasingly difficult beyond this distance. If dual frequency observations are used to eliminate the ionospheric delay; if water vapour radiometers (WVRs) or tropospheric estimation are used to minimise the tropospheric delay; and if orbits are estimated, then the distance over which ambiguities can be resolved will be increased significantly. For example, Blewitt (1988) cites a GPS survey with baselines up to 1933 km in which 94% of the ambiguities were resolved at the 99% confidence level.

There are a number of different strategies used to choose the correct integer values for the ambiguities. A number of different sets of hypothesised integer values for all ambiguities may be created with a test for the set with the lowest $\hat{\mathbf{v}}^T\mathbf{P}\hat{\mathbf{v}}$ (e.g. TRIMVEC^{TM}, Trimble Navigation Ltd, 1986). This has the disadvantage that the ambiguities must be either all resolved or all unresolved. A search for all ambiguities that are within 3 standard deviations of a single integer value may be used with these then resolved and the adjustment re-run to see if the determination of the remaining ambiguities is improved (e.g. PoPS^{TM}, WM Satellite Survey Company, 1987). A "bank" of

Kalman filters may be used to find the correct integer values (e.g. NOVAS, Wanless & Lachapelle, 1988). Blewitt (1988) outlines various strategies for ambiguity resolution. A study of the best strategy for ambiguity resolution is beyond the scope of this thesis. In the GPS phase adjustment simulations of Chapter 7, an iterative or progressive ambiguity resolution scheme is adopted similar to that of PoPS in which the best determined ambiguities are fixed to integers in a second adjustment. The remaining ambiguities from this second adjustment are then tested to see if they can now be resolved and, if so, fixed to integers in the next adjustment, and so on. If the errors in the ambiguities are large then the ambiguity free solution will be the best that can be achieved.

4.3.5 DUAL FREQUENCY

As noted above, one of the error sources that may prevent ambiguity resolution over long lines is that of ionospheric delay. If carrier phase observations are available on both L1 and L2 frequencies, a combined **ionosphere free phase observable**, written L1/L2 can be formed (e.g. King et al 1987). This, unfortunately, increases the influence of other error sources such as multipath (Schaffrin & Bock, 1987). On short baselines, where the ionospheric delay is virtually the same for both receivers and thus cancels in the explicit or implicit double differencing, it is best to form separate solutions for L1 and L2 and calculate the mean to reduce this noise. On longer lines (over 10 km , Hatch & Larson, 1985) the differential ionospheric delay may be large enough for the combined L1/L2 observable to be preferable. Schaffrin & Bock (1987) present a unified processing scheme with *a priori* constraints on the ionospheric delay which is equivalent to the mean of L1 and L2 for short baselines and to the combined L1/L2 for longer lines. This uses double difference observations (explicit double differencing) but the *a priori* VCV matrix of the double difference observations is constructed from a VCV of the undifferenced observations in which correlations are introduced for baseline dependent errors. Thus the method could be adapted to the undifferenced model used here (implicit double differencing).

Georgiadou & Kleusberg (1988) use the ionospheric delay, determined from dual frequency observations at one station, to estimate parameters of an ionospheric model. They use polynomials of first order in latitude and third order in hour angle of the sun. This model is then used to correct the single frequency observations from other stations. A combination of this approach and that of Schaffrin & Bock (1987) would be possible in which the

ionospheric parameters were estimated at the same time as the other geodetic parameters and where all observations (L1 from single frequency receivers, L1 and L2 from dual frequency receivers) were processed together.

An analysis of such techniques is beyond the scope of this thesis and in the simulations used here, one observation per receiver, per satellite, per epoch will be used. This may be thought of as being an ionosphere free observation such as L1/L2 or a corrected single frequency observation using the model of Georgiadou & Kleusberg (1988). Alternatively it may be considered to be an uncorrected single frequency L1 observation, in which case the effect of ionospheric delay on the solution should be considered.

4.4. GPS DATUM DEFINITION

If the datums of the terrestrial and GPS networks are defined by minimum constraints, e.g. by holding the appropriate number of parameters fixed or by the inner coordinate method (Pelzer, 1971), the datum definition will have introduced no strain. The estimates of translation, orientation and perhaps scale will then be affected by the datum definition but the strain parameters will be invariant.

For a terrestrial network the origin may be defined by holding the coordinates of one point fixed. The orientation may be defined by zenith distance and azimuth observations or by 3 more fixed coordinates of at least 2 more points. The scale may be defined by measured distances or another fixed coordinate. If necessary, the gravimetric datum may be defined by fixed deflections of the vertical at one point and either a fixed geoid height or a value for the geopotential at some point. In short the definition of the datum is reasonably transparent and it is relatively easy to ensure that it is not over-constrained.

In GPS adjustment the datum definition is more complex and is generally over-constrained. The reference system is defined, in part, by a set of tracking stations which are used to generate satellite ephemerides. There are no direct observations between these tracking stations and the stations of the survey network. The datum definition is transferred from the tracking stations to the survey stations via the satellite ephemerides. This is commonly a two step process with an orbit adjustment which produces satellite ephemerides followed by a multi-station adjustment where the orbits are held fixed. (The term **multi-station** includes the case of a baseline adjustment for which the number of stations is 2.) Alternatively, these two steps may be combined in a single orbit / station adjustment where both satellite ephemerides and survey station positions are estimated. The distinction between tracking stations and survey stations is then blurred as observations from all stations contribute to the orbit adjustment. The datum definition of the multi-station adjustment with fixed orbits and the combined orbit / station adjustment will be examined briefly. Both of these types of adjustment will be assessed in the covariance analysis of Chapter 7.

4.4.1 MULTI-STATION ADJUSTMENT WITH FIXED ORBITS.

The fixed satellite ephemerides, together with the force model, define a datum. The elements of any satellite would be sufficient, in theory, to define the origin, orientation and scale of an earth centred quasi-inertial reference frame. If the earth rotation parameters (polar motion and UT1) are considered to be known, an earth centred - earth fixed reference frame is also defined and the positions of receivers may be estimated in terms of this datum. If more than one satellite is held fixed the datum is over-constrained. If the ephemerides have been determined from a regional tracking network that surrounds, or is close to, the survey network, it is likely that the datum definitions inherent in each ephemeris will be consistent with each other and with that of the tracking network. If they have been generated from a network with a preponderance of tracking stations distant from the survey (say in the northern hemisphere for a survey in New Zealand) the possibility of discrepancy between these datum definitions is greater.

The estimation of receiver position relative to the geocentre is much weaker than the definition of the relative geometry of the survey network. If all station coordinates are estimated, the normal matrix will be non-singular but will be ill conditioned and the inversion may be numerically unstable due to the high correlations between the estimated coordinates. In such cases, systematic errors tend to have a disproportionately large effect and thus it is usual to hold the coordinates of one station fixed. This is a further over-constraint of the datum. Large errors between the fixed coordinates adopted and the unknown true coordinates of that point in the satellite ephemeris reference system, will distort the network. This is examined further in Chapter 7. Remondi (1984) suggests solving for the average and difference of the station coordinates in a two station (baseline) adjustment. This would be equivalent to holding one station fixed, estimating the coordinates of all other stations and estimating a translation of all stations relative to the datum of the satellite ephemerides. The accurately determined relative geometry is thus separated from the weakly determined absolute position. Another alternative is to estimate the coordinates of all stations by Bayesian estimation using *a priori* weights on the coordinate parameters (Bossler, 1972).

As noted above there is a definition of scale in the satellite ephemerides and the force model. The chosen value of the gravitational constant, GM, is effectively a scale factor for the size of the orbit. With GPS measurements, the

phase observable is converted to range through the speed of light. Thus there are two, possibly different, definitions of scale. In practice, any discrepancy between the scale defined by GM and that defined by the speed of light is unlikely to be distinguishable from an error in the atmospheric propagation model.

4.4.2 COMBINED ORBIT / STATION ADJUSTMENT.

There are various ways to define the datum in a combined orbit / station adjustment. The **fiducial station** concept (e.g. Davidson et al, 1985) is implemented by holding the coordinates of a number of tracking or fiducial stations fixed and estimating the orbits and coordinates of the survey stations. If six coordinates of three stations (e.g. 3 coordinates of one point, 2 coordinates of another and one coordinate of the third) are held fixed, the origin and orientation of an earth fixed datum are defined. Scale is defined by the observations. Typically, at least 3 points (9 coordinates) are held fixed (e.g. Davidson et al, 1985; Delikaraoglou, 1987) and thus the datum is over constrained. It is usually assumed that the coordinates are geocentric and that they are in terms of the axes of the reference system used to determine polar motion and UT1. There is potential for distortion of the adjustment if these assumptions are not correct. The satellite motions are sensitive to the true position of the geocentre and the model of satellite - receiver range is also sensitive to earth rotation. One of the advantages of the fiducial station concept is that the datum can be defined in the same way for each GPS campaign. Thus if deformation is to be determined from repeated GPS surveys, good results may be obtained from the fiducial station method. Any distortion caused by incorrect fiducial station coordinates will tend to be the same for both epochs (assuming no significant tectonic motion of the fiducial stations relative to each other) and will thus cancel. This investigation is principally concerned with the combination of terrestrial and GPS data and in this case the distortions due to fiducial station coordinate errors will not cancel.

An alternative datum definition is the **free net** concept (Beutler et al 1985) where the datum is defined by *a priori* weighted observations of all satellites in a Bayesian estimation scheme and by the coordinates of one station which is held fixed. The datum definition of the free net scheme is less "repeatable" because the *a priori* ephemeris errors will change from epoch to epoch and this may, or may not, be reflected in a change of the VCV of the *a priori*

satellite elements. However the free net scheme will be less subject to the distortions of an over defined datum.

There is a third possible option between these extremes in which the datum is defined by *a priori* weighted observations of the station coordinates and possibly also the satellite elements. The origin could be defined by 1 fixed station or by the weighted observations of all station coordinates. Coordinate variances should allow for possible tectonic motion of the tracking stations. Where station coordinates are very accurate this method will tend to the fiducial station method. Where they are poorly determined it will tend to the free net method. There are a number of advantages of such a scheme. There will be less distortion from an over defined datum than for the fiducial station method. The solution will have greater geometric strength than the free net concept and should thus be less sensitive to other systematic errors. Where good tracking station coordinates are not available, (e.g., New Zealand) they may be progressively improved over a number of GPS campaigns.

A common method used in network densification is to hold the coordinates of primary control points fixed and to distort the new data to fit. This avoids constantly changing coordinates for the primary control. However, it is well recognised that this technique is not appropriate for deformation adjustment. The fiducial station concept is equivalent to this method. It has proved useful in the U.S.A. where station coordinates are accurate and regularly monitored by SLR or VLBI. Despite this, there seems little justification for holding coordinates fixed which are known to have errors, however small. In New Zealand there are no VLBI or SLR stations and only TRANSIT Doppler coordinates with uncertainties of several meters are available to provide a geocentric datum. An SLR site and VLBI sites are available in eastern Australia more than 2000 km to the west of New Zealand and another SLR site is in West Australia over 5000 km from New Zealand. For the 1987 Australian GPS orbit determination pilot project (Rizos et al ,1987) observations were taken at 4 stations in Australia and one in New Zealand. Two of the Australian stations are adjacent to SLR sites and the remaining 3 have TRANSIT Doppler coordinates. Rizos et al (1987) note that the free network concept is more appropriate to this project than the fiducial station concept because of the uncertainties in the *a priori* station coordinates. They also intend to investigate Bayesian estimation using *a priori* station coordinates and satellite elements to define the datum.

4.5. GPS NETWORK AND DEFORMATION ADJUSTMENTS

The preceding discussion has been of the **GPS phase adjustment**, or **session adjustment**, using data from receivers that are simultaneously observing a set of satellites in one observing session. It is unlikely that enough receivers will be available to simultaneously observe from all stations in the network. The results of several observing sessions can be combined in a **GPS network adjustment**. The coordinates that result from the network adjustment can be used, together with coordinates of a terrestrial network adjustment, in a **terrestrial / GPS deformation adjustment**. The GPS data will then have passed through 3 successive adjustments. The GPS session and network adjustments could be combined in a multi-session adjustment as described by Rizos & Stolz (1988). This model has advantages where orbits are to be estimated as the orbital parameters can then be common to all observing sessions. However, for large networks and long observation campaigns, the number of observations and parameters in a multi-session adjustment may be a considerable drain on computer resources. For the simulations used here, each GPS observing session will be adjusted separately. The network of stations observed in a single session is referred to as a "sub-network".

The deformation parameters can be estimated directly from the terrestrial coordinates and the GPS sub-network coordinates without the need for a GPS network adjustment. This is easily implemented using existing deformation adjustment software by extending the parameter set to allow a different set of translations for each GPS sub-network. It is implicitly assumed that each of the sub-networks have the same orientation and scale but that they have different origins due to the standard practice of holding one arbitrarily chosen station fixed in each session adjustment. This model will be used for the simulations as it allows the effect of systematic errors on deformation parameters to be studied without the need to propagate the errors through the network adjustment stage. The parameters estimated are:

6 strain parameters
3 rotations
3 translations for each GPS sub-network

If the horizontal strain model recommended in Chapter 3 is adopted, the 3 vertical strain parameters will be held fixed.

This model is convenient for simulations but it is not recommended for processing GPS data for deformation analysis in practice. On the contrary, the GPS network adjustment step is an important part of the data editing and validation process required before deformation analysis begins. For example, errors in locating the antenna relative to the station mark may be detected at the network adjustment stage and anomalous results due to receiver malfunction or severe multipath may also be detectable. The repeatability of re-measured lines will be a guide as to the reliability of the GPS results although repeatability is not synonymous with accuracy and constant errors may be present that don't affect the repeatability.

The assumption that all sub-networks have the same orientation and scale is usually also made in a GPS network adjustment. It may be advisable to verify this by estimating rotation and scale parameter for each GPS sub-network also. These could then be tested for significant differences. Each GPS session would then require a minimum of 3 stations and preferably more. This highlights the complexity of datum definition in GPS adjustment as discussed in section 4.4. In a terrestrial network the datum is defined once for the whole network but there is a different datum definition for each of the GPS session adjustments that are combined in a GPS network adjustment. It will be assumed here that there are no significant scale or rotation differences between the GPS sub-networks.

Each station has only one set of terrestrial coordinates but may have several sets of GPS coordinates if it has been occupied in more than one observing session. Observed terrestrial coordinates are required for each point in the GPS network but, in practice, some GPS stations could have been included to provide strength to the network or to provide more accessible stations for future deformation surveys. Orbit tracking stations may have been used outside the zone for which the assumption of homogeneous strain is valid. If the network and deformation adjustments were separate these additional GPS points could be included in the GPS network adjustment but left out of the deformation adjustment. In the chosen combined network / deformation model, this problem may be overcome by adding approximate pseudo observed terrestrial coordinates for the extra points with *a priori* uncertainties so large (say 100 metres) that the extra observations do not affect the deformation adjustment.

The deformation model used is similar to the models described by Harvey (1985). For GPS coordinates $\mathbf{x}_{GPSij}$ of station i in sub-net j and corresponding terrestrial coordinates $\mathbf{x}_{TERi}$ the model is given by

$$\mathbf{x}_{GPSij} - (\mathbf{S} + \mathbf{R})\,\mathbf{x}_{TERi} - \mathbf{t}_j = \mathbf{0} \tag{4.5.1}$$

where $\mathbf{S}$ and $\mathbf{R}$ are the strain and rotation matrices and where $\mathbf{t}_j$ is the vector of translations for sub-net j. Adopting the topocentric model described in section 2.2.2

$$\mathbf{S} = \begin{pmatrix} e_{ee} & e_{en} & e_{ev} \\ e_{en} & e_{nn} & e_{nv} \\ e_{ev} & e_{nv} & e_{vv} \end{pmatrix} \tag{4.5.2}$$

$$\mathbf{R} = \begin{pmatrix} 1 & \omega_v & -\omega_n \\ -\omega_v & 1 & \omega_e \\ \omega_n & -\omega_e & 1 \end{pmatrix} \tag{4.5.3}$$

$$\mathbf{t}_j^T = (t_{ej}\,,\, t_{nj}\,,\, t_{vj}) \tag{4.5.4}$$

and

$$\mathbf{x}_{GPSij}^T = (e_{ij}\,,\, n_{ij}\,,\, v_{ij}) \tag{4.5.5}$$

$$\mathbf{x}_{TERi}^T = (e_i\,,\, n_i\,,\, v_i) \tag{4.5.6}$$

Linearising these equations in the general least squares model described in Appendix A gives

$$\mathbf{A}\,\delta\mathbf{d} + \mathbf{B}\,\mathbf{v} - \mathbf{w} = \mathbf{0} \tag{4.5.7}$$

where $\mathbf{A}$ is the matrix of partial derivatives of the equations with respect to the deformation parameters $\mathbf{d}$, $\mathbf{B}$ is the matrix of partial derivatives of the equations with respect to the coordinate observations $\mathbf{x}_{GPSij}$ and $\mathbf{x}_{TERi}$, and $\mathbf{w}$ is the vector of miscloses. This has solution (from equation A.1.17 in Appendix A)

$$\hat{\delta\mathbf{d}} = \left(\mathbf{A}^T (\mathbf{B}\mathbf{Q}\mathbf{B}^T)^{-1}\,\mathbf{A} + \mathbf{Q}_o^{-1}\right)^{-1} \mathbf{A}^T (\mathbf{B}\mathbf{Q}\mathbf{B}^T)^{-1}\,\mathbf{w} \tag{4.5.8}$$

where $\mathbf{Q}$ is the VCV matrix of the "observed" coordinates and where $\mathbf{Q}_o$ is the *a priori* VCV matrix of the deformation parameters. The $\mathbf{A}_{ij}$ matrix for station i and session j is

$$\mathbf{A}_{ij} = -\begin{pmatrix} e_i & 0 & 0 & n_i & v_i & 0 & 0 & -v_i & n_i & \cdots & 1 & 0 & 0 & \cdots \\ 0 & n_i & 0 & e_i & 0 & v_i & v_i & 0 & -e_i & \cdots & 0 & 1 & 0 & \cdots \\ 0 & 0 & v_i & 0 & e_i & n_i & -n_i & e_i & 0 & \cdots & 0 & 0 & 1 & \cdots \end{pmatrix} \tag{4.5.9}$$

$$\mathbf{d}^T = (e_{ee}\ e_{nn}\ e_{vv}\ e_{en}\ e_{ev}\ e_{nv}\ \omega_e\ \ \omega_n\ \ \omega_v\ \ \cdots\ \ t_{ej}\ t_{nj}\ t_{vj}\ \cdots) \tag{4.5.10}$$

where the vector $\mathbf{d}^T$ indicates the order of the parameters. The $\mathbf{B}_{ij}$ matrix for station i and sub-net j has the form

$$\mathbf{B}_{ij} = (\mathbf{0}\ \ \mathbf{0}\ \ \mathbf{I}\ \mathbf{0}\ \ \mathbf{0}\ \ -(\mathbf{S}+\mathbf{R})\ \mathbf{0}\ \ \mathbf{0}) \tag{4.5.11}$$

where the identity matrix $\mathbf{I}$ contains the partial derivatives of the equations with respect to $\mathbf{x}_{GPSij}$ and where $-(\mathbf{S}+\mathbf{R})$ contains the partial derivatives of the equations with respect to $\mathbf{x}_{TERi}$. The *a priori* estimates of the deformation parameters are used to calculate $(\mathbf{S}+\mathbf{R})$ and if the *a priori* model assumes zero strain and zero rotation then $(\mathbf{S}+\mathbf{R}) = \mathbf{I}$. In this case $\mathbf{B}$ is simply a differencing operator to generate terrestrial - GPS coordinate differences from the terrestrial and GPS "observed" coordinates. As a simple example, consider the case where the 3 sides of a triangle are observed in separate sessions.

Sub-net	Stations
1	1 , 2
2	1 , 3
3	2 , 3

The observation vector is

$$l = \begin{pmatrix} \mathbf{x}^T_{GPS11} \\ \mathbf{x}^T_{GPS21} \\ \mathbf{x}^T_{GPS12} \\ \mathbf{x}^T_{GPS32} \\ \mathbf{x}^T_{GPS23} \\ \mathbf{x}^T_{GPS33} \\ \mathbf{x}^T_{TER1} \\ \mathbf{x}^T_{TER2} \\ \mathbf{x}^T_{TER3} \end{pmatrix} \tag{4.5.12}$$

and if the *a priori* estimates of strain and rotation are zero, the **B** matrix is

$$\mathbf{B} = \begin{pmatrix} \mathbf{I} & 0 & 0 & 0 & 0 & 0 & -\mathbf{I} & 0 & 0 \\ 0 & \mathbf{I} & 0 & 0 & 0 & 0 & 0 & -\mathbf{I} & 0 \\ 0 & 0 & \mathbf{I} & 0 & 0 & 0 & -\mathbf{I} & 0 & 0 \\ 0 & 0 & 0 & \mathbf{I} & 0 & 0 & 0 & 0 & -\mathbf{I} \\ 0 & 0 & 0 & 0 & \mathbf{I} & 0 & 0 & -\mathbf{I} & 0 \\ 0 & 0 & 0 & 0 & 0 & \mathbf{I} & 0 & 0 & -\mathbf{I} \end{pmatrix} \qquad (4.5.13)$$

where each of the sub-matrices is of order 3 x 3. The partial derivatives in equations 4.5.9 and 4.5.13 are for the topocentric model where the coordinates and VCV have been converted to the topocentric system. Equations for such conversions are given in Appendix G.

The design matrices **A** and **B** given above are used in the program COSTRAIN (described briefly in Appendix F) to propagate the errors of simulated GPS session adjustments through to the parameters of a combined terrestrial / GPS deformation adjustment. The theory for this is given in section 5.6.

5. COVARIANCE ANALYSIS

5.1. SIMULATIONS

Simulations have a useful part to play in geodesy. When used before an observation campaign begins, they allow the testing of different observation schemes to ensure that the campaign objectives can be met in the most efficient manner. If adjustment software is to be written or modified, new models can be tested in a relatively simple form before the complexity of the full adjustment software is implemented.

The feature of simulations that is their principal advantage, namely that no observations are required, also leads to their principal disadvantage. The results are dependent on the assumptions made in formulating the adjustment model and these are not directly tested against the reality of observations. These assumptions are usually partly based on the results of other earlier adjustments. Of course, the circumstances of the campaign that is to be simulated may be different from those on which the assumptions are based. For a new observation technique like GPS, the assumptions will be more tentative than for established techniques like triangulation. However this is where simulations have their greatest value as there is less "established wisdom" on the best way to design an observation scheme for GPS than for triangulation. For conventional terrestrial observations the principles of network design are well known to surveyors, almost instinctive, and simulations are only needed to choose the best of several, basically sound, observation schemes. For GPS the basic rules of optimum observation scheduling have not yet been completely defined. The questions of satellite geometry, network geometry, tracking station geometry where orbits are to be determined, choice of parameters to be adjusted and the accuracy rather than the precision of the results need to be addressed. Simulations of specific observation schemes and adjustments assist here. To determine the accuracy of simulated adjustments, the technique of covariance analysis can be used.

Simulations, in their simplest form, involve the calculation of the VCV matrix of the adjusted parameters. Adopting the parametric least squares model described in Appendix A.2,

$$\mathbf{L} = f(\mathbf{x}) \qquad (5.1.1)$$

in parameters $\mathbf{x}$ and observables $\mathbf{L}$. The linearised observation equations are

$$\mathbf{w} + \mathbf{v} = \mathbf{A}\,\delta\mathbf{x} \qquad (5.1.2)$$

The stochastic model is defined by the VCV matrices of the observations $\mathbf{Q}$ and of the parameters $\mathbf{Q}_{x^o}$. The VCV of adjusted parameters is

$$\mathbf{Q}_{\hat{x}} = (\mathbf{A}^T\mathbf{P}\mathbf{A} + \mathbf{P}_{x^o}) \qquad (5.1.3)$$

If a Kalman filter adjustment is proposed the dynamic model must also be defined by the choice of Φ and $\mathbf{Q}_y$ (see section 4.3.3). The recursive equations

$$\tilde{\mathbf{Q}}_{x_i} = \Phi_i\,\hat{\mathbf{Q}}_{x_{i-1}}\,\Phi_i^T + \mathbf{Q}_{y_i} \qquad (5.1.4)$$

$$\mathbf{G}_i = \tilde{\mathbf{Q}}_{x_i}\,\mathbf{A}_i^T(\,\mathbf{Q}_i + \mathbf{A}_i\,\tilde{\mathbf{Q}}_{x_i}\,\mathbf{A}_i^T\,)^{-1} \qquad (5.1.5)$$

$$\hat{\mathbf{Q}}_{x_i} = (\,\mathbf{I} - \mathbf{G}_i\,\mathbf{A}_i\,)\,\tilde{\mathbf{Q}}_{x_i} \qquad (5.1.6)$$

are used starting in the first epoch with

$$\tilde{\mathbf{Q}}_{x_1} = \mathbf{Q}_{x^o} \qquad (5.1.7)$$

Simple simulations such as those above give the **precision** of the parameter estimates. They are based on the assumption that the functional and stochastic models are correct, and that there are no systematic errors. For deformation analysis the effects of systematic errors on the solution are of prime importance and the **accuracy** of the solution is required. Assumptions will still be required about the magnitude and behaviour of the systematic errors. These can be made more plausible than the simple assumption that systematic errors are zero.

5.2. COVARIANCE ANALYSIS IN LEAST SQUARES

The study of systematic errors in simulated least squares adjustments is known variously as **covariance analysis**, **sensitivity analysis** or **consider analysis** (Gelb, 1974; Bierman, 1977). These names arise because the **cross-covariance** matrix between systematic biases and the estimated parameters is used to determine the **sensitivity** of the solution to unadjusted parameters that are **considered** to be biased. The equations for covariance analysis in least squares adjustment may be found in a number of publications including Hatch & Goad (1973) and Bierman (1977). They are derived here as a means of introducing the notation and as a preparation for the more complex case of covariance analysis in a Kalman filter adjustment.

Systematic errors are considered to be errors in the *a priori* values of parameters that are not adjusted in the least squares (or Kalman filter) adjustment, but which are an integral part of the functional model. These may be physical constants that have been derived empirically and which are not known exactly. They may be observed, calculated or assumed values of variables used to reduce the observations or to generate the computed observations. They will often not appear explicitly in the model but appear implicitly in assumptions on which the model is based. For example, a triangulation adjustment model may be based on the assumptions that light waves travel in a straight line and that the theodolite and observed target are vertically over the station marks. The unadjusted parameters are then horizontal refraction and station eccentricity. The adjustment models for EDM and GPS observations may be based on an assumed speed of light through the atmosphere. The unadjusted parameter is then atmospheric delay. Errors in the *a priori* values of these parameters affect the misclose vector **w**, either through "correction" of the observations by an imperfect pre-processing step or as errors in the calculated observation. These **systematic errors** in the misclose vector **w** lead to perturbations in the solution. The model on which the observation equations are based (equation 5.1.1) is extended to explicitly include these unadjusted parameters. The complete model is

$$\mathbf{L} = f(\mathbf{x}, \mathbf{s}) \tag{5.2.1}$$

where $\mathbf{s}$ is the vector of unadjusted parameters. The *a priori* values $\mathbf{s}^o$ for these parameters have systematic errors $\delta\mathbf{s}$.

$$\delta \mathbf{s} = \mathbf{s}^o - \mathbf{s} \tag{5.2.2}$$

The **computed** misclose vector $\mathbf{w}^c$ is

$$\mathbf{w}^c = \boldsymbol{l} - \mathrm{f}(\mathbf{x}^o, \mathbf{s}^o) \tag{5.2.3}$$

whereas the **actual** or true misclose vector is

$$\begin{aligned} \mathbf{w}^a &= \boldsymbol{l} - \mathrm{f}(\mathbf{x}^o, \mathbf{s}) \\ &= \boldsymbol{l} - \mathrm{f}(\mathbf{x}^o, \mathbf{s}^o - \delta\mathbf{s}) \\ &= \boldsymbol{l} - \mathrm{f}(\mathbf{x}^o, \mathbf{s}^o) + \left(\frac{\partial \mathrm{f}}{\partial \mathrm{s}}\right)\delta\mathbf{s} \\ &= \mathbf{w}^c + \mathbf{A}_s\,\delta\mathbf{s} \end{aligned} \tag{5.2.4}$$

The matrix of partial derivatives $\mathbf{A}_s$ describes the **behaviour** of the systematic errors and the vector $\delta\mathbf{s}$ describes their **magnitudes**. Note that here the **error** $\delta\mathbf{s}$ is defined in the opposite sense to the **correction** $\delta\mathbf{x}$. The complete linearised model is

$$\mathbf{w}^c + \mathbf{v} = (\mathbf{A}_x \;\; \mathbf{A}_s)\begin{pmatrix} \delta\mathbf{x} \\ -\delta\mathbf{s} \end{pmatrix} \tag{5.2.5}$$

$$\mathbf{w}^c + \mathbf{A}_s\,\delta\mathbf{s} + \mathbf{v} = \mathbf{A}_x\,\delta\mathbf{x} \tag{5.2.6}$$

$$\mathbf{w}^a + \mathbf{v} = \mathbf{A}_x\,\delta\mathbf{x} \tag{5.2.7}$$

The model used in the computations is

$$\mathbf{w}^c + \mathbf{v} = \mathbf{A}_x\,\delta\mathbf{x} \tag{5.2.8}$$

The actual solution is

$$\begin{aligned} \delta\hat{\mathbf{x}}^a &= (\mathbf{A}_x{}^T\mathbf{P}\mathbf{A}_x + \mathbf{P}_{xo})^{-1}\left(\mathbf{A}_x{}^T\mathbf{P}\mathbf{w}^a + \mathbf{P}_{xo}(\boldsymbol{l}_x - \mathbf{x}^o)\right) \\ &= (\mathbf{A}_x{}^T\mathbf{P}\mathbf{A}_x + \mathbf{P}_{xo})^{-1}\left(\mathbf{A}_x{}^T\mathbf{P}\mathbf{w}^c + \mathbf{P}_{xo}(\boldsymbol{l}_x - \mathbf{x}^o)\right) \\ &\qquad + (\mathbf{A}_x{}^T\mathbf{P}\mathbf{A}_x + \mathbf{P}_{xo})^{-1}\,\mathbf{A}_x{}^T\mathbf{P}\mathbf{A}_s\,\delta\mathbf{s} \end{aligned} \tag{5.2.9}$$

(Note that this is the solution that would be obtained if the true values $\mathbf{s}$ were used. It is not the same as the solution that would be obtained if the parameters $\mathbf{s}$ were adjusted.) The computed solution is

$$\hat{\delta \mathbf{x}}^c = (\mathbf{A}_x^T \mathbf{P} \mathbf{A}_x + \mathbf{P}_{xo})^{-1} \left(\mathbf{A}_x^T \mathbf{P} \mathbf{w}^c + \mathbf{P}_{xo} (\boldsymbol{l}_x - \mathbf{x}^o) \right)$$

$$= \mathbf{Q}_{\hat{x}}^{c} \left(\mathbf{A}_x^T \mathbf{P} \mathbf{w}^c + \mathbf{P}_{xo} (\boldsymbol{l}_x - \mathbf{x}^o) \right) \qquad (5.2.10)$$

where

$$\mathbf{Q}_{\hat{x}}^{c} = (\mathbf{A}_x^T \mathbf{P} \mathbf{A}_x + \mathbf{P}_{xo})^{-1} \qquad (5.2.11)$$

is the **computed VCV** of the adjusted parameters and indicates their **precision**. The **perturbation** of the computed solution due to the systematic errors is therefore given by

$$\hat{\mathbf{p}} = -\mathbf{Q}_{\hat{x}}^{c} \mathbf{A}_x^T \mathbf{P} \mathbf{A}_s \, \delta \mathbf{s} \qquad (5.2.12)$$

where

$$\hat{\mathbf{p}} = \hat{\delta \mathbf{x}}^c - \hat{\delta \mathbf{x}}^a$$
$$= \hat{\mathbf{x}}^c - \hat{\mathbf{x}}^a \qquad (5.2.13)$$

Equation 5.2.12 may be written as

$$\hat{\mathbf{p}} = \mathbf{C} \delta \mathbf{s} \qquad (5.2.14)$$

$$\mathbf{C} = -\mathbf{Q}_{\hat{x}}^{c} \mathbf{A}_x^T \mathbf{P} \mathbf{A}_s \qquad (5.2.15)$$

where $\mathbf{C}$ is the cross covariance matrix between $\hat{\mathbf{p}}$ and $\delta \mathbf{s}$ and is known as the **sensitivity matrix**.

There are now two options for the use of equation 5.2.14. Given a vector of known systematic errors $\delta \mathbf{s}$, the perturbations $\hat{\mathbf{p}}$ may be calculated. Note that the **perturbations** to the solution vector can be calculated without calculating the solution vector itself. Thus, this technique can be used in simulations. This type of analysis is especially useful if there is a choice of different values for the *a priori* parameters $\mathbf{s}^o$ and the effect on the solution of this choice is required. For example, in GPS adjustment there may be several values for the coordinates of the fixed origin station(s) based on different earlier adjustments. There may be alternative integer values for the ambiguities that are to be fixed or a choice of different satellite ephemerides. This type of analysis is used by

the program **ORAN** and equation 5.2.12 appears in the mathematical description of the program (Hatch & Goad, 1973). It is an option of the program **DASH** developed for this investigation. (See Appendix F for a brief description of **ORAN** and **DASH**.)

The second option is to consider the systematic errors $\delta\mathbf{s}$ to be stochastic variables with known variances and covariances. In practice this is often closer to reality. The magnitude of the systematic errors is not known (if it were known the model could be corrected) but some idea of their variances and, possibly, covariances is often available. In other words, the vector $\delta\mathbf{s}$ is assumed to have zero expectation value and known VCV matrix $\mathbf{Q}_s$

$$E(\delta\mathbf{s}) = 0 \tag{5.2.16}$$

$$E(\delta\mathbf{s}\ \delta\mathbf{s}^T) = \mathbf{Q}_s \tag{5.2.17}$$

Applying the law of propagation of variances to the equation

$$\hat{\mathbf{x}}^a = \hat{\mathbf{x}}^c - \mathbf{C}\delta\mathbf{s} \tag{5.2.18}$$

and assuming that $\hat{\mathbf{x}}^c$ and $\delta\mathbf{s}$ are uncorrelated,

$$\begin{aligned}\mathbf{Q}_{\hat{x}}^{a} &= \mathbf{Q}_{\hat{x}}^{c} + \mathbf{C}\mathbf{Q}_s\mathbf{C}^T \\ &= \mathbf{Q}_{\hat{x}}^{c} + \mathbf{Q}_{\hat{p}}\end{aligned} \tag{5.2.19}$$

where $\mathbf{Q}_{\hat{x}}^{c}$ is the computed VCV of the parameters given in equation 5.2.11 and where the **perturbation covariance matrix** is

$$\mathbf{Q}_{\hat{p}} = \mathbf{C}\mathbf{Q}_s\mathbf{C}^T \tag{5.2.20}$$

The actual VCV matrix $\mathbf{Q}_{\hat{x}}^{a}$ is also called the **consider covariance matrix** (Bierman, 1977).

It was assumed above that the systematic errors are not correlated with the computed parameters. This is dependent on their being uncorrelated with the observations $\boldsymbol{l}$ or the pseudo observations of the parameters $\boldsymbol{l}_x$. If any of the

a priori values of the unadjusted parameters $\mathbf{s}^o$ have been derived from an earlier adjustment of the observations $\boldsymbol{l}$ (or observations correlated with $\boldsymbol{l}$) then this assumption will not be valid. Similarly it will not be valid if, for example, $\boldsymbol{l}_x$ and $\mathbf{s}^o$ were derived from a common adjustment. If the correlations between $\mathbf{s}^o$ and $\boldsymbol{l}_x$ or $\boldsymbol{l}$ are non zero and known, equation 5.2.19 can be extended to account for the cross-covariance matrix between the adjusted parameters and the perturbations. The assumption that these correlations are zero is usually reasonable and will be adopted for the remainder of this development.

The matrix $\mathbf{Q}_{\hat{p}}$ has two roles. Firstly as the VCV matrix of the perturbations $\hat{\mathbf{p}}$ it indicates the expected magnitude of the perturbations. Secondly, when added to the computed VCV $\mathbf{Q}_{\hat{x}}^c$ it gives the actual or consider VCV $\mathbf{Q}_{\hat{x}}^a$. This actual VCV indicates the **accuracy** of the adjusted parameters as distinct from $\mathbf{Q}_{\hat{x}}^c$ which indicates their **precision**. Its use as an measure of accuracy depends on:

(i) the completeness of the set of systematic errors $\delta\mathbf{s}$,
(ii) the correctness of $\mathbf{Q}_s$ and,
(iii) the correctness of the functional model contained in $\mathbf{A}_s$.

If the systematic errors are uncorrelated ($\mathbf{Q}_s$ diagonal) and only the diagonal terms of $\mathbf{Q}_{\hat{p}}$ are required, it may be more convenient to calculate the perturbations with equation 5.2.14 rather than the perturbation covariance matrix with equation 5.2.20. In this case the diagonal terms in $\mathbf{Q}_{\hat{p}}$ are equal to the squares of the perturbations $\hat{\mathbf{p}}$ provided that the systematic errors δs are chosen to be equal to their standard deviations σ_s. The perturbation variances may be obtained this way with less computational effort than by calculating the full VCV matrix. If the systematic errors are correlated with each other (e.g., tropospheric delay errors at different stations in a GPS adjustment) or if the covariances of the perturbations are required (e.g., for subsequent analysis of GPS baselines and networks) equation 5.2.20 should be used. Both options are available in the program **DASH**.

In both cases, the combined effect of **all** the systematic errors in $\delta\mathbf{s}$ is obtained. The effect of individual errors or groups of errors may also be of interest. From the sensitivity matrix $\mathbf{C}$, the **perturbation matrix** Π can be formed (Bierman, 1977).

$$\Pi = \mathbf{C}\ \mathbf{Diag}(\delta s_1, \delta s_2, \ldots, \delta s_n) \qquad (5.2.21)$$

This may be generated by multiplying each column of $\mathbf{C}$ by its corresponding error δs. The element $\Pi(i,j)$ gives the perturbation to the estimated parameter $\delta\hat{x}_i$ due to systematic error δs_j. In practice, the combined effect of groups of similar systematic errors may be required. For example, all errors in the satellite elements may be in one group and the tropospheric delay parameters in another group. The perturbation due to a group of systematic errors can be determined by adding the appropriate columns of the perturbation matrix.

The calculation of the effect of individual or grouped systematic errors can also be applied to perturbation covariance analysis. A perturbation covariance matrix $\mathbf{Q}_{\hat{p}i}$ could be generated for each systematic error δs_i.

$$\mathbf{Q}_{\hat{p}i} = \mathbf{c}_i\, \sigma_{si}^2\, \mathbf{c}_i^T \qquad (5.2.22)$$

where $\mathbf{c}_i$ is the i 'th column vector of the sensitivity matrix $\mathbf{C}$ and where σ_{si}^2 is the variance of systematic error parameter δs_i. If the systematic errors are uncorrelated then

$$\mathbf{Q}_{\hat{p}} = \mathbf{Q}_{\hat{p}1} + \mathbf{Q}_{\hat{p}2} + \ldots + \mathbf{Q}_{\hat{p}n} \qquad (5.2.23)$$

In practice, some of the systematic errors will be correlated with each other and the complete decomposition of 5.2.22 and 5.2.23 will not be possible. Also the large amount of data generated may be difficult to interpret. In general, $\delta\mathbf{s}$ may be partitioned into groups $\delta\mathbf{s}_i$ for which a perturbation covariance matrix $\mathbf{Q}_{\hat{p}i}$ is required and in such a way that there are no correlations between groups. Thus $\mathbf{Q}_s$ is a block diagonal matrix

$$\mathbf{Q}_s = \begin{pmatrix} \mathbf{Q}_{s1} & \mathbf{0} & \cdot & \cdot & \mathbf{0} \\ \mathbf{0} & \mathbf{Q}_{s2} & \cdot & \cdot & \mathbf{0} \\ \cdot & \cdot & \cdot & \cdot & \cdot \\ \cdot & \cdot & \cdot & \cdot & \cdot \\ \mathbf{0} & \mathbf{0} & \cdot & \cdot & \mathbf{Q}_{sn} \end{pmatrix} \qquad (5.2.24)$$

The sensitivity matrix $\mathbf{C}$ is also partitioned column-wise according to the partitioning of $\delta\mathbf{s}$

$$\mathbf{C} = (\mathbf{C}_1, \mathbf{C}_2, \ldots\ldots, \mathbf{C}_n) \tag{5.2.25}$$

Thus

$$\mathbf{Q}_{\hat{p}_i} = \mathbf{C}_i \ \mathbf{Q}_{si} \ \mathbf{C}_i^T \tag{5.2.26}$$

and equation 5.2.23 still applies.

This partitioning of $\delta\mathbf{s}$ into groups of parameters is simply for convenience in analysing the results. It does not preclude the possibility of having a separate group for each parameter (if $\mathbf{Q}_s$ diagonal) or one group for all parameters. It allows the effect of, say, all orbital errors on a GPS solution to be determined without the need to consider the effect of an error in each element of each satellite.

5.3. COVARIANCE ANALYSIS IN THE KALMAN FILTER

In Bierman (1977) the effects of un-estimated biases and random processes on a Kalman filter adjustment is considered. The derivation is similar to that above for least squares. The equations for Kalman filter adjustment are presented in section 4.3.3. It will be assumed that the parameters **x** and **s** are dynamically independent.

$$\begin{pmatrix} \delta \mathbf{x} \\ -\delta \mathbf{s} \end{pmatrix}_i = \begin{pmatrix} \Phi_x & \mathbf{0} \\ \mathbf{0} & \Phi_s \end{pmatrix}_i \begin{pmatrix} \delta \mathbf{x} \\ -\delta \mathbf{s} \end{pmatrix}_{i-1} + \begin{pmatrix} \mathbf{y} \\ -\mathbf{z} \end{pmatrix}_i \tag{5.3.1}$$

where **y** is the vector of dynamic model errors in the estimated parameters **x**, where **z** is the vector of dynamic model errors in the un-estimated parameters **s** , and where Φ_x and Φ_s are the transition matrices for vectors **x** and **s**. As above, $\delta\mathbf{x}$ is a vector of corrections and $\delta\mathbf{s}$ is a vector of errors.

Prediction

From equation 5.2.13

$$\hat{\mathbf{p}}_i = \delta\hat{\mathbf{x}}^c{}_i - \delta\hat{\mathbf{x}}^a{}_i \tag{5.3.2}$$

$$\tilde{\mathbf{p}}_i = \delta\tilde{\mathbf{x}}^c{}_i - \delta\tilde{\mathbf{x}}^a{}_i \tag{5.3.3}$$

The prediction step equations for the actual and computed parameters are

$$\begin{aligned} \delta\tilde{\mathbf{x}}^a{}_i &= \Phi_{x_i}\, \delta\hat{\mathbf{x}}^a{}_{i-1} \\ &= \Phi_{x_i}\, (\delta\hat{\mathbf{x}}^c{}_{i-1} - \hat{\mathbf{p}}_{i-1}) \end{aligned} \tag{5.3.4}$$

$$\delta\tilde{\mathbf{x}}^c{}_i = \Phi_{x_i}\, \delta\hat{\mathbf{x}}^c{}_{i-1} \tag{5.3.5}$$

and thus from equations 5.3.2, 5.3.3, 5.3.4 and 5.3.5

$$\tilde{\mathbf{p}}_i = \Phi_{x_i}\, \hat{\mathbf{p}}_{i-1} \tag{5.3.6}$$

It will be assumed, at this stage, that $\hat{\mathbf{p}}_i$ and $\delta\hat{\mathbf{x}}^c{}_i$ are uncorrelated as was assumed for the least squares adjustment above. This depends on the assumption that the *a priori* estimates of the systematic parameters $\mathbf{s}^o$ and the dynamic model errors $\mathbf{z}_i$ are uncorrelated with the observations l , the pseudo observed parameters l_x and the dynamic model corrections $\mathbf{y}_i$. Then,

$$\hat{\mathbf{Q}}_{x}{}^{a}{}_{i} = \hat{\mathbf{Q}}_{x}{}^{c}{}_{i} + \hat{\mathbf{Q}}_{p_i} \tag{5.3.7}$$

The prediction of the VCV matrices is given by

$$\begin{aligned} \tilde{\mathbf{Q}}_{x}{}^{a}{}_{i} &= \Phi_{x_i} \hat{\mathbf{Q}}_{x}{}^{a}{}_{i-1} \Phi_{x_i}{}^{T} + \mathbf{Q}_{y_i} \\ &= \Phi_{x_i} (\hat{\mathbf{Q}}_{x}{}^{c}{}_{i-1} + \hat{\mathbf{Q}}_{p_{i-1}}) \Phi_{x_i}{}^{T} + \mathbf{Q}_{y_i} \end{aligned} \tag{5.3.8}$$

and

$$\tilde{\mathbf{Q}}_{x}{}^{c}{}_{i} = \Phi_{x_i} \hat{\mathbf{Q}}_{x}{}^{c}{}_{i-1} \Phi_{x_i}{}^{T} + \mathbf{Q}_{y_i} \tag{5.3.9}$$

thus

$$\tilde{\mathbf{Q}}_{p_i} = \Phi_{x_i} \hat{\mathbf{Q}}_{p_{i-1}} \Phi_{x_i}{}^{T} \tag{5.3.10}$$

where the **predicted** VCV also satisfies the equation

$$\tilde{\mathbf{Q}}_{x}{}^{a}{}_{i} = \tilde{\mathbf{Q}}_{x}{}^{c}{}_{i} + \tilde{\mathbf{Q}}_{p_i} \tag{5.3.11}$$

From equation 5.3.1, the prediction equations for the systematic biases $\delta\mathbf{s}$ can be written.

$$\delta\mathbf{s}_i = \Phi_{s_i} \delta\mathbf{s}_{i-1} + \mathbf{z}_i \tag{5.3.12}$$

$$\mathbf{Q}_{s_i} = \Phi_{s_i} \mathbf{Q}_{s_{i-1}} \Phi_{s_i}{}^{T} + \mathbf{Q}_{z_i} \tag{5.3.13}$$

Filter

Next the equations for the filter or measurement update step are developed. Writing equation 5.2.4 for epoch i

$$\mathbf{w}^{a}{}_{i} = \mathbf{w}^{c}{}_{i} + \mathbf{A}_{s_i} \delta\mathbf{s}_i \tag{5.3.14}$$

The actual filter measurement update equation that would be obtained if the true values $\mathbf{s}_i$ were used is

$$\begin{aligned} \delta\hat{\mathbf{x}}^{a}{}_{i} &= (\mathbf{I} - \mathbf{G}_i\mathbf{A}_{x_i})\delta\tilde{\mathbf{x}}^{a}{}_{i} + \mathbf{G}_i\mathbf{w}^{a}{}_{i} \\ &= (\mathbf{I} - \mathbf{G}_i\mathbf{A}_{x_i})(\delta\tilde{\mathbf{x}}^{c}{}_{i} - \tilde{\mathbf{p}}_i) + \mathbf{G}_i\mathbf{w}^{c}{}_{i} + \mathbf{G}_i\mathbf{A}_{s_i}\delta\mathbf{s}_i \\ &= \delta\hat{\mathbf{x}}^{c}{}_{i} - (\mathbf{I} - \mathbf{G}_i\mathbf{A}_{x_i})\tilde{\mathbf{p}}_i + \mathbf{G}_i\mathbf{A}_{s_i}\delta\mathbf{s}_i \end{aligned} \tag{5.3.15}$$

where the update equation for the computed estimate is

$$\delta\hat{\mathbf{x}}^c_i = (\mathbf{I} - \mathbf{G}_i\mathbf{A}_{x_i})\delta\tilde{\mathbf{x}}^c_i + \mathbf{G}_i\mathbf{w}^c_i \tag{5.3.16}$$

and thus for the perturbations

$$\hat{\mathbf{p}}_i = (\mathbf{I} - \mathbf{G}_i\mathbf{A}_{x_i})\tilde{\mathbf{p}}_i - \mathbf{G}_i\mathbf{A}_{s_i}\,\delta\mathbf{s}_i \tag{5.3.17}$$

Note that these equations can also be derived by comparing the complete model (Bierman, 1977)

$$\begin{pmatrix}\delta\hat{\mathbf{x}}^a\\ -\delta\mathbf{s}\end{pmatrix}_i = \left[\begin{pmatrix}\mathbf{I} & \mathbf{0}\\ \mathbf{0} & \mathbf{I}\end{pmatrix} - \begin{pmatrix}\mathbf{G}\\ \mathbf{0}\end{pmatrix}_i (\mathbf{A}_x\ \mathbf{A}_s)_i\right]\begin{pmatrix}\delta\tilde{\mathbf{x}}^a\\ -\delta\mathbf{s}\end{pmatrix}_i + \begin{pmatrix}\mathbf{G}\\ \mathbf{0}\end{pmatrix}_i \mathbf{w}^c_i \tag{5.3.18}$$

with the model used in computations

$$\delta\hat{\mathbf{x}}^c_i = (\mathbf{I} - \mathbf{G}_i\mathbf{A}_{x_i})\,\delta\tilde{\mathbf{x}}^c_i + \mathbf{G}_i\,\mathbf{w}^c_i \tag{5.3.19}$$

The equations for the update of the VCV matrix of the perturbations is more complex than for the prediction step because the errors $\delta\mathbf{s}_i$ in epoch i are correlated with earlier epochs (equations 5.3.12, 5.3.13) and thus with $\tilde{\mathbf{p}}_i$. Systematic errors that are invariant in time will be considered first.

5.3.1 CONSTANT SYSTEMATIC ERRORS

For constant systematic errors, $\delta\mathbf{s}_i$ is not changed at the prediction stage (being constant), nor at the filter stage (being unadjusted) and thus

$$\delta\mathbf{s}_i = \delta\mathbf{s} \qquad \forall\, i \tag{5.3.20}$$

Given a sensitivity matrix $\hat{\mathbf{C}}_{i-1}$ for epoch i–1 where

$$\hat{\mathbf{p}}_{i-1} = \hat{\mathbf{C}}_{i-1}\delta\mathbf{s} \tag{5.3.21}$$

as in equation 5.2.14, and using equations 5.3.4, 5.3.2, 5.3.5 and 5.3.21

$$\begin{aligned}\delta\tilde{\mathbf{x}}^a_i &= \Phi_{x_i}\,\delta\hat{\mathbf{x}}^a_{i-1}\\ &= \Phi_{x_i}(\delta\hat{\mathbf{x}}^c_{i-1} - \hat{\mathbf{p}}_{i-1})\\ &= \delta\tilde{\mathbf{x}}^c_i - \Phi_{x_i}\hat{\mathbf{C}}_{i-1}\delta\mathbf{s}\end{aligned} \tag{5.3.22}$$

Thus

$$\begin{aligned}\tilde{\mathbf{p}}_i &= \delta\tilde{\mathbf{x}}^c_i - \delta\tilde{\mathbf{x}}^a_i \\ &= \Phi_{x_i}\hat{\mathbf{C}}_{i-1}\delta\mathbf{s} \\ &= \tilde{\mathbf{C}}_i\delta\mathbf{s}\end{aligned} \tag{5.3.23}$$

where

$$\tilde{\mathbf{C}}_i = \Phi_{x_i}\hat{\mathbf{C}}_{i-1} \tag{5.3.24}$$

From equation 5.3.17

$$\begin{aligned}\hat{\mathbf{p}}_i &= (\mathbf{I} - \mathbf{G}_i\mathbf{A}_{x_i})\tilde{\mathbf{p}}_i - \mathbf{G}_i\mathbf{A}_{s_i}\delta\mathbf{s} \\ &= (\mathbf{I} - \mathbf{G}_i\mathbf{A}_{x_i})\tilde{\mathbf{C}}_i\delta\mathbf{s} - \mathbf{G}_i\mathbf{A}_{s_i}\delta\mathbf{s} \\ &= \hat{\mathbf{C}}_i\delta\mathbf{s}\end{aligned} \tag{5.3.25}$$

where

$$\hat{\mathbf{C}}_i = (\mathbf{I} - \mathbf{G}_i\mathbf{A}_{x_i})\tilde{\mathbf{C}}_i - \mathbf{G}_i\mathbf{A}_{s_i} \tag{5.3.26}$$

Equations 5.3.24 and 5.3.26 can be used to generate the sensitivity matrix at each epoch and thus to calculate the perturbations and perturbation VCV using equation 5.3.25 and

$$\hat{\mathbf{Q}}_{p_i} = \hat{\mathbf{C}}_i\mathbf{Q}_s\hat{\mathbf{C}}_i^T \tag{5.3.27}$$

The calculation starts at epoch 1 with

$$\tilde{\mathbf{C}}_1 = \mathbf{0} \tag{5.3.28}$$

$$\hat{\mathbf{C}}_1 = -\mathbf{G}_1\mathbf{A}_{s_1} \tag{5.3.29}$$

The vector of systematic errors may be partitioned into groups of similar errors as in section 5.2 above and a consider covariance matrix generated for each group.

5.3.2 DYNAMIC SYSTEMATIC ERRORS

To use equations 5.3.6 and 5.3.17 to calculate the perturbation vector, the dynamic model errors $\mathbf{z}_i$ in equation 5.3.12 must be specified at each epoch. It is more convenient to treat these errors as stochastic variables with zero mean and known $\mathbf{Q}_z$. Equation 5.3.10 can be used in the prediction step to calculate the predicted consider covariance matrix. To apply the propagation of variances to equation 5.3.17 , the cross covariance matrix between $\tilde{\mathbf{p}}_i$ and $\delta\mathbf{s}_i$ is required and must be generated at the prediction and filter stage as with the other VCV matrices. To derive the prediction and filter equations for this cross covariance matrix, the combined vector

$$\hat{\mathbf{q}}_i = \begin{pmatrix} \hat{\mathbf{p}} \\ \delta\mathbf{s} \end{pmatrix}_i \tag{5.3.30}$$

is formed with VCV matrix

$$\hat{\mathbf{Q}}_{q_i} = \begin{pmatrix} \hat{\mathbf{Q}}_p & \hat{\mathbf{Q}}_{ps} \\ \hat{\mathbf{Q}}_{ps}^T & \hat{\mathbf{Q}}_s \end{pmatrix}_i \tag{5.3.31}$$

From equations 5.3.6 and 5.3.12

$$\tilde{\mathbf{q}}_i = \begin{pmatrix} \tilde{\mathbf{p}} \\ \delta\mathbf{s} \end{pmatrix}_i = \begin{pmatrix} \Phi_x & \mathbf{0} \\ \mathbf{0} & \Phi_s \end{pmatrix}_i \begin{pmatrix} \hat{\mathbf{p}} \\ \delta\mathbf{s} \end{pmatrix}_{i-1} + \begin{pmatrix} \mathbf{0} \\ \mathbf{z} \end{pmatrix}_i \tag{5.3.32}$$

From equations 5.3.10 and 5.3.13

$$\tilde{\mathbf{Q}}_{q_i} = \begin{pmatrix} \Phi_x & \mathbf{0} \\ \mathbf{0} & \Phi_s \end{pmatrix}_i \hat{\mathbf{Q}}_{q_{i-1}} \begin{pmatrix} \Phi_x^T & \mathbf{0} \\ \mathbf{0} & \Phi_s^T \end{pmatrix}_i + \begin{pmatrix} \mathbf{0} & \mathbf{0} \\ \mathbf{0} & \mathbf{Q}_z \end{pmatrix}_i \tag{5.3.33}$$

and thus

$$\tilde{\mathbf{Q}}_{p_i} = \Phi_{x_i} \hat{\mathbf{Q}}_{p_{i-1}} \Phi_{x_i}^T \tag{5.3.34}$$

$$\tilde{\mathbf{Q}}_{ps_i} = \Phi_{x_i} \hat{\mathbf{Q}}_{ps_{i-1}} \Phi_{s_i}^T \tag{5.3.35}$$

$$\tilde{\mathbf{Q}}_{s_i} = \Phi_{s_i} \hat{\mathbf{Q}}_{s_{i-1}} \Phi_{s_i}^T + \mathbf{Q}_{z_i} \tag{5.3.36}$$

From equation 5.3.17 (remembering that $\delta \mathbf{s}_i$ is unadjusted and thus unaltered in the filter step)

$$\hat{\mathbf{q}}_i = \begin{pmatrix} \hat{\mathbf{p}} \\ \delta \mathbf{s} \end{pmatrix}_i = \begin{pmatrix} \mathbf{I} - \mathbf{G}\mathbf{A}_x & -\mathbf{G}\mathbf{A}_s \\ \mathbf{0} & \mathbf{I} \end{pmatrix}_i \begin{pmatrix} \tilde{\mathbf{p}} \\ \delta \mathbf{s} \end{pmatrix}_i \tag{5.3.37}$$

and propagating the VCV

$$\hat{\mathbf{Q}}_{q_i} = \begin{pmatrix} \mathbf{I} - \mathbf{G}\mathbf{A}_x & -\mathbf{G}\mathbf{A}_s \\ \mathbf{0} & \mathbf{I} \end{pmatrix}_i \tilde{\mathbf{Q}}_{q_i} \begin{pmatrix} (\mathbf{I} - \mathbf{G}\mathbf{A}_x)^T & \mathbf{0} \\ -(\mathbf{G}\mathbf{A}_s)^T & \mathbf{I} \end{pmatrix}_i \tag{5.3.38}$$

Thus

$$\hat{\mathbf{Q}}_{p_i} = (\mathbf{I} - \mathbf{G}_i\mathbf{A}_{x_i})\,\tilde{\mathbf{Q}}_{p_i}\,(\mathbf{I} - \mathbf{G}_i\mathbf{A}_{x_i})^T - (\mathbf{I} - \mathbf{G}_i\mathbf{A}_{x_i})\,\tilde{\mathbf{Q}}_{ps_i}\,\mathbf{A}_{s_i}{}^T\mathbf{G}_i{}^T - \mathbf{G}_i\mathbf{A}_{s_i}\,\tilde{\mathbf{Q}}_{ps_i}{}^T(\mathbf{I} - \mathbf{G}_i\mathbf{A}_{x_i})^T + \mathbf{G}_i\mathbf{A}_{s_i}\,\tilde{\mathbf{Q}}_{s_i}\,\mathbf{A}_{s_i}{}^T\mathbf{G}_i{}^T \tag{5.3.39}$$

$$\hat{\mathbf{Q}}_{ps_i} = (\mathbf{I} - \mathbf{G}_i\mathbf{A}_{x_i})\,\tilde{\mathbf{Q}}_{ps_i} - \mathbf{G}_i\mathbf{A}_{s_i}\,\tilde{\mathbf{Q}}_{s_i} \tag{5.3.40}$$

$$\hat{\mathbf{Q}}_{s_i} = \tilde{\mathbf{Q}}_{s_i} \tag{5.3.41}$$

This sequence is started at the first epoch with

$$\tilde{\mathbf{Q}}_{p_1} = \mathbf{0} \tag{5.3.42}$$

$$\tilde{\mathbf{Q}}_{ps_1} = \tilde{\mathbf{Q}}_{sp_1} = \mathbf{0} \tag{5.3.43}$$

$$\tilde{\mathbf{Q}}_{s_1} = \mathbf{Q}_{s^o} \tag{5.3.44}$$

5.4 DYNAMIC MODEL ERRORS

In section 5.3.2 above, the effect of dynamic errors in the systematic or unadjusted parameters was considered. Now the effect of a time dependence in adjusted parameters that have been modelled as constants is investigated. In a standard least squares adjustment, all adjusted parameters implicitly have a constant dynamic model (unless a new parameter is introduced for each epoch as with GPS clock errors). Even where a time dependent function such as a polynomial is used to model a variable, the estimated parameters are the constant coefficients of that function.

What, then, is the effect of choosing a constant dynamic model, explicitly in a Kalman filter adjustment or implicitly in a least squares adjustment, for parameters that change with time? This is a special case of the situation where an incorrect dynamic model has been used for some or all of the adjusted parameters. The equations for this general situation are developed first and then applied to the special case. The principal application for this study is the tropospheric delay which is sometimes modelled by a set of constant estimated parameters in GPS and VLBI least squares adjustments.

5.4.1 GENERAL CASE: ERRONEOUS DYNAMIC MODEL FOR ADJUSTED PARAMETERS

Suppose that an incorrect dynamic model has been used for some or all of the adjusted parameters. The dynamic model used in the computations is

$$\delta \mathbf{x}^c_i = \Phi_{c_i}\, \delta \mathbf{x}^c_{i-1} + \mathbf{y}^c_i \qquad (5.4.1)$$

and the actual dynamic model is

$$\delta \mathbf{x}^a_i = \Phi_{a_i}\, \delta \mathbf{x}^a_{i-1} + \mathbf{y}^a_i \qquad (5.4.2)$$

Prediction

At the prediction step

$$\delta \tilde{\mathbf{x}}^c_i = \Phi_{c_i}\, \delta \hat{\mathbf{x}}^c_{i-1} \qquad (5.4.3)$$

$$\delta \tilde{\mathbf{x}}^a_i = \Phi_{a_i}\, \delta \hat{\mathbf{x}}^a_{i-1} \qquad (5.4.4)$$

and the perturbations are defined as in equations 5.3.2 and 5.3.3. Thus

$$\mathbf{p}_i = \delta\mathbf{x}^c{}_i - \delta\mathbf{x}^a{}_i \tag{5.4.5}$$

$$\tilde{\mathbf{p}}_i = \delta\tilde{\mathbf{x}}^c{}_i - \delta\tilde{\mathbf{x}}^a{}_i \tag{5.4.6}$$

$$\hat{\mathbf{p}}_i = \delta\hat{\mathbf{x}}^c{}_i - \delta\hat{\mathbf{x}}^a{}_i \tag{5.4.7}$$

Defining

$$\Delta\Phi_i = \Phi_{c_i} - \Phi_{a_i} \tag{5.4.8}$$

$$\Delta\mathbf{y}_i = \mathbf{y}_{c_i} - \mathbf{y}_{a_i} \tag{5.4.9}$$

Then from equations 5.4.1, 5.4.2, 5.4.5, 5.4.8 and 5.4.9

$$\begin{aligned}\mathbf{p}_i &= \Phi_{c_i}\,\delta\hat{\mathbf{x}}^c{}_{i-1} + \Phi_{a_i}\,\delta\hat{\mathbf{x}}^a{}_{i-1} + \mathbf{y}_{c_i} - \mathbf{y}_{a_i} \\ &= \Phi_{a_i}\,\mathbf{p}_{i-1} + \Delta\Phi_i\,\delta\mathbf{x}^c{}_{i-1} + \Delta\mathbf{y}_i\end{aligned} \tag{5.4.10}$$

and similarly

$$\tilde{\mathbf{p}}_i = \Phi_{a_i}\,\hat{\mathbf{p}}_{i-1} + \Delta\Phi_i\,\delta\hat{\mathbf{x}}^c{}_{i-1} \tag{5.4.10}$$

thus

$$(\mathbf{p}_i - \tilde{\mathbf{p}}_i) = \Phi_{a_i}(\mathbf{p}_{i-1} - \hat{\mathbf{p}}_{i-1}) + \Delta\Phi_i(\delta\mathbf{x}^c{}_{i-1} - \delta\hat{\mathbf{x}}^c{}_{i-1}) + \Delta\mathbf{y}_i \tag{5.4.11}$$

These perturbations, as distinct from those described in the sections above, depend on the estimated parameters. In the absence of observations, the perturbations cannot be calculated but their VCV matrix can be calculated. The VCV of the perturbations is propagated using

$$\tilde{\mathbf{Q}}_{p_i} = E\left[(\mathbf{p}_i - \tilde{\mathbf{p}}_i)(\mathbf{p}_i - \tilde{\mathbf{p}}_i)^T\right] \tag{5.4.12}$$

$$\hat{\mathbf{Q}}_{p_i} = E\left[(\mathbf{p}_i - \hat{\mathbf{p}}_i)(\mathbf{p}_i - \hat{\mathbf{p}}_i)^T\right] \tag{5.4.13}$$

$$\hat{\mathbf{Q}}_{x^c{}_i} = E\left[(\delta\mathbf{x}^c{}_i - \delta\hat{\mathbf{x}}^c{}_i)(\delta\mathbf{x}^c{}_i - \delta\hat{\mathbf{x}}^c{}_i)^T\right] \tag{5.4.14}$$

The cross covariance matrix between $\hat{\mathbf{p}}$ and $\hat{\mathbf{x}}^c$ (and between $\tilde{\mathbf{p}}$ and $\tilde{\mathbf{x}}^c$) is also required. Forming the combined vector of perturbation errors and estimated parameter errors.

$$\tilde{\mathbf{r}}_i = \begin{pmatrix} (\mathbf{p} - \tilde{\mathbf{p}}) \\ (\delta\mathbf{x}^c - \delta\tilde{\mathbf{x}}^c) \end{pmatrix}_i \tag{5.4.15}$$

$$\hat{\mathbf{r}}_i = \begin{pmatrix} (\mathbf{p} - \hat{\mathbf{p}}) \\ (\delta\mathbf{x}^c - \delta\hat{\mathbf{x}}^c) \end{pmatrix}_i \tag{5.4.16}$$

with VCV matrix

$$\hat{\mathbf{Q}}_{r_i} = \begin{pmatrix} \hat{\mathbf{Q}}_p & \hat{\mathbf{Q}}_{pxc} \\ \hat{\mathbf{Q}}_{xcp} & \hat{\mathbf{Q}}_{xc} \end{pmatrix}_i \tag{5.4.17}$$

Then from equations 5.4.1, 5.4.3 and 5.4.11

$$\begin{pmatrix} (\mathbf{p} - \tilde{\mathbf{p}}) \\ (\delta\mathbf{x}^c - \delta\tilde{\mathbf{x}}^c) \end{pmatrix}_i = \begin{pmatrix} \Phi_a & \Delta\Phi \\ \mathbf{0} & \Phi_c \end{pmatrix}_i \begin{pmatrix} (\mathbf{p} - \hat{\mathbf{p}}) \\ (\delta\mathbf{x}^c - \delta\hat{\mathbf{x}}^c) \end{pmatrix}_{i-1} + \begin{pmatrix} \Delta\mathbf{y} \\ \mathbf{y}^c \end{pmatrix}_i \tag{5.4.18}$$

The VCV propagates according to

$$\tilde{\mathbf{Q}}_{r_i} = \begin{pmatrix} \Phi_a & \Delta\Phi \\ \mathbf{0} & \Phi_c \end{pmatrix}_i \hat{\mathbf{Q}}_{r_{i-1}} \begin{pmatrix} \Phi_a{}^T & \mathbf{0} \\ \Delta\Phi^T & \Phi_c{}^T \end{pmatrix}_i + \begin{pmatrix} \mathbf{Q}_{\Delta y} & \mathbf{Q}_{\Delta y y^c} \\ \mathbf{Q}_{y^c \Delta y} & \mathbf{Q}_{y^c} \end{pmatrix}_i \tag{5.4.19}$$

and thus

$$\tilde{\mathbf{Q}}_{p_i} = \Phi_{a_i} \hat{\mathbf{Q}}_{p_{i-1}} \Phi_{a_i}{}^T + \Delta\Phi_i \hat{\mathbf{Q}}_{xc_{i-1}} \Delta\Phi_i{}^T + \Phi_{a_i} \hat{\mathbf{Q}}_{pxc_{i-1}} \Delta\Phi_i{}^T + \Delta\Phi_i \hat{\mathbf{Q}}_{pxc}{}^T{}_{i-1} \Phi_{a_i}{}^T + \mathbf{Q}_{\Delta y_i} \tag{5.4.20}$$

$$\tilde{\mathbf{Q}}_{pxc_i} = \Phi_{a_i} \hat{\mathbf{Q}}_{pxc_{i-1}} \Phi_{c_i}{}^T + \Delta\Phi_i \hat{\mathbf{Q}}_{xc_{i-1}} \Phi_{c_i}{}^T + \mathbf{Q}_{\Delta y y^c{}_i} \tag{5.4.21}$$

$$\tilde{\mathbf{Q}}_{xc_i} = \Phi_{c_i} \hat{\mathbf{Q}}_{xc_{i-1}} \Phi_{c_i}{}^T + \mathbf{Q}_{y^c{}_i} \tag{5.4.22}$$

Filter

The equations for the actual and computed adjusted parameters at the filter step are

$$\begin{aligned}\hat{\delta\mathbf{x}}^{a}_{i} &= (\mathbf{I} - \mathbf{G}_i\mathbf{A}_i)\tilde{\delta\mathbf{x}}^{a}_{i} + \mathbf{G}_i\mathbf{w}_i \\ &= (\mathbf{I} - \mathbf{G}_i\mathbf{A}_i)\tilde{\delta\mathbf{x}}^{c}_{i} - (\mathbf{I} - \mathbf{G}_i\mathbf{A}_i)\tilde{\mathbf{p}}_i + \mathbf{G}_i\mathbf{w}_i \end{aligned} \quad (5.4.23)$$

$$\hat{\delta\mathbf{x}}^{c}_{i} = (\mathbf{I} - \mathbf{G}_i\mathbf{A}_i)\tilde{\delta\mathbf{x}}^{c}_{i} + \mathbf{G}_i\mathbf{w}_i \quad (5.4.24)$$

Thus from equations 5.4.7, 5.4.23, 5.4.24

$$\hat{\mathbf{p}}_i = (\mathbf{I} - \mathbf{G}_i\mathbf{A}_i)\tilde{\mathbf{p}}_i \quad (5.4.25)$$

Forming the combined vector $\hat{\mathbf{r}}_i$

$$\hat{\mathbf{r}}_i = \begin{pmatrix} \hat{\mathbf{p}} \\ \hat{\delta\mathbf{x}}^{c} \end{pmatrix}_i$$

$$= \begin{pmatrix} \mathbf{I} - \mathbf{G}\mathbf{A} & \mathbf{0} \\ \mathbf{0} & \mathbf{I} - \mathbf{G}\mathbf{A} \end{pmatrix}_i \begin{pmatrix} \tilde{\mathbf{p}} \\ \tilde{\delta\mathbf{x}}^{c} \end{pmatrix}_i + \begin{pmatrix} \mathbf{0} \\ \mathbf{G} \end{pmatrix}_i \mathbf{w}_i \quad (5.4.26)$$

and propagating the VCV

$$\hat{\mathbf{Q}}_{r_i} = \begin{pmatrix} \mathbf{I}-\mathbf{G}\mathbf{A} & \mathbf{0} \\ \mathbf{0} & \mathbf{I}-\mathbf{G}\mathbf{A} \end{pmatrix}_i \tilde{\mathbf{Q}}_{r_i} \begin{pmatrix} (\mathbf{I}-\mathbf{G}\mathbf{A})^T & \mathbf{0} \\ \mathbf{0} & (\mathbf{I}-\mathbf{G}\mathbf{A})^T \end{pmatrix}_i$$

$$+ \begin{pmatrix} \mathbf{0} \\ \mathbf{G} \end{pmatrix}_i \mathbf{Q}_i \begin{pmatrix} \mathbf{0} & \mathbf{G}^T \end{pmatrix}_i \quad (5.4.27)$$

Thus

$$\hat{\mathbf{Q}}_{p_i} = (\mathbf{I} - \mathbf{G}_i\mathbf{A}_i)\,\tilde{\mathbf{Q}}_{p_i}\,(\mathbf{I} - \mathbf{G}_i\mathbf{A}_i)^T \quad (5.4.28)$$

$$\hat{\mathbf{Q}}_{pxc_i} = (\mathbf{I} - \mathbf{G}_i\mathbf{A}_i)\,\tilde{\mathbf{Q}}_{pxc_i}\,(\mathbf{I} - \mathbf{G}_i\mathbf{A}_i)^T \quad (5.4.29)$$

$$\hat{\mathbf{Q}}_{xc_i} = (\mathbf{I} - \mathbf{G}_i\mathbf{A}_i)\tilde{\mathbf{Q}}_{xc_i}\,(\mathbf{I} - \mathbf{G}_i\mathbf{A}_i)^T + \mathbf{G}_i\,\mathbf{Q}_i\,\mathbf{G}_i^T \quad (5.4.30)$$

This sequence starts at the first epoch with

$$\tilde{\mathbf{Q}}_{p_1} = \mathbf{0} \tag{5.4.31}$$

$$\tilde{\mathbf{Q}}_{pxc_1} = \tilde{\mathbf{Q}}_{xcp_1} = \mathbf{0} \tag{5.4.32}$$

$$\tilde{\mathbf{Q}}_{xc_1} = \mathbf{Q}_{xo} \tag{5.4.33}$$

The consider covariance matrix is calculated by applying the propagation of variances to the equation 5.4.7

$$\hat{\mathbf{Q}}_{xa_i} = \hat{\mathbf{Q}}_{xc_i} + \hat{\mathbf{Q}}_{p_i} - \hat{\mathbf{Q}}_{pxc_i} - \hat{\mathbf{Q}}_{pxc_i}^T \tag{5.4.34}$$

and thus the contribution to the consider covariance matrix is

$$\Delta\hat{\mathbf{Q}}_{x_i} = \hat{\mathbf{Q}}_{p_i} - \hat{\mathbf{Q}}_{pxc_i} - \hat{\mathbf{Q}}_{pxc_i}^T \tag{5.4.35}$$

where

$$\hat{\mathbf{Q}}_{xa_i} = \hat{\mathbf{Q}}_{xc_i} + \Delta\hat{\mathbf{Q}}_{x_i} \tag{5.4.36}$$

Note that $\Delta\hat{\mathbf{Q}}_{x_i}$ is not necessarily a positive definite matrix. In fact it is possible for the consider variances to be smaller than the computed variances (Gelb, 1974) with $\Delta\hat{\mathbf{Q}}_{x_i}$ having a generally negative contribution to the consider covariance matrix.

5.4.2 SPECIAL CASE: DYNAMIC ERRORS FOR CONSTANT ADJUSTED PARAMETERS

These equations are now applied to the case where a constant parameter dynamic model has been used for time varying parameters. The **x** vector is partitioned into the vectors **d** with correct dynamic model and **e** with erroneous dynamic model.

$$\mathbf{x} = \begin{pmatrix} \mathbf{d} \\ \mathbf{e} \end{pmatrix} \tag{5.4.37}$$

The actual and computed dynamic models are given by

$$\Phi_a = \begin{pmatrix} \Phi_d & \mathbf{0} \\ \mathbf{0} & \Phi_e \end{pmatrix} \tag{5.4.38}$$

$$\Phi_c = \begin{pmatrix} \Phi_d & \mathbf{0} \\ \mathbf{0} & \mathbf{I} \end{pmatrix} \tag{5.4.39}$$

$$\mathbf{y}^a = \begin{pmatrix} \mathbf{y}^d \\ \mathbf{y}^e \end{pmatrix} \tag{5.4.40}$$

$$\mathbf{y}^c = \begin{pmatrix} \mathbf{y}^d \\ \mathbf{0} \end{pmatrix} \tag{5.4.41}$$

$$\mathbf{Q}_{ya} = \begin{pmatrix} \mathbf{Q}_{yd} & \mathbf{0} \\ \mathbf{0} & \mathbf{Q}_{ye} \end{pmatrix} \tag{5.4.42}$$

$$\mathbf{Q}_{yc} = \begin{pmatrix} \mathbf{Q}_{yd} & \mathbf{0} \\ \mathbf{0} & \mathbf{0} \end{pmatrix} \tag{5.4.43}$$

and thus

$$\Delta\Phi = \begin{pmatrix} \mathbf{0} & \mathbf{0} \\ \mathbf{0} & \mathbf{I} - \Phi_e \end{pmatrix} \tag{5.4.44}$$

$$\Delta\mathbf{y} = \begin{pmatrix} \mathbf{0} \\ -\mathbf{y}^e \end{pmatrix} \tag{5.4.45}$$

$$\mathbf{Q}_{\Delta y} = \begin{pmatrix} \mathbf{0} & \mathbf{0} \\ \mathbf{0} & \mathbf{Q}_{ye} \end{pmatrix} \tag{5.4.46}$$

From equations 5.4.41 and 5.4.45, it is seen that $\mathbf{y}^c$ and $\Delta\mathbf{y}$ are uncorrelated provided that $\mathbf{y}^d$ and $\mathbf{y}^e$ are uncorrelated as has been assumed (equation 5.4.42). Thus

$$\mathbf{Q}_{\Delta y y^c} = \mathbf{0} \tag{5.4.47}$$

Now equations 5.4.38, 5.4.39, 5.4.43, 5.4.44, 5.4.46 and 5.4.47 may be substituted into the prediction equations 5.4.20, 5.4.21 and 5.4.22. Equations 5.4.28, 5.4.29, and 5.4.30 are used at the filter step and the initial values are given by equations 5.4.31, 5.4.32 and 5.4.33.

5.5. CHOICE OF GAIN MATRIX

In Kalman filtering the equation for the gain matrix

$$\mathbf{G}_i = \tilde{\mathbf{Q}}_{x_i} \mathbf{A}_i^T (\mathbf{Q}_i + \mathbf{A}_i \tilde{\mathbf{Q}}_{x_i} \mathbf{A}_i^T)^{-1} \qquad (5.5.1)$$

is based on the least squares condition that

$$\sum_i \left(\mathbf{v}_i^T \mathbf{P}_i \mathbf{v}_i \; + \; \delta\hat{\mathbf{x}}_i^T \mathbf{Q}_{xo_i}^{-1} \delta\hat{\mathbf{x}}_i \; + \; \hat{\mathbf{y}}_i^T \mathbf{Q}_{y_i}^{-1} \hat{\mathbf{y}}_i \right) = \text{minimum} \qquad (5.5.2)$$

If the adjustment model is correct and if the observations, *a priori* parameters and dynamic model errors are normally distributed then the matrix $\tilde{\mathbf{Q}}_{x_i}$ is also the VCV matrix of the predicted parameters $\tilde{\mathbf{x}}_i$. In this case the filter is said to be optimal.

However, this investigation includes sub-optimal filters where there are systematic errors in some unadjusted parameters and errors in the dynamic modelling of some adjusted parameters. The choice of sub-optimal filter may be made to minimise computer storage and execution time or due to limits on our knowledge of the true model. The use of constant parameters to model time dependent variables like tropospheric delay may be so that a least squares adjustment can be used instead of the more complicated Kalman filter. Whatever the reason for using a sub-optimal filter, the computed matrix $\tilde{\mathbf{Q}}_{x_i}$ above, now written $\tilde{\mathbf{Q}}_{xc_i}$, is not the same as the actual VCV of the predicted parameters, written $\tilde{\mathbf{Q}}_{xa_i}$. Which of these two matrices should be used to calculate the gain matrix in equation 5.5.1?

If the least squares condition of equation 5.5.2 is to be applied, $\tilde{\mathbf{Q}}_{xc_i}$ is used. The equations developed in the sections above can then be used to determine the actual covariance matrix of the **least squares solution** and the perturbations (or perturbation VCV) of that solution. If $\tilde{\mathbf{Q}}_{xa_i}$ were to be used to calculate the gain matrix, the result would be the **consider filter solution** (Bierman, 1977). This is not the least squares solution, nor is it the optimum solution which is only obtained by estimating all uncertain parameters with the correct model. The distinction between **consider analysis** and **consider filtering** is noted by Bierman (1977) where a discussion is also found on some of the gain matrices that can be used in sub-optimal filters.

The VCV of the consider filter solution is of interest only if the data is to be adjusted with such a filter. If the data is to be adjusted by application of the least squares condition of equation 5.5.2, then the perturbations and the actual or consider covariance matrix of that solution are required. The consider filter will not be used for simulated adjustments in this investigation and thus in all cases the gain matrix is calculated with

$$\mathbf{G}_i = \tilde{\mathbf{Q}}_{xc_i} \mathbf{A}_i^T (\mathbf{Q}_i + \mathbf{A}_i \tilde{\mathbf{Q}}_{xc_i} \mathbf{A}_i^T)^{-1} \qquad (5.5.3)$$

5.6. COVARIANCE ANALYSIS AND DEFORMATION

5.6.1 THE COVARIANCE ANALYSIS EQUATIONS

In section 4.5 the deformation model was presented that will be used to study the effects of systematic errors on deformation parameters. Now that the equations of covariance analysis have been developed, they can be applied to this case. The linearised general model $F(\mathbf{d},\mathbf{x})$ in deformation parameters $\mathbf{d}$ and observed coordinates $\mathbf{x}$ is (equation 4.5.1)

$$\mathbf{x}_{GPSj} - (\mathbf{S} + \mathbf{R})\,\mathbf{x}_{TER} - \mathbf{t}_j = \mathbf{0} = F(\mathbf{d},\mathbf{x}) \tag{5.6.1}$$

where $\mathbf{x}_{GPSj}$ is the GPS coordinates of sub-net j, $\mathbf{x}_{TER}$ is the terrestrial coordinates of the same points, $\mathbf{S}$ and $\mathbf{R}$ are the strain and rotation matrices and $\mathbf{t}_j$ is the vector of translations for sub-net j. From the *a priori* estimates of the parameters $\mathbf{d}_o$, the *a priori* strain, rotation and translation matrices are $\mathbf{S}_o$, $\mathbf{R}_o$ and $\mathbf{t}_{oj}$. The misclose vector $\mathbf{w}_j$ is simply

$$\mathbf{w}_j = -F(\mathbf{d}_o,\mathbf{x}_j) = (\mathbf{S}_o + \mathbf{R}_o)\,\mathbf{x}_{TER} + \mathbf{t}_{oj} - \mathbf{x}_{GPSj} \tag{5.6.2}$$

It will be assumed for simplicity that only one set of coordinates is affected by systematic errors, in this case the GPS coordinates. These have perturbations $\mathbf{p}_{xj}$ which represent the difference between the computed GPS coordinates $\mathbf{x}^c_{GPSj}$ used as observations in the deformation adjustment, and the actual coordinates $\mathbf{x}^a_{GPSj}$ that would have been obtained if no systematic errors had been present in the GPS adjustment. Thus

$$\mathbf{p}_{xj} = \mathbf{x}^c_{GPSj} - \mathbf{x}^a_{GPSj} \tag{5.6.3}$$

$$\mathbf{w}^c_j = (\mathbf{S}_o + \mathbf{R}_o)\,\mathbf{x}_{TER} + \mathbf{t}_{oj} - \mathbf{x}^c_{GPSj} \tag{5.6.4}$$

$$\begin{aligned}\mathbf{w}^a_j &= (\mathbf{S}_o + \mathbf{R}_o)\,\mathbf{x}_{TER} + \mathbf{t}_{oj} - \mathbf{x}^a_{GPSj} \\ &= \mathbf{w}^c_j + \mathbf{p}_{xj}\end{aligned} \tag{5.6.5}$$

The solution to the deformation adjustment is given by equation 4.5.8

$$\hat{\delta\mathbf{d}} = \left(\mathbf{A}^T(\mathbf{B}\mathbf{Q}\mathbf{B}^T)^{-1}\mathbf{A} + \mathbf{Q}_o^{-1}\right)^{-1}\mathbf{A}^T(\mathbf{B}\mathbf{Q}\mathbf{B}^T)^{-1}\mathbf{w} \tag{4.5.8}$$

where

$$\mathbf{w}^T = (\mathbf{w}_1^T, \mathbf{w}_2^T, \ldots, \mathbf{w}_j^T, \ldots) \tag{5.6.7}$$

and thus the computed and actual vectors of estimated deformation parameters are

$$\hat{\delta \mathbf{d}}^c = \left(\mathbf{A}^T (\mathbf{B}\mathbf{Q}\mathbf{B}^T)^{-1}\mathbf{A} + \mathbf{Q}_o^{-1}\right)^{-1} \mathbf{A}^T (\mathbf{B}\mathbf{Q}\mathbf{B}^T)^{-1}\mathbf{w}^c \tag{5.6.8}$$

$$\begin{aligned}\hat{\delta \mathbf{d}}^a &= \left(\mathbf{A}^T (\mathbf{B}\mathbf{Q}\mathbf{B}^T)^{-1}\mathbf{A} + \mathbf{Q}_o^{-1}\right)^{-1} \mathbf{A}^T (\mathbf{B}\mathbf{Q}\mathbf{B}^T)^{-1}\mathbf{w}^a \\ &= \hat{\delta \mathbf{d}}^c + \left(\mathbf{A}^T (\mathbf{B}\mathbf{Q}\mathbf{B}^T)^{-1}\mathbf{A} + \mathbf{Q}_o^{-1}\right)^{-1} \mathbf{A}^T (\mathbf{B}\mathbf{Q}\mathbf{B}^T)^{-1}\mathbf{p}_x \end{aligned} \tag{5.6.9}$$

where

$$\mathbf{p}_x^T = (\mathbf{p}_{x1}^T, \mathbf{p}_{x2}^T, \ldots, \mathbf{p}_{xj}^T, \ldots) \tag{5.6.10}$$

The computed VCV of the deformation parameters is

$$\mathbf{Q}_{\hat{d}}{}^c = \left(\mathbf{A}^T (\mathbf{B}\mathbf{Q}\mathbf{B}^T)^{-1}\mathbf{A} + \mathbf{Q}_o^{-1}\right)^{-1} \tag{5.6.11}$$

From equations 5.6.8 and 5.6.9, the perturbations in the deformation solution $\hat{\mathbf{p}}_d$ are

$$\begin{aligned}\hat{\mathbf{p}}_d &= \hat{\delta \mathbf{d}}^c - \hat{\delta \mathbf{d}}^a \\ &= -\left(\mathbf{A}^T (\mathbf{B}\mathbf{Q}\mathbf{B}^T)^{-1}\mathbf{A} + \mathbf{Q}_o^{-1}\right)^{-1} \mathbf{A}^T (\mathbf{B}\mathbf{Q}\mathbf{B}^T)^{-1}\mathbf{p}_x \end{aligned} \tag{5.6.12}$$

or

$$\hat{\mathbf{p}}_d = \mathbf{D}\,\mathbf{p}_x \tag{5.6.13}$$

$$\mathbf{D} = -\left(\mathbf{A}^T (\mathbf{B}\mathbf{Q}\mathbf{B}^T)^{-1}\mathbf{A} + \mathbf{Q}_o^{-1}\right)^{-1} \mathbf{A}^T (\mathbf{B}\mathbf{Q}\mathbf{B}^T)^{-1} \tag{5.6.14}$$

where $\mathbf{D}$ is the sensitivity matrix of the deformation adjustment. Given the sensitivity matrix $\mathbf{C}_j$ of GPS session adjustment j , and the GPS systematic biases $\delta\mathbf{s}_j$, the perturbations in the deformation parameters due to the errors in session j are given by

$$\hat{\mathbf{p}}_{dj} = \mathbf{D}\mathbf{C}_j\,\delta\mathbf{s}_j \tag{5.6.15}$$

where $\mathbf{DC}_j$ gives the sensitivity of the deformation parameters to systematic errors in the GPS carrier phase observations. Alternatively, given the VCV matrix of the systematic biases $\mathbf{Q}_{sj}$ or the perturbation VCV $\mathbf{Q}_{p_{x_j}}$ due to, say, a time varying systematic error (section 5.3.2) or an erroneous dynamic model (section 5.4), the perturbation VCV $\mathbf{Q}_{\hat{p}_{dj}}$ for the deformation adjustment due to these errors in session j can be calculated using

$$\mathbf{Q}_{\hat{p}_{dj}} = \mathbf{DC}_j \, \mathbf{Q}_{sj} \, \mathbf{C}_j^T \mathbf{D}^T \qquad (5.6.16)$$

$$\mathbf{Q}_{\hat{p}_{dj}} = \mathbf{D} \, \mathbf{Q}_{p_{x_j}} \, \mathbf{D}^T \qquad (5.6.17)$$

Using the above equations 5.6.15 to 5.6.17 in conjunction with covariance analysis of GPS session adjustments, it is possible to determine, for example, the effect of orbital errors for a particular session on the deformation adjustment. This is more useful than simply using the sensitivity matrix $\mathbf{D}$ to determine the effect on the deformation adjustment, of coordinate errors of unspecified cause.

5.6.2 DERIVED 2D STRAIN PARAMETERS

Given a VCV matrix of the strain parameters e_{ee} , e_{en} , e_{nn} , the variances of the derived 2D shear strain parameters γ_1 , γ_2 and the dilatation s_{2D} can be easily derived using the Jacobian matrices given in Welsch (1983) or Harvey (1985). For $\mathbf{e}^T = (e_{ee} , e_{en} , e_{nn})$ and $\mathbf{f}^T = (\gamma_1 , \gamma_2 , s_{2D})$

$$VCV_f = \begin{pmatrix} 1 & 0 & -1 \\ 0 & 2 & 0 \\ \frac{1}{2} & 0 & \frac{1}{2} \end{pmatrix} VCV_e \begin{pmatrix} 1 & 0 & \frac{1}{2} \\ 0 & 2 & 0 \\ -1 & 0 & \frac{1}{2} \end{pmatrix} \qquad (5.6.18)$$

This equation differs from that of Welsch (1983) and Harvey (1985) due to the different definition of the dilatation used here. The situation is more complex for the total shear strain γ because the partial derivatives of γ with respect to γ_1 and γ_2 depend on the actual values of γ , γ_1 and γ_2 . In other words, the uncertainty in the total shear strain cannot be determined without knowing the direction ψ of the maximum shear strain. As simulations are used, the value of ψ is not known.

This is analogous to the derivation of the length of a line from its components. Given uncertainties in the baseline components, the error in the length of the line cannot be determined without knowing its direction. However the maximum and minimum eigenvalues of the baseline component VCV may be used to determine the maximum and minimum uncertainty in the baseline length. These eigenvalues are the squares of the semi-major and semi-minor axes of the 1σ error ellipsoid of the baseline. The same procedure can be used to determine the maximum and minimum uncertainty in γ. From the VCV of the shear strains γ_1 and γ_2 (a sub-matrix of VCV_f in equation 5.6.18)

$$VCV_g = \begin{pmatrix} \sigma^2_{\gamma 1} & \sigma_{\gamma 1 \gamma 2} \\ \sigma_{\gamma 2 \gamma 1} & \sigma^2_{\gamma 2} \end{pmatrix} \tag{5.6.19}$$

the maximum and minimum eigenvalues may be derived and the square roots of these are $\sigma_{\gamma\,max}$ and $\sigma_{\gamma\,min}$. Given a perturbation VCV the same procedure may be used to determine the maximum and minimum 1σ perturbation in γ.

5.7. SUMMARY OF COVARIANCE ANALYSIS EQUATIONS

In the sections above the theory has been developed that will be used in the simulation of terrestrial and GPS deformation surveys. Common to all simulations is the definition of a set of adjusted parameters, an observation scheme and the functional and stochastic models. The functional model is contained in the matrix of partial derivatives $\mathbf{A}_x$ and the stochastic model is defined by the VCV matrices $\mathbf{Q}$ and $\mathbf{Q}_x$. These are sufficient for a simple simulation using least squares as in section 5.1. If a Kalman filter adjustment is to be simulated, the dynamic model must also be defined by specifying Φ and $\mathbf{Q}_y$.

The model is assumed to be correct for a simple simulation but it is generally expected that some systematic errors will be present, especially for a complex observation system like GPS. Therefore in section 5.2, the concept of errors in additional unadjusted parameters implicit in the model was introduced. To apply this, the set of unadjusted parameters $\mathbf{s}$ must be defined, together with the extended functional model $\mathbf{A}_s$ and the biases in those parameters $\delta\mathbf{s}$. The sensitivity matrix and perturbations to the solution are then calculated. If the errors $\delta\mathbf{s}$ are regarded as zero - mean stochastic variables with known VCV $\mathbf{Q}_s$, rather than biases with known values $\delta\mathbf{s}$, the perturbation covariance matrix can be calculated.

If a Kalman filter adjustment with constant systematic errors is to be simulated, the equations of section 5.3.1 can be used to generate the sensitivity matrix at each epoch. The perturbation vector and/or the perturbation covariance matrix are derived from the sensitivity matrix as above. If some of the systematic errors in the Kalman filter adjustment have a non-constant dynamic model, the perturbations cannot be calculated without specifying the dynamic model errors $\mathbf{z}$ at each epoch. However, the equations of section 5.3.2 may be used to generate the covariance matrix of the perturbations at each epoch.

Given postulated errors in the dynamic model, the equations of section 5.4.1 can be used to generate the VCV matrix of the perturbation due to this error at each epoch. The perturbation vector itself cannot be calculated without the observations. The cross-covariance matrix between the perturbations and the adjusted parameters is also required at each epoch. The case that will be considered for simulations here is that of the adjusted parameter which is

assumed to be constant but which has a non-constant dynamic model in reality. This case is described in section 5.4.2.

The computed VCV matrix of the coordinates, the sensitivity matrix, the VCV of the systematic errors and the perturbation VCV matrices due to dynamic systematic errors and an erroneous dynamic model may used to determine the perturbations of deformation parameters for a given terrestrial / GPS network scheme and deformation model. The equations and the procedure for this analysis are given in section 5.6.

This does not exhaust the possibilities for covariance analysis but it is all that will be considered here. Other possibilities are: the study of the effects of incorrect observation VCV matrix $\mathbf{Q}$ (for example, the effect of using a diagonal VCV matrix for correlated observations); and the study of the effects of incorrect *a priori* parameter VCV matrix $\mathbf{Q}_{x^o}$ (for example, unduly optimistic or pessimistic variances on the *a priori* parameters).

In the most complex case that will be considered, the vector $\mathbf{s}$ is partitioned for convenience into groups of parameters which are stochastically and dynamically independent ($\mathbf{Q}_s$, Φ, $\mathbf{Q}_y$ block diagonal).

(1) The computed VCV of the parameters $\hat{\mathbf{Q}}_x{}^c$ is calculated.

(2) A perturbation vector $\hat{\mathbf{p}}$ is generated for each group of systematic errors.

(3) A perturbation covariance matrix $\hat{\mathbf{Q}}_p$ is generated for the perturbations due to each group of systematic errors, whether constant or dynamic.

(4) A perturbation covariance matrix $\hat{\mathbf{Q}}_p$ for the perturbations due to the use of an erroneous dynamic model is calculated.

(5) The contribution of the errors in (4) $\Delta\hat{\mathbf{Q}}_x$ to the consider covariance matrix is calculated.

(6) By summing the VCV matrices from (1), (3) and (5), the actual or consider covariance matrix $\hat{\mathbf{Q}}_{xa}$ is generated.

(7) The results of this analysis are used as the data for 1 sub-network of a simulated deformation adjustment. The computed VCV, perturbation VCVs and consider VCV of the deformation parameters are determined from the data from several such sub-networks.

6. GPS SYSTEMATIC ERRORS

6.1. INTRODUCTION

To study the effect of systematic errors on GPS adjustment, the **behaviour** of the error (how the observations are affected) and the **magnitude** of the error must be defined. The error analysis used in this investigation is partly based on the program ORAN (Hatch & Goad, 1973). An example of covariance analysis using ORAN is found in Stolz et al (1984). The capabilities of ORAN have been extended with a suite of programs described in Appendix F. The techniques of covariance analysis are described in Chapter 5. The behaviour and magnitude of the systematic errors that will be dealt with in this study, are discussed in the following sections.

In the observation equation for undifferenced carrier beat phase in section 4.2.1,

$$\phi_{bj}^{i}(T_j) = -\left(f_0/c \right) \rho_j^i(T_j) + f_0 \left(c^i(T_j^i) - c_j(T_j) \right) + n_j^i - \phi_{atmos} + \phi_{noise} \qquad (4.2.12)$$

the satellite receiver range $\rho_j^i(T_j)$ appears. This is calculated from the *a priori* receiver position vector at the time of reception and the satellite position vector at the time of transmission. The receiver position vector is given by the station coordinates in an earth fixed (EF) reference frame. The origin of this frame will not necessarily be coincident with the centre of mass. The satellite position vector in an earth centred inertial (ECI) reference frame may be given by a set of initial elements at some epoch and a force model. These allow the calculation of the satellite position vector at the time of transmission of the observed signal. To calculate the satellite - receiver vector, the 7 parameters that describe the relationship between the EF reference frame of the receiver coordinates and the ECI reference frame in which the satellite motions are calculated are also required. These 7 parameters are: translation (the 3 coordinates of the centre of mass in the EF reference frame), rotation (given by the adopted models of precession and nutation and the observed values of polar motion and UT1) and scale. The scale of the satellite orbits in the ECI reference frame is defined by the value of the earth's gravitational constant GM as noted in section 4.4.

The errors in calculating the geometric range may be categorised as follows:

(a) The errors in station coordinates with respect to the EF reference frame.

(b) The errors in the transformation between this EF reference frame and the ECI reference frame in which the satellite motions are calculated.

(c) The errors in the satellite initial elements with respect to this ECI reference frame.

(d) The error in the time tag of the observation used to calculate the time of transmission and the time of reception of the signal.

(e) The errors in the force model used to calculate the satellite position at the time of transmission.

To relate the geometric range to the observed carrier beat phase, the effect of errors in the other terms in equation 4.2.12 should also be considered. These are the atmospheric delay (tropospheric and ionospheric), clock biases (clock phase errors, errors in fixed ambiguities, cycle slips) and other noise sources such as multipath, antenna phase centre positioning errors, biases between the channels tracking different satellites and random errors of the phase measuring process.

6.2. STATION COORDINATES AND REFERENCE FRAME ERRORS

ORAN generates partial derivatives of the range with respect to receiver station coordinates. If the coordinates are held fixed they are potential systematic errors. The coordinate axes used by ORAN are east, north and height at each station. Note that this is not the same as the (east, north, vertical) topocentric coordinate system illustrated in diagram 2.2.1 and used for deformation analysis. In the east, north, height (ORAN) system, the height axis is normal to the ellipsoid at each point and thus the orientation of the axes is different for each point. In the topocentric system the vertical axis is normal to the ellipsoid at the chosen origin point. For stations close to the origin, the axes of the ORAN system are close to being parallel to those of the topocentric system (an angle of approximately 1° between the axes over 110 km).

In Chapter 4.4, the GPS datum definition is discussed for:

(1) Multi-station adjustment with 1 fixed station and fixed orbits.

(2) Orbit adjustment using the fiducial station concept with 3 or more fixed stations.

(3) Orbit adjustment using the free net concept with 1 station held fixed. *A priori* weighted observations of the other station coordinates may be used to provide additional datum definition

The multi-station adjustment with fixed orbits is the most common configuration for GPS adjustment and for such adjustments, the effect of an error in the station coordinates with respect to the centre of mass is considered. This is comprised of the error of the station coordinates with respect to the EF reference frame and the error in the coordinates of the centre of mass in this frame. With only 1 fixed station these two errors are indistinguishable.

For GPS surveys in New Zealand, 2 levels of error for fixed station coordinates are adopted.

(i) σ_e , σ_n , σ_h = 3 metres for a GPS receiver on a station coordinated by TRANSIT Doppler.

(ii) σ_e , σ_n , σ_h = 10 metres for receivers on other stations. The *a priori* coordinates may be derived from a GPS pseudo-range point position or by transformation from NZGD-49 to the chosen EF reference frame.

These values will also be adopted as *a priori* uncertainties for the adjusted coordinates.

The fiducial station concept depends on accurate station coordinates but these are not available in the Australasian region to the extent that they are in North America (see section 7.6). The coordinates of 1 station may be used to define the origin of the EF reference frame in which case the coordinate errors of this point are, by definition, zero. The uncertainty in the coordinates of the origin station with respect to the centre of mass, pole and Greenwich meridian should then be accounted for in adopting errors for the transformation between the EF reference frame and the ECI reference frame. The coordinate errors adopted for other fiducial stations are the errors with respect to the origin station. This procedure allows us to separate the common coordinate errors (reference frame errors) from relative coordinate errors. It will be assumed that the origin station receiver is collocated with an SLR or VLBI site and that the other stations have TRANSIT Doppler coordinates. The origin station coordinates are considered to be without error and the other fiducial station are considered to have 1σ uncertainties of 3 metres in each component. For the uncertainty in the position of the centre of mass in the EF reference frame, 0.5 metres in each coordinate is adopted (Stolz et al, 1987). This includes any uncertainty in the connection between the SLR / VLBI reference point and the GPS antenna.

Errors of 0.01" in polar motion and UT1 are adopted, which are equivalent to 0.3 metres at the surface of the earth. These are the values used by Stolz et al (1984) and are conservative. Reigber et al (1987) have corroborated this by demonstrating that the differences between earth rotation parameters derived from SLR and VLBI are of the order of 0.0025" for polar motion and 0.07 msec (0.001") for the length of day. Conservative values have been chosen to allow for any uncertainty between the axes of the chosen EF reference frame and the reference axes used in the determination of the earth rotation parameters.

The value of GM adopted for GRS-80 and WGS-84 is $3986005 \times 10^8\ m^3s^{-2}$ (Moritz, 1980b, Decker, 1986) and the value adopted for the GEM T1 gravity field model based on satellite tracking data is $3986004.36 \times 10^8\ m^3s^{-2}$ (Marsh et al, 1987). These values differ by 0.16 ppm and so 0.2 ppm has been adopted as the uncertainty in the value of GM. Beutler et al (1987b) show that an error of 1 ppm in GM will result in an error of only 0.07 ppm in the baseline estimate. This assumes that the GPS orbits are to be held fixed and the effect may be different if the satellite elements are also to be estimated.

6.3 ORBIT ERRORS

ORAN provides partial derivatives of the observations with respect to the 6 initial satellite elements (position and velocity components) and the force model parameters. These are calculated from the partial derivatives of the observation with respect to the satellite position vector at the time of transmission and the **variational partials**. From Rizos et al (1987)

$$\frac{\partial \rho}{\partial \mathbf{x_o}} = \frac{\partial \rho}{\partial \mathbf{r}} \cdot \frac{\partial \mathbf{r}}{\partial \mathbf{x_o}} \qquad (6.3.1)$$

where ρ is the satellite receiver range, $\mathbf{r}$ is the satellite position vector at the time of transmission, $\mathbf{x_o}$ are the orbit parameters of interest (initial elements and the force parameters), and $\frac{\partial \mathbf{r}}{\partial \mathbf{x_o}}$ are the variational partials.

The errors in initial elements may be given in the height, cross-track, along-track (HCL) system. The H or height axis is in the direction of the radius vector of the satellite; the C or cross track axis is normal to the orbital plane and the L or along track axis is orthogonal to H and C. For the nearly circular GPS orbits the L axis lies close to the direction of the velocity vector. A study of GPS orbit estimation by other researchers (Bertiger et al, 1986; Beutler et al, 1986; Lichten & Border, 1987) revealed that the radial or height component H of the satellite elements is the best determined, the along track component L is generally the worst determined and the accuracy of the cross track component C is closer to that of L than H. The error in L is typically 2 to 4 times that of H. Therefore, HCL errors in the initial elements of 5 metres for H, 12 meters for C and 15 meters for L have been adopted. The total error budget is 19.85 metres. It is assumed that the errors in $\dot{H}$, $\dot{C}$, $\dot{L}$ as a proportion of the total velocity (4 km/sec) are approximately the same as the errors in H , C , L as a proportion of the position vector magnitude (26 000 km). Thus the errors adopted for the initial velocity components are 0.8 mm/sec for $\dot{H}$, 1.8 mm/sec for $\dot{C}$ and 2.4 mm/sec for $\dot{L}$ with a total velocity error budget of 3.1 mm/sec. These HCL$\dot{H}\dot{C}\dot{L}$ errors are assumed to be uncorrelated and it is assumed that there are no correlations between satellites. These last assumptions will not generally be true as the satellite elements will all have been generated from the same tracking network through the same adjustment software. Nevertheless, in the absence of any information as to what the correlations could be, it is a necessary assumption. It is often stated in GPS literature that

an error of 20 metres in the orbits will result in an error of 1 ppm in an estimated GPS baseline. The orbit error of approximately 20 metres assumed here should thus result in errors in the network of the order of 1 ppm. Where orbits are to be adjusted, the values above will be adopted as the uncertainties in the *a priori* satellite elements.

R. W. King (personal communication, 1987) has studied the accuracy of the broadcast ephemeris and identified cross track errors of typically a few metres but occasionally 20 - 80 metres. The along track errors are typically 10 - 15 metres but sometimes as large as 150 metres. For extrapolated orbits such as these, the assumed error of 20 meters may be optimistic. For global post-processed orbits based on pseudo-range observations, such as the precise ephemeris, 20 metres may be somewhat conservative. Regional orbits have been determined using carrier beat phase observations with accuracies at the few metre level (e.g. Bertiger et al, 1986; Beutler et al, 1986; Lichten & Border, 1987; Delikaraoglou, 1987). Therefore, if orbits have been generated from a regional tracking network using carrier phase observations (such as the Australian orbit determination pilot project described in Rizos et al (1987) orbit errors much less than 20 metres may be expected.

In equation 5.2.4, used to develop the covariance analysis equations, a linear relationship is assumed between the size of an error and its effect on the observations and thus on the adjusted parameters. Given the effect of 20 metre orbit errors on an adjustment, the effect of greater or smaller orbit errors can easily be determined using this assumed linear relationship. If a regional orbit determination project has provided orbits with accuracies of say 4 metres, the calculated effects of 20 metre orbit errors may be reduced by a factor of 5. The two levels of orbit error that will be considered in this thesis are 20 metres as described above for globally determined ephemerides and 4 metres (1/5 of the above H,C,L,$\dot{H}$,$\dot{C}$,$\dot{L}$ errors) for ephemerides from a regional orbit determination campaign. This latter figure is probably pessimistic.

The force parameters that will be considered to be in error are those of the gravity field and direct solar radiation pressure. Drag is insignificant at GPS satellite altitudes and, for the short arcs of 3 to 6 hours that will be considered here, reflected radiation (albedo) pressure, and tidal effects on the gravity field are also insignificant (King et al, 1987). The error in the earth's gravitational constant GM is discussed above under the reference frame parameters. The

error in the gravity field is taken to be the formal uncertainties in the GEM-9 model (Lerch et al, 1979) up to degree and order 8. Stolz et al (1984) note that these uncertainties are likely to be pessimistic as more accurate gravity field models such as GEM-L2 or GEM-T1 are now available. Solar radiation pressure is assumed to be modelled to within 5% of the total effect. This is the uncertainty assumed by Bertiger et al (1986) and Kroger et al (1986) in covariance analyses of orbit determination and is also likely to be pessimistic.

6.4 TROPOSPHERIC DELAY

A number of recent studies (e.g., Lichten & Border, 1987; Stephens & Skrumeda, 1987; Tralli et al, 1988) have demonstrated that the effect of tropospheric delay errors on GPS phase adjustments, may be reduced by estimating tropospheric zenith delay parameters. Adjustments are simulated in Chapter 7 where the observations are corrected *a priori* for tropospheric delay using meteorological observations and:

- no tropospheric delay parameters are estimated,
- the zenith tropospheric delay is estimated as a constant parameter
- the zenith tropospheric delay is estimated as a 1st order Gauss-Markov process (see Appendix D for a description of the 1st order Gauss-Markov process).

The tropospheric range delay in the direction of a satellite may be described in terms of the zenith delay τ_z and a mapping function $m(z,\alpha)$ which is dependent on the zenith distance z and azimuth α of the satellite - receiver vector.

$$\tau(z,\alpha) = \tau_z \, m(z,\alpha) \tag{6.4.1}$$

The zenith delay is usually separated into two components: the "dry" and "wet" delays. The zenith dry delay is of the order of 2.2 to 2.3 metres and can be modelled to within a centimetre from the measured surface pressure (Tralli et al, 1988). The zenith wet delay is of the order of 10 to 30 cm and is difficult to model accurately. The uncertainty in the wet delay is often equated with the uncertainty in the **total** tropospheric delay.

The assumption of spherical symmetry is usually applied to simplify the mapping function in which case equation 6.4.1 may be written

$$\tau(z) = \tau_z \, m(z) \tag{6.4.2}$$

The complexity of the mapping function used depends on the accuracy required and the maximum zenith distance of an observed satellite. See Davis et al (1985) and Davis, (1986) for detailed description of mapping functions and their errors. For simulations, a very precise mapping function is not required as it is needed only to describe the general behaviour of the

tropospheric delay error. ORAN uses the mapping function (Hatch & Goad, 1973)

$$m(z) = \frac{1}{0.026 + \cos(z)} \qquad (6.4.3)$$

The partial derivative of the carrier beat phase observation with respect to the parameter τ_z is given by the mapping function.

Surface meteorological observations may be used in a tropospheric model such as Hopfield or Saastamoinen (Hopfield, 1969; Saastamoinen, 1973), to determine a value for the tropospheric zenith delay τ_z. A stochastic model can be developed for the **residual error** in the zenith delay. It is clear that the zenith delays are not independent for stations a few kilometres apart. The total delay will be highly correlated for all stations as it only varies from about 1.9 to 2.6 m over the earth. The correlation of the residual zenith delay will be less than that of the total delay and will depend on the distance between stations, the spatial variability of the troposphere and the accuracy of the tropospheric model. If atmospheric modelling is improved the residual delay error will become increasingly dominated by errors in meteorological observations and local atmospheric conditions which are independent at each station. Thus an increase in tropospheric model accuracy will tend to reduce the correlation in residual delay between adjacent stations. The dependence of correlation with distance can be modelled by the choice of a spatial correlation function and the definition of a correlation distance. For exponential correlation functions the correlation distance is typically defined as the distance at which the correlation is equal to e^{-1} (0.368).

The variability of the residual zenith delay in time can also be modelled by the choice of a temporal correlation function and a correlation time. Thus the stochastic model for the residual delay may be defined by three parameters. These are:

(1) The variance of the zenith delay at a point σ^2_{trop}. If the 1st order Gauss-Markov process is used to model the zenith delay, σ^2_{trop} is considered to be the steady state variance (see Appendix D).

(2) The correlation distance D_{trop} for a spatial correlation function.

(3) The correlation time T_{trop} for a temporal correlation function for those cases where the tropospheric zenith delay error is not considered to be constant.

6.4.1 CONSTANT TROPOSPHERIC DELAY ERROR

When the tropospheric zenith delay error is considered to be constant throughout the observation session, the stochastic model is defined by the zenith delay variance and the correlation distance. As noted above, the magnitude of the correlation distance is related to the variance. Where the correlation between stations is high (short baselines) the effect of the tropospheric delay error will tend to cancel in the explicit or implicit observation differencing between stations. On long baselines where the correlation is low, the full effect of the tropospheric errors will appear in the adjustment. Thus the magnitude of σ^2_{trop} determines the magnitude of tropospheric effects on long baselines where the correlation $\rho(\infty) = 0$. For a given σ^2_{trop}, the magnitude of D_{trop} determines the correlation and thus the level of tropospheric effects on short baselines (less than D_{trop}). If σ^2_{trop} is specified, it can be used together with a reasonable estimate of troposphere induced errors in short baselines, to derive an appropriate D_{trop}. The height error is the most useful for this analysis as it is this component that is most affected by a differential error in tropospheric delay between stations, and the perturbation in height is similar for ambiguity fixed and ambiguity free adjustments (see section 7.3). It should be remembered that the value obtained for D_{trop} is specific to the choice of σ^2_{trop} and will be different for more or less accurate atmospheric modelling.

In the discussion on orbit errors in section 6.3, the linear relationship between the magnitude of a systematic error and its effect on the adjustment was noted. This linear relationship will only apply to tropospheric errors if the variance is considered to be independent of the correlation distance. If a change in the assumed variance is accompanied by a change in the assumed value for the correlation distance, the net effect will depend on baseline length and will be non-linear. Therefore the adopted values for σ^2_{trop} and D_{trop} need to be chosen with care.

Coco & Clynch (1982) tested the Hopfield model (Hopfield 1969) against radiosonde data in western Texas and found that the uncertainty in the zenith delay ranged from 3.9 to 5.4 cm with a mean error of 4.2 cm. They also summarised studies of tropospheric models by other researchers which indicate uncertainties in the zenith tropospheric delay ranging from 1.6 to 5.7

cm. Herring (1986) considers the uncertainty of tropospheric zenith delay derived from surface meteorological data to be in the range of 2 to 5 cm. Bertiger et al (1986) use a value of 5 cm zenith tropospheric delay error in their covariance analysis while Kroger et al (1986) use 2 cm. Given the weak correlation between surface observations of humidity and integrated tropospheric water vapour (Reber & Swope, 1972), an uncertainty of 2 cm is considered to be too optimistic. The uncertainty adopted here for tropospheric zenith delay error σ_{trop} is 2% of the total zenith delay which is approximately equal to 48 mm.

A Gaussian spatial correlation function is used for the tropospheric delay error

$$\rho(b) = \exp\left(-\frac{b^2}{D_{trop}^2}\right) \qquad (6.4.4)$$

where $\rho(b)$ is the correlation between two stations and b is the length of the baseline. From this correlation function, the relationship between σ_{trop}^2, D_{trop} and the uncertainty in height on short GPS baselines may be determined. Beutler et al (1987b) derive the expression

$$\sigma_{\Delta h}(b) = \frac{\sigma_{\Delta trop}(b)}{\cos(z_{max})} \qquad (6.4.5)$$

where $\sigma_{\Delta h}(b)$ is the uncertainty in the GPS estimated height between stations, $\sigma_{\Delta trop}(b)$ is the between - stations tropospheric zenith delay error and z_{max} is the maximum zenith distance at which satellites are observed. A similar relationship is demonstrated for VLBI from simulated data by Herring (1986). For the simulations here $z_{max} = 75°$ is adopted. If the uncertainty in the tropospheric delay σ_{trop} is the same at both stations

$$\sigma_{\Delta trop}^2(b) = 2\,\sigma_{trop}^2\left(1 - \rho(b)\right) \qquad (6.4.6)$$

The correlation $\rho(b)$ is zero for baselines much longer than the correlation distance so $\sigma_{trop} = 48$ mm implies $\sigma_{\Delta trop}(\infty) = 68$ mm. For long baselines with $z_{max} = 75°$, the height error from residual tropospheric delay alone, is $\sigma_{\Delta h}(\infty) = 260$ mm from equation 6.4.5. For baselines significantly less than the correlation distance

$$\rho(b) \approx 1 - \frac{b^2}{D_{trop}^2} \qquad (6.4.7)$$

Thus, from equations 6.4.6 and 6.4.7

$$\sigma_{\Delta trop}(b) = \frac{\sqrt{2}\,\sigma_{trop}\,b}{D_{trop}} \qquad (6.4.8)$$

and substituting into equation 6.4.5

$$\sigma_{\Delta h}(b) = \frac{\sqrt{2}\,\sigma_{trop}\,b}{D_{trop}\cos(z_{max})}$$

$$= \frac{\sigma_{\Delta trop}(\infty)\,b}{D_{trop}\cos(z_{max})}$$

$$= \frac{\sigma_{\Delta h}(\infty)\,b}{D_{trop}} \qquad (6.4.9)$$

The height uncertainty expressed as a proportion of the baseline length, $\varepsilon_{\Delta h}$ is then

$$\varepsilon_{\Delta h} = \frac{\sigma_{\Delta h}(\infty)}{D_{trop}} \qquad (6.4.10)$$

with $\sigma_{\Delta h}(\infty)$ =260 mm for the chosen z_{max} . $\varepsilon_{\Delta h}$ is in units of ppm if D_{trop} is given in km and $\sigma_{\Delta h}(\infty)$ is given in mm. Note that if an improvement in atmospheric modelling (smaller σ_{trop} and thus smaller $\sigma_{\Delta h}(\infty)$) is accompanied by a reduction in the correlation distance D_{trop} , the net effect, from equation 6.4.10, may be no improvement in the proportional height error on short baselines although the absolute error on long baselines will be improved. This is in agreement with the comments of Beutler et al (1987c) that tropospheric modelling is better for large networks than for small networks.

Kouba et al (1986) use a correlation distance of 30 km (which is noted as being a somewhat arbitrary choice) but this is based on a $\sigma_{\Delta h}(\infty)$ of about 80 mm and results in $\varepsilon_{\Delta h}$ of about 2.7 ppm. This low value of $\sigma_{\Delta h}(\infty)$ is based on 24 hour VLBI solutions and may reflect the averaging that occurs in a 24 hour period. If D_{trop} = 30 km is used with σ_{trop} = 48 mm, $\varepsilon_{\Delta h}$ will be equal to 8.7 ppm. Height errors of this magnitude from all error sources are uncommon in GPS adjustments and these values are not reasonable for the contribution to height error from the residual tropospheric delay error alone. Ladd (1986)

reports height uncertainties of 1.6 ppm from dual frequency observations in California of baselines ranging from 10 km to 56 km. This error will be mostly due to troposphere and orbits. Sideris & Schwarz (1986) use the formula

$$\sigma_{\Delta h}(b) = 20 + 1.8\ b \qquad (6.4.11)$$

where $\sigma_{\Delta h}(b)$ is the relative error in millimetres from all error sources and where b is the baseline length in kilometres. They note that this is consistent with the relative height errors of the order of 2 to 3 ppm generally achieved in practice. Coco & Clynch (1982) found that for inter-station distances of 150 to 200 km, $\sigma_{\Delta trop} \approx \sigma_{trop}$ which implies $\rho \approx 0.5$ (equation 6.4.6). If $\rho = 0.5$ and $b = 175$ km are substituted in equation 6.4.4 the result is $D_{trop} = 210$ km and from equation 6.4.10, $\varepsilon_{\Delta h} = 1.2$ ppm. This is generally consistent with the total error budget given by equation 6.4.11.

The best estimate for the correlation distance for New Zealand conditions lies between these extremes of 30 km and 210 km. The correlation distance of 30 km may be appropriate for a tropospheric model accurate to 20 mm but it leads to unrealistically large errors if used with the chosen value of $\sigma_{trop} = 48$ mm. The correlation distance of 210 km, derived from the study of Coco & Clynch (1982) may be appropriate to continental climates such as that of the plains of western Texas where the data was obtained, but in New Zealand the climatic zones may change from maritime to alpine or from semi arid plains to temperate rainforest in less than 200 km. Relative height errors greater than those described by equation 6.4.11 are expected. It is considered that in New Zealand, a realistic proportional height error on baselines less than the correlation distance due to differential tropospheric delay errors is 3.5 ppm. A correlation distance of approximately 75 km is then implied by equation 6.4.10. Diagram 6.4.1 shows the values of the correlation $\rho(b)$, the differential height error $\sigma_{\Delta h}(b)$ and the proportional height error $\varepsilon_{\Delta h}$ for different baseline lengths based on these assumed values of $\sigma_{trop} = 48$ mm and $D_{trop} = 75$ km.

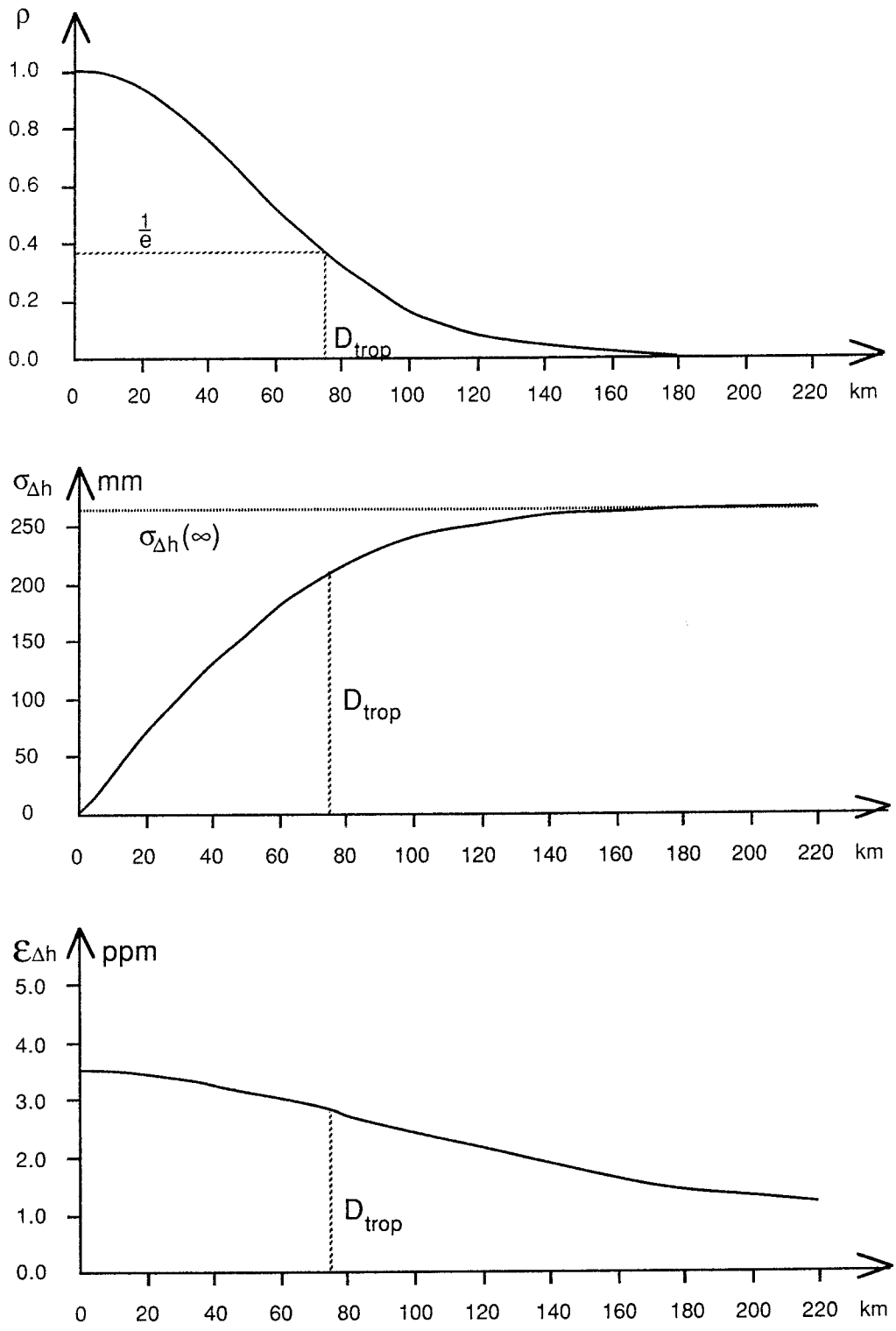

Diagram 6.4.1 Zenith Tropospheric Delay Error.

Spatial correlation coefficient (ρ); Baseline height error ($\sigma_{\Delta h}$); Baseline height proportional error ($\varepsilon_{\Delta h} = \sigma_{\Delta h}/b$) for correlation distance D_{trop} = 75 km and uncertainty in the zenith tropospheric delay σ_{trop} = 48 mm.

6.4.2 TIME DEPENDENT TROPOSPHERIC DELAY ERROR

If the 1st order Gauss-Markov process is used to model the temporal variations of the tropospheric delay error (see Appendix D), the correlation function is given by

$$\rho(\Delta t) = \exp\left(-\frac{\Delta t}{T_{trop}}\right) \tag{6.4.12}$$

Tralli et al (1988) used the 1st order Gauss-Markov process to model tropospheric delay and determined values for the correlation time from water vapour radiometer (WVR) observations. They assumed that the dry component of the tropospheric delay was modelled perfectly and that all the uncertainty was due to the difficulty of modelling the wet component. Thus the error in the wet delay was equated with the error in the **total** tropospheric delay. The WVR observations were used to quantify the errors in zenith delay derived from the use of surface meteorological observations in a tropospheric model. When the phase observations had been corrected for tropospheric delay using the surface meteorological observations they found the best results using σ_{trop} = 100 mm and T_{trop} = 16 hours. If their value of 16 hours is adopted with the σ_{trop} adopted here of 48 mm, the rate of change of the troposphere will be constrained to a level less that that of their adjustment. Considering the variation of the tropospheric delay error $\sigma_{\Delta trop}(\Delta t)$ between observation epochs Δt apart,

$$\sigma^2_{\Delta trop}(\Delta t) = 2\,\sigma^2_{trop}\left(1 - \rho(\Delta t)\right) \tag{6.4.13}$$

and for $\Delta t << T_{trop}$

$$\rho(\Delta t) \approx 1 - \frac{\Delta t}{T_{trop}} \tag{6.4.14}$$

Thus

$$\sigma_{\Delta trop}(\Delta t) = \sqrt{\frac{2\,\Delta t}{T_{trop}}}\,\sigma_{trop} \tag{6.4.15}$$

If, T_{trop} = 4 hours and σ_{trop} = 48 mm, are adopted, this will allow approximately the same rate of change of tropospheric delay error between measurement epochs as if the values, σ_{trop} = 100 mm and T_{trop} = 16 hours, had been used. The adopted T_{trop} = 4 hours is also near the mid-point of the correlation times of 0.2 to 10 hours determined by Tralli et al (1988) from WVR

data. Note that the relationship between correlation distance D_{trop} , σ_{trop} and $\sigma_{\Delta trop}(b)$ in equation 6.4.8 is different from that of the correlation time T_{trop} , σ_{trop} and $\sigma_{\Delta trop}(\Delta t)$ in equation 6.4.15. This is due to the different spatial and temporal correlation functions in equations 6.4.4 and 6.4.12.

6.4.3 MAPPING FUNCTION ERRORS

The mapping function used in equation 6.4.2 to relate the zenith delay to the delay in the direction of the satellite, assumes spherical symmetry and a certain vertical atmospheric structure. Davis (1986) considers the effect of errors in the elevation angle dependence of the mapping function. The mapping function is assumed to have the form

$$m(z) = \frac{1}{\cos(z) + a \tan(z)} \qquad (6.4.16)$$

Considering the effect of an error in the constant a , the partial derivative of the observation with respect to a is

$$\frac{\partial \tau(z)}{\partial a} \approx \frac{\tau_z \sin(z)}{\cos^3(z)} \qquad (6.4.17)$$

Davis considers the effect on VLBI solutions, of a 10% error in the value of a where $a \approx 0.001$. The same error magnitude is adopted here for GPS adjustment.

The effect of azimuthal asymmetry is also considered by Davis based on the work of Gardner (1977) on the effect of horizontal refractivity gradients on laser ranging. The largest effect is due to horizontal temperature gradients (Gardner, 1977) and given a gradient ∇T in °K / km, the partial derivative is (Davis, 1986)

$$\frac{\partial \tau}{\partial \nabla T} = \left(\frac{56.8}{\cos(z)\cot(z)} - 0.219 \frac{\left(1 + \frac{1}{2}\sin^4(z)\right)}{\cos^3(z)\cot(z)} \right) \cos(\theta) \qquad (6.4.18)$$

where θ is the angle between the azimuth to the satellite and the azimuth of the maximum temperature gradient. Davis considers an error in ∇T of 0.01 °K / km and finds that this gives close agreement with the results of Gardner based on radiosonde data from Maryland. This is adopted here also.

6.5 IONOSPHERIC DELAY

The effect of the ionosphere on GPS carrier phase observations is a delay of metres to tens of metres (actually it is a phase advance but it can be described as a negative delay). The delay is greatest a few hours after local noon and least around 0400 hours local time. Its magnitude also depends on the 11.5 year solar activity cycle. Many of the good results reported for GPS have been from observations during the solar cycle minimum of 1985 - 86. The introduction of GPS to New Zealand will come at a time of increasing solar activity with the peak of the cycle expected in 1991. Almost all the effect of ionospheric delay can be eliminated through the use of dual frequency receivers but these are more expensive than single frequency receivers. The effect of the ionospheric delay on the adjustment of single frequency observations will be considered in the simulations.

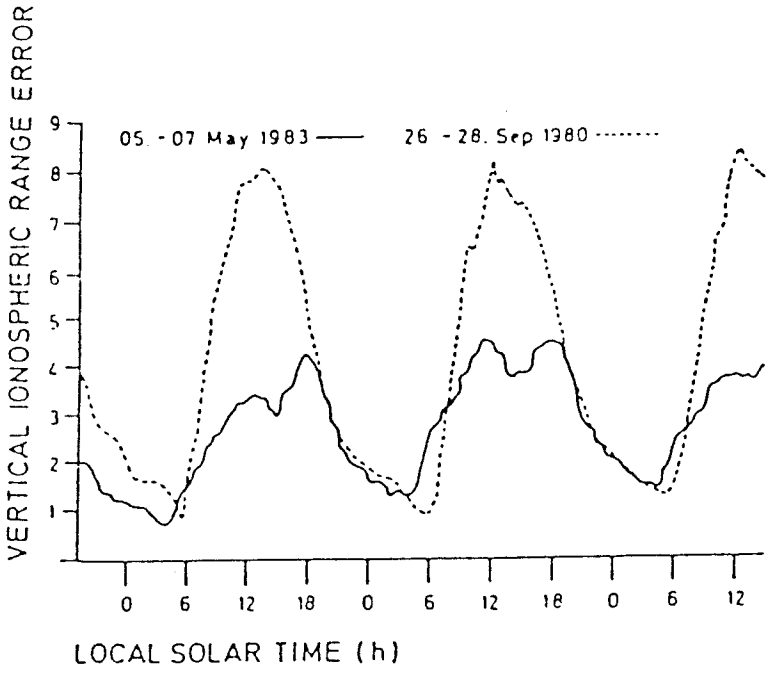

Diagram 6.5.1 Diurnal variation in zenith ionospheric delay at L1 frequency at latitude 39° N after Campbell et al (1986).

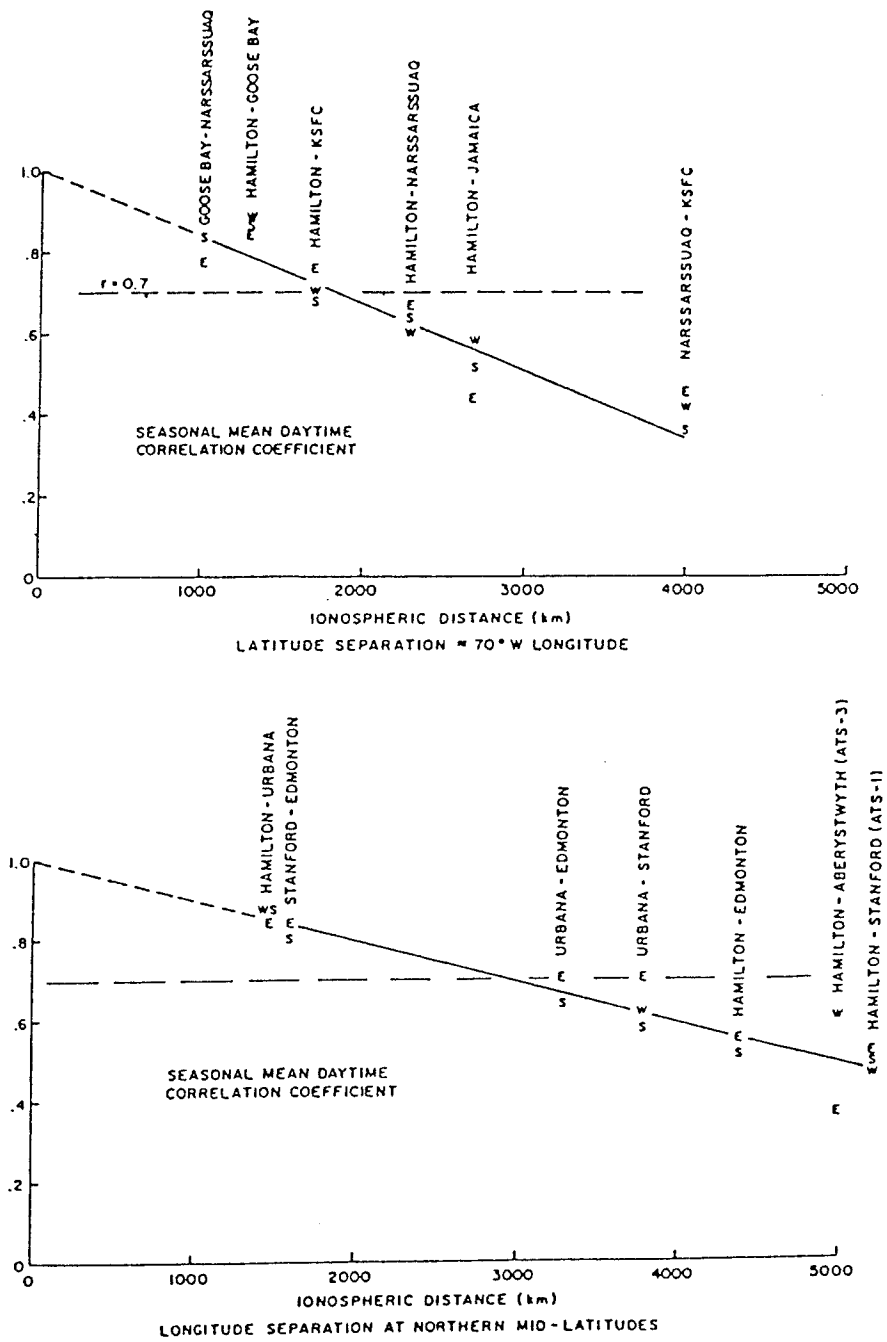

Diagram 6.5.2 Correlation coefficient of ionospheric delay vs station separation in latitude and longitude. After Klobuchar (1983).

During the peak of the solar cycle, the use of single frequency receivers for accurate geodetic surveys will be limited to night time observations through the minimum of the diurnal cycle, when the ionospheric delay is 10 - 20% of the daytime peak. Diagram 6.5.1 from Campbell et al (1986) shows the zenith

ionospheric delay at latitude 39°N for 1980 which was a maximum of the solar cycle. The delay is less than 3 metres for several hours at night. At the minimum of the solar cycle, the maximum daytime zenith delay at these latitudes is of the order of 3 metres or less (Partis & Brunner, 1988). The ionospheric model developed by Klobuchar (1986) is considered to be accurate to 50%. Therefore an uncertainty of σ_{ion} = 1.5 metres is adopted for the residual zenith ionospheric delay assuming night observations during peak solar activity or day observations during minimum solar activity.

Diagram 6.5.2 from Klobuchar (1983) shows the ionospheric correlation distance (ρ = 0.368) to be about 4000 km north - south and about 6000 - 7000 km east - west. This is the correlation distance for the total ionospheric delay and it may be different for the residual ionospheric delay after modelling to the 50% level assumed above. Clynch & Coco (1986) note that the largest gradients in the zenith ionospheric delay will be 4 m / 1000 km and 1 m / 1000 km at solar maximum and minimum respectively. Taking the latter figure as being appropriate for the mean gradient when the total delay is 3 metres, and assuming the gradient is also modelled to 50% gives $\sigma_{\Delta ion}$(1000 km) = 0.5 m.

Assuming the same spatial correlation function for the ionosphere as for the troposphere, and applying equations 6.4.4 and 6.4.6 to the ionospheric delay

$$\sigma^2_{\Delta ion}(b) = 2\,\sigma^2_{ion}\left(1 - \exp\left(-\frac{b^2}{D^2_{ion}}\right)\right) \qquad (6.5.1)$$

gives $D_{ion} \approx 4180$ km which is consistent with the results of Klobuchar (1983) above. Applying equation 6.4.10 to the ionosphere for baselines less than the correlation distance

$$\varepsilon_{\Delta h} = \frac{\sqrt{2}\,\sigma_{ion}}{D_{ion}\cos(z_{max})}$$

$$= \frac{\sigma_{\Delta h}(\infty)}{D_{ion}} \qquad (6.5.2)$$

and adopting a correlation distance of 4000 km with z_{max} = 75° gives $\varepsilon_{\Delta h}$ = 2.05 ppm. Ladd (1986) from a study of 30 baselines observed during the day during minimum solar activity, found height errors of 1.6 ppm from dual frequency data and 2.16 ppm from single frequency data which implies a

height error due to the ionosphere alone, of 1.45 ppm. Thus the chosen parameters σ_{ion} = 1.5 m , D_{ion} = 4000 km seem reasonable if slightly pessimistic. Note however, that these values would be optimistic by a factor of 5 or more, if applied to single frequency daytime observations at a time of maximum solar activity.

From diagram 6.5.1, the maximum rate of change of ionospheric delay is seen to be of the order of 2 m in a 2 hour observing session. Assuming again that this is modelled to 50% and applying equations 6.4.12 and 6.4.13 to the ionospheric delay

$$\sigma^2_{\Delta ion}(\Delta t) = 2\,\sigma^2_{ion}\left(1 - \exp\left(-\frac{\Delta t}{T_{ion}}\right)\right) \qquad (6.5.3)$$

gives a correlation time of T_{ion} = 8 hours for the 1st order Gauss-Markov process.

The ionospheric mapping function is derived from the assumption that the ionosphere is concentrated in a thin homogeneous spherical layer at a known height above the earth. From Georgiadou & Kleusberg (1988)

$$\tau_{ion}(z) = \frac{\tau^z_{ion}}{\cos(z')} \qquad (6.5.4)$$

where

$$z' = \sin^{-1}\left(\frac{R}{R + H}\cos(z)\right) \qquad (6.5.5)$$

$\tau_{ion}(z)$ is the ionospheric delay in the satellite receiver range, τ^z_{ion} is the ionospheric zenith delay, z is the zenith distance to the satellite, z' is the zenith distance of the signal path at the ionospheric layer, R is the radius of the earth and H is the ionospheric height which is assumed to be 400 km.

6.6 CLOCK ERRORS

The clock phase errors (section 4.2.1) are too large and too variable, relative to the measurement precision, to be held fixed at *a priori* values. These will be estimated or eliminated in some way and are thus not considered to be systematic errors. Four methods of dealing with these errors are:

(1) observation differencing (explicit differencing, section 4.2.2),
(2) implicit differencing which is equivalent to (1), (see section 4.3.1)
(3) estimation using clock polynomials,
(4) estimation as a random walk process in a Kalman filter adjustment.

The implicit differencing option (2) is used in the simulated adjustments. It has been verified in simulations, that the same results are obtained using explicit differencing (1). The random walk model was also used with a rate of increase of variance of $(10^{-10})^2$ sec^2 / sec which is appropriate for the quartz oscillators generally used in GPS receivers. The results of this simulated random walk adjustment were identical to the implicit and explicit differencing adjustments.

Receiver oscillators perform a dual role in generating carrier phase observations. The oscillator generates the reference frequency which is combined with the received signal to produce the beat phase. This observation is then given a time tag based on the time scale maintained by the oscillator. The time tags are used to calculate the *a priori* satellite - receiver range. An iterative process, described by Remondi (1985) and King et al (1987), is used to calculate the satellite position at the time of transmission and the receiver position at the time of reception. An error in the time tag, which is the input of this iterative routine, will cause an error in the *a priori* carrier beat phase observation. In section 4.2.2, a set of parameters were introduced to describe the time tag error, written $te_j(t_i)$, for receiver j at time t_i. The first order effect of time tag error on the calculation of geometric satellite-receiver range is given by

$$\rho_j^i\left(t_j + te_j(t_j)\right) = \rho_j^i(t_j) + te_j(t_j)\,\dot{\rho}_j^i(t_j) + \ldots \qquad (6.6.1)$$

where $\dot{\rho}$ is the rate of change of range (range rate). The maximum range rate has been calculated for GPS satellites allowing for earth rotation. It is approximately 760 m/sec. If the time tag error is 1 μsec the effect of the carrier beat phase will be less than 0.76 mm which is less than the phase measurement error of a few millimetres. Over an observation period of say 3

hours (approximately 10^4 seconds) a crystal receiver clock with a stability of 1 part in 10^{10} will not change its error by more than 1 μsec. It is assumed that the time tags have been obtained from the pseudo-range solution with an accuracy of the order of 1 μsec (300 metres) and thus the effect of time tag errors of this magnitude, is negligible.

An undetected cycle slip is a systematic error and could be modelled as an unestimated parameter if the receiver, satellite and epoch are specified. However, a cycle slip may occur at any epoch for any observed satellite - receiver pair and thus, even considering the possibility of only 1 cycle slip per observing session, there are as many possibilities for its placement as there are observations. The perturbation of the solution will be different for each of these possibilities and the analysis will be further complicated if several cycle slips per observing session are considered. This analysis is not attempted here. It is assumed that the observation output rate is sufficiently high (1 observation every few seconds) that there is no difficulty in distinguishing between cycle slips and between-epoch changes in the double differences due to other errors such as atmospheric delay, multipath, receiver coordinates or orbits.

6.7 RECEIVER AND ANTENNA ERRORS

The errors of multipath, antenna phase centre position errors, inter-channel biases and the random errors associated with the phase measurement process are included under this heading. The effects of these errors on the observations will be independent of the length of the baseline and will thus be most noticeable on short baselines where the errors due to orbits and atmospheric propagation delay are least. Brunner et al (1986) demonstrate that a comparison of a wide variety of GPS surveys with "ground truth" indicates an accuracy of 10 mm + 2 ppm. The 10 mm constant error is due to a combination of all the baseline independent errors listed above. Brunner et al describe the zero baseline, short baseline and small network tests that can be used to quantify the effects of these error sources. The errors they found with the WM 101 receiver are, in all cases, less than 10 mm.

Georgiadou & Kleusberg (1987) note variations in the ionospheric delay determined from L1 / L2 phase observations of several centimetres on a 3.5 metre baseline. These variations repeat every sidereal day as does the receiver - satellite geometry. The errors are attributable to multipath or to variations in the location of the L1 and L2 antenna phase centres. The effect of multipath on dual frequency ionosphere free observations is of concern. However it should be noted that the TI 4100 antenna, used to collect the data above, is particularly sensitive to multipath (R.W. King, personal communication, 1987) and that smaller errors may be obtained with other antenna designs. The elimination of multipath errors by antenna design or signal processing is the subject of on-going research. The effect of multipath is not considered in these simulations due to the lack of a suitable model for its behaviour. High frequency multipath noise can be accommodated by an increase in the phase observation uncertainty. If a low frequency effect is also present, as detected by Georgiadou & Kleusberg (1987), the errors will not cancel and cannot be considered to be normally distributed.

An uncertainty of 5 mm is assigned to undifferenced phase observations with one observation every 2 minutes. If the errors are random, this is equivalent to a 10 mm uncertainty for observations taken every 30 seconds and is a pessimistic estimate of the receiver noise.

6.8 SUMMARY OF SYSTEMATIC ERRORS

Receiver Coordinates (fixed orbits)	
Doppler coordinated sites	± 3.0 m (east, north, height)
Other	± 10.0 m (east, north, height)
(these include centre of mass position uncertainty)	
Receiver Coordinates (adjusted orbits)	
SLR / VLBI origin station	± 0 m by definition
Other receivers on Doppler sites	± 3.0 m (east, north, height)
Reference Frame	
Centre of mass (adjusted orbits)	± 0.5 m (x, y, z)
Polar motion, UT1	± 0.01 arcsec (0.3 m)
GM	± 0.2 ppm
Orbits and force model	
Global	20 m (5 m, 12 m, 15 m HCL)
Regional	4 m (1 m, 2.4 m, 3 m HCL)
Gravity field	100% of GEM-9 to (8,8)
Solar radiation	5%
Troposphere	
Zenith delay	0.048 m (2%)
Correlation distance	75 km
Correlation time	4 hours
Ionosphere	
Zenith delay	1.5 m
Correlation distance	4000 km
Correlation time	8 hours
Receiver measurement error (all receiver and antenna errors)	
2 minute data	0.005 m

7. TERRESTRIAL / GPS COMBINATION

7.1. SATELLITE GEOMETRY AND SELECTION

For terrestrial observation campaigns, the design of a geometrically strong network is an important factor in obtaining the most accurate results. When using GPS, the best satellite geometry is an important consideration in obtaining the highest accuracy. The choice of satellite geometry is governed by the choice of observing time and, if the number of satellites that can be observed by the receiver is less than the number visible, the set of observed satellites. The geometric dilution of precision (GDOP) is often used to select satellites and observation time for GPS surveys. This gives the optimum satellite geometry for an instantaneous point position using pseudo ranges but not necessarily the best geometry for a GPS carrier phase adjustment in which the ambiguities are estimated. Good geometry for the ambiguity free solution is necessary so that the ambiguities can be resolved to integers and the more accurate ambiguity fixed solution can proceed. This is especially important when the inter-station distances are of the order of 20 to 30 km or more, which is typical for geodetic networks. Ambiguity resolution becomes more difficult for GPS lines of this length and, if the best satellite geometry is not chosen, it may not be possible to resolve the ambiguities to their correct integer values.

The BDOP1 (bias dilution of precision) factor developed by Merminod (1988) and described briefly in Appendix E, indicates the **relative precision** of GPS ambiguity free phase adjustments which use different satellite geometries. Can it also be used to indicate **relative accuracy** when systematic errors are considered?

The sensitivity matrix $\mathbf{C}$ which describes the sensitivity of the adjusted parameters to systematic errors in the unadjusted parameters is (section 5.2)

$$\mathbf{C} = -\mathbf{Q}_{\hat{x}}\, c\, \mathbf{A}_x^T \mathbf{P} \mathbf{A}_s \qquad (7.1.1)$$

This is used to determine the perturbation VCV matrix of the adjusted parameters $\mathbf{Q}_{\hat{p}}$ and thus the actual VCV matrix of the adjusted parameters $\mathbf{Q}_{\hat{x}}\, a$ which gives the parameter accuracies (if the assumptions of the covariance analysis are correct).

$$\mathbf{Q}_{\hat{p}} = \mathbf{C}\mathbf{Q}_s\mathbf{C}^T \qquad (7.1.2)$$

$$\mathbf{Q}_{\hat{x}a} = \mathbf{Q}_{\hat{x}}{}^{c} + \mathbf{Q}_{\hat{p}} \qquad (7.1.3)$$

The precision is given by the computed VCV matrix $\mathbf{Q}_{\hat{x}}{}^{c}$ and thus there will be a tendency for a more precise adjustment (smaller $\mathbf{Q}_{\hat{x}}{}^{c}$) to be less sensitive to systematic errors (smaller **C** by equation 7.1.1). The perturbations will tend to be smaller (equation 7.1.2) and thus the adjusted parameters will tend to be more accurate (equation 7.1.3). The principle that the choice of a geometrically strong (precise) network will limit the influence of systematic errors is well known for terrestrial geodetic adjustments. It may also be applied to GPS but, due to the complexity of the GPS adjustment, an intuitive assessment of geometric strength is less reliable. This is where simulations and covariance analysis are helpful. Covariance analysis may be used to determine the relative accuracy of different satellite geometries but this is a time consuming process as the number of possible observing sessions is large. Therefore the BDOP1 factor will be used in these studies to choose the best satellite geometry. First, its suitability as an indicator of relative accuracy must be checked in comparison with the more commonly used GDOP.

Two 120 minute observation sessions and the simulated 18 satellite constellation described in section 4.1, were used to compare the merits of GDOP and BDOP1 as indicators of the best satellite geometry.

Session A:

TIME	0730 – 0930.
SATELLITES	2 , 4 , 7 , 9 , 12 , 14.
BDOP1	2.61
GDOP	ranges from 2.82 to 13.60. It is **below** 5 for most of the observing session.

Session B:

TIME	0830 – 1030.
SATELLITES	4 , 7 , 9 , 12 , 14. (2 has set)
BDOP1	1.37
GDOP	ranges from 2.82 to 96.83. It is **above** 5 for most of the observing session.

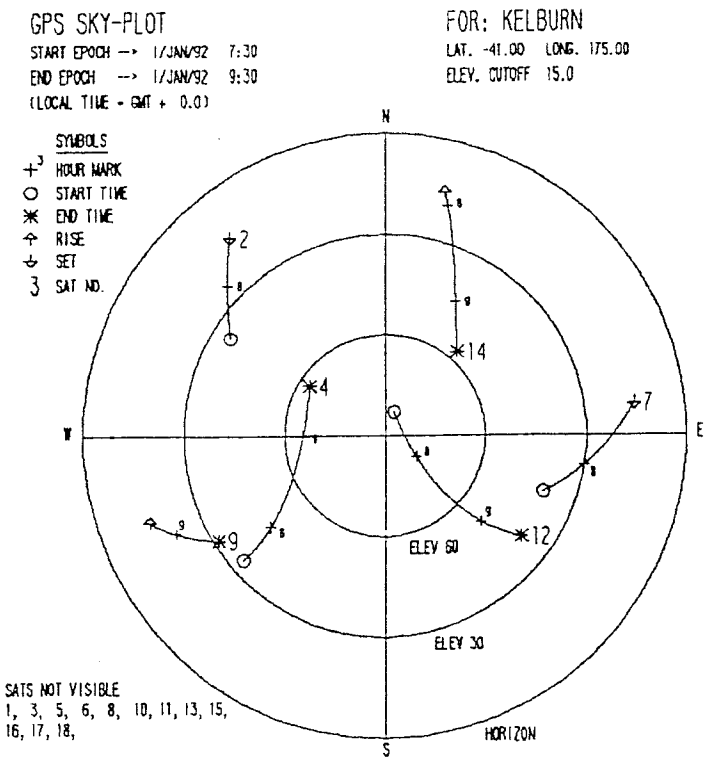

Session A

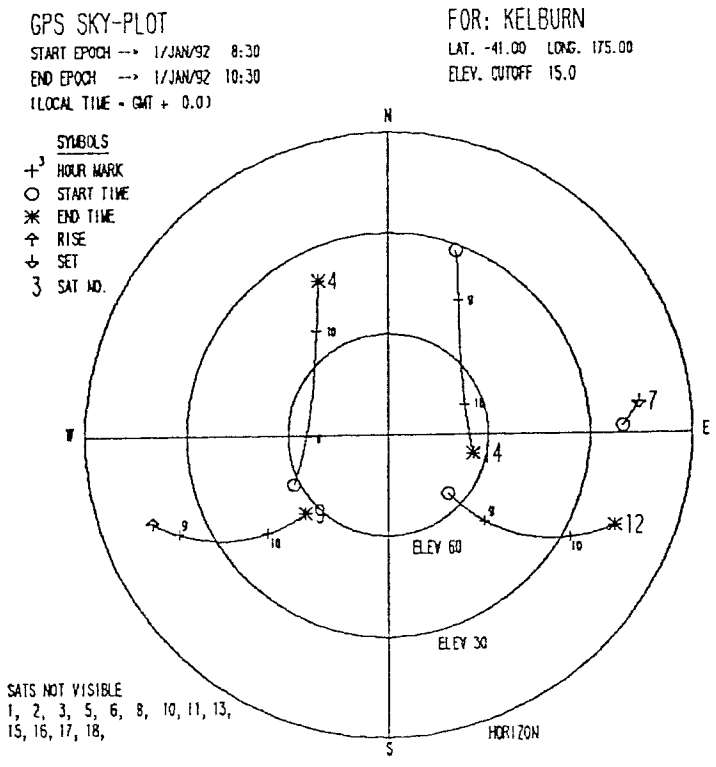

Session B

Diagram 7.1.1 Sky-plots of observing sessions used to evaluate BDOP1 as an indicator of the optimum satellite geometry

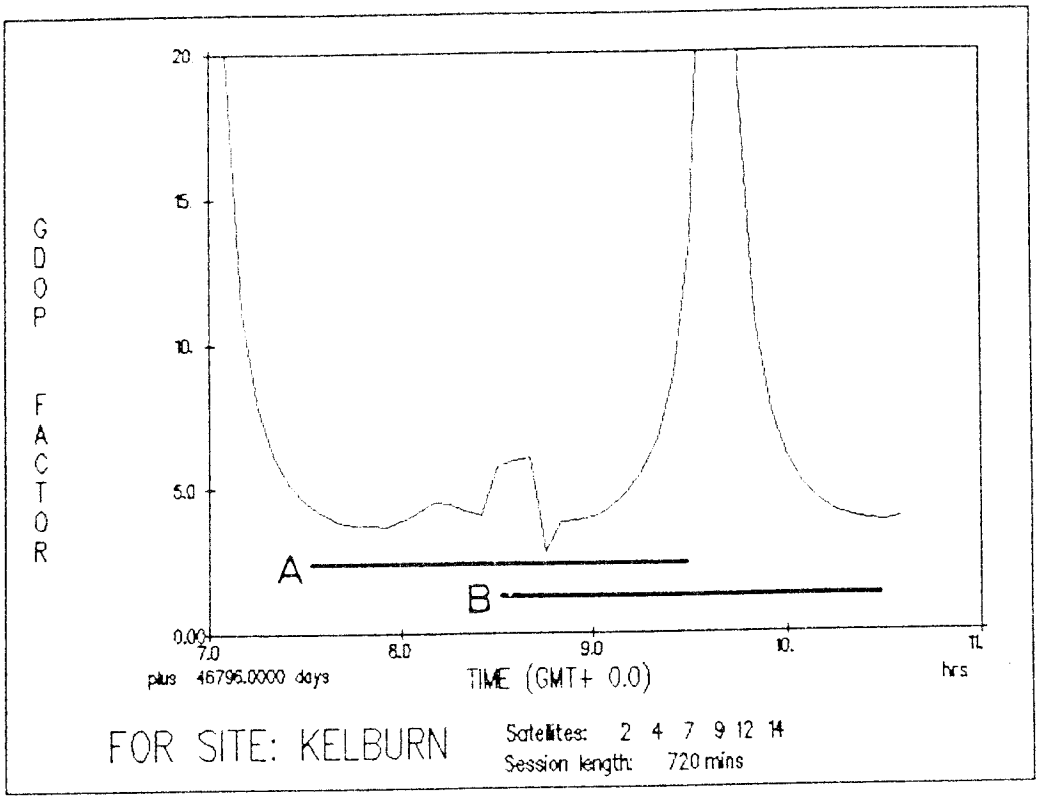

GDOP

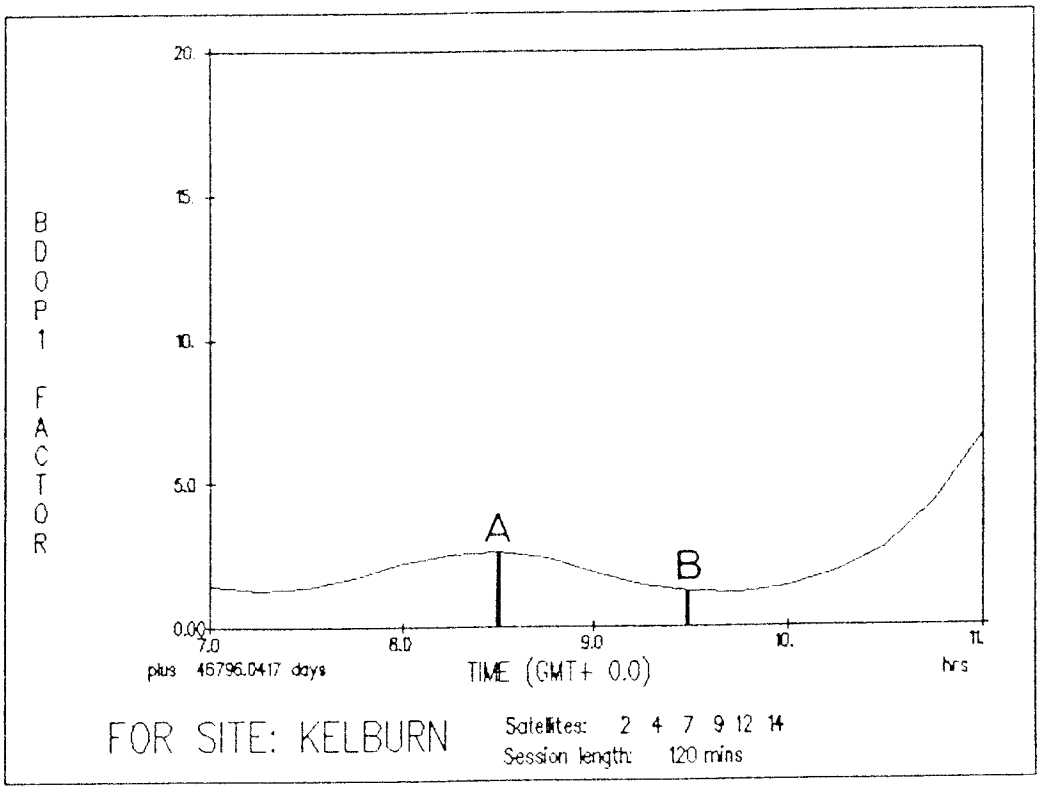

BDOP1

Diagram 7.1.2 GDOP and BDOP1 for the period of simulated observations.

The sky-plots for these sessions are shown in diagram 7.1.1 and the GDOP and BDOP1 values for the period of interest are shown in diagram 7.1.2. In comparing the GDOP and BDOP1 plots, note that the **range** of GDOP values over the session should be compared with the **single** BDOP1 value at the mid-point of the session. This is because GDOP depends on instantaneous geometry and BDOP1 is defined by the geometry over the whole observation period. If low GDOP values are used as an indicator of the best geometry, session A will be chosen. If low BDOP1 values are used to indicate good geometry, session B will be chosen.

TABLE 7.1.1 Evaluation of BDOP1 as an indicator of good satellite geometry.

Sess.	Dist.	Precision	Origin	Orbit	Tropo.	Total
A	7.2 km	0.017	0.020	0.018	0.044	0.054
B	7.2 km	0.009	0.019	0.013	0.023	0.034
A	28.4 km	0.018	0.081	0.067	0.164	0.196
B	28.4 km	0.009	0.080	0.048	0.085	0.127
A	107.6 km	0.018	0.312	0.230	0.406	0.562
B	107.6 km	0.009	0.346	0.170	0.214	0.441

- Session A: BDOP1 = 2.61 GDOP generally less than 5
- Session B: BDOP1 = 1.37 GDOP generally greater than 5
- Errors are baseline vector errors expressed in metres (rss of east, north and height errors)
- Total error is rss of precision, origin, orbit, tropospheric errors

Covariance analysis was applied to simulations of GPS adjustment of carrier phase data on 3 baselines. The lengths of these baselines are 7.2 km , 28.4 km and 107.6 km. The observation sigma was chosen to be 0.005 m for undifferenced phase observations every 2 minutes. Orbit errors of approximately 20 metres; origin coordinate errors of 10 m in each component and a 2% tropospheric zenith delay error with a correlation distance of 75 km and a correlation time of 4 hours were considered. The magnitude and behaviour of these errors are discussed in Chapter 6. The results of the analysis for the 3 baselines are summarised in table 7.1.1. The errors, given in metres, are the root sum square (rss) of the east, north and height errors and

thus indicate the baseline vector error. The precision refers to the computed uncertainty from the least squares solution. The total error is the root sum square of the precision and the perturbations due to origin coordinates, orbits and troposphere.

Note that the precision in session B is approximately twice as good as that of session A. The ratio of the precisions in sessions A and B is equal to the ratio of the BDOP1 values. This is an independent check on the use of BDOP1 as a measure of precision. It can be seen from the total error, that the results of session B are also more accurate than those of session A. Thus the better geometry in session B (as indicated by the BDOP1) leads to a greater resistance to systematic error as expected from equations 7.1.1, 7.1.2 and 7.1.3. The baseline perturbation due to tropospheric error in session B is approximately half that of session A. The perturbation due to orbit errors is about 30% less in session B. It is interesting however, to note the anomalous results for the perturbation due to origin coordinate error. For the short and medium length lines, this perturbation is virtually the same for sessions A and B. On the long line it is greater in session B which conflicts with the perturbations due to orbit and troposphere. What could be the cause of this?

Bock et al (1984) demonstrate that GPS carrier phase can be used to estimate a point position with an accuracy of several metres. It is this sensitivity of the observations to absolute station position that may cause conflict with the errors in the fixed coordinates. Presumably this conflict is greatest when the GPS solution is strongest (strong satellite geometry and thus low BDOP). This example indicates that errors in the origin coordinates can have a greater effect when the satellite geometry is good than when it is poor. However, it would be unwise to generalise from this example without further study.

The results in table 7.1.2 show the total errors in the east, north and vertical components. The component that shows the greatest improvement from session A to session B in all cases, is the east component. When ambiguities are resolved and held fixed, it is well known that the east component generally shows the greatest improvement. In these simulations the ambiguities are not fixed but the solution with the best geometry for estimating them has the best determined east baseline component.

This close relationship between the ambiguities and the east baseline components is a well known feature of GPS adjustment but the reason for it is not known. It is sometimes assumed that it is due to the present limited constellation but this example demonstrates that it will also be a feature of the full 18 satellite constellation.

TABLE 7.1.2 Baseline component errors for sessions A and B

Sess.	Dist.	East	North	Height	Total
A	7.2 km	0.041	0.015	0.033	0.054
B	7.2 km	0.017	0.015	0.025	0.034
A	28.4 km	0.141	0.052	0.126	0.196
B	28.4 km	0.065	0.053	0.094	0.127
A	107.6 km	0.407	0.174	0.346	0.562
B	107.6 km	0.265	0.181	0.302	0.441

- Session A: BDOP1 = 2.61 GDOP generally less than 5
- Session B: BDOP1 = 1.37 GDOP generally greater than 5
- Errors are rss of precision, origin, orbit, tropospheric errors in metres
- Total error is baseline vector error (rss of east, north and height errors)

In general, these results indicate that BDOP1 may be used as an indication of the **best satellite geometry** for the ambiguity free solution, that it can be used as an indication of **relative precision**, and that it may be used, with qualification, as an indication of **relative accuracy**. The qualification is that the relative accuracy depends on the nature and the magnitude of the systematic errors. For example, if the origin coordinate errors are large and the orbit and tropospheric errors are small the BDOP1 will be less suitable as an indicator of relative accuracy. Nevertheless, for GPS phase adjustment, BDOP1 is to be preferred to GDOP for satellite selection and observation time selection. The use of GDOP should be limited to point positioning with pseudo-ranges: the application it was designed for. For small networks with baselines of less than 10 km it may be reasonable to assume that the ambiguities can be resolved even with relatively poor geometry. In such cases the BDOP3 factor (see Appendix E), which indicates the relative precision of ambiguity fixed

adjustments, may be more appropriate for selecting the optimum satellite geometry.

BDOP1 has been used in the simulations that follow in this chapter, to choose the optimum observation time. The simulated observing sessions are 2 hours long with a maximum of 6 observed satellites from the 18 satellite constellation. These are listed in table 7.1.3. The sessions used correspond to 4 of the 5 BDOP1 minima between 0 and 1200 hours in the BDOP1 plot of diagram E.1 in Appendix E. The session from 0845 to 1045 hours, corresponding to the BDOP1 minimum at 0945 hours, has not been used in the simulations as it is too close to the observing sessions before and after to allow for receiver redeployment. The sky plots of the 4 sessions used are shown in diagram 7.1.3. Note that the time scale of these observing sessions is arbitrarily defined as a simulated ephemeris is used.

TABLE 7.1.3 Simulated Observation Sessions

Session	BDOP1	Time	Satellites
1	1.29	2300 - 0100	3 , 5 , 6 , 8 , 15 , 17
2	0.83	0230 - 0430	3 , 5 , 7 , 8 , 10 , 16
3	1.29	0615 - 0815	2 , 4 , 5 , 7 , 12 , 14
4	1.28	1100 - 1300	4 , 9 , 11 , 13 , 14 , 16

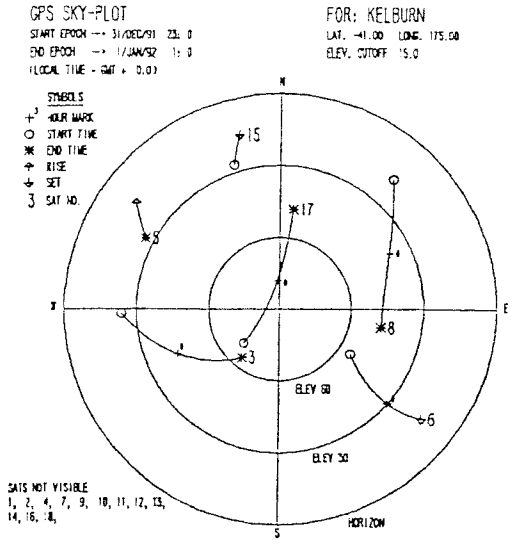

Session 1

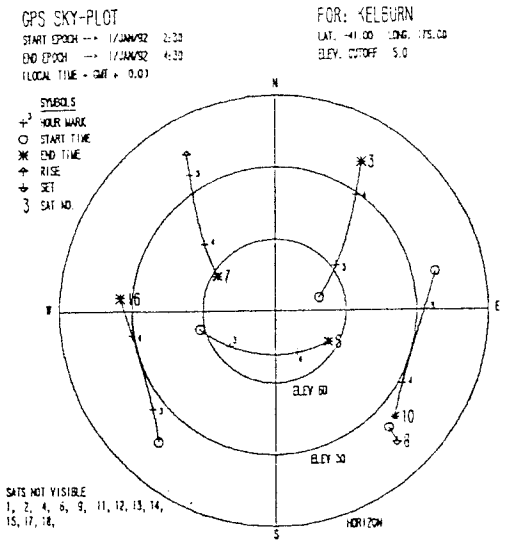

Session 2

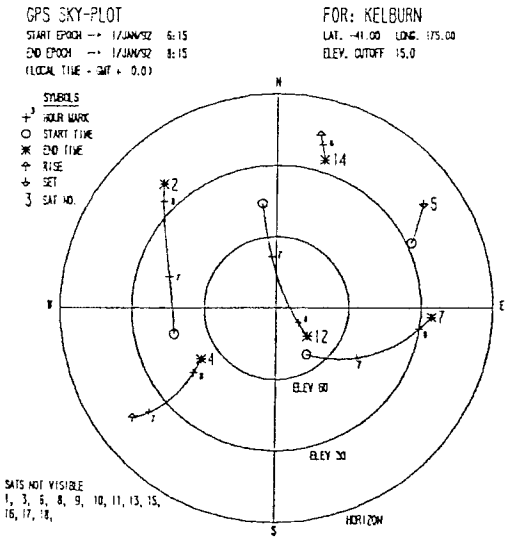

Session 3

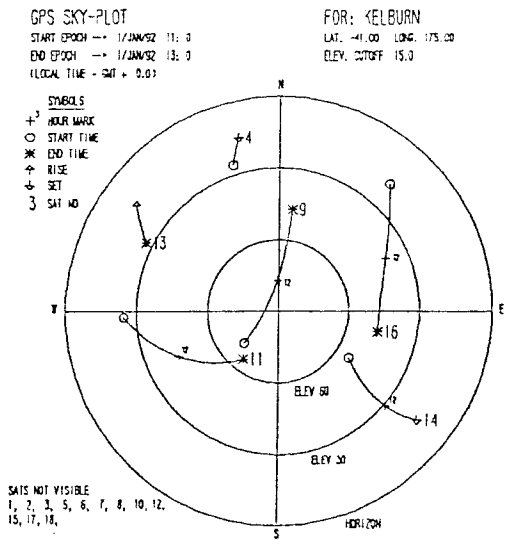

Session 4

Diagram 7.1.3 Sky-plots of simulated observing sessions with low BDOP1 to be used in the simulations of GPS network adjustment.

7.2 ACCURACY AND PRECISION

In the simulations above, measurement noise of 0.005 m for 2 minute data was adopted. This is equivalent, if the measurement errors are random and uncorrelated, to noise of 0.010 for 30 second data. This is a pessimistic value for the **random** component of the measurement error but the precisions given in table 7.1.1 are very optimistic when compared with the total error. The classical method of dealing with this problem is to scale the output variances by the *a posteriori* variance factor $\hat{\sigma}_0^2$. This may be a 3 step process as the GPS data may pass through 3 successive adjustments. At the session or baseline adjustment step, $\hat{\sigma}_0^2$ will be affected by random errors and by systematic errors that change during the session (e.g., orbits, tropospheric delay, multipath). When GPS session figures or baselines are combined in a network adjustment, $\hat{\sigma}_0^2$ for this adjustment is likely to be greater than 1 due to the effects of those systematic errors that change between sessions. Finally, if the GPS data is combined with terrestrial data, variance component estimation (VCE) may be used to determine the relative accuracy of the GPS and terrestrial data and $\hat{\sigma}_0^2 > 1$ for the GPS data is likely again due to the effects of those error sources that were constant during the observation campaign (e.g., origin station coordinates).

The use of $\hat{\sigma}_0^2$ to scale the *a posteriori* VCV matrices is based on the assumption that the measurement errors are random with unknown variance. In practice, with GPS the random component is often very small and has little effect on the solution due to the high redundancy. The major component of the measurement error is generally systematic and to inflate the *a posteriori* variances and covariances by a single factor only goes part way towards the generation of more realistic *a posteriori* statistics. To investigate the validity of using $\hat{\sigma}_0^2$ to scale the *a posteriori* VCV matrix, the ratio of total error to precision was calculated for the east, north, height baseline components and for the total baseline error of the 3 lines in used in section 7.1 above. The ratio for each component is the square root of the ideal *a posteriori* variance factor for that component. The ratio for the total baseline error is the square root of the ideal *a posteriori* variance factor for the baseline. If the ratios for all components are of similar magnitude, the use of a single scale factor for the variances and covariances is valid. The ratios are given in table 7.2.1 for session B and similar results were obtained for session A.

Table 7.2.1 Ratio of total error to precision for baseline components using the simulations of ambiguity free adjustment in section 7.1 for session B.

	Length of line		
	7.2 km	**28.4 km**	**107.6 km**
East	2.4	9.3	37.9
North	5.0	17.7	60.3
Height	6.3	23.5	75.5
Total	3.8	14.1	49.0

The precisions of the north and height baseline components are more optimistic (require larger *a posteriori* variance factors) than the precision of the east component. If a single variance factor is used for a baseline, e.g., $(3.8)^2$ for the 7.2 km line, the variance of the east component will be pessimistic and the variance of the north and height components will still be optimistic. If a multi-station adjustment with lines of different length as above is used, the discrepancy will be compounded as the variances on the short line will be pessimistic and those of the long line will be optimistic. In this example, the appropriate variance factor for the height component on the long line $(75.5)^2$ is more than 900 times the appropriate variance factor for the east component of the short line $(2.4)^2$.

Correct statistical procedures for the *a posteriori* analysis of least squares adjustment such as VCE tend to break down when the underlying assumptions (random errors) are false. This is particularly true for GPS adjustment where the influence of systematic errors is generally greater than the effect of random errors. The scaled VCV matrix in the example above, will still be much more realistic than the unscaled VCV and for many purposes will be adequate. Testing for the significance of estimated deformation parameters is an important part of deformation analysis and for this, good *a posteriori* statistics are required. There are 2 procedures that can be used to improve the *a posteriori* statistics of a GPS adjustment.

(1) Use the actual VCV derived from covariance analysis for statistical testing. The assumptions on the magnitude and behaviour of the systematic errors will need to be tested extensively against the results of actual adjustments.

(2) Include extra parameters in the adjustment model with appropriate *a priori* uncertainties and estimate corrections for them along with the other parameters (e.g., estimate tropospheric zenith delay parameters

and orbital parameters). This will increase the computed variances of the adjusted parameters and will decrease the perturbations. In other words, the solution will be more accurate and less precise so that the ratio of total error to precision will be closer to unity and the solution errors will become dominated by random influences.

If these procedures are followed, techniques such as VCE and significance testing of deformation parameters will be more reliable.

7.3. AMBIGUITY RESOLUTION

The importance of the ambiguity resolution step in GPS phase adjustment was mentioned in section 7.1 and any study of the accuracy of GPS should give some consideration to the likelihood that some, but not necessarily all, of the ambiguities will be resolvable and the benefits that may result if they are resolved. The estimated horizontal coordinates (particularly the east coordinate) are generally found to be more accurate when the ambiguities are resolved. However, it is not reasonable to assume that all ambiguities can always be resolved. A progressive ambiguity resolution scheme is proposed here. After each adjustment, the most accurately determined ambiguity is resolved to the nearest integer (if possible) and the adjustment is run again with this ambiguity held fixed. The simulated observations on the 28.4 km line used in section 7.1 above were used to study this scheme. This is about the length of baseline beyond which ambiguity resolution becomes difficult.

The total errors in the ambiguities (rss of precision and perturbations due to origin, orbit and tropospheric errors) are shown in diagram 7.3.1. As more ambiguities are held fixed, those remaining become more accurately determined. Table 7.3.1 shows the total error of the most accurately determined ambiguity at each step. This indicates the difficulty of the resolution of each ambiguity. In session A (high BDOP1) the ambiguity associated with satellite 7 has an error of nearly one cycle in the first (ambiguity free) adjustment but by the time it is resolved after adjustment 5, its error is only 0.14 cycles. The ambiguity that is the most difficult to resolve in session A, is the one associated with satellite 9. In adjustment 2 it has an error of 0.29 cycles. If the ambiguity resolution is to proceed this ambiguity must be fixed to the nearest integer in adjustment 3.

In session B there are only 5 satellites and thus only 4 ambiguities to resolve. The ambiguity associated with satellite 14 is the most difficult to resolve. In adjustment 2 it has an error of 0.25 cycles which is fixed to the nearest integer in adjustment 3. The errors in the ambiguity free adjustment in session B are significantly less than those of session A (diagram 7.3.1). However the error in the ambiguity that is resolved at each step is similar for both sessions (table 7.3.1).

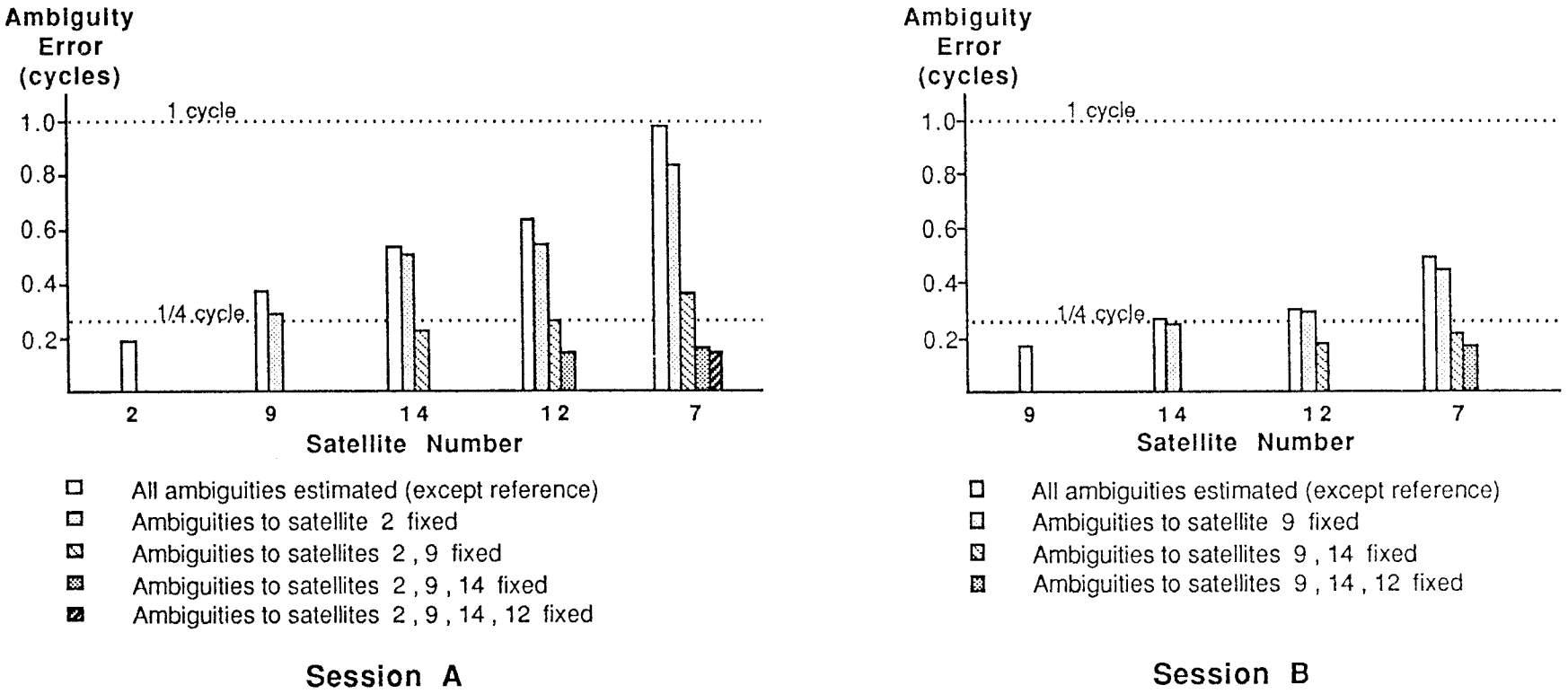

Diagram 7.3.1 Progressive resolution of ambiguities and accuracy of remaining estimated ambiguities on a 28.4 km line with simulated sessions A and B described in section 7.1

Table 7.3.1 Total ambiguity error at time of resolution (rss of precision and perturbations due to origin, orbit and tropospheric errors).

Session A

Adjustment	Next ambiguity to be fixed (satellite number)	Error in previous adjustment (cycles)
1	All estimated	–
2	2	0.19
3	9	0.29
4	14	0.22
5	12	0.15
6	7	0.14

Session B

1	All estimated	–
2	9	0.18
3	14	0.25
4	12	0.18
5	7	0.17

Next, the accuracy of the baseline determination at each step of the ambiguity resolution process is considered. The total error, which again includes the precision and the perturbations due to origin coordinates, orbits and troposphere, is illustrated in diagram 7.3.2 for the east, north and height baseline components. In session A, the east component improves as each ambiguity is resolved. The east component error is reduced by 75% with ambiguity resolution. The north component error is virtually unaltered by ambiguity resolution and the height component error is reduced by 25%. In session B, ambiguity resolution causes virtually no change to the accuracy of the north and height components and the improvement in the east component is slight. This is because the ambiguities are already well determined in session B so there is little to be gained from their correct resolution. Note also, that the ambiguity that is hardest to resolve in session A (satellite 9) gives the greatest improvement when correctly resolved.

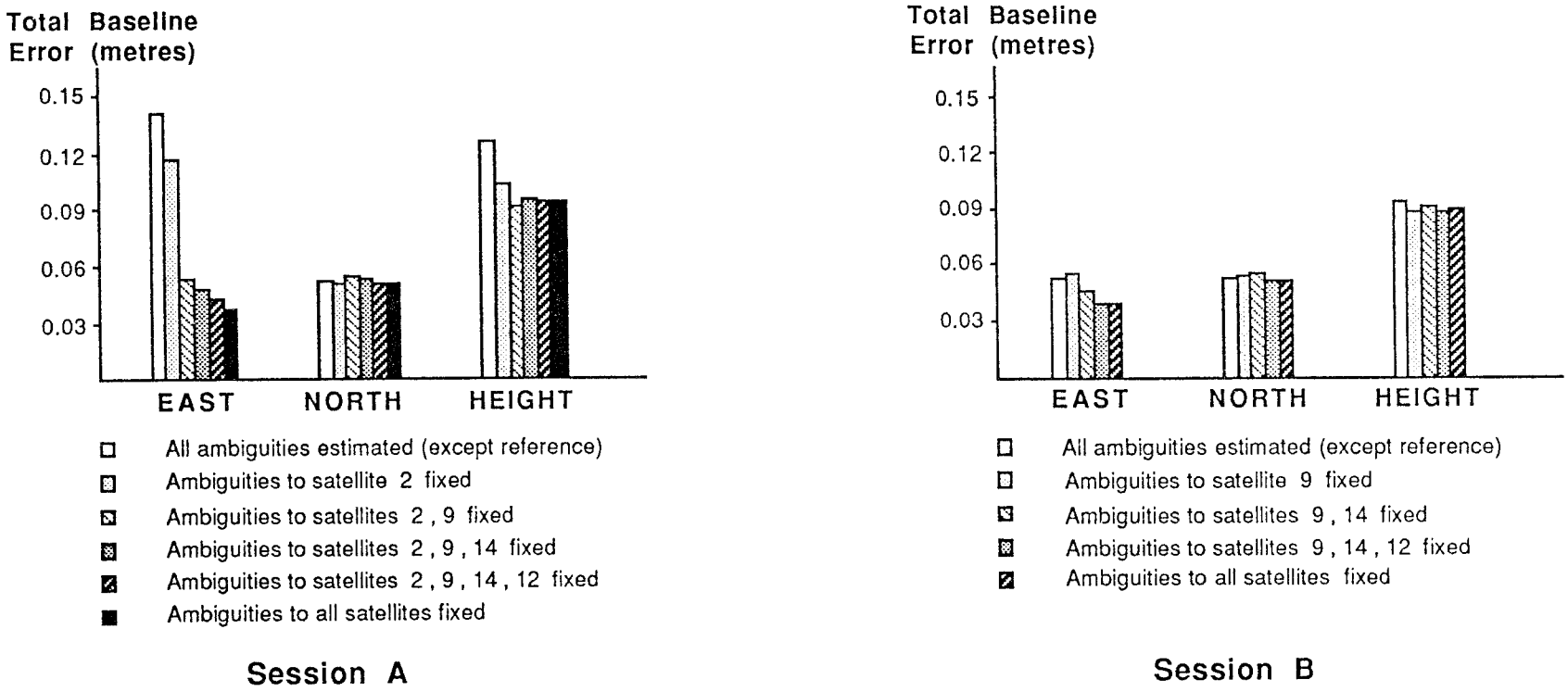

Diagram 7.3.2 Accuracy of baseline as ambiguities are progressively resolved on a 28.4 km line with simulated sessions A and B described in section 7.1

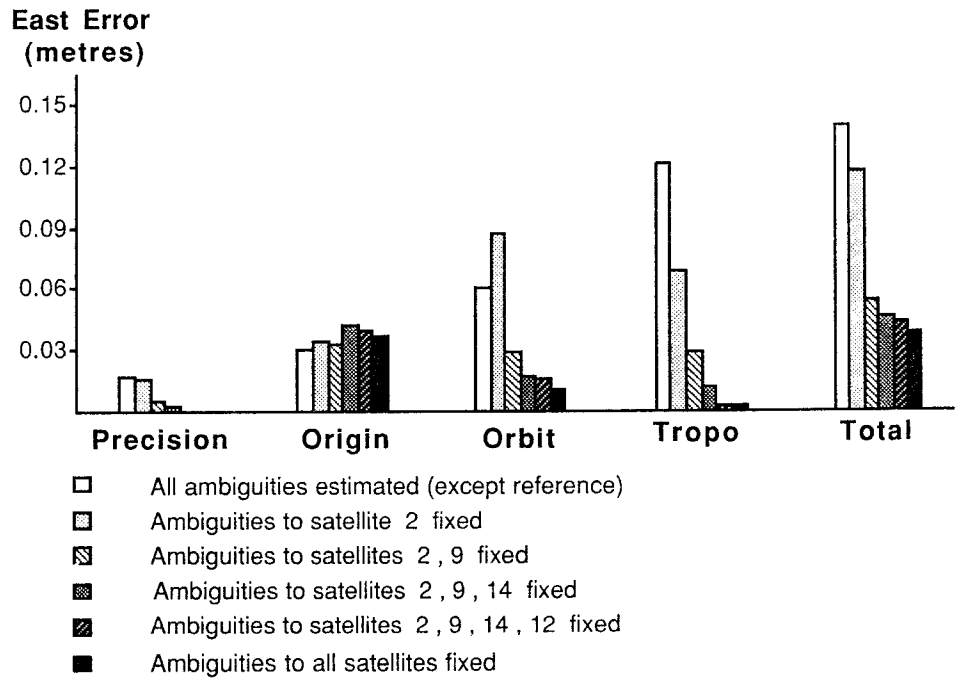

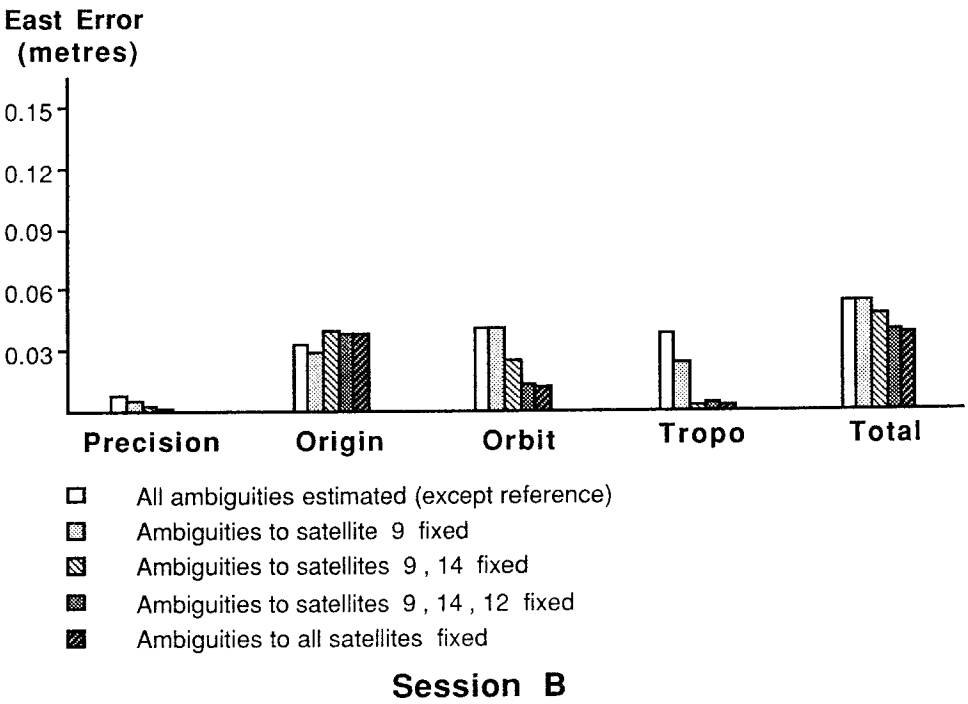

Diagram 7.3.3 Errors in east baseline component with ambiguities progressively resolved on a 28.4 km line with simulated sessions A and B described in section 7.1

Diagram 7.3.3 shows the contribution of the different error sources considered, to the east baseline component error. The errors in both sessions, due to measurement noise (precision), orbit and troposphere decrease significantly, as the ambiguities are resolved. The most dramatic improvement is in the tropospheric perturbation. However the origin perturbation is slightly greater in the ambiguity fixed adjustment than in the ambiguity free adjustment. Thus it seems again, that the stronger adjustment (ambiguity fixed) is more sensitive to an over-constraint of the datum. A similar effect was noted in section 7.1 for differing satellite geometries.

If a baseline is observed several times and the same origin coordinates are used in the adjustment each time, the east coordinates of the ambiguity fixed solution will exhibit better repeatability than those of the ambiguity free solution. The errors that change from one observation session to the next (measurement noise, orbits, troposphere) have much smaller effects in the ambiguity fixed solution. The origin error will tend to have the same effect on all adjustments and will thus not greatly affect the repeatability. Repeatability provides a measure of the error sources that do not average out within an observation session but which change significantly between repeated baseline observations in a campaign. It is insensitive to those error sources that are constant during the days to weeks of an observation campaign but which may change significantly in the years between campaigns. Repeatability is also insensitive to constant errors such as those of the origin coordinates in GPS adjustment. The error sources that change between observation campaigns are of concern in deformation analysis as the effects of these errors may not be readily distinguished from deformation. If deformation is to be estimated from two GPS observation campaigns the effect of origin coordinate errors may be minimised by using the same coordinates in both campaign adjustments. When triangulation and GPS are to be combined for deformation analysis the full effect of the origin coordinate errors will appear in the estimated deformation parameters.

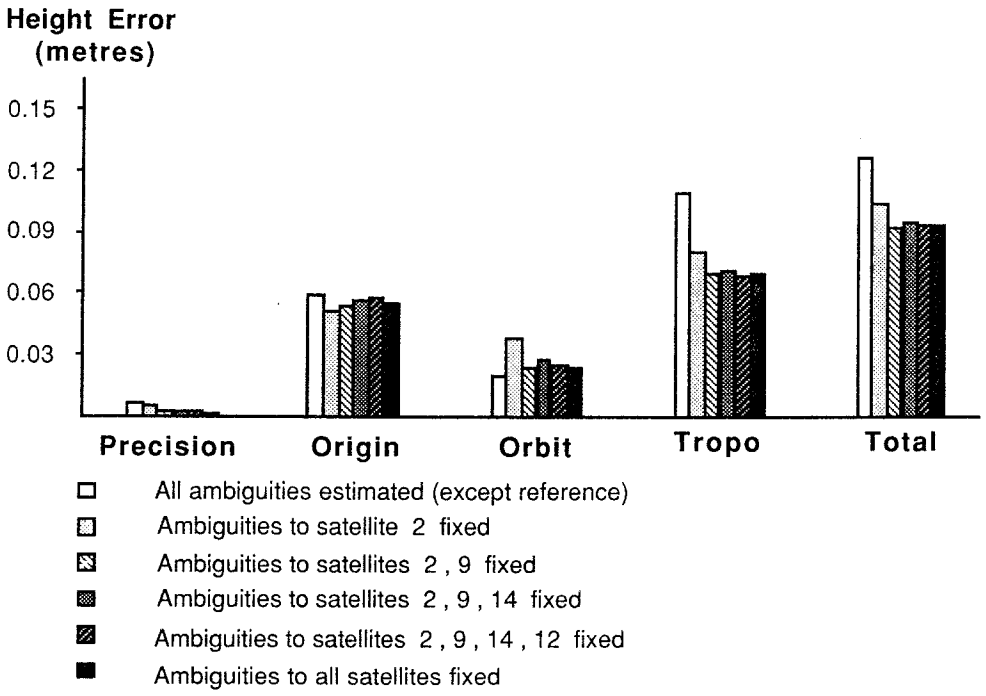

Session A

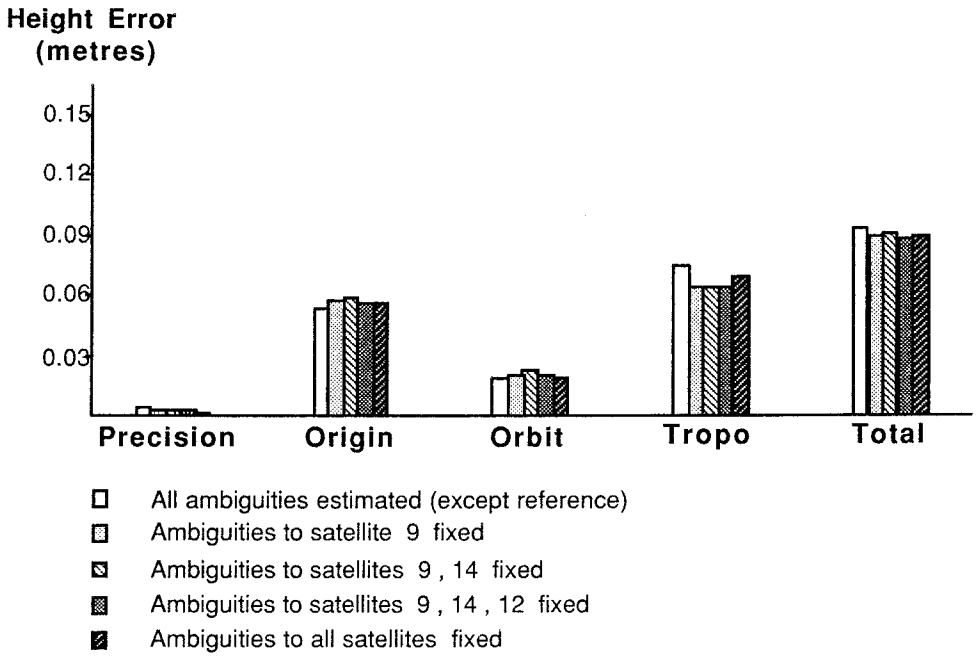

Session B

Diagram 7.3.4 Errors in height baseline component with ambiguities progressively resolved on a 28.4 km line with simulated sessions A and B described in section 7.1

Diagram 7.3.4 shows the contribution of the different errors sources considered, to the height baseline component error. In session A there is a reduction in the height error due to troposphere but in session B the accuracy of the ambiguity free solution and the ambiguity fixed solution are virtually identical. For a GPS survey in which accurate heights are the main requirement, it is debatable whether it is advisable to attempt to resolve the ambiguities. Given the slight improvement in height with ambiguity resolution and the risk of introducing significant errors by choosing the wrong integer value, the nett effect may be a reduction in height accuracy.

The horizontal strain parameters are of principal interest in this investigation and the effect of ambiguity resolution on the estimation of these parameters is studied in the following sections. The test adopted for ambiguity resolution is that the ambiguities are resolvable if the total (consider) error is less than 0.5 cycles at the 95% confidence level. This is true when the 1σ consider error is less than or equal to 0.255 cycles (0.049 m using the full L1 wavelength). It should be noted that if 100 ambiguities are resolved at, or close to, the 95% confidence level, 5 can be expected to be incorrectly resolved. The solution will then be biased by the incorrectly fixed ambiguities. The adopted procedure for simulating ambiguity resolution is as follows.

(1) Simulate an adjustment in which all ambiguities are estimated (except the reference ambiguities; section 4.3.2)
(2) Identify those ambiguities with total (consider) error less than 0.049 m.
(3) Hold these fixed in a new simulated adjustment.
(4) Return to (2) and repeat until all ambiguities are resolved or until all remaining ambiguities fail the test criteria.

A number of ambiguities may be resolved at each step. Applying this procedure to the examples above, it can be seen from table 7.3.1, that all ambiguities can be resolved in session B, but that in session A the process stops after the ambiguity to satellite 2 is resolved. The most accurate of the remaining ambiguities, the one to satellite 9, has an accuracy of 0.29 cycles which is above the test value. From diagram 7.3.2, it can be seen that the biggest improvement to the east baseline component occurs if this ambiguity is resolved. As it cannot be resolved under the chosen test limit, the improvement in the east component is much less than when all are resolved, and thus the baseline estimate in session A (high BDOP1, low GDOP) will be less accurate than that in session B (low BDOP1, high GDOP).

Significant errors may still be present in a GPS baseline after the ambiguities have been successfully resolved. Even greater errors will be present if any of the ambiguities have been fixed to the wrong value. Those errors that cause the ambiguity estimates to take on non-integer values have not been eliminated by ambiguity fixing. Their influence has simply been changed and, hopefully, diminished. Where possible, it is preferable to improve the adjustment model, perhaps with extra parameters to model the systematic errors, and thus effectively eliminate their effects. The ambiguities will then be resolved with greater certainty as their estimates will be close to integers.

7.4. GPS NETWORK GEOMETRY

7.4.1 PRINCIPLES OF GPS NETWORK DESIGN

In designing a GPS survey campaign for deformation analysis, the choice of station locations will be mostly dictated by the need to re-occupy as many existing stations as possible. Therefore, although many of the restrictions of triangulation network design do not apply to GPS (e.g., the need for station intervisibility), the first GPS deformation surveys are likely to be of similar design to the triangulation surveys of the past. The triangulation stations, which are often high with difficult access, should be included in the GPS networks because they have the longest record of geodetic observation. The GPS networks may also include extra stations at more accessible locations so that future re-observations with GPS are possible at lower cost. In the following simulations a GPS observation campaign is adopted that re-occupies the stations of the Castle point - New Plymouth EDS, used as a case study in Chapter 3. The inclusion of extra GPS stations will not be considered except tracking stations for orbit improvement in section 7.6.

This still leaves the question of the best way to deploy the receivers in each observation session. In considering observation strategies where stations are occupied a number of times Morgan (1987) states: *"This is considered undesirable as it increases the possibility of blunders occurring in the re-establishment of the station relative to the initial occupation."* If such blunders (e.g., an error in the measurement of antenna height) are considered likely, I regard the re-occupation of stations several times as not undesirable but **essential** to ensure that these errors do not go undetected. The recommendation that such re-occupations be minimised, for reasons other than that of economy, is only valid if the station marks are considered to be temporary marks, established for the GPS campaign and with no geodetic role in the past or future. This will rarely be the case and is certainly not the case for deformation surveys. Hothem (1986) recommends that all stations be occupied at least twice and that 80% be occupied at least 3 times for regional deformation surveys where the accuracy specification is 0.1 ppm. For local deformation surveys with an accuracy specification of 1 ppm he recommends that 80% be occupied at least twice and that 40% be occupied at least 3 times. I consider these recommendations to be reasonable for deformation surveys. If a station is occupied once and anomalous deformation results are obtained for

that station, doubts will later arise as to whether earth deformation or antenna eccentricity has been detected.

The optimum level of redundancy in the network is another point to consider in the context of GPS network design. Gross and systematic errors are more likely to be detected when the redundancy is high. This is especially important in deformation analysis where it is necessary to distinguish between geodetic and geophysical strain. Also it may be some time after an observation campaign is finished before all data has been processed and re-observation of suspect stations after the campaign has finished may be very expensive. If a high redundancy network has been observed, it may be possible to delete outlying observations or reduce their weight in the adjustment without the need for re-observation. These advantages of high redundancy cannot be easily tested without real data from GPS observation campaigns but the effect on the accuracy of extra observations that increase the redundancy can be determined.

The final point that will be considered is whether direct observations of long lines crossing or "bracing" the network should be used, or whether only only short lines between adjacent stations should be observed. Morgan (1987) states *"I do not favour designs that use long 'crossing' lines as such lines will be dominated by the systematic orbital contributions rather than by random contributions."* This will be tested using covariance analysis. Long "crossing" or "bracing" lines will be added to the networks to see if the results are improved or degraded. The principal criterion for whether a GPS network has been improved will be the maximum consider error in the total shear strain γ (see section 5.6.2).

7.4.2 CONFIGURATION OF THE SIMULATED ADJUSTMENT

The Castle Point - New Plymouth terrestrial EDS network is basically, a linear chain of braced quadrilaterals. It is assumed that a GPS survey of this network would start at one end of the chain and progress steadily to the other end with a number of receivers being shifted to new stations for each observing session. It is assumed that 4 receivers are used and the following schemes are considered.

Medium Redundancy

Move 2 receivers between sessions: 2 common stations.

High Redundancy

Move 1 receiver between sessions: 3 common stations.

A low redundancy scheme with only one receiver in each session being common to the previous session has not been considered. With such a scheme the connection between sessions would be completely dependent on the data from one receiver and on the correct positioning of the antenna at the common point in both sessions. Errors would only be detected if a loop of multi-station sessions was observed and even then, might not be distinguishable from other errors if the loop were large. A loop is not readily formed in the linear EDS chain without occupying extra stations. If observations proceeded through the EDS chain without a loop being formed and with only one station common to successive sessions, the result would be the similar to an unclosed traverse.

A medium redundancy network scheme was simulated and the effect of extra observation sessions that simulate a high redundancy scheme was then considered. The effect of an extra session with long lines crossing the network was also considered. The 9 station north west sub-network of the Castle Point - New Plymouth EDS as illustrated in diagram 3.4.2 was used. The GPS observation sessions are described in table 7.4.1 and illustrated in diagram 7.4.1. The times of 4 observing session in a 14 hour day, based on the optimum satellite geometry, are listed in table 7.1.3. Where more than 4 observation sessions were required, these satellite sessions were repeated one sidereal day (23 hours 56 minutes) later. A "standard" single frequency GPS multi-station adjustment with implicit double differencing was simulated. The systematic errors considered, are listed in table 7.4.4 and have been discussed in detail in Chapter 6.

Table 7.4.2 describes how these sessions can be combined to form networks and the number of station re-occupations are listed in table 7.4.3. The 7 session network virtually meets the specifications of Hothem (1986) for regional deformation surveys (100% of stations occupied at least twice and 80% occupied at least 3 times). The 6 session network virtually meets his specifications for local deformation surveys (80% of stations occupied at least twice and 40% occupied at least 3 times).

Table 7.4.1 Simulated observation sessions for NW EDS network.

Observation Session	Stations	Day	Satellite Session
Medium redundancy			
1	1 , 2 , 3 , 4	1	1
2	3 , 4 , 5 , 6	1	2
3	5 , 6 , 7 , 9	1	3
4	5 , 7 , 8 , 9	1	4
Extra sessions for high redundancy			
5	2 , 3 , 4 , 5	2	1
6	4 , 5 , 6 , 7	2	2
Extra session to brace the network			
7	1 , 2 , 8 , 9	2	3

Table 7.4.2 Simulated GPS network configurations to test the effect of different levels of redundancy

Network	Description	Sessions
4 session	Medium redundancy	1 , 2 , 3 , 4
5 session	Medium redundancy braced	1 , 2 , 3 , 4 , 7
6 session	High redundancy	1 , 2 , 3 , 4 , 5 , 6
7 session	High redundancy braced	1 , 2 , 3 , 4 , 5 , 6 , 7

Table 7.4.3 Station re-occupations

Network	≥ 2 occupations	≥ 3 occupations
4 session	67%	11%
5 session	100%	11%
6 session	78%	56%
7 session	100%	78%

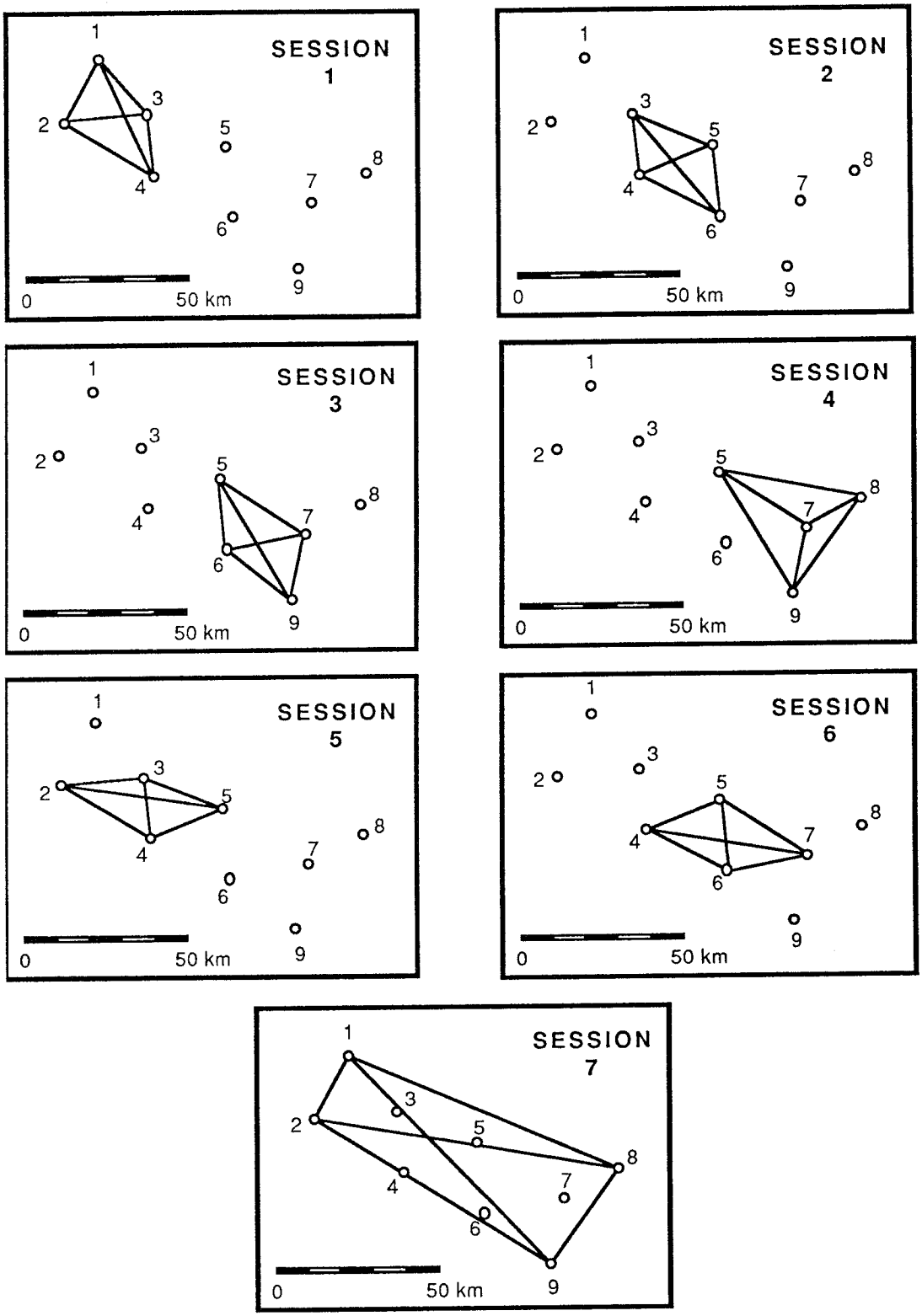

Diagram 7.4.1 Simulated GPS network observations sessions

Table 7.4.4 Systematic errors considered for covariance analysis.

Origin Coordinates	10.0 m (east, north, height).
Polar motion, UT1	0.01 arcsec (0.3 m).
Orbits	20 m (5 m, 12 m, 15 m HCL).
Gravity field	100% of GEM-9 to (8,8).
Solar radiation	5% of total effect.
Troposphere	0.048 m (2%) zenith delay. 75 km correlation distance. 4 hours correlation time in a 1st order Gauss Markov process.
Tropospheric mapping function	10% in "a" (equation 6.4.16). 0.01 °K / km temperature gradient
Ionosphere	1.5 m zenith delay. 4000 km correlation distance. 8 hours correlation time in a 1st order Gauss Markov process.
Measurement error	0.005 m (2 minute data).

The origin coordinate errors were assumed to be completely correlated between sessions. In other words, it was assumed that a preliminary network adjustment had allowed an accurate determination of the relative coordinates of the stations adopted as the origin in each session and that the assumed 10 m error in each component was therefore common to each session adjustment. The force parameters and earth rotation parameters were also assumed to be completely correlated between session adjustments. All other systematic errors were assumed to be completely independent between session adjustments.

In propagating the systematic errors through to the estimated deformation parameters, a VCV matrix of the terrestrial coordinates is also required. For this the VCV of a 3D OPERA adjustment of horizontal directions, zenith distances, EDM distances and astronomical observations was used.

7.4.3 AMBIGUITY RESOLUTION

The choice of base station was made so as to minimise the distances to other stations. Other choices were also used and verified that the coordinate estimates in the ambiguity free solution are unaffected by the choice of base station. However the ambiguities associated with stations close to the base station, are more accurately determined than those associated with stations further away. By minimising the distance from base station to all other stations the process of ambiguity resolution is made easier. Therefore the base station chosen was the station closest to the centroid of the session network. For similar reasons, the base satellite chosen was the one closest to the centre of the constellation by inspection of the sky-plots in diagram 7.1.3. These satellites are also closest to the zenith and thus their carrier phases will be least affected by tropospheric and ionospheric delay errors. The results of the ambiguity resolution are summarised in table 7.4.5. Note that 3 ambiguities in session 4 and 10 ambiguities in session 7 could not be resolved using the test outlined in section 7.3. Up to 3 adjustments in some cases were required before the iterative ambiguity resolution procedure was halted, either when all were resolved or when the remaining ambiguities were too inaccurate to be resolved. A total of 92 ambiguities were resolved. About half of these had accuracies close to the test value (less than 0.5 cycles at the 95% confidence level) while the others were resolved at higher confidence levels. Therefore two or three ambiguities would be expected to be incorrectly resolved with a resultant biasing of the adjustment.

Other choices of base satellite were also tested and it was found that the ambiguity resolution was generally more difficult than with the base satellite in the centre of the constellation. For example, using satellite 12 as base satellite in session 3, all 15 ambiguities were resolved but with satellite 2 as base satellite only 7 could be resolved. The extent to which these findings can be generalised is not certain. It was assumed that all satellites had the same magnitude of orbit errors but in practice this will not be the case and a satellite

with large orbit errors may be inappropriate as a base satellite regardless of the geometry. Further investigations are required.

Table 7.4.5 Ambiguity resolution in simulated session adjustments.

Observation Session	Base station	Base Satellite	Ambiguities resolved
1	3	17	15 of 15
2	4	5	15 of 15
3	6	12	15 of 15
4	7	9	**12** of 15
5	3	17	15 of 15
6	6	5	15 of 15
7	1	12	**5** of 15
Total			92 of 105

In these simulations the origin station (the station with fixed coordinates) was chosen, for convenience, to be the base station (the station with fixed reference ambiguities) although this is not necessary. Other stations were also tried as origin stations to see if there was any difference in the perturbation of the ambiguities due to origin coordinate errors. These perturbations were found to be identical for all choices of origin station.

7.4.4 DUAL FREQUENCY

If a dual frequency ambiguity free solution is to be simulated, it is reasonable to suppose that the effects of the ionospheric delay on the L1/L2 combined observation are negligible. Thus, if the effect of the ionosphere on the simulations of single frequency ambiguity free adjustment is neglected, the accuracy of a dual frequency ambiguity free adjustment is obtained. If a dual frequency adjustment in which the ambiguities are to be resolved is to be simulated, the situation becomes more complex. The L2 carrier phase observations are also ambiguous and thus the ambiguity resolution problem is, in effect, doubled. The ionosphere free phase observable, which is a linear combination of L1 and L2 phase observations, has a non integral ambiguity which is a linear combination of the L1 and L2 phase ambiguities. The combination of L1 and L2 integer ambiguities that give a combined L1/L2 ambiguity closest to the estimated value from the ambiguity free solution must

be determined. This approach and some of the difficulties are described briefly by King et al (1987).

From the 2 signals with frequencies f_{L1} and f_{L2} the combinations L1 + L2 with frequency $(f_{L1} + f_{L2})$ and L1 – L2 with frequency $(f_{L1} - f_{L2})$ can be formed. The L1 and L2 frequencies are 1575.42 MHz and 1227.60 MHz respectively and the combined signals thus have frequencies of 2803.02 MHz (wavelength of 10.7 cm) and 347.82 MHz (wavelength of 86.2 cm). An alternative approach to dual frequency ambiguity resolution proposed by Counselman et al (1979) and Hatch and Larson (1985) is to resolve the "wide lane" ambiguity (86.2 cm) first. *A priori* constraints on the differential ionosphere or accurate dual frequency pseudo-range data may be required on long baselines (Bender and Larden, 1985). If the wide lane ambiguity resolution is successful, the resulting solution is more accurate and the "narrow lane" (10.7 cm) ambiguities can then be resolved with greater certainty. For codeless receivers that square the L1 and L2 carrier phases (double the frequency) such as the Macrometer Mini Mac, the wide lane and narrow lane wavelengths are 43.1 cm and 5.3 cm respectively and ambiguity resolution will be more difficult.

No attempt has been made to simulate the complexities of dual frequency ambiguity resolution. In general, the extra L2 observations and the wide lane / narrow lane technique should allow resolution of the ambiguities with greater certainty than for the single frequency adjustment. In any case, the dual frequency ambiguity resolution will not be less certain than that of single frequency because, if necessary, the L1 and L2 ambiguities could be determined independently and then used in a solution of the ionospheric free L1/L2 combination. Therefore it is assumed that all ambiguities that can be resolved in a single frequency adjustment, can be resolved in an adjustment of the L1/L2 combination. Some of those ambiguities that are not resolved in the single frequency adjustment may be resolvable with dual frequency but the conservative approach is taken here and it is assumed that they are also not resolved. Therefore, as with the ambiguity free simulations, dual frequency ambiguity fixed adjustments are simulated by simply neglecting the effect of the ionosphere on the simulations of single frequency ambiguity fixed adjustments. It should be remembered in the following discussion, that the actual improvement in accuracy with dual frequency vs single frequency observations is likely to be greater than the improvement obtained from the simulations because the likelihood of improved ambiguity resolution.

7.4.5 RESULTS

It was found in the simulations, that the errors in the tropospheric mapping function have negligible effects on the coordinate estimates and on the deformation parameters. The assumed error in the elevation dependence of the tropospheric delay perturbed the total shear strain by less than 3 parts in 10^9 in all cases. The horizontal temperature gradient was considered for 4 different azimuths of maximum gradient (0°, 45°, 90° and 135°) and found to affect the total shear strain by less than 2 parts in 10^9 in all cases. An elevation cut-off angle of 15° was used for the data in these simulations because of the risk of increased multipath at lower elevation angles. The effect of these errors would be greater at lower elevation angles (Davis, 1986) and may be significant in some cases for VLBI because the directional antennas used in VLBI are less sensitive to multipath and observations to lower elevation angles are often used. These mapping function parameters were also found to have insignificant effects in simulations where the tropospheric zenith delay was estimated (see section 7.5). Therefore these parameters will not be considered further.

The effect of the considered errors in all force parameters (solar radiation and the earth's gravity field) on the total shear strain is less than 4.2 parts in 10^8 in all cases and is thus negligible when compared with other error sources. In an orbit adjustment, especially one covering several days satellite tracking, these parameters may have a significant effect. For the 2 hour observation periods and fixed orbits of these simulations, the force models are clearly more than adequate to propagate the satellite positions forwards and backwards 1 hour from the epoch of the initial satellite elements. The effect of the considered errors in earth rotation parameters on the total shear strain is less than 1.4 parts in 10^8 in all cases. The estimated rotations were perturbed by up to 0.015 arcsec. These errors may also be considered to be negligible despite the pessimistic estimate of the earth rotation parameter errors. The force parameters and the earth rotation parameters will not be considered further except for simulations where the orbits are estimated (section 7.6).

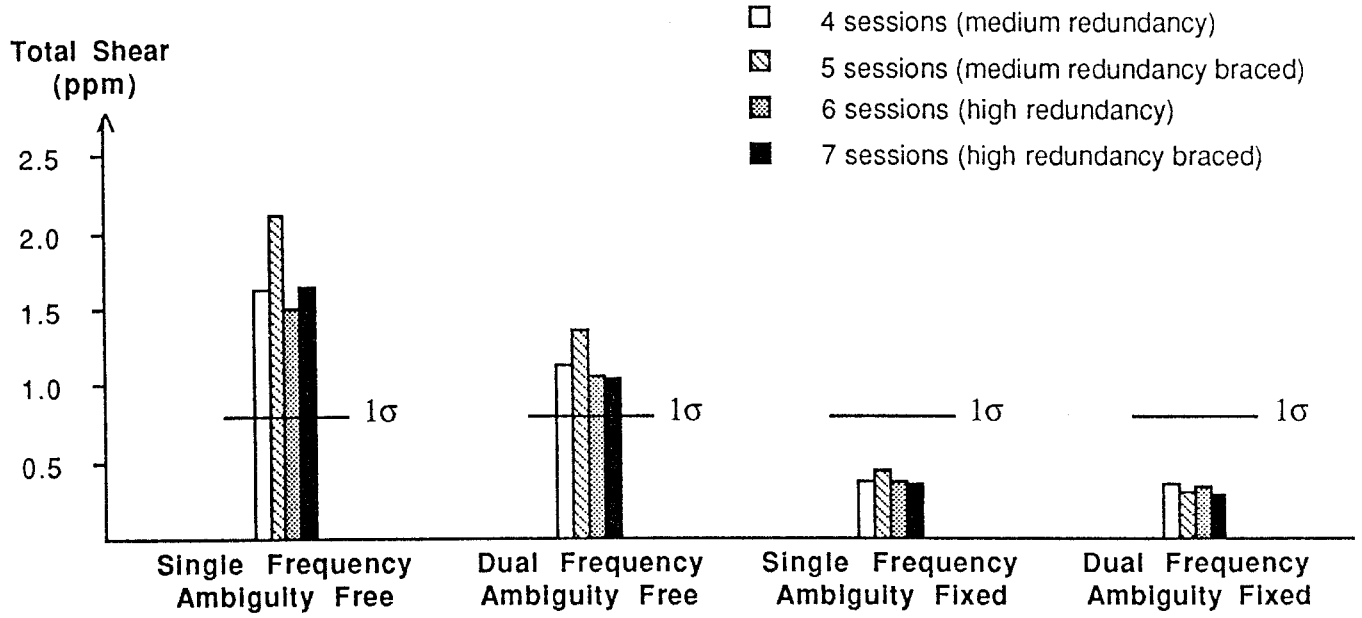

Diagram 7.4.2 Perturbation of **total shear strain** γ due to errors in origin coordinates, orbits, troposphere and (for single frequency) ionosphere. Precision of the estimate of γ is shown as the line marked "1σ".

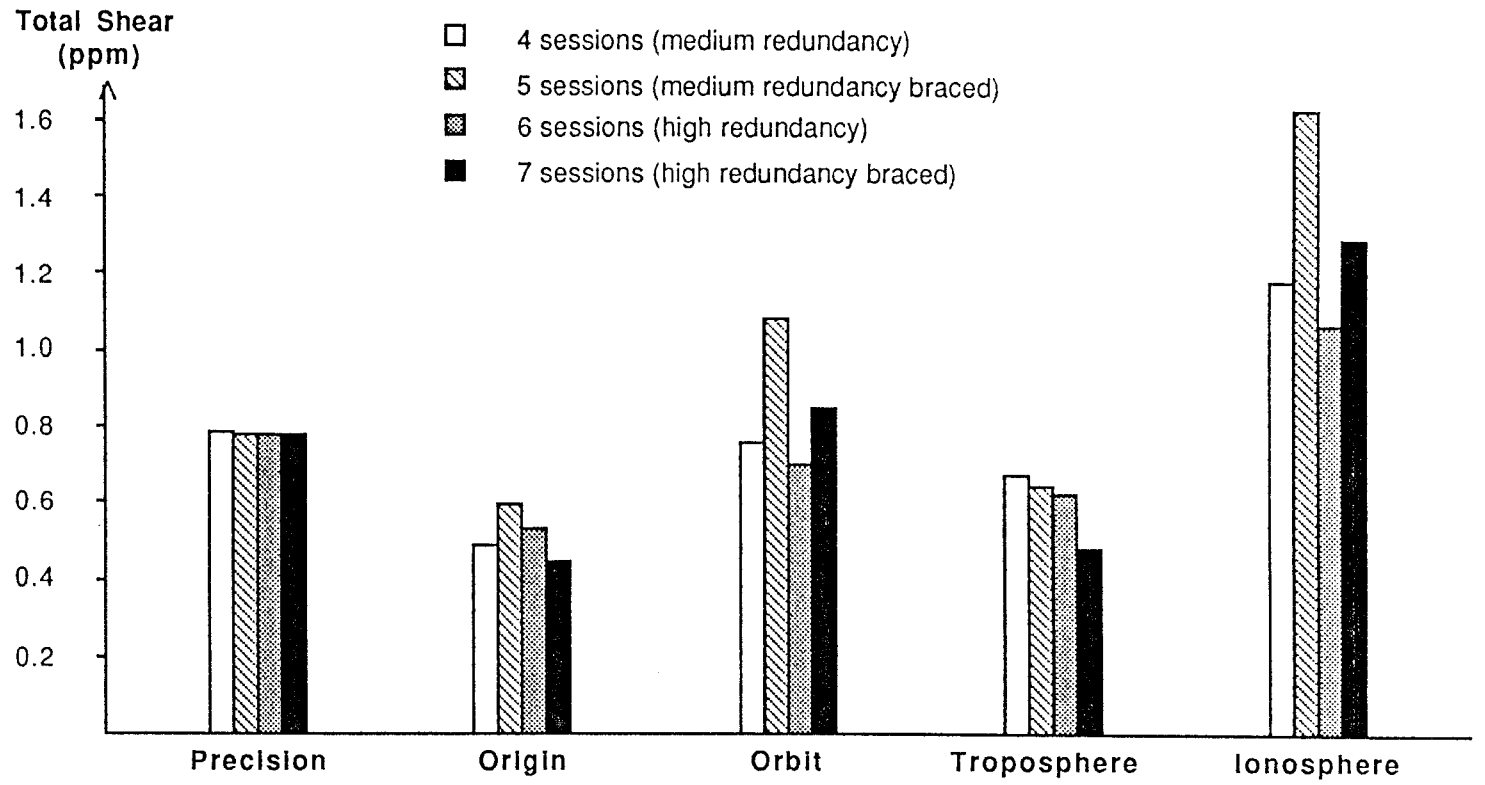

Diagram 7.4.3 Precision and the perturbations from principal GPS error sources, in estimate of total shear strain γ for **ambiguity free** adjustments.

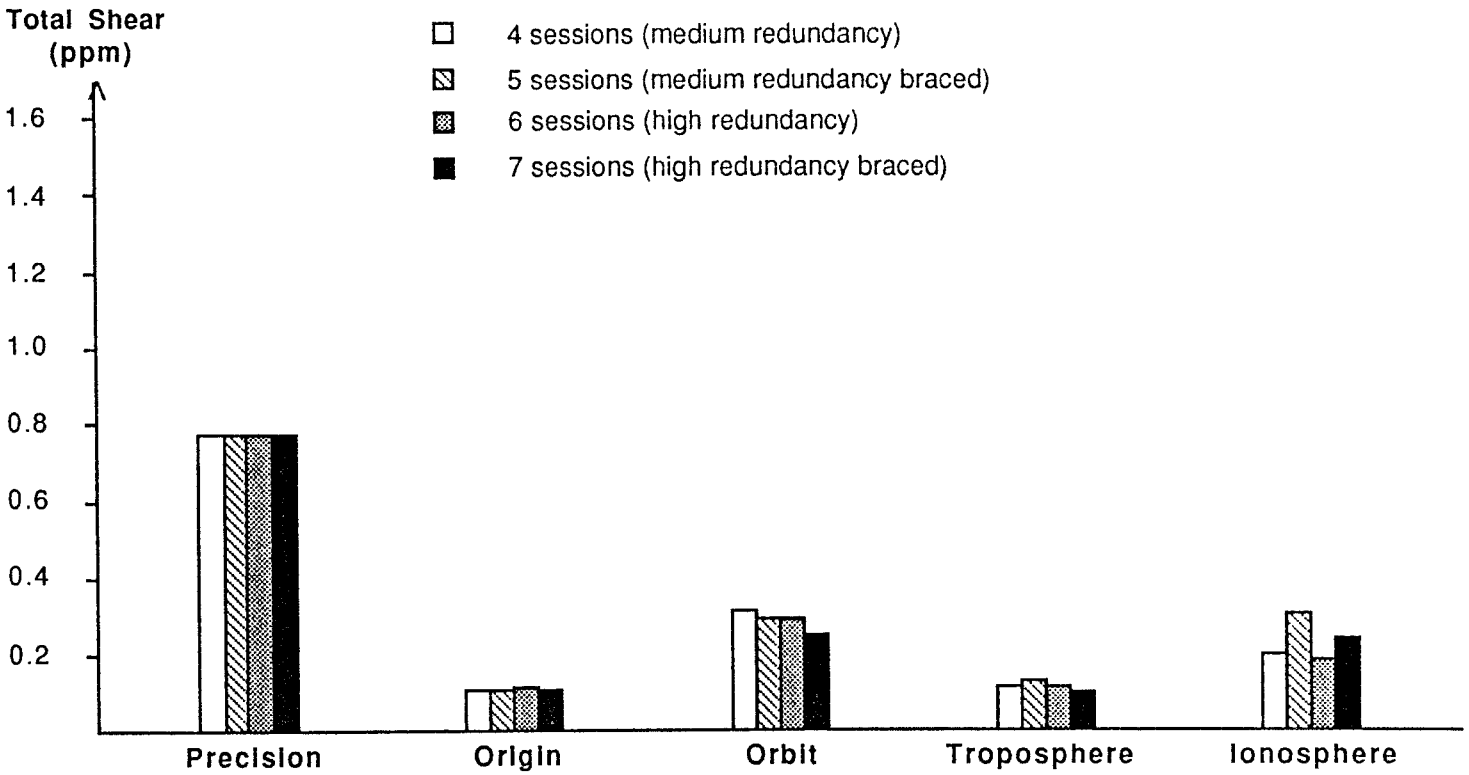

Diagram 7.4.4 Precision and the perturbations from principal GPS error sources, in estimate of total shear strain γ for **ambiguity fixed** adjustments.

The effect of the other GPS error sources, origin coordinates, orbits, tropospheric delay and (for single frequency) ionospheric delay on the determination of total shear strain are shown in diagram 7.4.2. The results are shown for single and dual frequency, ambiguity fixed and ambiguity free adjustments of the 4, 5, 6 and 7 session networks of table 7.4.2. The precision is virtually identical for all adjustments as it is dominated by the precision of the the 3D terrestrial network which is common to all adjustments. For the single frequency ambiguity free adjustments, the networks that incorporate the long lines (5 session and 7 session) have greater errors in the total shear strain γ than the others (4 session and 6 session). However for the dual frequency and ambiguity fixed adjustments, the high redundancy braced network (7 session) has the most accurately determined γ. This is surprising as the ambiguities were not resolved for the long baselines in session 7 and yet this session can be used to improve the results of sessions 1 to 6 in which most of the ambiguities were resolved.

The individual contributions of the major error sources to the error in the determination of γ, are shown in diagram 7.4.3 for ambiguity free adjustments of the 4, 5, 6 and 7 session networks. The perturbation due to orbit errors is greatest for the networks incorporating the long lines (5 session and 7 session) and the perturbation due to ionospheric errors exhibits a similar behaviour to that of the orbit errors. This increase in perturbation with the inclusion of long lines, is partly offset by the decrease in the perturbation due to tropospheric error as redundancy increases. In diagram 7.4.4 the same breakdown of error contributions is shown for solutions in which the ambiguities have been resolved. The errors are all less than those of the ambiguity free solutions (except the precision which, as noted above, is dominated by the precision of the terrestrial coordinates) and it is interesting to note that the effect of the orbit errors decreases as the redundancy increases: i.e. the orbital errors on the long lines do not degrade the results in this case.

The comment by Morgan (1987), quoted above, that long crossing lines are undesirable because of the increased influence of systematic errors, appears to be valid to some extent for networks of single frequency observations in an ambiguity free adjustment, especially when the network redundancy is not high. His comment is based on an analysis of Phase I of the South Australian GPS survey which generally has these characteristics (Morgan et al, 1986).

The comment is not necessarily true for for dual frequency adjustments or for adjustments in which most of the ambiguities are correctly resolved.

The increase in accuracy due to the extra observations in sessions 5, 6 and 7 is small but it can be concluded, for dual frequency and/or ambiguity fixed adjustments, that the general effect of the additional redundancy is an increase in accuracy as well as an increase in reliability as noted earlier. The decision on the "correct" level of redundancy will depend, in part, on economic considerations but for deformation surveys, I consider that the recommendations of Hothem (1986) on multiple re-occupation of all stations should apply and therefore, that the 7 session scheme for this network is preferable to the 4, 5 and 6 session schemes.

A comparison of diagrams 7.4.3. and 7.4.4 shows that the perturbation of γ due to origin coordinate error is reduced by ambiguity fixing. This is despite the fact that the perturbation of the **baseline components** due to the origin errors, is not greatly reduced by ambiguity fixing as noted in section 7.3. From a closer study of the results it becomes apparent that the character of this perturbation is changed with ambiguity fixing. Taking the 7 session network as a typical example, the correlation of the perturbations in e_{ee} and e_{nn} due to origin error is 0.19 for the ambiguity free case and 0.93 for the ambiguity fixed case. The small correlation in the ambiguity free adjustment indicates that an origin error may cause different scale errors in the east and north directions. This affects the shear strain component γ_1 and thus the total shear γ. The high correlation in the ambiguity fixed case means that the effect of an origin error is close to being a pure scale change, equal in all directions. Thus, while ambiguity resolution does not significantly reduce the perturbation of the coordinates due to origin error, it does reduce the perturbation of γ.

It is expected, from the change in character of this perturbation, that the determination of the dilatation, s_{2D} will not be greatly improved by ambiguity resolution. Diagram 7.4.5 shows the perturbations in s_{2D} for ambiguity fixed and ambiguity free adjustments of the 4, 5, 6 and 7 session networks. The ambiguity fixed adjustments are more accurate than the ambiguity free adjustments but, by comparison with diagram 7.4.2, it can be seen that the improvement with ambiguity resolution is less significant than for γ. After the ambiguities have been resolved the perturbations due to the major systematic errors are at about the 1σ (precision) level.

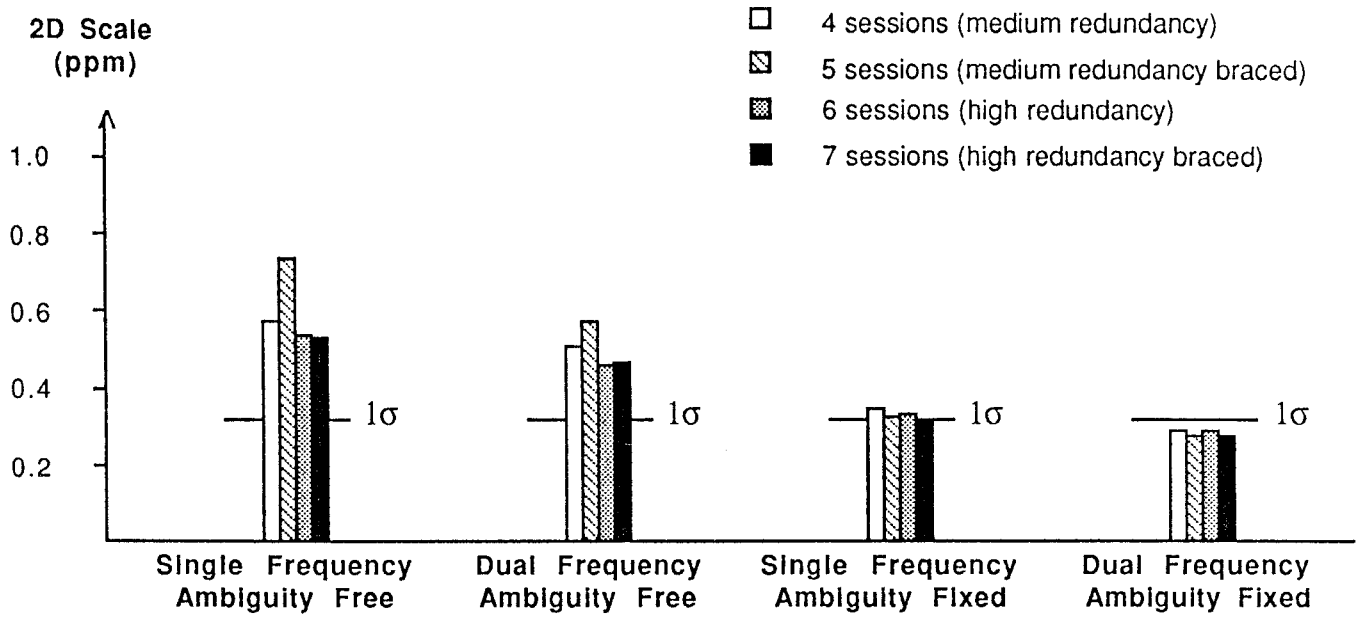

Diagram 7.4.5 Perturbation of **2D scale** s_{2D} due to errors in origin coordinates, orbits, troposphere and (for single frequency) ionosphere. Precision of the estimate of s_{2D} is shown as the line marked "1σ".

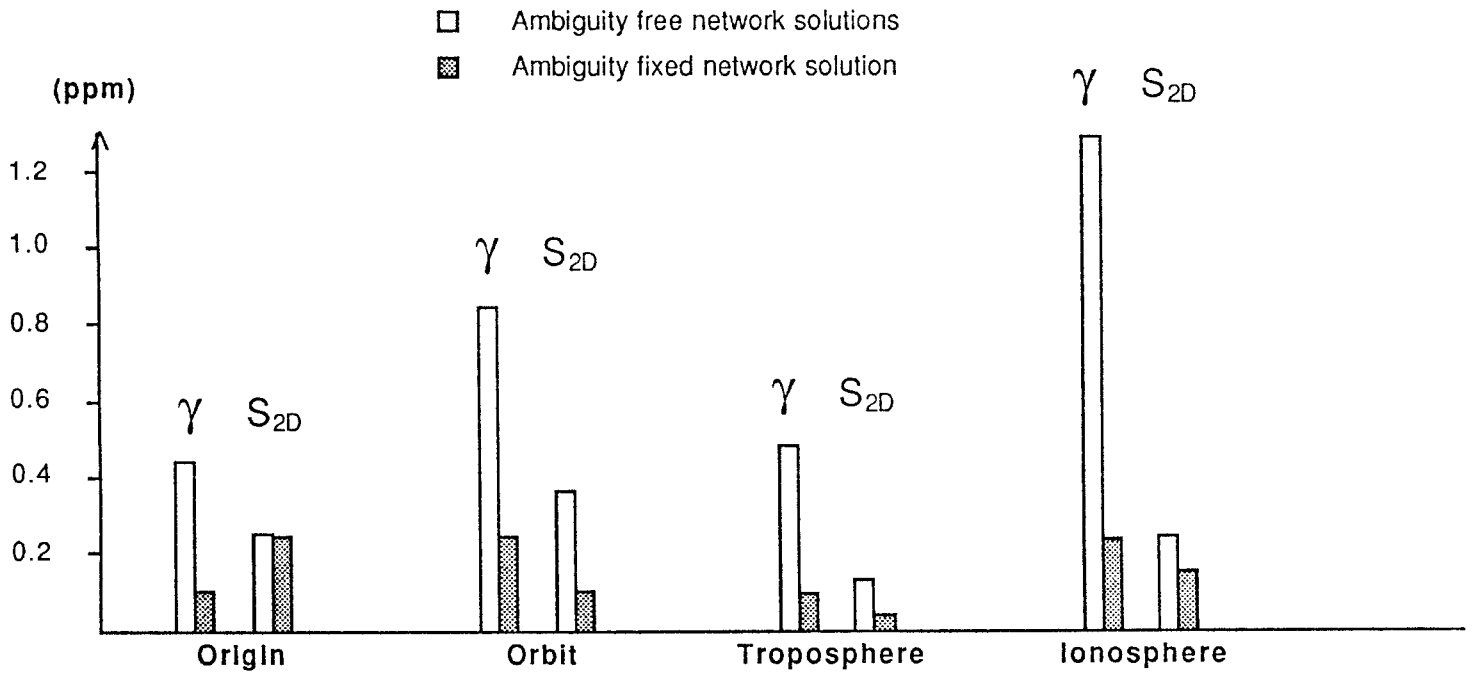

Diagram 7.4.6 Perturbations from principal GPS error sources, in estimate of **total shear strain** γ and **2D scale** s_{2D} for **ambiguity free** and **ambiguity fixed** adjustments of the 7 session network.

Diagram 7.4.6 shows the perturbations of γ and s_{2D} for ambiguity fixed and ambiguity free adjustments of the 7 session network. The origin perturbations show the change of character noted above, where the dominant effect of this error source is a total shear error in the ambiguity free case and a dilatation error in the ambiguity fixed case. All perturbations in γ are reduced substantially by ambiguity resolution but the origin perturbation in s_{2D} is not reduced and the reduction in the ionospheric perturbation is less significant for s_{2D} than for γ. Thus the principal source of scale error in an ambiguity fixed adjustment is the origin coordinate error with the ionospheric error next in importance for single frequency observations. The principal sources of shear strain in ambiguity fixed adjustments are orbital errors and, for single frequency observations, ionospheric delay.

Table 7.4.6 Covariance analysis of the errors in deformation parameters from a 3D adjustment of **terrestrial data** and **GPS data** .
Min γ and **max** γ are the minimum and maximum possible errors in γ. The actual error depends on the direction of maximum shear strain ψ.

Param	Units	Precision	Origin	Orbit	Tropo	Total
e_{ee}	ppm	0.40	0.24	0.14	0.03	0.48
e_{nn}	ppm	0.57	0.27	0.18	0.09	0.67
e_{en}	ppm	0.37	0.05	0.11	0.05	0.40
ω_e	arcsec	1.24	0.06	0.09	0.20	1.26
ω_n	arcsec	1.05	0.09	0.09	0.18	1.07
ω_v	arcsec	0.24	0.01	0.04	0.01	0.25
s_{2D}	ppm	0.31	0.25	0.11	0.05	0.42
γ_1	ppm	0.77	0.10	0.25	0.09	0.82
γ_2	ppm	0.75	0.09	0.23	0.10	0.79
min γ	ppm	0.74	0.09	0.22	0.08	0.79
max γ	ppm	0.77	0.10	0.25	0.10	0.82
t_e	m	0.05	10.00	0.01	0.00	10.00
t_n	m	0.06	10.00	0.01	0.01	10.00
t_v	m	0.27	10.00	0.02	0.04	10.00

Table 7.4.6 gives the errors in all deformation parameters for the 7 session network of ambiguity fixed, dual frequency session adjustments. The errors in the translations for each session differed by only 10% or less and average values are shown here. The principal error in the translations is due to the 10

m uncertainty in the origin coordinates. The other main effect of the origin errors is the dilatation as noted above. The errors due to tropospheric zenith delay have been substantially reduced by ambiguity resolution except for the station height errors and these appear as perturbations in the rotations about the east and north axes.

7.4.6 SUMMARY

(1) Ambiguity resolution significantly reduces the error in the total shear strain γ. The total error in γ for the ambiguity fixed adjustments was found to be 20% - 30% of the error in the ambiguity free adjustments. The improvement in dilatation s_{2D} error with ambiguity resolution is less significant with the error for the ambiguity fixed adjustments being about 45% - 60% of that of the ambiguity free adjustments. If GPS is combined with triangulation surveys observed before the advent of EDM, the scale is effectively undefined in the terrestrial data and the accuracy of the determination of s_{2D} is of little concern.

(2) Not all ambiguities could be resolved at the 95% confidence level and some of those unresolved were on relatively short lines between adjacent network stations (session 4). With 105 ambiguities to resolve in the 7 session network, some of those resolved could be expected to be incorrect using a test value at the 95% confidence level. The incorrectly resolved ambiguities are likely to significantly bias the solution. A more stringent test is required, combined with an adjustment model which reduces the effects of the error sources that affect ambiguity resolution. The principal error sources are ionospheric delay, tropospheric delay, orbit errors and origin coordinate errors.

(3) Dual frequency observations increase the accuracy of the solution but, for the greatest benefit, should be accompanied by a reduction in the other major error sources. The elimination of one of the four major error sources without a reduction in the effect of the others will be of limited benefit. Hothem (1986) recommends the use of dual frequency observations for regional and local deformation surveys. In the following sections only the use of dual frequency observations will be considered and the other important error sources will be studied.

(4) Even with the relatively simple observations schemes considered, given dual frequency observations and resolved ambiguities, the contribution of GPS systematic errors to the total uncertainty in the estimate of γ is less than the precision. The precision is dominated by the precision of the terrestrial data and it was demonstrated in Chapter 3 that there may also be significant systematic errors in the terrestrial data even for high precision surveys such as the Castle Point - New Plymouth EDS used here. If the reliability of the ambiguity resolution can be improved, the major concern in the use of terrestrial and GPS data for horizontal deformation analysis will be the systematic errors in the terrestrial data. This is also true for the estimation of dilatation. The total perturbation in s_{2D} for the dual frequency - ambiguity fixed case is of the order of 0.3 ppm whereas, in Chapter 3, systematic errors of more than 2 ppm between night and day EDM observations were noted.

7.5. TROPOSPHERIC DELAY

In section 7.4 it was demonstrated for the Castle Point – New Plymouth EDS, that for the estimation of horizontal strain, the accuracy of GPS data is greater than that of the terrestrial data provided the ambiguities can be correctly resolved to their integer values. The test level for ambiguity resolution used was a limit of 0.5 cycles in the total ambiguity error at the 95% confidence level and 92 of the 105 ambiguities could be resolved at this level. However, the likelihood that some of these would be incorrectly resolved with a resultant biasing of the solution was noted. It would be desirable to reduce the effects of the major GPS error sources so that the ambiguities could be resolved at a higher confidence level, say 99%.

The data from GPS deformation surveys that is to be combined with past terrestrial data will also be used with future GPS survey data to estimate deformation. If deformation is to be detected with confidence in the shortest possible time, a higher accuracy than the 1 - 2 ppm of the terrestrial surveys will be sought. If one of the aims of the GPS surveys is the detection of uplift or subsidence, accurate heights will be required and ambiguity resolution does not greatly improve the accuracy of GPS heights (see section 7.3). Therefore, means of reducing the effects of the major error sources in GPS adjustment have been investigated. These major error sources considered are ionospheric delay, tropospheric delay, orbital errors and origin coordinate errors.

It is assumed, as in section 7.4 above, that the effect of ionospheric delay may be made negligible by the use of dual frequency observations. The effect of origin coordinate errors may be reduced if a survey connection between the origin station and the nearest TRANSIT Doppler station is considered to be available. The uncertainty of the Doppler coordinates is assumed to be 3 m in each component. There are 3 stations in the Castle Point – New Plymouth EDS with Doppler coordinates. It is assumed that precise orbits from some regional or global orbit determination project are available with accuracies of 4 m at the 1σ level ($^1/_5$ of the orbit errors adopted in sections 7.1 - 7.4). In section 7.6 estimation of orbital parameters in the GPS session adjustment is examined.

The major remaining error source is the tropospheric delay. The use of water vapour radiometers (WVRs) is frequently suggested as a means of reducing this error. However these are expensive and their use on stations with difficult access would add to the logistical problems of a GPS survey campaign. Also they do not give tropospheric delay directly but must be calibrated in a process subject to its own errors and assumptions. Davis (1986) describes the calibration of WVRs in detail. Tralli et al (1988) compared GPS adjustments using WVR data with those in which the tropospheric zenith delay was modelled as a 1st order Gauss-Markov process and estimated along with the other parameters. They found results from the 2 methods comparable. An ideal model would be one where the tropospheric zenith delay parameters were estimated with WVR data being used to assist in the estimation and with WVR calibration parameters included in the adjustment. Then the GPS data would assist in the calibration of the WVRs and the WVR data would provide information on spatial and temporal variations in the tropospheric delay. Otherwise the main value of WVRs may be to determine the stochastic properties (correlation time T_{trop} , steady state variance σ^2_{trop} , and with several WVRs, correlation distance D_{trop}) of the tropospheric delay as noted by Tralli et al (1988).

However, given the marginal benefit of using WVR data, even in a humid environment as demonstrated by Tralli et al 1988, it seems difficult to justify the extra expense of their use. The estimation of tropospheric zenith delay parameters offers a much cheaper alternative. Three different adjustment models have been considered for the tropospheric delay:

(1) Surface meteorological observations are used to determine the zenith tropospheric delay. The residual error of 2% (approximately 0.048 m) is ignored.

(2) Surface meteorological observations are used as for (1) above and the residual zenith delay error is estimated as a constant bias for each station. The *a priori* variance used is $(0.048\ m)^2$ and the *a priori* correlations of the parameters are given by a Gaussian function (equation 6.4.4) with a correlation distance of 75 km as described in section 6.4.

(3) Surface meteorological observations are used as for (1) above and the residual zenith delay error for each station is modelled as a 1st order Gauss-Markov process and estimated in a Kalman filter adjustment. The *a priori* variances and covariances are as for (2) above.

The first model is the one that was been adopted in sections 7.1 to 7.4. The perturbations can be calculated due to the residual tropospheric errors which are considered to be 1st order Gauss-Markov processes. For the second model, the equations developed in section 5.4 can be used to determine the effect of an error in the dynamic model used in the adjustment. In this case the assumed dynamic model is that of a constant parameter while the actual dynamic model is considered to be the 1st order Gauss-Markov process. In the third model it is assumed that the correct dynamic model has been used in the adjustment and thus the direct effect of the tropospheric errors has been eliminated. The simulation results of the third model will therefore be somewhat optimistic as no account is taken of the possibility of the correlation time used in the dynamic model being significantly incorrect. Tralli et al (1988) used correlation times of 1 hour and 10 hours in their experiment, to test the sensitivity of the solution to the choice of this parameter. The differences in the baseline repeatability for these extreme values was of the order of 10% to 20%. The equations of section 5.4.1 could also be used to evaluate the sensitivity of the solution to the choice of correlation time. Such a study, while potentially valuable, is beyond the scope of this investigation and only the simpler case of the effect of dynamic model errors in the constant parameter model is considered.

The suitability of the constant bias model for the zenith tropospheric delay (model 2) will obviously depend on the change in the actual tropospheric delay during the observation session. Thus it is expected that the errors in this model will be dependent in some way, on the ratio of the session length to the correlation time. If the session length is a small fraction of the correlation time the results of models 2 and 3 should be similar. If the session length is greater than the correlation time the results of models 1 and 2 should be similar.

Two criteria have been used to judge the relative merits of the 3 tropospheric models above: the ease of ambiguity resolution and the errors in the height component of baselines. Perturbations in heights and ambiguities are the principal effects of residual tropospheric delay errors. If the errors in the ambiguities can be kept low, ambiguity resolution will ensure that the tropospheric perturbation of the horizontal coordinates and strain parameters is minimal. Table 7.5.1 shows the total error for the least accurately determined ambiguity in session 7. This session has inter-station distances up to 95 km

and is more sensitive to tropospheric errors than the sessions with shorter lines. The maximum ambiguity errors are shown for the 3 tropospheric models assuming correlation times T_{trop} of 1, 2, 4, 8, and 16 hours. The expected (1σ) change in zenith tropospheric delay during the 2 hour observing session Δ_{trop} is also shown based on the correlation time and the steady state variance σ^2_{trop} of $(0.048\ m)^2$.

Table 7.5.1 Maximum ambiguity errors (cycles) for session 7 with correlation times, T_{trop} of 1, 2, 4, 8, and 16 hours. 1 GMP is the 1st order Gauss-Markov process. Δ_{trop} is the 1σ modelled change in tropospheric zenith delay during the 2 hour observation session.

		Tropospheric model		
T_{trop} (hrs)	Δ_{trop} (m)	Not estimated (cycles)	Constant (cycles)	1 GMP (cycles)
1	0.063	0.63	0.59	0.19
2	0.054	0.62	0.37	0.18
4	0.043	0.62	0.28	0.18
8	0.032	0.62	0.24	0.18
16	0.023	0.61	0.21	0.18

The ambiguity errors shown are the total errors including the precision of the adjustment and the perturbations due to orbital errors and origin station coordinates. It is not useful to consider the tropospheric errors in isolation because one of the effects of estimating tropospheric zenith delay parameters (or indeed any extra parameters) is an increase in the computed parameter variances (decrease in precision) and an increase in perturbations from other error sources. In all the examples presented here, the decrease in perturbation that comes from the elimination of the tropospheric error is greater than the increase from the other error sources but if the orbit or origin coordinate errors were large this would not necessarily be the case. This highlights the need to tackle all major error sources simultaneously rather than attempting to eliminate the effect of one error source while ignoring the effect of other, possibly more serious, errors.

When the correlation time is 1 hour (half of the session length) the results from the constant parameter tropospheric model are only slightly (6%) better than those from the model where the tropospheric delay error is ignored. With a

correlation time of 16 hours (8 times the session length) the results from the constant parameter model are nearly as good as those where the tropospheric delay is correctly modelled as a 1st order Gauss-Markov process.

The criterion for ambiguity resolution has been tightened here to require total errors of less than 0.5 cycles at the 99% confidence level for an ambiguity to be resolvable. Ambiguities meet this criterion if their total error is less than 0.194 cycles or 0.037 m. This was applied using the ambiguity resolution scheme outlined in section 7.3, to the adjustments with a correlation time of 4 hours. For models 1 and 2 where tropospheric parameters were not estimated or were estimated as constant parameters, 6 ambiguities could not be resolved. In both cases they could not be resolved at the 95% confidence level either. When the tropospheric zenith delay was estimated as a 1st order Gauss-Markov process, the worst determined ambiguity could be immediately resolved at the 99% confidence level. Thus, for ambiguity resolution, the Kalman filter adjustment with the tropospheric zenith delays modelled as 1st order Gauss-Markov processes is generally superior to the other 2 models, especially for networks with inter-station distances of the order of 100 km as in session 7. This conclusion must be qualified by reiterating that the errors of the Kalman filter adjustment may be optimistic as it has been assumed that the correlation time used in the adjustment is correct. Also the constant parameter model would probably be improved if the zenith delays were modelled as constant parameters in a first or second order polynomial. This would allow them to be estimated in a standard least squares adjustment without the need to adopt the Kalman filter algorithm.

Table 7.5.2 Height errors for a 90.1 km line in session 7 for ambiguity fixed and ambiguity free adjustments of the 3 tropospheric models.

	Tropospheric model		
	Not estimated	**Constant**	**1 GMP**
	metres (ppm)	metres (ppm)	metres (ppm)
Ambiguity free	0.219 (2.43)	0.094 (1.04)	0.067 (0.74)
Ambiguity fixed	0.219 (2.43)	0.092 (1.02)	0.103 (1.14)

The relative height errors for a 90.1 km baseline in session 7, are given in Table 7.5.2 for ambiguity fixed and ambiguity free adjustments using the 3 tropospheric models listed above. For tropospheric models 1 and 2, only 9 of

the 15 ambiguities were resolved in the ambiguity fixed adjustments as noted above.

The height errors in models 2 and 3, where the tropospheric zenith delay parameters are estimated, are less than half of those in model 1 where they are not estimated. Thus some form of estimation of the tropospheric parameters is desirable if accurate heights are required. The relative merits of the constant parameter model (2) and the 1st order Gauss-Markov process (3) are less obvious here. Model 3 is better than model 2 when the ambiguities are free but worse, in this case, when they are fixed. This is not true for all baselines and most showed a slight improvement of around 10% in the height errors when the ambiguities were resolved. Nevertheless it demonstrates that the improvement in horizontal coordinates and horizontal strain parameters that comes with ambiguity resolution, may be at the expense of the station height coordinates.

Table 7.5.3 Covariance analysis of the errors in deformation parameters from a 3D adjustment of **terrestrial data** and **GPS data**.

Param	Units	Precision	Origin	Orbit	Total
e_{ee}	ppm	0.40	0.10	0.05	0.41
e_{nn}	ppm	0.57	0.10	0.06	0.59
e_{en}	ppm	0.37	0.01	0.03	0.37
ω_e	arcsec	1.24	0.01	0.07	1.24
ω_n	arcsec	1.05	0.09	0.08	1.06
ω_v	arcsec	0.24	0.00	0.01	0.24
s_{2D}	ppm	0.31	0.10	0.04	0.33
γ_1	ppm	0.77	0.04	0.06	0.77
γ_2	ppm	0.75	0.02	0.06	0.75
$\min \gamma$	ppm	0.74	0.02	0.06	0.75
$\max \gamma$	ppm	0.77	0.04	0.06	0.77
t_e	m	0.053	3.000	0.002	3.000
t_n	m	0.058	3.000	0.003	3.000
t_v	m	0.269	3.000	0.015	3.012

In Table 7.5.3, results are presented of a combined terrestrial / GPS deformation adjustment of the 7 session network using the origin and orbit error assumptions as above and with the tropospheric zenith delays estimated as 1st order Gauss-Markov processes. The ambiguities have all been

resolved. The magnitude of the precision is dominated by the computed uncertainties of the terrestrial coordinates and, relative to this, the GPS errors are insignificant.

Table 7.5.4 Covariance analysis of the errors in deformation parameters from **repeated GPS surveys.**

Param	Units	Precision	Origin	Orbit	Total
e_{ee}	ppm	0.03	0.10	0.05	0.11
e_{nn}	ppm	0.05	0.10	0.06	0.13
e_{en}	ppm	0.02	0.01	0.03	0.04
ω_e	arcsec	0.06	0.01	0.07	0.10
ω_n	arcsec	0.04	0.09	0.08	0.13
ω_v	arcsec	0.01	0.00	0.01	0.01
s_{2D}	ppm	0.03	0.10	0.04	0.11
γ_1	ppm	0.06	0.03	0.06	0.09
γ_2	ppm	0.04	0.02	0.06	0.08
$\min\gamma$	ppm	0.04	0.02	0.06	0.08
$\max\gamma$	ppm	0.06	0.03	0.06	0.09
t_e	m	0.001	3.000	0.002	3.000
t_n	m	0.001	3.000	0.002	3.000
t_v	m	0.008	3.000	0.015	3.000

Table 7.5.4 shows the results of a simulated deformation adjustment based on repeated GPS observations. While this is not the direct subject of this thesis, it is difficult to separate the study of deformation using terrestrial / GPS observations from that of GPS / GPS observations because the GPS surveys will be designed for both roles. The GPS data used for the first epoch, is the simulated GPS adjustment used in section 3.4.4. This is the computed VCV of a 9 receiver, single session observation of the 9 network stations with the tropospheric delays estimated as 1st order Gauss-Markov processes and all ambiguities resolved. The data from the second epoch is the 7 session network adjustment used above. Only systematic errors from one epoch are considered. Thus the precision of the deformation parameters depends on the precisions of **both** GPS surveys and the systematic errors are those of **one** GPS survey. Allowing for systematic errors in both epochs, these results indicate that horizontal strain estimated from repeated GPS surveys can be accurate to 1 - 2 parts in 10^7 provided accurate orbits (errors $\leq$ 4 m) and origin coordinates (errors $\leq$ 3 m) are used in an adjustment of dual frequency data

where tropospheric zenith delay parameters are estimated. In such an adjustment the resolution of all ambiguities in the network should be possible at the 99% confidence level.

7.6. ORBIT ESTIMATION

In section 7.5 above it was assumed that precise orbits with accuracies of 4 meters were available from some source. The possibility of estimating orbital parameters together with the station coordinates is now considered. One question which must be addressed for orbit estimation, is whether to adopt the fiducial station concept or the free net concept (section 4.4). A number of successful orbit estimation campaigns in North America have been based on the fiducial station concept in which the coordinates of accurately determined fiducial stations are held fixed. These are generally co-located with VLBI or SLR sites and the coordinates of these points are considered to have uncertainties of a few centimetres. In the eastern Australian region the SLR site at Orroral has good coordinates with respect to the geocentre but any other tracking sites in the area will probably depend on TRANSIT Doppler coordinates; e.g., the Townsville and the Wellington sites for the Australian GPS orbit determination pilot project (Rizos et al, 1987). Another SLR site is available in Western Australia at Yaragadee but being 5000 km from New Zealand, the mutual visibility for satellites is not extensive. Also this site is nearly co-linear with Orroral and Wellington and therefore does not contribute greatly to the tracking network geometry. The VLBI sites at Tidbinbilla, Parkes and Fleurs are too close to Orroral (< 300 km) to provide good geometry for orbits to be used in New Zealand over 2000 km away. There is a VLBI baseline from Tidbinbilla near Orroral to a radio antenna at Hobart but this baseline has uncertainties at the several metre level (Harvey, 1985).

Given GPS satellite tracking stations on Doppler sites with coordinate uncertainties at the few metre level, is the fiducial station concept appropriate? To investigate this, a simple simulated tracking network was chosen involving 3 of the 5 stations of the Australian GPS orbit determination pilot project. These are Orroral and Townsville in eastern Australia and Wellington in New Zealand. These stations, and the other stations of the GPS orbit determination project, are illustrated in diagram 7.6.1.

For the covariance analysis, a reference frame specific to the orbit campaign was defined. The coordinates of Orroral were held fixed and were also considered to be without error in the covariance analysis. Thus the reference frame origin is defined by the adopted coordinates of Orroral, and is not necessarily located at the centre of mass. The uncertainty in the coordinates of

the centre of mass in this reference frame was taken to be 0.5 m in X, Y and Z. Other considered errors were adopted as described in Chapter 6 and these are summarised in table 7.6.1. The tropospheric zenith delay errors were estimated as 1st order Gauss-Markov processes as described in section 7.5.

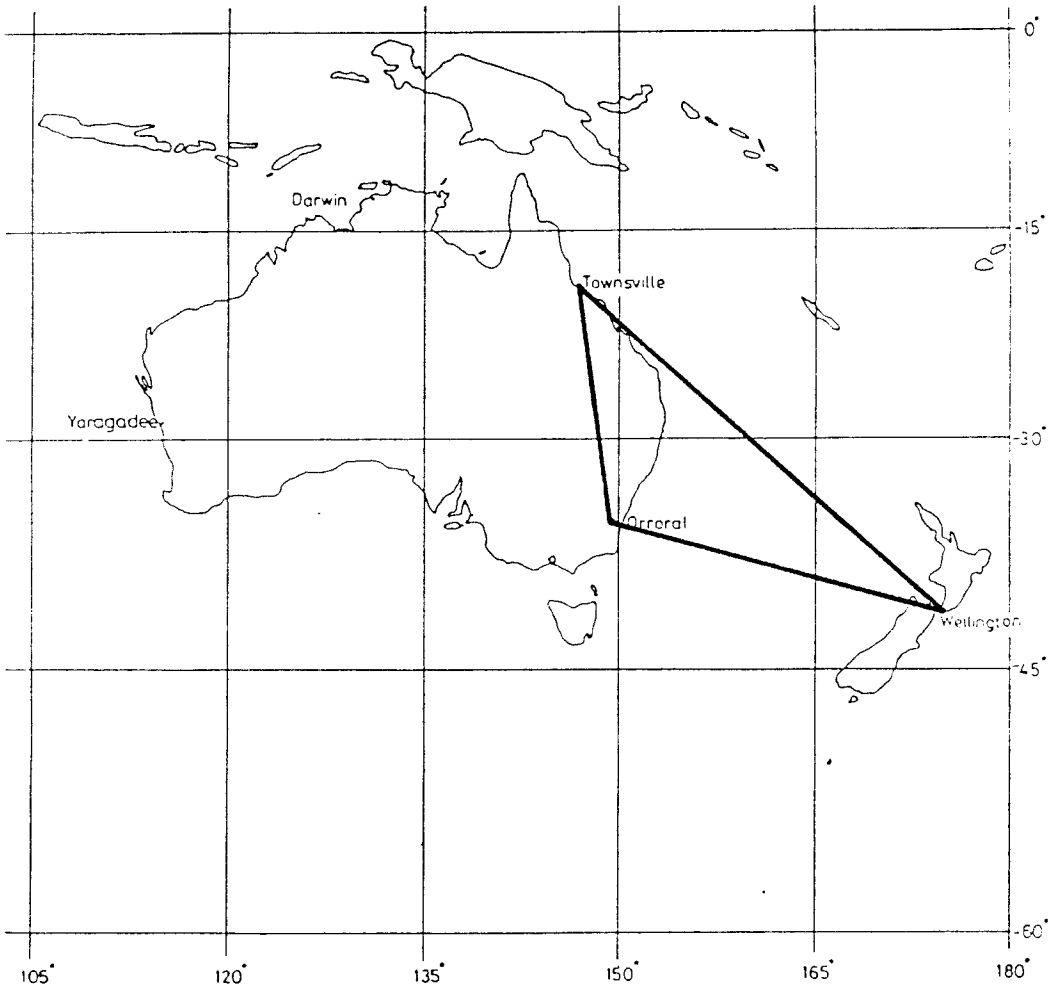

Diagram 7.6.1 Orbit tracking network for simulated orbit / network adjustment.

Satellite observation session 1 (table 7.1.3) was adopted for the 4 receivers in the survey network, but at the 3 tracking stations, observations were considered to have begun 2 hours before, and ended 2 hours after this session. Thus the simulated schedule is 6 hours of observations from the 3 tracking stations (2100 hours to 0300 hours) and 2 hours of observations from the 4 survey stations (2300 hours to 0100 hours). The same satellite session was repeated every sidereal day, for the 7 survey networks illustrated in diagram 7.4.1. For the simulations in sections 7.1 to 7.5 above, 2 minute data

was used with σ = 0.005 m. Because of the increased length of the observing session, 4 minute data with σ = 0.0035 m was adopted for this simulation. One session was tested at both rates and the results agreed to at least 2 significant figures. Given the nature of the assumptions on which the covariance analysis is based, this difference is not considered to significantly degrade the value of the results.

Table 7.6.1 *A priori* uncertainties of observations, adjusted and unadjusted parameters in the simulation of a combined orbit / network adjustment.

OBSERVATIONS	
4 minute data	0.0035 m
2 minute data (test only)	0.005 m
ADJUSTED PARAMETERS	
Receiver Coordinates	
Survey stations	3.0 m (east, north, height)
Tracking stations (free net)	3.0 m (east, north, height)
Orbits	
Initial elements	20 m (5 m, 12 m, 15 m HCL)
Troposphere	
Zenith delay	0.048 m (2%)
Correlation distance	75 km
Correlation time	4 hours
UNADJUSTED PARAMETERS	
Receiver Coordinates	
Origin	0 m by definition
Tracking stations (fiducial)	3.0 m (east, north, height)
Reference Frame	
Centre of mass	0.5 m (x, y, z)
Polar motion, UT1	0.01 arcsec (0.3 m)
GM	0.2 ppm
Force model	
Gravity field	100% of GEM-9 to (8,8)
Solar radiation	5%

The base station and base satellite adopted for each session were those given in table 7.4.5. The distances from the base station to the other survey stations are of the order of 20 to 40 km for sessions 1 to 6 and up to 90 km in session 7. The distances to the Wellington station are of the order of 190 km to 240 km and the distances to the Australian stations are of the order of 2300 km to 3400 km. Thus it was expected that the ambiguities associated with network stations would be easily resolved as in section 7.5, that the ambiguities associated with Wellington might be resolved with some difficulty and that the ambiguities associated with the Australian stations would be unresolvable.

Table 7.6.2 Total errors in baseline components for selected representative baselines on day 7. Free net adjustment.

ALL AMBIGUITIES ESTIMATED

Length	East		North		Height	
km	m	ppm	m	ppm	m	ppm
22.5	0.012	(0.54)	0.005	(0.24)	0.018	(0.80)
91.2	0.025	(0.28)	0.017	(0.19)	0.029	(0.31)
243.2	0.082	(0.34)	0.037	(0.15)	0.066	(0.27)
2318.0	0.462	(0.20)	0.440	(0.19)	0.444	(0.19)

NEW ZEALAND AMBIGUITIES FIXED

Length	East		North		Height	
km	m	ppm	m	ppm	m	ppm
22.5	0.003	(0.15)	0.002	(0.11)	0.009	(0.38)
91.2	0.007	(0.07)	0.014	(0.15)	0.022	(0.24)
243.2	0.032	(0.13)	0.022	(0.09)	0.041	(0.17)
2318.0	0.189	(0.08)	0.345	(0.15)	0.394	(0.17)

The large uncertainties adopted for the coordinates of Townsville and Wellington suggest that the fiducial network concept is inappropriate. This was tested in a simulation with the 3 tracking stations fixed. It was found that many of the ambiguities in the survey network could not be resolved at the 99% confidence level. Thus the results are worse than if orbital elements accurate to 20 m were held fixed. The 3 metre station coordinate errors resulted in satellite position errors up to 80 m. This large increase in error is due to the use of ambiguous range measurements. The perturbations in the ambiguities

were up to 10 m (50 cycles). Thus, as expected, the fiducial station concept requires station coordinates much more accurate than are available in the region at the time of writing. Over the next few years it may be expected that international VLBI and GPS campaigns will result in improved tracking station coordinates in Australia and New Zealand. At that stage the fiducial station concept will become more viable. However, as noted in section 4.4, there seems little justification for holding stations fixed that are known to have coordinate errors. It would be preferable to use Bayesian estimation with *a priori* weights on the coordinates. These weights should allow for tectonic motion between Australia and New Zealand.

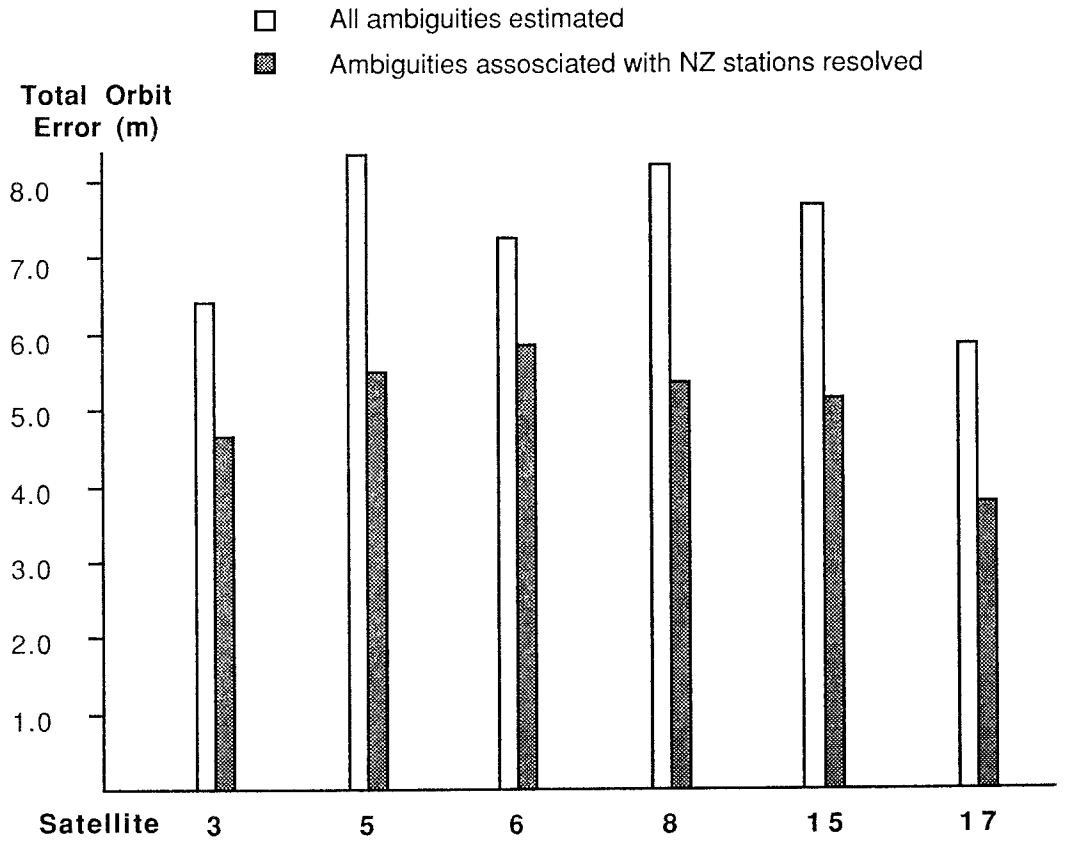

Diagram 7.6.2 Total consider errors for initial satellite positions in simulated orbit / network adjustment on day 7.

The free net concept was then adopted with one station (Orroral) held fixed and with all other stations estimated with *a priori* uncertainties of 3 m in each component. Table 7.6.2 shows the accuracies obtained for a range of baselines. All ambiguities in the survey network were resolved at confidence

levels well above the 99% level. Also it was found that all ambiguities associated with Wellington were resolved at the 99% confidence level. None of the ambiguities associated with the Australian stations could be resolved as the 1σ errors were generally greater than 0.5 cycles.

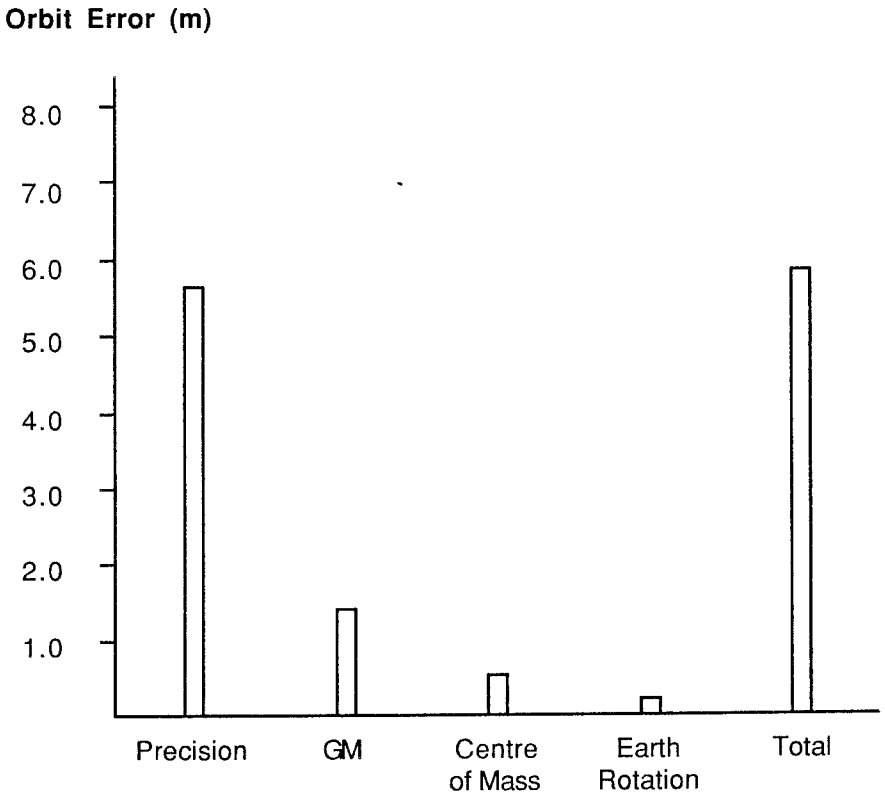

Diagram 7.6.3 Simulated errors in satellite 6, day 7 from the adjustment in which New Zealand ambiguities were fixed. The errors due to solar radiation and the geopotential model are too small to be plotted.

The accuracies of the estimated satellite initial positions are shown in diagram 7.6.2 for ambiguity free adjustment and the adjustment in which the ambiguities in New Zealand were fixed. The results are shown for day 7 which showed slightly greater accuracy than the other days, presumably because of the longer lines in the survey network. It is seen that with only 1 day's tracking and only 3 widely spaced tracking stations, accuracies close to the 4 m assumed in section 7.5 are achieved. A breakdown of the error sources is given in diagram 7.6.3 for satellite 6 on day 7 in the adjustment where New Zealand ambiguities were resolved. The errors for the other satellites were similar.

Given 7 days data from 5 widely spaced sites, as in the GPS orbit determination pilot project (Rizos et al, 1987), the figure of 4 m is likely to be a conservative value for the orbit accuracy achievable. Also, one result of orbit determination projects will be the improvement of tracking station coordinates from the several metre level assumed here, to the several decimetre level that these simulations indicate is achievable from 1 day's data. As more data is collected, improved station coordinates will ensure better orbits and a bootstrapping procedure can be used.

It should be noted, however that caution is required in interpreting these results. The effects of the major systematic error sources have been eliminated by including them in the set of adjusted parameters. However, increasing the adjusted parameter set increases the sensitivity of the adjustment to other systematic errors including those that have not been considered here. For example, there may be complex interactions between multipath and the ionospheric correction for dual frequency observations (Georgiadou & Kleusberg, 1987b) which require further study. Overall the results obtained here are considered to be a realistic, if not conservative, estimate of the present potential accuracy of GPS in this region. As more data becomes available, higher accuracy can be expected.

The orbit estimation simulations with ambiguities resolved in New Zealand were used to simulate a combined terrestrial / GPS deformation adjustment. As in section 7.5 above, the effect of the systematic GPS errors was insignificant (0.014 ppm in γ and 0.007 ppm in s_{2D}) compared with the terrestrial errors.

Of interest for earth deformation studies in New Zealand, is the determination of the baseline from Orroral to Wellington. The accuracy of the east component is particularly important as the relative motion of the Pacific and Australian plates is mostly east - west (section 2.3.2). The total error in the east component ranged from 0.189 m to 0.246 m for the 7 days tracking. The major part of this error is random and would therefore be reduced by taking the mean result over the 7 days. Separating the random component from the systematic bias it was found that the mean result has a random error of 0.086 m and a systematic bias of 0.042 m giving a total uncertainty of 0.095 m. Given relative plate motion of approximately 0.05 m/yr, these results suggest that the motion

of points in New Zealand relative to Australia could be detected in 4 years at the 95% confidence level (1.96σ).

In another study of orbit determination in this region, Thornton & Beckman (1986) used covariance analysis to predict decimetre level orbits and centimetre level errors over 2000 - 3000 km baselines, from 4 hours data. These high accuracies were based on predicted future capabilities of the system. In particular, 0.01 m errors were assumed for the fiducial station coordinates, tropospheric calibration to 0.0075 m was assumed using WVR data and it was assumed that improvements in receiver design allowed unambiguous carrier phase to be measured. These are considered to be rather optimistic estimates of the present capabilities of the system, particularly the first assumption which includes the error in the survey connection between the VLBI reference point (the intersection of the antenna axes) and the phase centre of the GPS antenna. The assumption of unambiguous carrier phase would require high accuracy pseudo-ranges on both frequencies and the future availability of L2 pseudo-ranges for civilian users is not certain. The simulations presented in this thesis are based on present capabilities at the time of writing and future improvements, while likely, are not assumed.

7.7. TERRESTRIAL SYSTEMATIC ERRORS

The analysis of this Chapter has been principally concerned with errors in GPS observations and adjustment. There are two reasons for this. Firstly, the systematic errors of terrestrial networks have been extensively studied in the past. Secondly, systematic errors in GPS are generally much larger than the random errors and thus require special scrutiny. However, it has been demonstrated that by choosing appropriate adjustment models, the effect of GPS errors on horizontal strain parameters may be reduced to the point where they are insignificant when compared with terrestrial errors. The major systematic error source in terrestrial networks is probably refraction but it is difficult to simulate the effects of refraction. One error source which may be readily simulated is the uncertainty in the shape of the earth's gravity field and this is studied using the same techniques as were used for GPS errors.

The uncertainty in the shape of the gravity field can be expressed as errors in the deflections of the vertical and geoid height. When terrestrial observations of the same type are used in two epochs, it is often reasonable to assume that the change in the geoid between epochs is small and that the deflections and geoid height errors are therefore the same in both epochs. If different observations are used in the two epochs, e.g., horizontal directions and EDM or EDM and GPS, the effects of these errors will not cancel and care is required to determine the deflections and geoid heights accurately. The program OPERA 2.3, described briefly in section 3.4.2 and Appendix F, generates partial derivatives for the deflections of the vertical and the geoid height and these can be considered to be systematic errors in a 3D terrestrial network adjustment.

Errors of 1" are assumed for the deflections of the vertical ξ and η. These errors are likely to be dominated, in mountainous areas, by the effects of local masses and therefore it is assumed that the errors are uncorrelated over the 20 km - 30 km distance between geodetic stations. Errors of 1 m are assumed for the determination of geoid height (N). Kearsley (1986) demonstrates that relative geoid heights can be determined to an accuracy of 2 - 3 ppm from gravity data. Given the mountainous environment of many of New Zealand's deformation surveys, and the proximity to the sea where gravity data is poor, a relative geoid height error of 5 ppm is adopted. For simulations, only an approximate covariance function is required and, for simplicity, the Gaussian

function used for tropospheric and ionospheric errors is adopted for the geoid height errors also.

$$\rho_N(b) = \exp\left(-\frac{b^2}{D_N^2}\right) \tag{7.7.1}$$

where b is the baseline distance between stations, D_N^2 is the correlation distance and $\rho_N(b)$ is the correlation. In section 6.4, the correlation function was used to determine the correlation distance from an assumed total error and a relative error. The same procedure may be adopted here. Adapting equations 6.4.7 and 6.4.8,

$$\rho_N(b) \approx 1-\frac{b^2}{D_N^2} \tag{7.7.2}$$

for distances less than the correlation distance and

$$\sigma_{\Delta N}(b) \approx \frac{\sqrt{2}\,\sigma_N\, b}{D_N} \tag{7.7.3}$$

where $\sigma_{\Delta N}(b)$ is the relative geoid height error and σ_N is the absolute geoid height error. From the above assumptions, $\sigma_N = 1$ m and $\frac{\sigma_{\Delta N}(b)}{b} = 5 \times 10^{-6}$. Thus the correlation distance is approximately $D_N = 280$ km.

The program DASH was used to simulate an adjustment of the terrestrial data using horizontal directions, EDM distances, astro azimuth observations with the ellipsoidal heights assigned an *a priori* uncertainty of 1 m. The results of this adjustment were then used in a simulated deformation adjustment with the GPS data set used in section 3.4.4. The results are given in table 7.7.1.

The effect of these systematic errors is generally insignificant except for η which affects the azimuth observations directly. In this example, 4 azimuth observations were used and the error in η caused rotations about all axes. The mechanism for this is not understood but it is connected with the multiple azimuth observations. When only one azimuth observation was used, the only significant effect of the error in η was a simple azimuth rotation (ω_v) as expected. The effect of η on the azimuth observations caused a small amount of shear strain to the network in this example but this was less than 0.1σ. Thus,

unless the errors in the deflections of the vertical and the relative geoid heights are significantly greater than the 1" and 5 ppm assumed here, these errors may be considered to be insignificant when compared with other errors in the terrestrial data. Of course, if the deflections of the vertical were neglected completely in the terrestrial network adjustment, errors of tens of arcseconds could cause significant distortion. Similarly if geoid heights were poorly modelled or not modelled at all, significant distortion could be expected.

Table 7.7.1 Covariance analysis of the errors in deformation parameters from a 3D adjustment of **terrestrial data** and **GPS data** due to errors in the geoid height N and deflections of the vertical ξ and η .

Param	Units	Precision	N	ξ	η	Total
e_{ee}	ppm	0.39	0.03	0.00	0.01	0.39
e_{nn}	ppm	0.57	0.03	0.00	0.04	0.58
e_{en}	ppm	0.37	0.03	0.00	0.03	0.37
ω_e	arcsec	3.59	0.01	0.03	1.25	3.80
ω_n	arcsec	2.91	0.01	0.03	1.29	3.18
ω_v	arcsec	0.23	0.00	0.01	0.40	0.46
s_{2D}	ppm	0.31	0.03	0.00	0.01	0.31
γ_1	ppm	0.76	0.03	0.01	0.05	0.76
γ_2	ppm	0.75	0.06	0.00	0.06	0.75
min γ	ppm	0.74	0.03	0.00	0.02	0.75
max γ	ppm	0.76	0.06	0.01	0.07	0.77
t_e	m	0.112	0.002	0.002	0.184	0.215
t_n	m	0.104	0.002	0.001	0.127	0.164
t_v	m	0.978	0.002	0.007	0.163	0.992

8. CONCLUSIONS AND RECOMMENDATIONS

The combination of terrestrial and GPS data for deformation analysis is likely to take two forms. Firstly, terrestrial and GPS surveys conducted in one deformation epoch (the period of time for which earth deformation can be considered to be negligible) will be combined to provide a comparison of the accuracies of the two techniques and any systematic differences between them (e.g., a scale difference). This is essentially a verification of the new technique (GPS) and a calibration of the different data sets with respect to each other. Secondly, terrestrial data from one epoch will be used with GPS data from another epoch to estimate deformation. The interpretation of these results will depend, in part, on the verification / calibration step.

The analysis in these two cases will be similar. The terrestrial and GPS data sets will first be adjusted separately to identify outliers and ensure internal consistency. The data sets will then be combined to see if any systematic differences are detected. One method of detecting such systematic differences is to use the coordinates from the terrestrial and GPS network adjustments in a deformation adjustment. If the terrestrial and GPS observations are from the same epoch, any differences will be geodetic strain; strain caused by systematic errors in the observations or adjustment. This will provide an indication of the accuracy of a deformation adjustment using combined observations. If the observations are from different epochs, and if the estimated strain is significantly greater than the geodetic strain expected from systematic errors, the result can be considered to be geophysical strain; the object of the investigation. Thus, for verification / calibration and for deformation analysis, the detection of deformation between sets of coordinates obtained from independent terrestrial and GPS network adjustments is necessary.

It is recommended that simultaneous terrestrial and GPS surveys be conducted to allow the verification of the new observation technique (GPS) and to allow the calibration of the observation types with respect to each other. This process involves the determination of orientation and scale differences, relative accuracies of the observation types and the magnitude of geodetic strain in combined adjustments.

The estimation of relative uplift or subsidence from terrestrial and GPS data has been only briefly considered in this thesis. The principal limitation is the determination of accurate relative geoid heights. This depends on the accuracy and coverage of the gravity data base; both land based and marine. In New Zealand, all points lie within about 100 km of the sea and the coverage and accuracy of gravity data off-shore may be a limiting factor in the estimation of relative geoid heights. **It is recommended that the New Zealand gravity data base be evaluated in terms of the estimation of accurate relative geoid heights to allow the combination of precise levelling and GPS data for the estimation of relative vertical movements.**

The topocentric strain model has been adopted for analysis. In terrestrial networks, the determination of the height coordinate is generally less accurate than that of the horizontal coordinates. In GPS adjustments with unresolved ambiguities, the principal axes of the 3D error ellipsoids of network stations generally lie close to the east, north and height directions with the north axis being near the semi-minor axis and either the east or the height axes being near the semi-major axis. Thus, for an analysis of errors it is convenient to adopt the east, north, vertical axes of the topocentric system. If some of the parameters of the 3D topocentric deformation model are held fixed, the results are close to those of the 2D strain model that has been used effectively in the past in New Zealand.

Homogeneous deformation has been assumed here for simplicity. This assumption is generally only suitable in New Zealand for networks of small extent (20 km or less in some areas). Given the high density of terrestrial observations in many areas it may be appropriate to use heterogeneous deformation models in the future. **It is recommended that heterogeneous deformation models be investigated, particularly with regard to their sensitivity to systematic errors.**

In Chapters 2 and 3 the parameters of 3D homogeneous strain were studied from geometric and numerical viewpoints. It was found that the vertical extensional strain parameter e_{vv} is not well determined from geodetic data and that the deformation adjustment is not significantly biased when it is held fixed at zero, even in the presence of height differences between data sets of 1 metre or more. It was found that the vertical shear strain parameters e_{ev} and

e_{nv} are highly correlated with the rotations about the horizontal axes ω_n and ω_e . When the vertical shear strains and the horizontal rotations are estimated together, they are very sensitive to systematic errors in the horizontal coordinates which makes their interpretation difficult. The decision on whether to estimate e_{ev} and e_{nv} requires care as it has a significant effect on the estimates of the other parameters. When e_{ev} and e_{nv} are held fixed at zero, the horizontal strain estimates are close to those obtained in earlier studies from plane or 2D strain models. These have proved useful for the interpretation of deformation and show close agreement with geological and geophysical data. Thus it is advisable to hold the vertical shear strains fixed at zero.

In an adjustment combining terrestrial and GPS data, the rotations about the horizontal axes ω_e and ω_n are dependent on the different reference system definitions and have little value for the interpretation of deformation. Similarly, estimates of the 3 translation parameters depend on the arbitrary definition of the origin in both networks and have little value for deformation analysis. Nevertheless, these parameters are generally non-zero and should be estimated. The azimuth rotation about the vertical axis, ω_v , has potential value for the detection of differential tectonic rotation between regions in New Zealand. However, the level of uncertainty in astronomical azimuth observations is such that it is unlikely that such rotations will be detected with confidence in the near future. The parameters with the greatest potential value for combined terrestrial / GPS deformation analysis are the 3 horizontal strain parameters, e_{ee} , e_{en} and e_{nn} . **It is recommended that the parameters estimated in the topocentric model should be the 3 horizontal strains, e_{ee} , e_{en} , e_{nn} , the 3D rotations, ω_e , ω_n , ω_v , and 3D translations, t_e , t_n , t_v .**

Various method of generating 3D data sets from essentially horizontal terrestrial surveys were considered. For terrestrial networks incorporating EDM slope distances, it was found that best results were obtained from 3D adjustments. For the examples used here, errors greater than 1 metre in height did not introduce significant geodetic strain provided the height variances were realistic. In smaller networks with steeper lines this conclusion may not be valid. Geodetic strain was introduced if any changes were made to the heights between the network adjustment and the deformation adjustment; even where the changed heights were more accurate than those originally

used. **It is recommended that terrestrial observation data sets that include EDM slope distances, be adjusted in a 3D network adjustment model and that the coordinates of this adjustment be used without alteration in the deformation adjustment.**

For triangulation networks with only one distance provided to define scale, it was found that the results of a 2D adjustment could be used to create a 3D data set provided the variances on the adopted heights were realistic. It was also found that triangulation adjustments were generally insensitive to 1 - 2 metre changes in the heights. If no heights are available with the triangulation data, GPS heights could be used although the estimated rotations about the horizontal axes would then have no physical meaning. **It is determined that 3D terrestrial data sets may be created from 2D triangulation adjustments, provided realistic variances are assigned to heights.**

The scale difference between day and night EDM observations was found to be inhomogeneous and significant geodetic strain was detected between adjustments using day observed and night observed distances. If both day and night observed EDM distances were always available in geodetic networks the mean distance could be used as a more accurate definition of scale. However this mean cannot always be formed and where it is available, significant systematic errors may still be present. **It is recommended that improved atmospheric models be investigated to account for the scale difference between EDM distances observed during the day and at night. It is further recommended that the line ratio technique be adopted for the adjustment of EDM observations where the observation schedule makes this appropriate.**

The terrestrial networks analysed had multiple azimuth observations and a test was devised to see if geodetic strain was introduced by systematic errors in these observations. It was found that no significant strain was introduced despite significant discrepancies between the observations. **It is recommended that multiple azimuth observations in a terrestrial network not be rejected *a priori* but that they be assigned realistic variances and subjected to outlier detection tests as with all observations. The observation variances should include the effects of any uncertainty in the deflection of the vertical at the observation point.**

The resolution of integer ambiguities is an important step in GPS adjustment especially for horizontal coordinates and, ultimately, the horizontal strain parameters. Selection of the best satellite geometry assists in obtaining estimates of the ambiguities accurate enough to allow them to be fixed to their correct integer values. It was found that the commonly used GDOP is not appropriate as an indicator of the best geometry for the crucial ambiguity free adjustment. The BDOP factors are based on simulations of the carrier phase adjustment and are therefore more appropriate indicators of the best satellite geometry. **It is recommended that the bias dilution of precision (BDOP) factors be used to select the best satellite geometry in preference to the geometric dilution of precision (GDOP).**

Use of the *a posteriori* variance factor to scale the computed VCV of the adjusted parameters is a standard technique in least squares analysis, particularly for a new type of observation where errors are not well known *a priori* . This technique assumes that observations have random errors with an unknown variance. In the case of GPS, the random observation error is often smaller than the systematic errors. This is especially true at this early stage in the development of GPS processing methods. Standard statistical procedures tend to become unreliable in these circumstances. It was demonstrated in a simulated multi-station adjustment, that the use of a single scale factor for the VCV matrix may result in very optimistic variances for some coordinates and very pessimistic variances for others. **It is suggested that the consider VCV matrix derived from covariance analysis is preferable to a scaled computed VCV matrix for statistical testing of estimated parameters in the presence of significant systematic errors.**

The accuracies of east coordinates and horizontal strain parameters are significantly improved by the correct resolution of integer ambiguities. However the improvement in the accuracy of height coordinates is small and, in some cases, the height accuracy is degraded by ambiguity resolution. The exception to this is for orbit adjustment where all coordinates are improved by ambiguity resolution. However, incorrectly resolved ambiguities will bias the solution. **For GPS surveys where accurate heights are the principal requirement and where orbital parameters are not estimated, the advisability of resolving the ambiguities is questioned.**

If ambiguities are resolved the effect of an origin coordinate error on a GPS adjustment is mainly a scale error. If inconsistent origin coordinates are used for different session adjustments, there will be variations in scale throughout the network and hence geodetic strain. If deformation is to be estimated from repeated GPS surveys, it is important that consistent origin coordinates be used to process the data from both epochs. It may be necessary to readjust the raw GPS data from the first epoch using better origin coordinates than were available at the time of observation. The default option for many GPS software packages is to use a C/A code position from each session as an origin coordinate. This option should not be used for deformation surveys. **It is recommended that the origin coordinates used for each session adjustment in a GPS campaign be consistent with each other. Where repeated GPS surveys are used for deformation analysis, it is recommended that consistent origin coordinates be used in processing the data from the both epochs.**

Hothem (1986) recommends that all stations in a regional deformation survey be occupied at least twice and that 80% be occupied at least 3 times. The first recommendation is considered to be essential for deformation surveys to ensure that errors in locating the antenna over the ground mark are identified at the network adjustment stage. Three occupations may allow set-up errors to be accommodated without re-measurement but the 80% requirement could be relaxed to limit costs. The requirement of 2 occupations should not be relaxed for any stations that are to be used for deformation analysis. No matter how carefully the antenna is set up, doubts are likely to arise later if anomalous results are obtained. **It is recommended that all stations in a GPS deformation survey network be occupied at least twice and that the majority be occupied at least 3 times.**

The base station - base satellite concept was adopted here for choosing the reference ambiguities that are fixed to ensure a non-singular normal matrix (other choices of reference ambiguities are also possible). Although the choice of reference ambiguities does not affect the estimates of coordinates in the ambiguity free solution, it was found that the resolution of ambiguities was facilitated by having the base station near the centroid of the session network and having the base satellite near the centroid of the satellite constellation. **It is recommended that the base station used to define the reference ambiguities be chosen to be near the centroid of the deformation**

network stations in each observation session. It is recommended that the base satellite be chosen near the centre of the satellite constellation for the session.

The use of single frequency night-time observations was considered and it was found that good results can be achieved if most ambiguities are correctly resolved. However, the resolution of these ambiguities with confidence requires the reduction of the major error sources of ionosphere, troposphere, orbits and origin coordinates. Dual frequency observations will be essential for accurate daytime observations during periods of maximum solar activity. The use of orbit adjustment to reduce orbit and origin coordinate errors requires dual frequency observations. Furthermore, the GPS surveys that are used in combination with terrestrial data will also be of value in combination with future GPS surveys and the use of dual frequency observations will significantly increase their value. **It is recommended that dual frequency observations be used for GPS deformation surveys.**

It was found that ambiguity resolution and the accuracy of height coordinates were significantly improved when tropospheric zenith delay parameters were estimated. The estimation of the tropospheric zenith delay as a constant parameter was tested. It was found that the improvement in accuracy depended on the rate of change of the actual tropospheric delay error. GPS deformation surveys that are to be combined with terrestrial data will tend to involve the occupation of high triangulation stations where changes in the weather are often rapid. The constant parameter model may be inappropriate in such circumstances. The possibility of using low order polynomials to model tropospheric delay in a standard least squares adjustment has not been tested here. **It is recommended that tropospheric zenith delay parameters be estimated. It is further recommended that the use of low order polynomials in a standard least squares adjustment to model the tropospheric delay be evaluated as an alternative to the Kalman filter model.**

The simulations of the estimation of tropospheric delay parameters using the 1st order Gauss-Markov process may be optimistic as no allowance was made for the possibility of the dynamic model being incorrect. **It is recommended that the studies on the estimation of tropospheric parameters in this thesis, be extended to determine the sensitivity of the**

adjustment to errors in the stochastic parameters adopted for the tropospheric model. It is also recommended that the 2nd order Gauss Markov process be evaluated as an alternative dynamic model for tropospheric and ionospheric delay.

These studies have confirmed the results of other researchers, that the effects of tropospheric errors can be substantially reduced by the estimation of tropospheric delay parameters. The extra benefits that may be obtained by the use of water vapour radiometers (WVRs) is doubtful. However, if the tropospheric estimation adjustment is found to be sensitive to the stochastic model adopted, WVRs may have a useful role to play. **It is recommended that the use of WVRs not be adopted as a requirement for earth deformation surveys until such time as the benefits, compared with the alternative of tropospheric estimation, can be shown to outweigh the costs. However it is recommended that WVRs be evaluated as a means of determining the stochastic properties of the troposphere in New Zealand conditions.**

No account has been taken in these studies, of the effects of multipath. Improvements in antenna design may result in this error source being effectively eliminated in the future, for carrier phase observations at least. Nevertheless this requires further study. The presence of reflective snowfields adjacent to many stations in the existing deformation networks may cause problems. **It is recommended that the effects of multipath be investigated further.**

The reduction of orbital errors, along with the reduction of tropospheric and ionospheric errors is an important step in ensuring that ambiguities can be resolved at high confidence levels. Tracking data will need to be archived along with the deformation network data to allow for improved future adjustments, e.g., as improved tracking station coordinates become available. Regional orbit determination campaigns have some advantages over global campaigns as relatively high accuracies can be achieved without the need for extensive data sets and the logistical problems in data collection are less for regional campaigns. Also there are advantages in having a tracking network reference frame defined by the coordinates of stations entirely within one tectonic plate. However, improved results are also likely if the tracking network is extended to include stations outside the region.

The origin coordinate error is also eliminated by orbit adjustment. This error is due to a discrepancy between the definition of the reference frame origin given by the coordinates of the fixed station and that given by the elements of the fixed orbits. When the orbital elements are adjusted with one station held fixed (the free net concept) this over-constraint of the datum definition is eliminated. The fiducial station method of orbit determination has proved useful in North America where there are many sites with accurate coordinates. These are regularly monitored by SLR and VLBI. In the region around New Zealand there are few such sites. Furthermore, the broad zone of deformation through New Zealand will limit the useful life of any accurate coordinates that may be determined there in the future. The fiducial station method involves an unnecessary over-constraint of the datum. The best method is considered to be Bayesian estimation with 1 fixed station and *a priori* variances on the coordinates of other stations. These variances should allow for possible tectonic motion of the tracking stations. Over several GPS campaigns, this method will allow steady improvement of station coordinates. **It is recommended that regional or global orbit determination be used for GPS deformation surveys. It is recommended that Bayesian estimation be used with no more than 1 fixed station.**

Covariance analysis has been used extensively in this thesis to study the effects of systematic errors, principally those of the GPS observations. It has been used to determine the relative merits of different observation schemes and adjustment models. It has been demonstrated that *a posteriori* statistics are often very optimistic and that the use of a single variance scale factor may not be sufficient to ensure reliable statistics. The estimation of deformation parameters in a least squares adjustment is relatively straightforward. It is the interpretation of parameter estimates that requires the greatest skill and reliable statistics are vital if geophysical strain is to be distinguished from geodetic strain. **It is recommended that covariance analysis be used in the planning of GPS surveys and in the analysis of the results of GPS adjustments. It is recommended that the assumptions on which this covariance analysis is based be continually assessed for New Zealand conditions by comparison with the results achieved in practice.**

REFERENCES

ANGUS-LEPPAN, P.V., 1979. Network adjustment by the ratio method and its meteorological basis. **Aust. J. Geod. Photo. Surv., 31**, 15-26.

BENDER, P.L., LARDEN, D.R., 1985. GPS carrier phase ambiguity resolution over lang baselines. Proc. 1st Int. Symp. Prec. Pos. GPS, U.S. Dept. of Commerce, NOAA, Rockville, Md., May, 1985.

BERTIGER, W., WU, S.C., BORDER, J.S., LICHTEN, S.M., WILLIAMS, B.G., WU, J.T., 1986. High precision GPS orbit determination using March 1985 demonstration data. Presented, American Institute of Aeronautics & Astronautics, 24th Aerospace Sciences Meeting, Jan. 1986, Reno, Nevada.

BEUTLER, G., GURTNER, W., BAUERSIMA, I., LANGLEY, R., 1985. Modeling and estimating the orbits of GPS satellites. Proc. 1st Int. Symp. Prec. Pos. GPS, U.S. Dept. of Commerce, NOAA, Rockville, Md., May, 1985.

BEUTLER, G., GURTNER, W., ROTHACHER, M., SCHILDKNECHT, T., BAUERSIMA, I., 1986. Determination of GPS orbits using double difference carrier phase observations from regional networks. Proc. 4th Int. Geod. Symp. Sat. Pos., University of Texas, Austin, Tex., 28 April - 2 May, 1986.

BEUTLER, G., BAUERSIMA, I., GURTNER, W., ROTHACHER, M., 1987a. Correlations between simultaneous GPS double difference carrier phase observations in the multistation mode: Implementation considerations and first experiences. **Manuscripta Geodaetica, 12**, 40-44.

BEUTLER, G., BAUERSIMA, I., GURTNER, W., ROTHACHER, M., SCHILDKNECHT, T., 1987b. Atmospheric refraction and other important biases in GPS carrier phase observations. IUGG XIX General Assembly, Vancouver, Aug. 1987.

BEUTLER, G., BAUERSIMA, I., BOTTON, S., GURTNER, W., ROTHACHER, M., SCHILDKNECHT, T., 1987c. Accuracy and biases in the geodetic application of the Global Positioning System. IUGG XIX General Assembly, Vancouver, Aug. 1987.

BEVIN, A.J., FORSTER,T.A., 1973. Evaluation of the laser geodimeter for precise measurement. **N.Z. Surv., 27**, 410-434.

BEVIN, A.J., 1981. Geodetic surveys for earth deformation. Misc Series 5, Royal Society of N.Z., 87-96.

BEVIN, A.J., OTWAY, P.M., WOOD, P.R., 1984. Geodetic monitoring of crustal deformation in New Zealand. Misc. Series 7, Royal Society of N.Z., 13-60.

BIBBY, H.M., 1973. The reduction of geodetic survey data for the detection of earth deformation. Report 84, Geophysics Division, Dept Scientific & Industrial Research, N.Z.

BIBBY, H.M., 1975. Crustal strain from triangulation in Marlborough, New Zealand. **Tectonophysics, 29**, 529-540.

BIBBY, H.W., WALCOTT, R.I., 1977. Earth deformation and triangulation in New Zealand. **N.Z. Surv., No.252**, 741-762.

BIBBY, H.M., 1981. Geodetically determined strain across the southern end of the Tonga-Kermadec-Hikurangi subduction zone. **Geophys. J. R. Astr. Soc., 66**, 513-533.

BIBBY, H.M., 1982. Unbiased estimate of strain from triangulation data using the method of simultaneous reduction. **Tectonophysics, 82**, 161-174.

BIERMAN, G.J., 1977. **Factorization methods for discrete sequential estimation**. Academic Press, Orlando. 241p.

BLEWITT, G., 1988. Ambiguity resolution. 3rd Annual GPS Geodesy Workshop, J.P.L., March 1988.

BLICK, G.H. 1986. Geodetic determination of crustal strain from old survey data in Central Otago. Bull. 24, Royal Society of N.Z., 47-54

BOCK, Y., ABBOT, R.I., COUNSELMAN, C.C., GOUREVITCH, S.A., KING, R.W., PARADIS, A.R., 1984. Geodetic accuracy of the Macrometer model V-1000. **Bull. Geod., 58(2).**

BOCK, Y., GOUREVITCH, S.A., COUNSELMAN, C.C., KING, R.W., ABBOT, R.I., 1986. Interferometric analysis of GPS phase observations. Submitted to **Manuscripta Geodaetica, 11**, 282-288.

BOMFORD, G., 1980. **Geodesy.** 4th Ed, Oxford University Press. 855p.

BOSSLER, J.D., 1972. Bayesian inference in geodesy. PhD Dissertation, Dept Geodetic Science, Ohio State University, 79p.

BOYES, W.S., 1971. Horizontal and vertical crustal movement in the Inangahua earthquake of 1968. Bull. 9, Royal Society of N.Z., 61-72.

BRUNNER, F.K., FRASER, C.S., 1978. An atmospheric turbulent transfer model for EDM reduction. Proc. Int. Symp. EDM and Influence Atmos. Refraction., Wagening, P. Richardus (ed), 304-334.

BRUNNER, F.K., COLEMAN, R., HIRSCH, B., 1981. A comparison of computation methods for crustal strains from geodetic measurements. **Tectonophysics, 71**, 281-298.

BRUNNER, F.K., CHAMBERLAIN, S.M., FREI, E., 1986. Test measurements using the WM 101. **Österreichischen Zeitschrift, Vermessungswesen, Photogrammetrie, 74**, 141-154.

BRUNNER, F.K., COLEMAN, R., 1988. Strain effects near Palmdale associated with the San Fernando earthquake (1971). submitted to **Tectonics.**

BUCY, R.S., JOSEPH, P.D., 1968. **Filtering for stochastic processes with applications to guidance.** Interscience, New York. 195p

CAMPBELL, J., MANIATIS, T., MÜLLER, A., VIERBUCHEN, J., LOHMAR, F.J., 1986. On the generation of ionospheric refraction corrections for single frequency GPS measurements. Proc. 4th Int. Geod. Symp. Sat. Pos., University of Texas, Austin, Tex., 28 April - 2 May, 1986.

CASPARY, W.F., 1987. Concepts of network and deformation analysis. Monograph No. 11, School of Surveying, University of N.S.W. 183p.

CHISHOLM, G.S. 1987. Integration of GPS into hydrographic survey operations. Unisurv S-29, School of Surveying, University of N.S.W.

CLYNCH, J.R., COCO, D.S., 1986. Error characteristics of high quality geodetic GPS measurements: clocks, orbits and propagation effects. Proc. 4th Int. Geod. Symp. Sat. Pos., University of Texas, Austin, Tex., 28 April - 2 May, 1986.

COCO, D.S., CLYNCH, J.R., 1982. The variability of the tropospheric range correction due to water vapor fluctuations. Proc. 3rd Int. Geod. Symp. Sat. Doppler Pos., University of Texas, Las Cruces, N.M., Feb, 1982.

COLEMAN, R., LAMBECK, K., 1983. Crustal motion in south-eastern Australia: Is there geodetic evidence for it?. **Aust. J. Geod. Photo. Surv., 39**, 1-26.

COUNSELMAN, C.C., III, SHAPIRO, I.I., GREENSPAN, R.L., COX, D.B., Jr, 1979. Backpack VLBI terminal with subcentimeter capability. Radio Interferometry Techniques for Geodesy, NASA Conference Publication 2115, NASA Scientific and Technical Information Office, Washington, D.C., 409-414.

CROSS, P.A., 1983. Advanced least squares applied to position fixing. Working Paper No. 6, Dept Land Surveying, North East London Polytechnic. 205p.

DAVIDSON, J.M., THORNTON, C.L., VEGOS, C.J., YOUNG, L.E., Y UNCK, T.P., 1985. The March 1985 demonstration of the fiducial network concept for GPS geodesy: A preliminary report. Proc. 1st Int. Symp. Prec. Pos. GPS, U.S. Dept. of Commerce, NOAA, Rockville, Md., May, 1985.

DAVIS, J.L., HERRING, T.A., SHAPIRO, I.I., ROGERS, A.E.E, ELGERED, G., 1985. Geodesy by radio interferometry: Effects of atmospheric modeling errors on estimates of baseline length. **Radio Science, 20(6)**, 1593-1607.

DAVIS, J.L., 1986. Atmospheric propagation effects on radio interferometry. Scientific Rpt 1, Air Force Geophysics Laboratory, USAF, Hanscom, Mass.

DECKER B.L., 1986. World geodetic system 1984. Proc. 4th Int. Geod. Symp. Sat. Pos., University of Texas, Austin, Tex., 28 April - 2 May, 1986.

DELIKARAOGLOU, D., 1987. On principles, methods and recent advances in studies towards a GPS - based control system for Geodesy and Geodynamics. Preprint, NASA Technical Memorandum, Goddard.

DENYS, P.H., 1987. The analysis of second order electronic distance measuring equipment for monitoring local deformation. MSurv Thesis, Dept. of Surveying, University of Otago, N.Z.

DERMANIS, A., LIVIERATOS, E., 1983. Applications of deformation analysis in geodesy and geodynamics. **Reviews of Geophysics and Space Physics, 21(1)**, 41-50.

ECKELS, R., 1987. Surveying with GPS in Australia. Unisurv Report S-28, University of N.S.W.

EEG, J., KRARUP, T., 1973. Integrated geodesy. Internal Report 7, Danish Geodetic Institute, Copenhagen.

EISSFELLER, B., HEIN, G.W., 1986. A contribution to 3D operational geodesy. Part 4: The observation equations of satellite geodesy in the model of integrated geodesy. Heft 17, Universität der Bundeswehr, München, 190p.

ELGERED, G., DAVIS, J.L., HERRING, T.A., SHAPIRO, I.I., 1987. Measuring, modeling, and estimating the wet atmospheric delay in VLBI and GPS geodetic systems. Pres. A.G.U Spring meeting, Baltimore, May 1987.

FRANK, F.C., 1966. Deduction of earth strains from survey data. **Bull. Seismol. Soc. Am., 56**, 35-42.

GAPOSCHKIN, E.M., KOLACZEK, B., (Eds) 1981. **Reference coordinate systems for earth dynamics**. D. Reidel, Dordrecht, Holland, 396p

GARDNER, C.S., 1977. Correction of laser tracking data for the effects of horizontal refractivity gradients. **Applied Optics, 16**, 2427-2432.

GELB, A., 1974. **Applied optimal estimation**. M.I.T. Press Cambridge, Mass. 374p.

GEORGIADOU, Y., KLEUSBERG, A., 1987. Ionospheric refraction and multipath effects in GPS carrier phase observations. IUGG XIX General Assembly, Vancouver, Aug. 1987.

GEORGIADOU, Y., KLEUSBERG, A., 1988. On the effect of ionospheric delay on geodetic relative GPS positioning. **Manuscripta Geodaetica, 13**, 1-8.

GOAD, C.C., 1985. Precise relative position determination using Global Positioning System carrier phase measurements in a non-difference mode. Proc. 1st Int. Symp. Prec. Pos. GPS, U.S. Dept. of Commerce, NOAA, Rockville, Md., May, 1985.

GRAFAREND, E., SCHAFFRIN, B., 1976. Equivalence of estimable quantities and invariants in geodetic networks, **Zeitschrift für.Vermessungswesen, 101(11)**, 485-491.

HANNAH, J., 1986. Accuracy estimates of, and the rejection criteria used on the observed quantities from the New Zealand EDS networks. Bull. 24, Royal Society of N.Z., 463-471.

HARVEY, B.R., 1985. The combination of VLBI and ground data for geodesy and geophysics. Unisurv S-27, School of Surveying, University of N.S.W.

HARVEY, B.R., 1987. Degrees of freedom - simplified. **Aust. J. Geod. Photo. Surv., 46 & 47**, December, 1987, 57-68.

HATCH, R., LARSON, K., 1985. Magnet-4100 GPS survey program processing techniques and test results. Proc. 1st Int. Symp. Prec. Pos. GPS, U.S. Dept. of Commerce, NOAA, Rockville, Md., May, 1985.

HATCH, W., GOAD, C., 1973. Mathematical description of the ORAN error analysis program. Wolf Research & Development Corp., Riverdale, Md.

HATHERTON, T., 1980. Shallow seismicity in New Zealand 1956 - 1975. **J. Royal Society, N.Z., 10**, 19-25.

HEIN, G.W., 1982a. A contribution to 3D operational geodesy. Part 1: Principle and observation equations of terrestrial type. Proc. Int. Symp. on Geodetic Networks and Computations, Reihe B, Nr 258/VII, Deutsche Geod. Komm., 31-64.

HEIN, G.W., 1982b. A contribution to 3D operational geodesy. Part 2: Concepts of solution. Proc. Int. Symp. on Geodetic Networks and Computations, Munich 1981, Reihe B, Nr 258/VII, Deutsche Geod. Komm., 65-85.

HEIN, G.W., LANDAU, H., 1983. A contribution to 3D operational geodesy. Part 3: OPERA – A multi-purpose program for operational adjustment of geodetic observations of terrestrial type. Reihe B, Nr 264, Deutsche Geod. Komm., 81p.

HENDERSON, J., 1937. The West Nelson earthquakes of 1929 with notes on the geological structure of West Nelson. **N.Z. J. Sci. Tech., 19**, 65-144.

HERRING, T.A., 1986. Precision of vertical position estimates from Very Long Baseline Interferometry. **J. Geophys. Res, 91**, 9177-9182.

HOPFIELD, H.S., 1969. Two quartic tropospheric refractivity profile for correcting satellite data. **J. Geophys. Res, 74**, 4487-4499.

HOTHEM, L.D., 1986. Subsidence studies with GPS: planning and field operation aspects. Proc. Deformation Measurements Workshop, Modern Methodology in Precise Engineering and Deformation Surveys - II, Massachusetts Institute of Technology, Oct 31 - Nov 1, 1986.

HSUI, A.T., TOKSOZ, M.N., 1981, Back arc spreading: trench migration, continental pull or induced convection. **Tectonophysics, 74**, 89-98.

JONES, H.E., 1971. Systematic errors in Tellurometer and Geodimeter measurements. **Can. Surv., 25(4)**, 406-423.

KAMP, P.J.J., 1984. Neogene and quarternary extent and geometry of the subducted Pacific plate beneath North Island, New Zealand: implications for Kaikoura tectonic. **Tectonophysics, 108**, 241-256.

KARIG, D.E., 1969. Kermadec Arc - New Zealand tectonic confluence. **N.Z. J. Geol. Geophys., 13**, 21-29

KEARSLEY, A.H.W., SIDERIS, M.G., KRYNSKI, J., FORSBERG, R. SCHWARZ, K.P., 1985. White Sands revisited. A comparison of techniques to predict deflections of the vertical. UCSE Report 30007, University of Calgary, Division of Surv. Eng., 166p.

KEARSLEY, A.H.W., 1986. Data requirements for determining precise relative geoid heights from gravimetry. **J. Geophys. Res., 91**, 9193-9201.

KING, R.W., MASTERS, E.G., RIZOS, C., STOLZ, A., COLLINS, J., 1987. **Surveying with GPS**. Dümmler Verlag, Bonn, 128p.

KLOBUCHAR, J.A., 1983. Ionospheric effects on earth - space propagation. Air Force Geophysics Laboratory, AFGL-tr-84-004.

KLOBUCHAR, J.A., 1986. Design and characteristics of the GPS ionospheric time delay algorithm for single frequency users. Proc. Position Location and Navigation Symposium, Las Vegas, NV, Nov. 1986.

KOUBA, J., LAMBERT, A., POPELAR, J., STEEVES, R.R., CANNON, W.C., 1986. Plans for VLBI and GPS monitoring network for geodesy and geodynamics in Canada. **Advances in Space Research, 6(9)**, 75-78.

KRAKIWSKY, E.J., 1981. A synthesis of recent advances in the method of least squares. Tech Rpt 42 (reprint) Dept Survey Engineering, University of New Brunswick.

KROGER, P.M., DAVIDSON, J.M., GARDNER, E.C., 1986. Mobile Very Long Baseline Interferometry and Global Positioning System measurement of vertical crustal motion. **J. Geophys. Res. 91**, 9169-9176.

LADD, J.W., 1986. Establishment of a 3-dimensional geodetic network using the Macrometer II^{TM} dual-band surveyor. **Bull. Geod. 60**, 255-264.

LANDAU, H., HEHL, K., EISSFELLER, B., HEIN, G.W. 1987. OPERA 2.3 user's guide. Institute of Astronomical and Physical Geodesy, University FAF, Munich.

LEE, L.P., 1978. First order geodetic triangulation of New Zealand 1909-49 and 1973-74. Tech. Series No. 1, Dept. Lands & Survey, New Zealand. 97p.

LERCH, F.J., KLOSKO, S.M., LAUBSCHER, R.E., WAGNER, C.A., 1979. Gravity model improvement using GEOS-3 (GEM-9 and GEM-10). **J. Geophys. Res., 84**, 3897-3915.

LICHTEN, S.M., BORDER, J.S., 1987. Strategies for high precision GPS orbit determination. **J. Geophys. Res. 92**, 12751-12762.

LIEBELT, P.B., 1967. **An introduction to optimal estimation**. Addison-Wesley, Reading, Mass, 273p.

LINDLOHR, W., WELLS, D., 1985. GPS design using undifferenced carrier beat phase observations. **Manuscripta Geodaetica, 10**, 255-295.

LIVIERATOS, E., VLACHOS, D., 1981. The influence of correlations in computing crustal strains from trigonometric network results. **Tectonophysics, 77**, 323-332.

MACKIE, J.B. 1982. The relationship between the WGS72 doppler satellite datum and the New Zealand Geodetic Datum 1949. Report 178, Geophysics Division, Dept. Scientific & Industrial Research, N.Z.

MACKIE, J.B., 1983. Transformation of coordinates from the World Geodetic System (WGS-72) doppler satellite datum to the New Zealand Geodetic Datum (NZGD-49). **N.Z. Surv., No. 262**, 412-420.

MARSH, J.G., LERCH, F.J., PUTNEY, B.H., CHRISTODOULIDIS, D.C., FELSENTREGER, T.L., SANCHEZ, B.V., SMITH, D.E., KLOSKO, S.M., MARTIN, T.V., PAVLIS, E.C., ROBBINS, J.W., WILLIAMSON, R.G., COLOMBO, O.L., CHANDLER, N.L., RACHLIN, K.E., PATEL, G.B., BHATI, S., CHINN, D.S., 1987. An improved model of the Earth's gravitational field: GEM-T1. NASA Tech. Memorandum, 4019.

MEISSL, P., 1982. Least squares adjustment.: a modern approach. Rpt 43, Geodetic Institute, Technical University, Graz.

MERMINOD, B., 1988. Resolution of the cycle ambiguities. Unpublished Report, School of Surveying, University of N.S.W.

MERMINOD, B., GRANT, D.B., RIZOS, C. 1988. A new approach to satellite selection and observation scheduling for GPS surveys. In prep., School of Surveying, University of N.S.W.

MERMINOD, B., RIZOS, C. 1988. A surveyor's perspective of Kalman filtering. **Aust. J. Geod. Photo. Surv., 49**, December, 1988, 1-38.

MORGAN, P., XING, C., ROGERS, C., 1986. An assessment of the internal precision and quality of GPS data from the S.A. geodetic network project. Research Project Report, School of Applied Science, Canberra College of Advanced Education, Canberra.

MORGAN, P., 1987. Models for GPS network design. **Aust. J. Geod. Photo. Surv., 46 & 47**, December, 1987, 41-55.

MORITZ, H., 1980a. **Advanced physical geodesy**. Abacus Press, Tunbridge Wells, 500p.

MORITZ, H., 1980b. Geodetic reference system 1980. **Bull. Geod. 54(3)**, 395-405.

NATIONAL COMMITTEE FOR GEOLOGICAL SCIENCES, 1973. Report on earth deformation studies. Royal Society of N.Z.

NORTON, T., 1987. Monitoring the precision of relative GPS positioning. Proc. RMIT Centenary GPS Conf., Melbourne, Victoria, Aug, 1987.

PARTIS, I.S., BRUNNER, F.K., 1988. The use of dual frequency Transit observations to determine ionospheric corrections for single frequency GPS. Proc. Int. Symp. on GPS, Qld, Oct 17-19, 1988.

PELZER, H., 1971. Zur analyse geodätischer deformationsmessungen. Reihe C, Nr 164, Deutsche Geod. Komm., 86p.

PERCIVAL, T., 1987. Detection of space vehicle clock errors by CSIRO. Proc. RMIT Centenary GPS Conf., Melbourne, Victoria, Aug, 1987.

PRECOTT, W.H., SAVAGE, J.C., KINOSHITA, W.T., 1979. Strain accumulation in the western United States between 1970 and 1978. **J.Geophys.Res., 84**, 5423-5435.

RAPP, R.H., 1981. The earth's gravity field to degree and order 180 using SEASAT altimeter data, terrestrial gravity data, and other data. Rpt. 322, Dept Geod. Sci. & Surv., Ohio State University.

REBER, E.E., SWOPE, J.R., 1972. On the correlation of the total precipitable water in a vertical column and absolute humidity at the surface. **J. Appl. Meteorology, 11**, 1322-1325.

REIGBER, C.H., SCHWINTZER, P., MÜLLER, H., BARTH, W., MASSMANN, F.H., 1987. The terrestrial reference frame underlying the GRIM earth model determination. XIX I.U.G.G. General Assembly, I.A.G, August 1987, Vancouver, B.C.

REILLY, W.I., 1979. Determination of geometric and gravimetric earth deformation parameters from geodetic observations. Report 140, Geophysics Division, Dept. Scientific & Industrial Research, N.Z.

REILLY, W.I., 1980. Three dimensional adjustment of geodetic networks with incorporation of gravity field data. Report 160, Geophysics Division, Dept. Scientific & Industrial Research, N.Z., 54p.

REILLY, W.I. 1986a. Crustal bending in Otago,New Zealand, from the evidence of geodetic measurements. Bull 24, Royal Society of N.Z., 65-73.

REILLY, W.I., 1986b. Heterogeneous strain in earth deformation. Report 210, Geophysics Division, Dept. Scientific & Industrial Research, N.Z.

REMONDI, B.W., 1984. Using the Global Positioning System (GPS) phase observable for relative geodesy: modeling, processing, and results. PhD Dissertation, Centre for Space Research, University of Texas at Austin. 360p.

REMONDI, B.W., 1985. Global Positioning System carrier phase: description and use. **Bull Geod, 59**, 361-377.

REYNERS, M., 1980. A microearthquake study of the plate boundary, North Island, New Zealand. **Geophys. J. R. astr. Soc.**, 63, 1-22.

RIZOS, C., STOLZ, A., 1985. Force modelling for GPS satellite orbits. Proc. 1st Int. Symp. Prec. Pos. GPS, U.S. Dept. of Commerce, NOAA, Rockville, Md., May, 1985.

RIZOS, C., GOVIND, R., STOLZ, A., LUCK, J.McK., 1987. The Australian GPS orbit determination pilot project. **Aust. J. Geod. Photo. Surv., 46 & 47**, December, 1987, 17-40.

RIZOS, C., STOLZ, A., 1988. The UNSW satellite measurement analysis software system (USMASS). **Aust. J. Geod. Photo. Surv., 48**, June, 1988, 1-28.

ROBERTSON, K.D., 1972. The use of line pairs in trilateration and traverse. **Survey Review, 165**, 290-306.

ROWE, G.H., 1981. Doppler satellite positioning. **N.Z. Surv., No. 258**, 608-624.

ROYAL SOCIETY OF NEW ZEALAND, EARTH DEFORMATION COMMITTEE 1985. Review of earth deformation studies in New Zealand. Misc. Series 13, Royal Society of N.Z., 108p

SAASTAMOINEN, J., 1973. Theory of atmospheric refraction. **Bull. Geod. 107**.

SAVAGE, J.C., BURFORD, R.O., 1970. Accumulation of tectonic strain in California. **Bull. Seismological Soc. America, 60(6)**, 1877-1896.

SCHAFFRIN, B., BOCK, Y., 1987. A unified scheme for processing GPS dual band phase observations. Submitted to **Manuscripta Geodaetica**.

SCHEIDEGGER, A.E., 1982. **Principles of geodynamics**. 3rd Ed; Springer-Verlag, 395p.

SIDERIS, M., SCHWARZ, K. 1986. The use of GPS and Doppler heights in NAVD. Proc. 4th Int. Geod. Symp. Sat. Pos., University of Texas, Austin, Tex., 28 April - 2 May, 1986.

SLATER, L.E., 1979. Can the ratios of single wavelength EDM data improve the resolution of small changes in line length? A comparison with multi-wavelength EDM data. **J. Geophys Res., 84**, 3659-3663.

SLATER, L.E., MCGARR, A., LANGBEIN, J.O., LINKER, M.F., 1983. Multiwavelength EDM measurements in Southern California. **Tectonophysics, 97.**

SMITH, E.G.C., DAVEY, F.J., 1984. Joint hypocentre determination of intermediate depth earthquakes in Fiordland, New Zealand. **Tectonophysics, 104**, 127-144.

STACEY, F.D., 1977. **Physics of the earth.** 2nd Ed; John Wiley & Sons, New York, 414p.

STEIN, W.L., 1986. NAVSTAR Global Positioning System 1986 status and plans. Proc. 4th Int. Geod. Symp. Sat. Pos., University of Texas, Austin, Tex., 28 April - 2 May, 1986.

STEPHENS, S.A., SKRUMEDA, L.L., 1987. Stochastic colored noise estimation of clocks and tropospheres in analysis of GPS geodetic data. Pres. Spring 1987 Meeting A.G.U.

STOLZ, A., MASTERS, E.G., RIZOS, C., 1984. Determination of GPS satellite orbits for geodesy in Australia. **Aust. J. Geod. Photo. Surv., 40**, 41-51.

STOLZ, A., RIZOS, C., HIRSCH, B., SCHUTZ, B.E., TAPLEY, B.D., 1987. An experiment to determine regional and global GPS satelite orbits. **Aust. J. Geod. Photo. Surv., 46 & 47**, December, 1987, 41-51.

SUGGATE, R.P., 1986. Astride a plate boundary. Bull. 24, Royal Society of N.Z., 1-17.

THOMSON, D.B., NASSAR, M.M., MERRY, C.L., 1974. Distortions of Canadian geodetic networks due to the neglect of deflections of the vertical and geoidal heights. **Can. Surv., 28**, 598-605.

THORNTON, C.L., BECKMAN, B.C., 1986. GPS-based system for regional geodesy in New Zealand and Australia. Proc. Int. Symp. Recent Crustal Movements of the Pacific Region, Wellington, N.Z. 9-14 Feb 1986, Royal Society of New Zealand, Bulletin 24, 213-221.

TORGE, W., 1980. **Geodesy**. Trans. by C. Jekeli, W. De Gruyeter, 254p.

TRALLI, D.M., DIXON, T.H., STEPHENS, S.A., 1988. The effect of wet tropospheric path delays on estimation of geodetic baselines in the Gulf of California using the Global Positioning System. **J. Geophys. Res.**, In Press.

TREUHAFT, R.N., LANYI, G.E., 1987. The effect of the dynamic wet troposphere on radio interferometric measurements. **Radio Science, 22(2)**, 251-265.

TRIMBLE NAVIGATION LTD, 1986. TRIMVEC^{TM} GPS survey software preliminary user's manual. Trimble Navigation Ltd, Sunnyvale California.

VAN DEN BERG, W.M., 1979. Whakamaru - Maraetai control survey computed by the use of scale factors. **N.Z. Surv., 29**, 124-140.

VANICEK, P., KRAKIWSKY, E.J., 1986. **Geodesy: The concepts**. 2nd Ed, North Holland, Amsterdam. 697p.

VINCENTY, T., 1975. Length ratios and scale unknowns in trilateration, **J. Surveying and Mapping**, ACSM, 35: 245-250.

VINCENTY, T., BOWRING, B.R., 1978. Application of three - dimensional geodesy to adjustment of horizontal networks. NOAA Tech. Mem. NOS NGS-13, 7p.

VINCENTY, T., 1980. Height - controlled three - dimensional adjustment of horizontal networks. **Bull. Geod., 54**, 37-43.

WALCOTT, R.I., 1978a. Present tectonics and late cenozoic evolution of New Zealand. **Geophys.J.R.Astr.Soc, 52**, 137-164.

WALCOTT, R.I., 1978b. Geodetic strains and large earthquakes in the axial tectonic belt of North Island, New Zealand. **J.Geophys.Res., 83**, 4419-4429.

WALCOTT, R.I., 1979. Plate motion and shear strain rates in the vicinity of the Southern Alps. Bull.18, Royal Society of N.Z., 5-12.

WALCOTT, R.I., 1984. The kinematics of the plate boundary zone through New Zealand: A comparison of short and long term deformations. **Geophys. J. R. Astr. Soc., 79**, 613-633.

WANLESS, B., LACHAPELLE, G., 1988. NOVAS - An automated program for the precise reduction of GPS static carrier phase observations. Submitted **Manuscripta Geodaetica.**

WARE, R.H., ROCKEN, C., HURST, K.J., 1985. A Global Positioning System baseline determination including bias fixing and water vapour radiometer corrections. **J. Geophys. Res., 91**, 9183-9192.

WELLMAN, H.W., 1955. New Zealand Quaternary tectonics. **Geologische Rundschau, 43**, 248-257.

WELLMAN, P., 1981. Crustal movement determined from repeat surveying – results from southeastern and southwestern Australia. **J. Geological Soc of Australia, 28**, 311-321.

WELSCH, W., 1980. Some techniques for monitoring and analysing deformations and control nets. Universität der Bundeswehr, München., Reprinted, University of N.S.W., October 1982, 193p.

WELSCH, W., 1981. Estimation of variances and covariances of geodetic observations. **Aust. J. Geod. Photo. Surv., 34**, 1-14.

WELSCH, W., 1982. Description of homogeneous horizontal strains and some remarks to their analysis. Proc. Int. Symp. on Geodetic Networks and Computations, Munich 1981, Reihe B Nr 258/VII, Deutsche Geod. Komm.

WELSCH, W., 1983. Finite element analysis of strain patterns from geodetic observations across a plate margin. **Tectonophysics, 97**, 57-71.

WELSCH, W., OSWALD, W., 1985. Variance analysis of satellite networks. Proc. 1st Int. Symp. Prec. Pos. GPS, U.S. Dept. of Commerce, NOAA, Rockville, Md., May, 1985.

WELSCH, W., 1986a. Some aspects of the analysis of geodetic strain observations in kinematic models. **Tectonophysics, 130**, 437-458.

WELSCH, W., 1986b. Problems of accuracies in combined terrestrial and satellite control networks. Proc. 4th Int. Geod. Symp. Sat. Pos., University of Texas, Austin, Tex., 28 April - 2 May, 1986.

WESSEL, P., WATTS, A.B., 1988. On the accuracy of marine gravity measurements. **J. Geophys. Res. 93**, 393-413

WM SATELLITE SURVEY COMPANY, 1987. PoPS^{TM} post - processing software. Magnavox Survey Systems Inc. and Wild Heerbrugg Survey Corporation.

APPENDIX A: LEAST SQUARES ADJUSTMENT.

A.1 GENERAL LEAST SQUARES

The equations are based on Bossler (1972) and Cross (1983) with some changes in the notation. Given a set of equations

$$F(\mathbf{x},\mathbf{L}) = \mathbf{0} \tag{A.1.1}$$

in parameters $\mathbf{x}$ and observables $\mathbf{L}$, a Taylor expansion is used to linearise about the *a priori* parameters $\mathbf{x}^o$ and the observations l.

$$\mathbf{A}\,\delta\mathbf{x} + \mathbf{B}\,\mathbf{v} - \mathbf{w} = \mathbf{0} \tag{A.1.2}$$

where

$$\mathbf{A} = \left(\frac{\partial F}{\partial x}\right)_{\mathbf{x}^o,l} \tag{A.1.3}$$

$$\mathbf{B} = \left(\frac{\partial F}{\partial L}\right)_{\mathbf{x}^o,l} \tag{A.1.4}$$

$$\mathbf{w} = -F(\mathbf{x}^o,l) \tag{A.1.5}$$

where the corrections to the *a priori* parameters are

$$\delta\mathbf{x} = \mathbf{x} - \mathbf{x}^o \tag{A.1.6}$$

and where the residuals are

$$\mathbf{v} = \mathbf{L} - l \tag{A.1.7}$$

It is assumed that in this development, that *a priori* pseudo observations of the parameters l_x are available with VCV matrix $\mathbf{Q}_{xo}$. The observations l have *a priori* VCV matrix $\mathbf{Q}$. The weight matrices of the observations $\mathbf{P}$ and parameters $\mathbf{P}_{xo}$ are the inverses of $\mathbf{Q}$ and $\mathbf{Q}_{xo}$ respectively assuming that the inverses exist. It is also assumed that the *a priori* variance factor σ_o^2 is the same for $\mathbf{Q}$ and $\mathbf{Q}_{xo}$ and is equal to unity. Equation A.1.2 has the solution

$$\hat{\delta\mathbf{x}} = \left(\mathbf{A}^T(\mathbf{B}\mathbf{Q}\mathbf{B}^T)^{-1}\mathbf{A} + \mathbf{P}_{xo}\right)^{-1}\left(\mathbf{A}^T(\mathbf{B}\mathbf{Q}\mathbf{B}^T)^{-1}\mathbf{w} + \mathbf{P}_{xo}\mathbf{w}_x\right) \tag{A.1.8}$$

where $\hat{}$ denotes the least squares estimate and where

$$\mathbf{w}_x = \mathit{l}_x - \mathbf{x}^\circ \tag{A.1.9}$$

This is the equation of Bossler (1972) extended for the general linear model of equation A.1.1. The vector of adjusted parameters is

$$\hat{\mathbf{x}} = \mathbf{x}^\circ + \delta\hat{\mathbf{x}} \tag{A.1.10}$$

with VCV matrix

$$\mathbf{Q}_{\hat{x}} = \left(\mathbf{A}^T (\mathbf{B}\mathbf{Q}\mathbf{B}^T)^{-1}\mathbf{A} + \mathbf{P}_{x^\circ}\right)^{-1} \tag{A.1.11}$$

The vector of estimated residuals is

$$\hat{\mathbf{v}} = \mathbf{Q}\mathbf{B}^T (\mathbf{B}\mathbf{Q}\mathbf{B}^T)^{-1} (\mathbf{w} - \mathbf{A}\delta\hat{\mathbf{x}}) \tag{A.1.12}$$

and the estimated *a posteriori* variance factor is

$$\hat{\sigma}_o^2 = (\hat{\mathbf{v}}^T\mathbf{P}\hat{\mathbf{v}} + \delta\hat{\mathbf{x}}^T\mathbf{P}_{x^\circ}\delta\hat{\mathbf{x}})/f \tag{A.1.13}$$

where the degrees of freedom f is given by

$$f = n - u + u_x \tag{A.1.14}$$

and where n = the number of observation equations,
u = the number of parameters and
u_x = the number of "significantly weighted" parameters.

See Bossler (1972) and Harvey (1985, 1987) for discussions on the degrees of freedom where some parameters have significant *a priori* weights.

It is common, for numerical convenience, to choose the *a priori* values of the parameters to be equal to the pseudo observed values.

$$\mathbf{x}^\circ = \mathit{l}_x \tag{A.1.15}$$

$$\mathbf{w}_x = \mathbf{0} \tag{A.1.16}$$

This gives the familiar equations of general least squares with *a priori* weights on the parameters (e.g. Krakiwsky, 1981).

$$\delta\hat{\mathbf{x}} = \left(\mathbf{A}^T (\mathbf{B}\mathbf{Q}\mathbf{B}^T)^{-1}\mathbf{A} + \mathbf{P}_{x^\circ}\right)^{-1} \mathbf{A}^T (\mathbf{B}\mathbf{Q}\mathbf{B}^T)^{-1}\mathbf{w} \tag{A.1.17}$$

Note for an iterated adjustment where $\mathbf{x}^o$ is changed for each iteration, that if equations A.1.15 - 17 are true for the first iteration, they will not be strictly true for subsequent iterations and the complete equation A.1.8 should be used. In the absence of *a priori* observations of the parameters, $\mathbf{P}_{xo}$ is zero and the equations are the same as those of Cross (1983).

A.2 PARAMETRIC LEAST SQUARES

This is a special case of the general least squares model above with explicit observation equations.

$$\mathbf{L} = f(\mathbf{x}) \tag{A.2.1}$$

or

$$F(\mathbf{x},\mathbf{L}) = f(\mathbf{x}) - \mathbf{L} = \mathbf{0} \tag{A.2.2}$$

From equations A.1.4 and A.2.2

$$\mathbf{B} = -\mathbf{I} \tag{A.2.3}$$

and thus

$$\mathbf{w} + \mathbf{v} = \mathbf{A}\delta\mathbf{x} \tag{A.2.4}$$

where

$$\begin{aligned} \mathbf{w} &= -F(\mathbf{x}^o, l\ ) \\ &= l\ - f(\mathbf{x}^o) \\ &= l\ - l^o \end{aligned} \tag{A.2.5}$$

with l^o the vector of *a priori* calculated observations. The vector $\mathbf{w}$ is often called the "misclose" or "observed minus calculated" vector. The solution to A.2.4 using A.1.8 and A.2.3 is

$$\hat{\delta\mathbf{x}} = (\mathbf{A}^T\mathbf{P}\mathbf{A} + \mathbf{P}_{xo}\ )^{-1}\ (\mathbf{A}^T\mathbf{P}\mathbf{w} + \mathbf{P}_{xo}\mathbf{w}_x\ ) \tag{A.2.6}$$

with

$$\mathbf{Q}_{\hat{x}} = (\mathbf{A}^T\mathbf{P}\mathbf{A} + \mathbf{P}_{xo}\ )^{-1} \tag{A.2.7}$$

$$\hat{\mathbf{v}} = \mathbf{A}\hat{\delta\mathbf{x}} - \mathbf{w} \tag{A.2.8}$$

as in Bossler (1972) These equations can be simplified if $\mathbf{x}^{\circ} = \boldsymbol{l}_x$

$$\hat{\delta\mathbf{x}} = (\mathbf{A}^T\mathbf{P}\mathbf{A} + \mathbf{P}_{x^{\circ}})^{-1}\mathbf{A}^T\mathbf{P}\mathbf{w} \tag{A.2.9}$$

and if $\mathbf{P}_{x^{\circ}} = \mathbf{0}$

$$\hat{\delta\mathbf{x}} = (\mathbf{A}^T\mathbf{P}\mathbf{A})^{-1}\mathbf{A}^T\mathbf{P}\mathbf{w} \tag{A.2.10}$$

$$\mathbf{Q}_{\hat{x}} = (\mathbf{A}^T\mathbf{P}\mathbf{A})^{-1} \tag{A.2.11}$$

APPENDIX B: RANK DEFECT OF THE CLOCK BIASES

B.1 THE NATURE AND SIZE OF THE RANK DEFECT

The normal matrix of the GPS adjustment will be singular if all the clock bias parameters of the undifferenced phase observation, $c_j(T_j)$, $c^i(T_j^i)$ and n_j^i, are included in the set of parameters to be estimated. A singular normal matrix indicates that the set of parameters to be estimated contains some information which has not been supplied, either through the observations or the model. Such a matrix has a number of zero eigenvalues, this number being equal to the rank defect.

The clock phase errors were introduced in equation 4.2.3, by considering a perfect oscillator or clock with which the receiver and satellite oscillators could be compared. If the clock phase errors are estimated relative to this perfect oscillator, two problems are created. Firstly, the perfect oscillator does not exist. Secondly, if it did exist there would be no means of comparing it directly with all the other oscillators. This is the information in the set of parameters which is not provided by the observations. The observations, being differences between received phase signals and local receiver oscillator phase, are sensitive only to **differences** between satellite and receiver clock phase error (see equation 4.2.12). Thus, in introducing the parameters of absolute clock phase error, the equivalent of a datum defect has been created. The **external** phase "geometry" is not defined by the set of observations. It is well understood in geodetic adjustment that absolute coordinates are not determined when all the observations are sensitive only to coordinate differences. There is a similar situation here with the clock phase errors.

One way to overcome this "datum defect" is to hold the clock phase errors of one (reference) oscillator fixed. Then the absolute phase is defined by the reference oscillator but only ambiguous phase observations are available to determine the unambiguous clock phase errors of all the other oscillators. That the clock phase errors are unambiguous was noted in their definition in equation 4.2.3. If observations of the satellite - receiver range were available that were more accurate than 1 carrier phase cycle (19 cm at the L1 frequency), the unambiguous clock phase errors of the other oscillators could be determined with respect to the reference oscillator. At present, pseudo-ranges with this accuracy are not available. Therefore, there is a rank defect of

1 for each of the other oscillators. This is equivalent to a configuration defect where the **internal** phase "geometry" is not defined by the set of observations.

To summarise; there is a "phase datum defect" caused by the attempt to estimate **absolute** clock phase error from observations of the **difference** between received satellite phase and receiver oscillator phase. There is a further "phase configuration defect" caused by the attempt to estimate **unambiguous** phase errors from **ambiguous** phase observations.

There are a number of methods which may be used to overcome a rank defect but the simplest method is to hold some of the parameters fixed (remove them from the set of parameters to be estimated). The phase datum and phase configuration defects may be overcome by holding some of the clock bias parameters fixed. To determine the number of parameters that should be fixed, consider an example with R receivers, S satellites and observations for T epochs. For simplicity it will be assumed that that all R receivers observe all S satellites for all T epochs. Therefore there is a complete set of RST phase observations. The total number of receiver clock phase errors is RT. The total number of satellite clock phase errors is ST and the total number of integer ambiguities is RS. If the clock phase errors of one oscillator are held fixed for all epochs to define the phase datum, T parameters are removed from the full set. The unambiguous phase relationships between this reference oscillator and the other $R+S-1$ oscillators are also required. This can be provided by holding $R+S-1$ parameters fixed. One possibility is to hold all these clock phase errors fixed for one epoch. Another possibility is to fix the required number of ambiguities so that the phase relationship can be transferred to all the other oscillators. Other combinations of parameters are also possible. Once the relationship between all oscillators has been defined in one epoch, the continuous phase tracking allows it to be maintained for all other epochs. An unambiguous definition of phase is provided for all oscillators in this example, by holding $R+S+T-1$ clock bias parameters fixed. This is therefore an intuitive estimate of the size of the rank defect in the clock biases.

It is noted in section 4.3.1 that the clock biases may be eliminated either by estimating them or by differencing observations to eliminate them. According to the fundamental differencing theorem (Lindlohr and Wells, 1985) both methods give the same result for the non-bias parameters provided the full set of linearly independent differenced observations is used and provided the

correlations introduced by differencing are accounted for in the observation weight matrix. This provides an analytical means of analysing the rank defect in the clock bias parameters complementing the intuitive analysis above. Using the fundamental differencing theorem, the reduction in the number of linearly independent observations caused by differencing can be equated with the number of estimable parameters that have been eliminated. This method of using the fundamental differencing theorem to determine the rank defects is found in Lindlohr and Wells (1985). A good starting point is the triple difference observation for which the number of clock biases is zero.

Given R receivers, S satellites and T epochs as above, there are RST undifferenced phase observations. From these observations, (R–1)(S–1)(T–1) **linearly independent** triple difference observations can be formed. (More than this number of **different** triple differences can be formed but the additional ones are linear combinations of this set.) Triple differencing changes the number of observations from RST to (R–1)(S–1)(T–1) ; a reduction of RS+ST+RT–R–S–T+1 . Under the fundamental differencing theorem, this reduction in the number of observations has resulted in an identical reduction in the number of estimable clock bias parameters. As there are zero clock biases in the triple difference model, the number of estimable clock bias parameters C_E in the undifferenced model is therefore

$$C_E = RS + ST + RT - R - S - T + 1 \qquad \text{(B.1.1)}$$

The clock biases are completely described by this number of parameters just as they are completely eliminated by reducing the number of observations by this amount. The total number of clock biases C_T in the undifferenced model is

$$C_T = RS + ST + RT \qquad \text{(B.1.2)}$$

The rank defect is

$$\begin{aligned} C_D &= C_T - C_E \\ &= R + S + T - 1 \end{aligned} \qquad \text{(B.1.3)}$$

This is equal to the rank defect determined intuitively above.

Similarly for the double difference adjustment model. The number of linearly independent double difference observations is $(R-1)(S-1)T$ and the reduction in the number of observations when $(R-1)(S-1)(T-1)$ triple differences are formed is $(R-1)(S-1)$. This is the number of estimable ambiguities but the total number is RS. Thus there is a rank defect of $R+S-1$.

$$C_E = RS - R - S + 1 \tag{B.1.4}$$

$$C_T = RS \tag{B.1.5}$$

$$C_D = R + S - 1 \tag{B.1.6}$$

B.2 OVERCOMING THE CLOCK BIAS RANK DEFECT

A distinction may be drawn, between the unknown true value of a parameter and its least squares estimate. Assuming for the moment, that the observations do not have any systematic errors and are normally distributed, then (Welsch, 1980)

$$E(\hat{x}) = x \tag{B.2.1}$$

where x is the true value of a parameter, $\hat{x}$ is the least squares estimate and $E(\ )$ is the expectation operator.This equation is only true for estimable parameters. Grafarend and Schaffrin (1976) prove that parameters are estimable if and only if they are invariant under any transformation which leaves the observations invariant. It is easily demonstrated that the clock biases are not estimable parameters. For example, an equal change of all oscillators in any epoch will alter the clock phase errors significantly but not the observed phases. If a change of one cycle is introduced into any oscillator for all epochs then by the definition of the ambiguity, a compensating change of one cycle will ensure that the observation remains unaltered. equation B.2.1 is therefore not true for clock biases.

These transformations do not produce any net change in the total clock bias $B_j^i(t_k)$ defined as

$$B_j^i(t_k) = f_0\, c^i(t_k) - f_0\, c_j(t_k) + n_j^i \tag{B.2.2}$$

where, for simplicity, a common time tag t_k has been assigned to the time dependent terms. From equations B.2.2 and 4.2.12 it can be seen that any transformation which leaves the observed phases invariant must leave the total clock bias invariant. Therefore,

$$E(\hat{B}_j^i(t_k)) = B_j^i(t_k)$$
$$= f_0\, c^i(t_k) - f_0\, c_j(t_k) + n_j^i \qquad \text{(B.2.3)}$$

and thus

$$f_0\, E(\hat{c}^i(t_k)) - f_0\, E(\hat{c}_j(t_k)) + E(\hat{n}_j^i) = f_0\, c^i(t_k) - f_0\, c_j(t_k) + n_j^i \qquad \text{(B.2.4)}$$

since the expectation of a sum of terms is the sum of the expectations of the individual terms (e.g., Liebelt, 1967). When a parameter is fixed, its expected value is set to the *a priori* value which, for the clock biases, is usually zero. Using equation B.2.4, the effects on other parameters can be determined.

As an example, consider undifferenced phase observations with one receiver clock error fixed every epoch and an ambiguity fixed for every receiver and every satellite. The fixed biases are as follows:

Ambiguities to receiver r fixed for all satellites.
Ambiguities to satellite s fixed for all receivers.
Clock of receiver t fixed for all epochs.

This can be expressed in terms of expectation values as

$E(\hat{n}_r^i) = 0$ for all satellites, i
$E(\hat{n}_j^s) = 0$ for all receivers, j
$E(\hat{c}_t(t_k)) = 0$ for all epochs, k

Clock error of satellite s

Using equation B.2.4 for receiver t and satellite s

$$f_0\, E(\hat{c}^s(t_k)) - f_0\, E(\hat{c}_t(t_k)) + E(\hat{n}_t^s) = f_0\, c^s(t_k) - f_0\, c_t(t_k) + n_t^s \qquad \text{(B.2.5)}$$

and eliminating the fixed parameters

$$f_0\, E(\hat{c}^s(t_k)) = f_0\, c^s(t_k) - f_0\, c_t(t_k) + n_t^s \qquad \text{(B.2.6)}$$

Clock errors of all receivers j

For satellite s and any other receiver j

$$f_0 E(\hat{c}^s(t_k)) - f_0 E(\hat{c}_j(t_k)) + E(\hat{n}_j^s) = f_0 c^s(t_k) - f_0 c_j(t_k) + n_j^s \quad \text{(B.2.7)}$$

Eliminating the fixed parameter and using equation B.2.6

$$f_0 E(\hat{c}_j(t_k)) = f_0 c_j(t_k) - f_0 c_t(t_k) + n_t^s - n_j^s \quad \text{(B.2.8)}$$

Clock errors of all other satellites i

For receiver r and any other satellite i

$$f_0 E(\hat{c}^i(t_k)) - f_0 E(\hat{c}_r(t_k)) + E(\hat{n}_r^i) = f_0 c^i(t_k) - f_0 c_r(t_k) + n_r^i \quad \text{(B.2.9)}$$

Substituting equation B.2.8 into B.2.9 for the case where j = r

$$f_0 E(\hat{c}^i(t_k)) = f_0 c^i(t_k) - f_0 c_t(t_k) + n_r^i + n_t^s - n_r^s \quad \text{(B.2.10)}$$

Ambiguities of satellites i and receivers j

Finally for any other satellite i and any other receiver j

$$f_0 E(\hat{c}^i(t_k)) - f_0 E(\hat{c}_j(t_k)) + E(\hat{n}_j^i) = f_0 c^i(t_k) - f_0 c_j(t_k) + n_j^i \quad \text{(B.2.11)}$$

and using equations B.2.8 and B.2.10

$$E(\hat{n}_j^i(t_k)) = n_j^i - n_j^s - n_r^i + n_r^s \quad \text{(B.2.12)}$$

This result is revealing in two ways. Firstly, equation B.2.12 shows that, for this example, the estimated ambiguities are in reality doubly differenced ambiguities even though undifferenced observations were used. Therefore this choice of reference clock biases gives estimated ambiguities with integral expectation values. The second point of interest is in the method used. The fixed ambiguity between satellite s and the reference clock t allowed the derivation of an expression for the clock phase error of satellite s (equation B.2.6). Using the fixed ambiguities from this satellite, expressions were derived for all other receiver clock phase errors (equation B.2.8) and thence all other satellite clock phase errors (equation B.2.10). In Appendix B.1 above it was suggested from an intuitive point of view, that the phase datum could be

transferred from the fixed clock to all other clocks through the fixed ambiguities. That idea is expressed analytically in this derivation.

In a complex observing session with satellites rising and setting and the possibility of receivers observing at slightly different times, such a simple scheme as that given above may not be possible. By analysing the method used, it may be seen that any group of fixed ambiguities will satisfy the rank defect provided that they provide a path from the reference oscillator to every other oscillator. It is worth noting that the estimated ambiguities do not depend on the reference oscillator. Only the clock error terms depend on this and these are estimated for each epoch. Therefore it is not necessary to have the same reference oscillator in every epoch. If receiver t in the above example stops observing, one of the other oscillators (including the satellite oscillators) may be chosen as the new reference without affecting the estimated ambiguities or other non-bias parameters. It should also be noted that the reference oscillator need not be that of the base station or base satellite used to choose the reference ambiguities.

Examples of the paths provided by reference ambiguities for the transfer of the phase datum are shown in Diagram B.2.1. In these diagrams there are 5 satellites and 6 receivers so the number of reference ambiguities required is 10. The top diagram shows the base station - base satellite concept. The other diagrams show more complicated examples and in these cases the expected values of the estimated parameters will have more complex forms. The expected values of the ambiguities will still be integers and will still be unaffected by a change of reference clock between epochs.

An algorithm for choosing fixed ambiguity parameters is relatively simple even for complex observing sessions. Considering the observations in the first epoch, the ambiguities are fixed from one station (base station) to all satellites and from one satellite (base satellite) to all receivers. All other ambiguities are included amongst the parameters to be estimated. In subsequent epochs, if observations become available to a new satellite, new ambiguities are introduced for all stations observing that satellite except for one reference ambiguity to an existing station (usually but not necessarily the base station). Similarly if a new receiver starts observing, new ambiguities are introduced for all observed satellites except for one reference ambiguity to an existing satellite (say the base satellite). In this way a link is provided from the new

oscillator to one of the existing oscillators. Thus the phase datum is transferred.

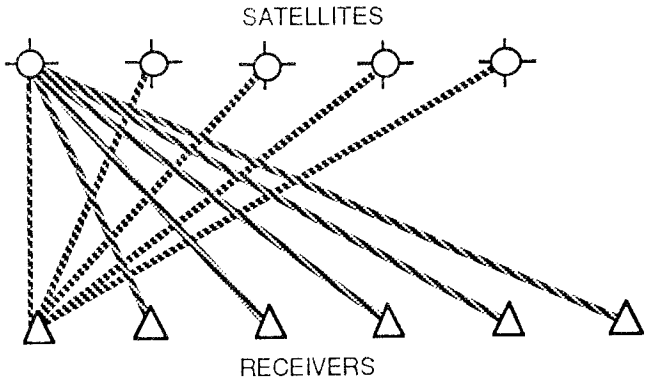

BASE STATION - BASE SATELLITE

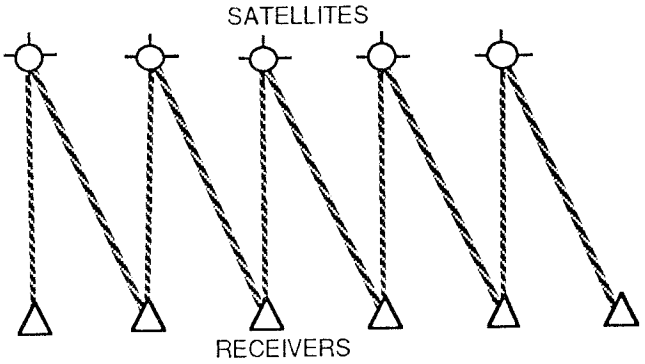

CHAIN

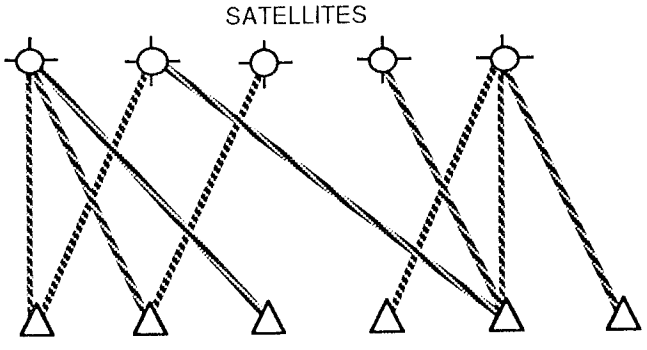

GENERAL

DIAGRAM B.2.1 Some choices of reference ambiguities.

APPENDIX C: RELATIONSHIP BETWEEN LEAST SQUARES AND KALMAN FILTERING

It has been demonstrated by Krakiwsky (1981) that for the trivial dynamic model,

$$\Phi_i = I \qquad \text{for all i} \tag{C.1}$$

$$\mathbf{Q}_{y_i} = \mathbf{0} \qquad \text{for all i} \tag{C.2}$$

the Kalman filter solution is identical to that of sequential least squares which, in turn, is identical to a single step least squares adjustment of all data provided that the observations are not correlated between epochs (a requirement of the Kalman filter algorithm). This equivalence is not immediately obvious from the Kalman filter equations in section 4.3.3. Krakiwsky (1981) uses matrix identities to convert 4.3.17, 4.3.14 and 4.3.15 to the form of the Bayes filter

$$\hat{\mathbf{Q}}_{x_i} = \left(\tilde{\mathbf{Q}}_{x_i}^{-1} + \mathbf{A}_i^T \mathbf{P}_i \mathbf{A}_i\right)^{-1} \tag{C.3}$$

$$\mathbf{G}_i = \hat{\mathbf{Q}}_{x_i} \mathbf{A}_i^T \mathbf{P}_i \tag{C.4}$$

$$\delta\hat{\mathbf{x}}_i = (I - \mathbf{G}_i \mathbf{A}_i)\, \delta\tilde{\mathbf{x}}_i + \mathbf{G}_i \mathbf{w}_i \tag{C.5}$$

With the trivial dynamic model of equations C.1 and C.2

$$\tilde{\mathbf{Q}}_{x_i} = \hat{\mathbf{Q}}_{x_{i-1}} \tag{C.6}$$

$$\hat{\mathbf{Q}}_{x_i} = \left(\hat{\mathbf{Q}}_{x_{i-1}}^{-1} + \mathbf{A}_i^T \mathbf{P}_i \mathbf{A}_i\right)^{-1} \tag{C.7}$$

$$\delta\tilde{\mathbf{x}}_i = \delta\hat{\mathbf{x}}_{i-1} \tag{C.8}$$

From C.4 and C.7

$$(I - G_i A_i) = (I - \hat{Q}_{x_i} A_i^T P_i A_i)$$

$$= (\hat{Q}_{x_i} \hat{Q}_{x_i}^{-1} - \hat{Q}_{x_i} A_i^T P_i A_i)$$

$$= \hat{Q}_{x_i} (\hat{Q}_{x_{i-1}}^{-1} + A_i^T P_i A_i - A_i^T P_i A_i)$$

$$= \hat{Q}_{x_i} \hat{Q}_{x_{i-1}}^{-1} \qquad (C.9)$$

and thus from C.4, C.5 and C.9

$$\delta\hat{x}_i = \hat{Q}_{x_i} (A_i^T P_i w_i + \hat{Q}_{x_{i-1}}^{-1} \delta\tilde{x}_i) \qquad (C.10)$$

Starting in epoch i = 1 with

$$\delta\hat{x}_{i-1} = w_x \qquad (C.11)$$

$$\hat{Q}_{x_{i-1}} = Q_{xo} = P_{xo}^{-1} \qquad (C.12)$$

then from C.7 and C.12

$$\hat{Q}_{x_1} = (A_1^T P_1 A_1 + P_{xo})^{-1} \qquad (C.13)$$

and from C.10, C.12, C.8, C.11,

$$\delta\hat{x}_1 = \hat{Q}_{x_1} (A_1^T P_1 w_1 + P_{xo} \delta\tilde{x}_i)$$

$$= (A_1^T P_1 A_1 + P_{xo})^{-1} (A_1^T P_1 w_1 + P_{xo} w_x) \qquad (C.14)$$

which may be compared with equations A.2.6 and A.2.7 for the parametric least squares model with *a priori* weights on the parameters. In general for epoch n

$$\hat{Q}_{x_n} = \left(\sum_{i=1}^{n} (A_i^T P_i A_i) + P_{xo} \right)^{-1} \qquad (C.15)$$

$$\delta\hat{x}_n = \left(\sum_{i=1}^{n} (A_i^T P_i A_i) + P_{xo} \right)^{-1} \left(\sum_{i=1}^{n} (A_i^T P_i w_i) + P_{xo} w_x \right) \qquad (C.16)$$

which is equal to the least squares solution where the weight matrix of the observations has the block diagonal form

$$\mathbf{P} = \begin{pmatrix} \mathbf{P}_1 & \mathbf{0} & & \mathbf{0} \\ \mathbf{0} & \mathbf{P}_2 & & \mathbf{0} \\ & & \cdot & \\ & & & \cdot \\ \mathbf{0} & \mathbf{0} & & \mathbf{P}_n \end{pmatrix} \qquad \text{(C.17)}$$

Thus, a least squares adjustment where the observations are uncorrelated between epochs, is equivalent to a Kalman filter adjustment with the trivial dynamic model of equations C.1 and C.2.

APPENDIX D: DYNAMIC MODELS

D.1 DYNAMIC MODEL THEORY

In section 4.3.3 the Kalman filter equations are presented. The prediction step of the Kalman filter adjustment depends on the dynamic or secondary model. In this appendix, equations are presented that allow the development of the two matrices that embody the dynamic model. These are the transition matrix Φ and the VCV matrix of the dynamic model errors $\mathbf{Q}_y$. The following development is based on that of Liebelt (1967) and Gelb (1974). A slightly different notation to that of section 4.3.3 is used initially. In this notation the prediction step of the Kalman filter adjustment is

$$\mathbf{x}(t) = \Phi(t,t_o)\,\mathbf{x}(t_o) + \mathbf{y}(t,t_o) \tag{D.1}$$

where $\mathbf{x}(t)$ is the state vector at epoch t, $\Phi(t,t_o)$ is the transition matrix from epoch t_o to epoch t and $\mathbf{y}(t,t_o)$ is the vector of dynamic model errors. The propagation of variances is given by

$$\mathbf{Q}_x(t) = \Phi(t,t_o)\,\mathbf{Q}_x(t_o)\,\Phi^T(t,t_o) + \mathbf{Q}_y(t,t_o) \tag{D.2}$$

For simple dynamic systems the matrices $\Phi(t,t_o)$ and $\mathbf{Q}_y(t,t_o)$ may be readily determined but in other cases these matrices must be derived from a knowledge of the time behaviour of system parameters and stochastic properties such as the auto-correlation function, error growth or steady state variance as discussed below. Complex models may need numerical integration but the models used in this thesis can be derived analytically. The starting point may be a linear differential equation of the form

$$\dot{\mathbf{x}}(t) = \mathbf{F}(t)\,\mathbf{x}(t) + \mathbf{G}(t)\,\mathbf{u}(t) \tag{D.3}$$

where the matrix $\mathbf{F}(t)$ describes the behaviour of the deterministic dynamic system and where the matrix $\mathbf{G}(t)$ describes the effect on the system dynamics of a vector of random variables $\mathbf{u}(t)$ known as forcing functions. The case where the matrices $\mathbf{F}$ and $\mathbf{G}$ are invariant in time will be considered and their time dependence is dropped in the following equations. In the adjustment of GPS observations, the system dynamics over the time interval between observations is of interest and this is no more than a few minutes. In cases where $\mathbf{F}$ and $\mathbf{G}$ change in time they may be considered to be step functions of time that are constant between observation epochs. Equation D.3 has the solution (Liebelt, 1967)

$$\mathbf{x}(t) = \Phi(t,t_o)\,\mathbf{x}(t_o) + \int_{t_o}^{t} \Phi(t,s)\,\mathbf{G}\,\mathbf{u}(s)\,ds \qquad (D.4)$$

The transition matrix satisfies the equations

$$\Phi(t_o,t_o) = \mathbf{I} \qquad (D.5)$$

$$\dot{\Phi}(t,t_o) = \mathbf{F}\,\Phi(t,t_o) \qquad (D.6)$$

and can be derived from the equation (Liebelt, 1967)

$$\begin{aligned}\Phi(t,t_o) &= \exp\left((t-t_o)\mathbf{F}\right) \\ &= \mathbf{I} + (t-t_o)\mathbf{F} + \tfrac{1}{2!}(t-t_o)^2\mathbf{FF} + \tfrac{1}{3!}(t-t_o)^3\mathbf{FFF} + \ldots\end{aligned} \qquad (D.7)$$

The propagation of the VCV matrix $\mathbf{Q}_x(t)$ is given by

$$\begin{aligned}\mathbf{Q}_x(t) &= E\left(\mathbf{x}(t),\mathbf{x}^T(t)\right) \\ &= \Phi(t,t_o)\,\mathbf{Q}_x(t_o)\,\Phi^T(t,t_o) + \\ &\qquad \int_{t_o}^{t}\int_{t_o}^{t} \Phi(t,s)\,\mathbf{G}\,E\left(\mathbf{u}(s),\mathbf{u}^T(r)\right)\,\mathbf{G}^T\Phi^T(t,r)\,ds\,dr \\ &= \Phi(t,t_o)\,\mathbf{Q}_x(t_o)\,\Phi^T(t,t_o) + \\ &\qquad \int_{t_o}^{t}\int_{t_o}^{t} \Phi(t,s)\,\mathbf{G}\,\mathbf{Q}_u(s,r)\,\mathbf{G}^T\Phi^T(t,r)\,ds\,dr\end{aligned} \qquad (D.8)$$

where it is assumed that $\mathbf{x}(t_o)$ and $\mathbf{u}(t)$ are uncorrelated and where $\mathbf{Q}_u$ is the VCV matrix of $\mathbf{u}(t)$. When the dynamic model is being used to predict behaviour over a relatively short interval it is common to assume that $\mathbf{u}(t)$ is a vector of random variables which are constant over the interval t_o to t. In the Kalman filter adjustment, which involves a series of predictions, each of the variables in $\mathbf{u}(t)$ then forms a **random sequence**. This is a time series of random variables whose values are available at discrete times (Liebelt, 1967). The integrals in equation D.4 and D.8 are then easily evaluated as

$$\mathbf{x}(t) = \Phi(t,t_o)\,\mathbf{x}(t_o) + \Phi(t,t_o)\,\mathbf{G}\,\mathbf{u}(t) \qquad (D.9)$$

$$\mathbf{Q}_x(t) = \Phi(t,t_o)\,\mathbf{Q}_x(t_o)\,\Phi^T(t,t_o) + \Phi(t,t_o)\,\mathbf{G}\,\mathbf{Q}_u(t,t_o)\,\mathbf{G}^T\Phi^T(t,t_o) \qquad (D.10)$$

where $\mathbf{Q}_u(t,t_o)$ is assumed to be constant over the prediction interval. By comparison with equations D.1 and D.2

$$\mathbf{y}(t,t_o) = \Phi(t,t_o)\,\mathbf{G}\,\mathbf{u}(t) \qquad (D.11)$$

$$\mathbf{Q}_y(t,t_o) = \Phi(t,t_o)\,\mathbf{G}\,\mathbf{Q}_u(t,t_o)\,\mathbf{G}^T\Phi^T(t,t_o) \qquad (D.12)$$

In the context of a Kalman filter adjustment of GPS data, these equations are based on the assumption that the random variables $\mathbf{u}(t)$ are step functions of time with the steps occurring at observation epochs. A more general assumption for the behaviour of $\mathbf{u}(t)$ is to assume that it is a vector of stationary, white, zero mean, **random processes**; a random process being the time-continuous equivalent of a random sequence. This is the assumption that will be made for the remainder of this development.

$$E\big(\mathbf{u}(t)\big) = \mathbf{0} \qquad (D.13)$$

$$E\big(\mathbf{u}(t),\mathbf{u}^T(s)\big) = \mathbf{Q}_u(t,s) = \delta(t-s)\,\Theta_u \qquad (D.14)$$

where Θ_u is known as the spectral density matrix of $\mathbf{u}(t)$ and where $\delta(t-s)$ is the Dirac delta function. The relationship between the spectral density matrix and the VCV matrix $\mathbf{Q}_u$ is discussed by Gelb (1974). The spectral density matrix Θ_u is assumed to be constant (i.e., $\mathbf{u}(t)$ is assumed to be a stationary random process) and thus equation D.8 then simplifies to

$$\mathbf{Q}_x(t) = \Phi(t,t_o)\,\mathbf{Q}_x(t_o)\,\Phi^T(t,t_o) + \int_{t_o}^{t} \Phi(t,s)\,\mathbf{G}\,\Theta_u\,\mathbf{G}^T\Phi^T(t,r)\,ds \qquad (D.15)$$

In the special case of Kalman filtering where $\mathbf{x}(t)$, $\mathbf{Q}_x(t)$ are required at discrete epochs t_i , equations D.4 and D.15 can be written in a more compact form.

$$\mathbf{x}_i = \Phi_i\,\mathbf{x}_{i-1} + \mathbf{y}_i \qquad (D.16)$$

$$\mathbf{Q}_{x_i} = \Phi_i\,\mathbf{Q}_{x_{i-1}}\,\Phi^T{}_i + \mathbf{Q}_{y_i} \qquad (D.17)$$

where

$$\mathbf{y}_i = \int_{t_{i-1}}^{t_i} \Phi\, \mathbf{G}\, \mathbf{u}\, dt \qquad (D.18)$$

$$\mathbf{Q}_{y_i} = \int_{t_{i-1}}^{t_i} \Phi\, \mathbf{G}\, \Theta_u\, \mathbf{G}^T \Phi^T\, dt \qquad (D.19)$$

The time-discrete propagation of variance in equation D.15 or D.17 may be written in time continuous form as (Gelb, 1974)

$$\dot{\mathbf{Q}}_x(t) = \mathbf{F}\, \mathbf{Q}_x(t) + \mathbf{Q}_x(t)\mathbf{F}^T + \mathbf{G}\Theta_u\mathbf{G}^T \qquad (D.20)$$

Therefore, given matrices **F** and **G** in equation D.3, a transition matrix can be found that satisfies D.5 and D.6 for simple models. For more complex models, equation D.7 can be used to derive Φ. Given the spectral density matrix Θ_u and using equation D.19, $\mathbf{Q}_{y_i}$ can be derived. If Θ_u is unknown and if $\dot{\mathbf{Q}}_x$ and $\mathbf{Q}_x$ are known, equation D.20 can be used to derive Θ_u and then equation D.19 is used as above to derive $\mathbf{Q}_{y_i}$.

D.2 DYNAMIC MODELS IN GPS ADJUSTMENT

If the Kalman filter is to be used for the adjustment of GPS phase data, a dynamic model must be chosen for the parameters. The dynamic models that are considered here are

- constant parameter,
- white noise,
- random walk, and
- first order Gauss Markov process.

The second order Gauss-Markov process is also briefly considered.

Constant Parameter.

This has the linear differential equation.

$$\dot{\mathbf{x}}(t) = \mathbf{0} \qquad (D.21)$$

and from in equation D.3 , **F** and **G** equal zero. From equations D.7 and D.19

$$\Phi_i = \mathbf{I} \qquad (D.22)$$

$$\mathbf{Q}_{y_i} = \mathbf{0} \tag{D.23}$$

giving the recursive equations

$$\tilde{\mathbf{x}}_i = \hat{\mathbf{x}}_{i-1} \tag{D.24}$$

$$\tilde{\mathbf{Q}}_{x_i} = \hat{\mathbf{Q}}_{x_i} \tag{D.25}$$

The auto-correlation function for epochs i and j is

$$\rho(i,j) = 1 \quad \text{for all } i, j \tag{D.26}$$

As noted in Appendix C, the constant parameter model is the dynamic model implicitly used in a standard least squares adjustment.

White Noise.

In this case the state vector at each epoch is independent of its value at any other epoch. The equation for the state vector and VCV matrix is

$$\mathbf{x}_i = \mathbf{y}_i \tag{D.27}$$

$$\mathbf{Q}_{x_i} = \mathbf{Q}_{y_i} \tag{D.28}$$

where $\mathbf{y}_i$ is a white noise random sequence. The transition matrix is therefore

$$\Phi_i = \mathbf{0} \tag{D.29}$$

and the auto-correlation function is

$$\rho(i,j) = \delta(i,j) \tag{D.30}$$

where $\delta(i,j)$ is the Dirac delta function. This model may be used for clock phase errors. Differencing observations to eliminate clock phase errors is equivalent to modelling the clock phases as a white noise process with infinite (or, at least, very large) variance σ_y^2.

Random Walk.

In this model, the rate of change of the parameter is a white noise random process.

$$\dot{\mathbf{x}}(t) = \mathbf{u}(t) \tag{D.31}$$

and thus

$$\mathbf{F} = \mathbf{0} \tag{D.32}$$

$$\mathbf{G} = \mathbf{I} \tag{D.33}$$

From equation D.7

$$\Phi_i = \mathbf{I} \tag{D.34}$$

From equation D.20

$$\dot{\mathbf{Q}}_x = \Theta_u \tag{D.35}$$

and thus the variance of **x** increases linearly with time when **u** is a stationary random process (constant Θ_u). From equation D.19,

$$\mathbf{Q}_{y_i} = \int_{t_{i-1}}^{t_i} \Theta_u \, dt$$

$$= (t_i - t_{i-1})\Theta_u$$

$$= (t_i - t_{i-1})\, \dot{\mathbf{Q}}_x \tag{D.36}$$

Considering a single variable x with variance σ_x^2 and a random process u with spectral density θ_u , then for epochs i and j with $j > i$

$$\sigma_{xj}^2 = \sigma_{xi}^2 + (t_j - t_i)\theta_u \tag{D.37}$$

and the covariance between epochs i and j is

$$\sigma_{xi\ xj} = \sigma_{xi}^2 \tag{D.38}$$

Thus the correlation function is

$$\rho(i,j) = \frac{\sigma_{xixj}}{\sigma_{xi}\,\sigma_{xj}}$$

$$= \frac{\sigma_{xi}^{\,2}}{\sigma_{xi}\sqrt{\sigma_{xi}^{\,2} + (t_j - t_i)\theta_u}}$$

$$= \frac{1}{\sqrt{1 + \dfrac{(t_j - t_i)\theta_u}{\sigma_{xi}^{\,2}}}} \qquad \text{(D.39)}$$

which diminishes with time. The random walk model can be used to model the behaviour of a clock with random frequency errors and with no systematic frequency drift or higher order terms. The random walk has also been used by Lichten & Border (1987) to model zenith tropospheric delay. This will be discussed further following the development of the first order Gauss-Markov process, which is also used to model tropospheric delay.

First Order Gauss - Markov Process.

The differential equation is (Gelb, 1974)

$$\dot{\mathbf{x}}(t) = -\beta\,\mathbf{x}(t) + \mathbf{u}(t) \qquad \text{(D.40)}$$

and the correlation function is

$$\rho(i,j) = e^{-\beta\Delta t} \qquad \text{(D.41)}$$

where $\Delta t = (t_j - t_i)$. Equation D.41 leads to an alternative name "exponentially correlated noise". Bierman (1977) calls it "coloured noise". The correlation time

$$T = \frac{1}{\beta} \qquad \text{(D.42)}$$

is the time period for which the auto-correlation is $e^{-1} = 0.368$. As T tends to zero this model tends towards white noise. As T tends to infinity ($\beta \rightarrow 0$) the model tends towards the random walk model. From equation D.3 it can be seen that if all parameters have the same factor β

$$\mathbf{F} = -\beta\mathbf{I} \qquad \text{(D.43)}$$

$$\mathbf{G} = \mathbf{I} \tag{D.44}$$

and using equations D.7 and D.19

$$\Phi_i = e^{-\beta\Delta t}\,\mathbf{I} \tag{D.45}$$

$$\mathbf{Q}_y = \frac{1}{2\beta}(1 - e^{-2\beta\Delta t})\Theta_u \tag{D.46}$$

From equation D.20

$$\dot{\mathbf{Q}}_x(t) = -2\beta\mathbf{Q}_x(t) + \Theta_u \tag{D.47}$$

After the system has been running for an infinite length of time it reaches the steady state where $\dot{\mathbf{Q}}_x(t) = \mathbf{0}$ and thus

$$\Theta_u = 2\beta\mathbf{Q}_{ss} \tag{D.48}$$

where $\mathbf{Q}_{ss}$ is the steady state VCV matrix of $\mathbf{Q}_x$. From equations D.46 and D.48

$$\mathbf{Q}_y = (1 - e^{-2\beta\Delta t})\mathbf{Q}_{ss} \tag{D.49}$$

This can also be derived by considering the propagation of variance in the steady state,

$$\begin{aligned}\mathbf{Q}_{ss} &= \Phi_i\mathbf{Q}_{ss}\Phi_i^T + \mathbf{Q}_y \\ &= e^{-\beta\Delta t}\,\mathbf{Q}_{ss}\,e^{-\beta\Delta t} + \mathbf{Q}_y\end{aligned} \tag{D.50}$$

This dynamic model has been used by Lichten & Border (1987); Stephens & Skrumeda, (1987); Elgered et al (1987) and Tralli et al (1988) to model the zenith tropospheric delay. It has the advantage over the random walk model that the variance is bounded by the steady state variance and does not increase to infinity over an infinite time period. The unbounded error growth of the random walk model is realistic for clock phase errors but it is not realistic for a physical system in dynamic equilibrium such as the earth's atmosphere.

In practice, when the zenith tropospheric delay is estimated in a Kalman filter adjustment the difference between the models is not as great as the above comments suggest. Any increase in variance during the prediction step is

countered by a decrease during the filter step as the observations act to correct the dynamic model. Lichten & Border (1987) found that using the random walk model for tropospheric delay gave better repeatability for orbits and baselines than the first order Gauss-Markov process. This may be due to an inappropriate choice of correlation time T or steady state variance σ_{ss}^2 but it demonstrates that the random walk model is, at least, adequate for estimating zenith tropospheric delay.

The effect of unestimated tropospheric errors on the solution is investigated (section 7.5) and in this case the choice of dynamic model is more critical. The unestimated parameters and their variances are not changed at the filter step and thus the errors in the dynamic model are not corrected by the observations. If the random walk model is used, the parameter variances, which increase with time, will be too large at the end of the observation period or too small at the start of the observation period (or both). In this thesis, the 1st order Gauss-Markov process is used to model tropospheric delay.

Note that the correlation function of the 1st order Gauss-Markov process shown in diagram D.1, has a non-zero gradient at the origin. A study of the temporal and spatial stochastic properties of the wet troposphere by Treuhaft & Lanyi (1987) using structure functions indicates that the correlation function should have zero gradient at the origin. The variance of the difference between tropospheric delays at epochs 1 and 2 is

$$\begin{aligned} \sigma_{1\text{-}2}^2 &= \sigma_1^2 + \sigma_2^2 - 2\sigma_{12} \\ &= \sigma_1^2 + \sigma_2^2 - 2\rho_{12}\,\sigma_1\,\sigma_2 \end{aligned} \qquad \text{(D.51)}$$

and if $\sigma_1 = \sigma_2 = \sigma$

$$\rho_{12} = 1 - \frac{\sigma_{1\text{-}2}^2}{2\sigma^2} \qquad \text{(D.52)}$$

From Treuhaft & Lanyi (1987)

$$\sigma_{1\text{-}2}^2 = C\,\Delta t^{\,\alpha} \qquad \text{(D.53)}$$

where C is a constant, Δt is the time interval and α ranges from $\frac{5}{3}$ for short time intervals to $\frac{2}{3}$ for long time intervals. Substituting this in equation D.52 and differentiating with respect to time gives

$$\frac{d\rho}{dt} = -\frac{\alpha C \Delta t^{\alpha-1}}{2\sigma^2} \qquad (D.54)$$

which is zero for $\Delta t = 0$.

Second Order Gauss-Markov Process.

One dynamic model having a correlation function with zero gradient at the origin is the second order Gauss-Markov process. The use of this model is beyond the scope of this thesis but it is described briefly because of its potential applications in modelling systematic errors such as the tropospheric delay. This has the differential equation

$$\ddot{\mathbf{x}}(t) = -2\beta\dot{\mathbf{x}}(t) - \beta^2\mathbf{x}(t) + \mathbf{u}(t) \qquad (D.55)$$

For $\mathbf{u}(t) = 0$ this is the differential equation of critically damped harmonic motion with an acceleration tending to restore equilibrium $-\beta^2\mathbf{x}(t)$, and a damping acceleration just sufficient to prevent oscillation $-2\beta\dot{\mathbf{x}}(t)$. The actual processes of atmospheric dynamics are complex but the use of this model to represent an atmospheric parameter, such as tropospheric delay, is equivalent to a grouping of the forces acting on the atmosphere into three categories:

(a) Those that tend to disturb the equilibrium, represented here by the random process $\mathbf{u}(t)$.

(b) Those that tend to restore equilibrium, represented here by $-\beta^2\mathbf{x}(t)$.

(c) Those that damp the energy and prevent oscillation, represented here by $-2\beta\dot{\mathbf{x}}(t)$.

This is intuitively pleasing as a simplification of the dynamics of atmospheric parameters. The correlation function of this model is (Gelb, 1974)

$$\rho(i,j) = (1 + \beta\Delta t)e^{-\beta\Delta t} \qquad (D.56)$$

which has a gradient

$$\frac{d\rho}{dt} = -\beta^2\Delta t\, e^{-\beta\Delta t} \qquad (D.57)$$

which is zero when $\Delta t = 0$. As with the first order Gauss-Markov process, the error growth is bounded by the steady state variance and the model may be completely defined by this steady state variance and the correlation time. This appears to be a model worthy of further study for describing the dynamics of tropospheric delay.

Comparison of Dynamic Models

The time behaviour of a parameter, its auto-correlation function and its variance are illustrated in diagram D.1 for the 4 dynamic models that will be used in this thesis (constant parameter, white noise, random walk, 1st order Gauss-Markov process). The constant parameter model needs no explanation. Although the value of the parameter may not be known its time dependence is known exactly (it is independent of time). In the white noise model the value of the parameter at any epoch is independent of its value at any other epoch. While significant fluctuations occur from epoch to epoch, the mean value of the parameter is constant. It will always lie within a few standard deviations of this mean. If the variance is sufficiently small this model may be approximated by the constant parameter model.

In the random walk model the parameter differs from its **previous value** by a random amount. This distinguishes it from the white noise model where the parameter differs from the **mean** by a random amount. Because the random walk parameter is not tied to the mean value it can drift away from it. The size of the dynamic model error variance determines how fast the parameter can drift and, given sufficient time, there is no limit to this drift.

The 1st order Gauss-Markov process lies between the white noise and random walk models. The unbounded drift of the random walk model is countered by an exponential drift back towards the mean position. Over short periods, where Δt is much less than the correlation time T , the behaviour is similar to that of a random walk in that it may be thought of as a series of random steps. Over long periods, where Δt is much greater than the correlation time T , the behaviour is similar to that of white noise in that the parameter always lies within a few standard deviations (the steady state standard deviation) of the mean.

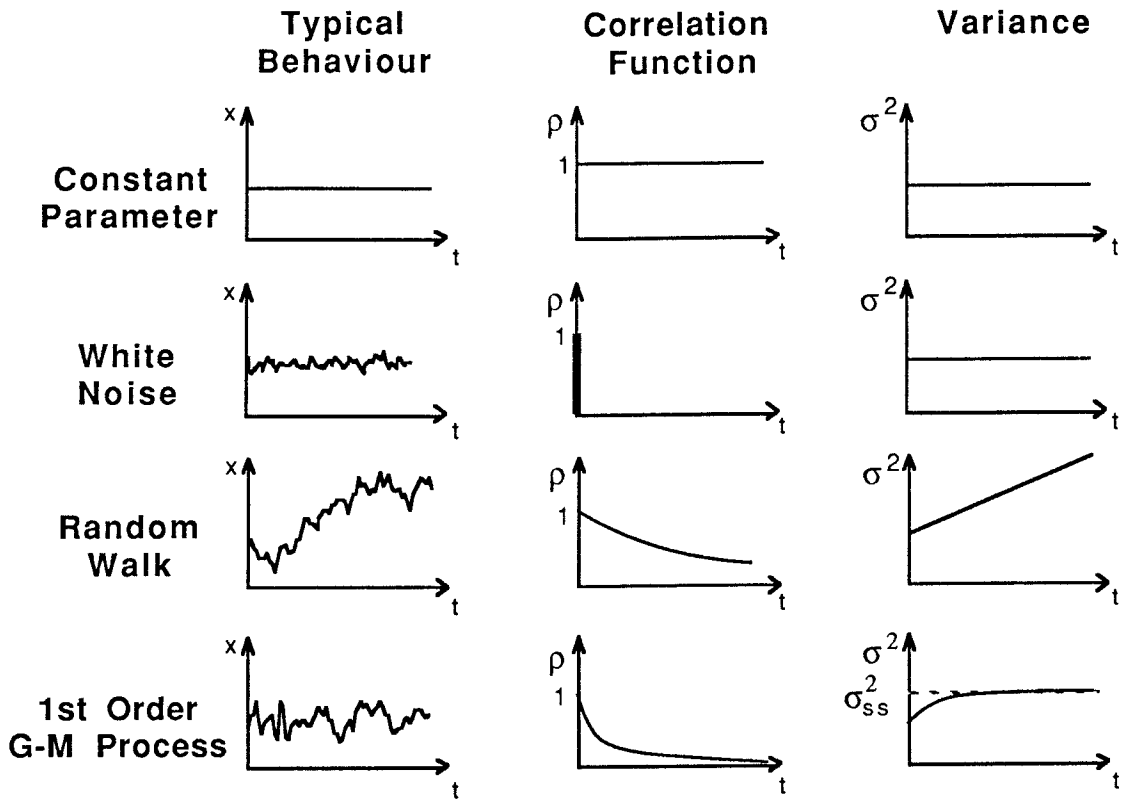

Diagram D.1 Comparison of Dynamic Models

APPENDIX E: BIAS DILUTION OF PRECISION (BDOP)

The geometric dilution of precision (GDOP) is frequently used as an indicator of good satellite geometry and is used for the purpose of choosing the optimum set of satellites and the optimum observation time. The GDOP is based on a solution of position and clock offset from 4 pseudo-ranges. It gives the geometric strength of the instantaneous GPS navigation solution. This differs from the baseline adjustment using integrated carrier phase in three important respects:

(a) It is governed by the **instantaneous** geometry whereas the GPS carrier phase adjustment is governed by the continually changing geometry of an observing session which may last for several hours.

(b) It gives the geometric strength of a **point position** whereas the GPS carrier phase adjustment is for **relative position** of 2 or more receivers.

(c) The pseudo-ranges are considered to be biased only by the errors of receiver oscillator. In a GPS carrier phase adjustment, the observation is also considered to be biased by satellite oscillator errors and integer ambiguities. The geometric strength of **ambiguous pseudo-range** (integrated carrier phase) is quite different to that of **pseudo-range**.

A simple example of the inappropriate nature of GDOP for GPS carrier phase adjustment is the fact that GDOP is undefined for 3 satellites (it would involve the estimation of 4 parameters from 3 observations) and yet three satellites can be used in a baseline solution using integrated carrier beat phase. Norton (1987) has reported that times of high GDOP (poor geometry for the pseudo-range solution) may be the **best** observing times for carrier phase adjustment.

Merminod et al (1988) describe a set of three indicators for dilution of precision that are tailored to the estimation of baseline components from an adjustment of GPS integrated carrier beat phase. These "bias dilution of precision" (BDOP) indicators provide the relative precision of

- baseline components in an ambiguity (bias) free solution (BDOP1),
- ambiguities in an ambiguity (bias) free solution (BDOP2) and
- baseline component in an ambiguity (bias) fixed solution (BDOP3).

Briefly, the algorithm, described in detail in Merminod (1988), involves the formation of the normal matrix for each observation epoch based on simulated

double difference observations. These are then accumulated for all epochs in the desired observation windows. The estimated parameters are components of a unit baseline and ambiguities (biases). The parameter vector may be partitioned into the coordinate sub-vector (subscript "c") and the bias sub-vector (subscript "b"). The normal matrix is partitioned similarly.

$$\mathbf{N}_{xx} = \begin{pmatrix} \mathbf{N}_{cc} & \mathbf{N}_{cb} \\ \mathbf{N}_{bc} & \mathbf{N}_{bb} \end{pmatrix} \tag{E.1}$$

This is inverted to produce the VCV of the adjusted parameters $\mathbf{Q}_{xx}$

$$\mathbf{Q}_{xx} = \mathbf{N}_{xx}^{-1}$$

$$= \begin{pmatrix} \mathbf{Q}_{cc} & \mathbf{Q}_{cb} \\ \mathbf{Q}_{bc} & \mathbf{Q}_{bb} \end{pmatrix} \tag{E.2}$$

If the ambiguities are fixed the sub matrices $\mathbf{N}_{cb}$, $\mathbf{N}_{bc}$ and $\mathbf{N}_{bb}$ are cut from the normal matrix and

$$\mathbf{Q}_{xx} = \mathbf{N}_{cc}^{-1} \tag{E.3}$$

The BDOP factors are defined as follows:

$$\text{BDOP1} = \sqrt{\text{trace}(\mathbf{Q}_{cc})} \tag{E.4}$$

$$\text{BDOP2} = \sqrt{\text{trace}(\mathbf{Q}_{bb})} \tag{E.5}$$

$$\text{BDOP3} = \sqrt{\text{trace}(\mathbf{N}_{cc}^{-1})} \tag{E.6}$$

Of these, Merminod et al (1988) show BDOP1 to be of the greatest value. The exact definition of BDOP2 depends on the method of dealing with the rank deficiency in the ambiguity parameters and thus it is not uniquely defined. The general behaviour of BDOP2 is almost identical to that of BDOP1; i.e. when the ambiguities are precisely estimated in an ambiguity free solution, the baseline components will also be precisely estimated. BDOP3 is the equivalent of an accumulated PDOP (position dilution of precision). An important step in

accurate positioning with GPS is the resolution of the integer ambiguities. If these ambiguities are not well determined in a ambiguity free solution, the correct ambiguity fixed solution cannot be found. If the ambiguities can be fixed to the correct integer values, an increase in solution precision for the (horizontal) coordinates is assured (BDOP3 is always less than BDOP1). A useful additional feature of the BDOP indicators is that they provide information on the effect of different observing session lengths.

The set of simulated elements for the 18 satellite constellation (section 4.1.1) was used to calculate GDOP and BDOP1. These were calculated for a receiver located at Kelburn, Wellington, New Zealand at approximate position 41°S, 175°E. An elevation cutoff of 15° was applied and the number of satellites visible at any instant varies between 4 and 6. The GDOP is calculated for all combinations of 4 visible satellites and the least of these GDOP values is plotted. For the symmetric 18 satellite constellation the satellite geometry repeats every 11 hours 58 minutes (with different satellites). Thus the factors are only plotted for 12 hours (diagram E.1(a)). BDOP1 has been calculated for observation times of 30, 60 and 120 minutes. The BDOP1 values have been plotted against the mid point of the observation session (diagram E.1(b)). Thus, for example, the plotted BDOP1 at 2h 30m for the 120 minute window is that for an observation session from 1h 30m to 3h 30m. The number of satellites that are visible at some stage during an observing session ranges from 4 to 7. BDOP1 is based on all satellites visible in an observing session. Diagram E.1(b) shows BDOP1 for the 30, 60 and 120 minute observation sessions.

Note in diagram E.1(a), the peaks in the GDOP plot at 0h 20m, 7h 00m and 9h 40m and, in diagram E.1(b), the BDOP1 minima at 0h 00m, 3h 45m, 7h 15m, and 9h 45m. Thus, 3 of the 4 BDOP1 minima correspond to the 3 GDOP maxima. The fourth BDOP1 minimum comes at an extended period of low GDOP. This is consistent with the findings of Norton (1987). Thus it appears that sharp peaks in the GDOP correspond to good observing sessions. The commonly accepted idea that low GDOP indicates good geometry for GPS carrier phase adjustment may be true in some circumstances but it appears to be more often wrong than right. The observing windows of all the BDOP1 maxima (centred at 1h 45m, 5h 30m, 8h 30m and 10h 45m) correspond to periods of relatively good (small) GDOP.

(a)

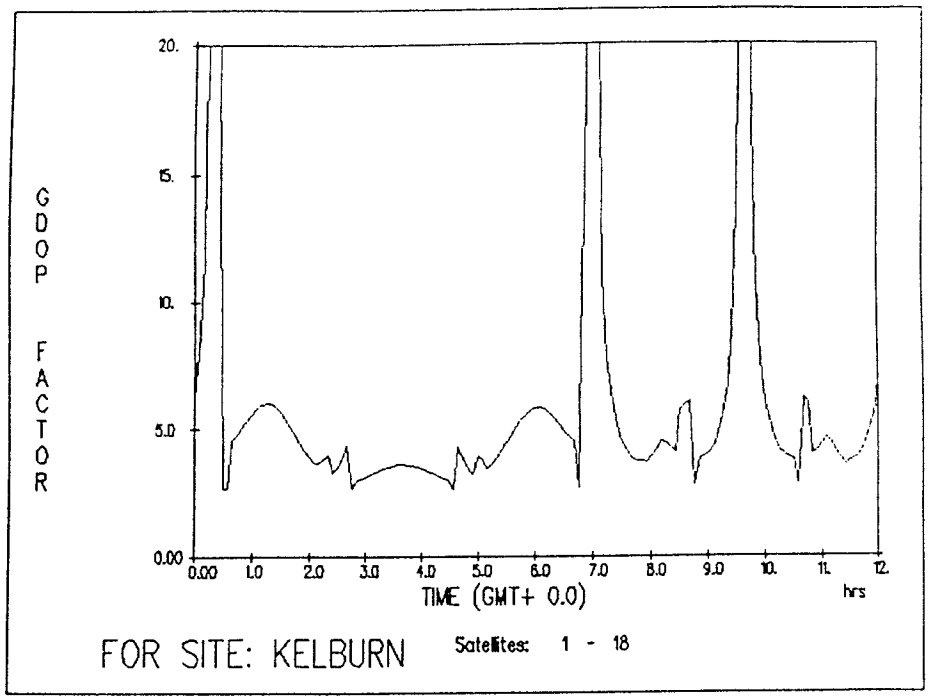

(b)

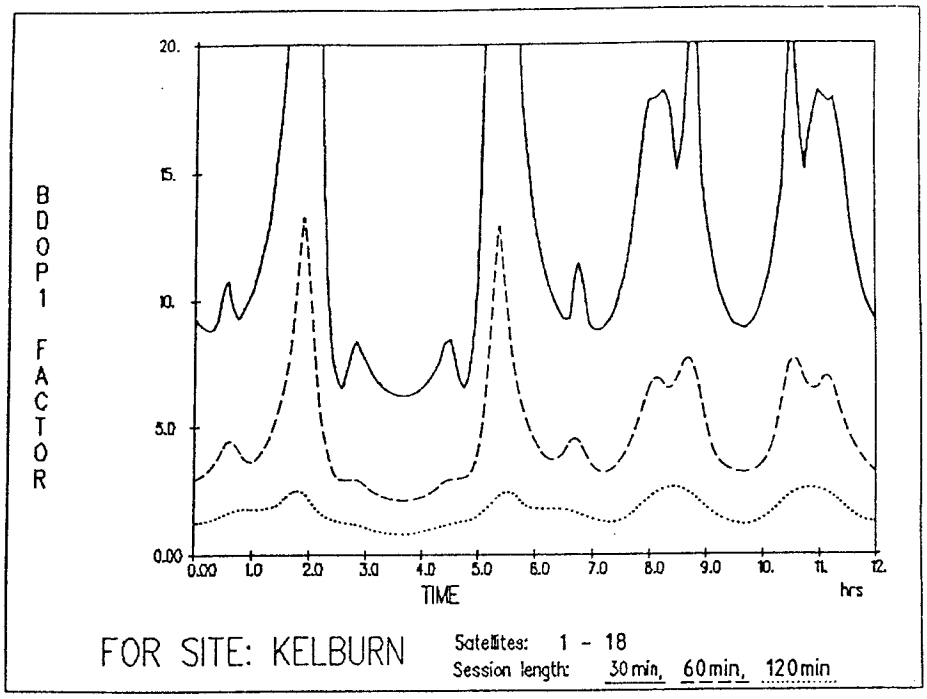

Diagram E.1 A comparison of GDOP and BDOP1

(a) The Geometric Dilution of Precision (GDOP) for the proposed 18 satellite constellation at Kelburn New Zealand. (41°S, 175°E).

(b) The Bias Dilution of Precision (BDOP1) for the same constellation and location for 30, 60 and 120 minute observation sessions.

Note the dramatic improvement (and smoothing of the plot) that occurs with longer observation sessions. Note also, that the best observing time with a 30 minute session is significantly better than the worst observing time with a 60 minute session. Even for the 2 hour observing session, the ratio of best to worst BDOP1 is more than 2 to 1. Thus, despite the 24 hour coverage of the 18 satellite constellation there will be some observing times that are significantly better than others. This has important implications for GPS survey design (Merminod et al 1988).

APPENDIX F: SOFTWARE

A number of programs were written for the analysis described in this thesis and programs written by other authors were also used. These are illustrated in diagrams F.1 and F.2. A brief description of the program system follows.

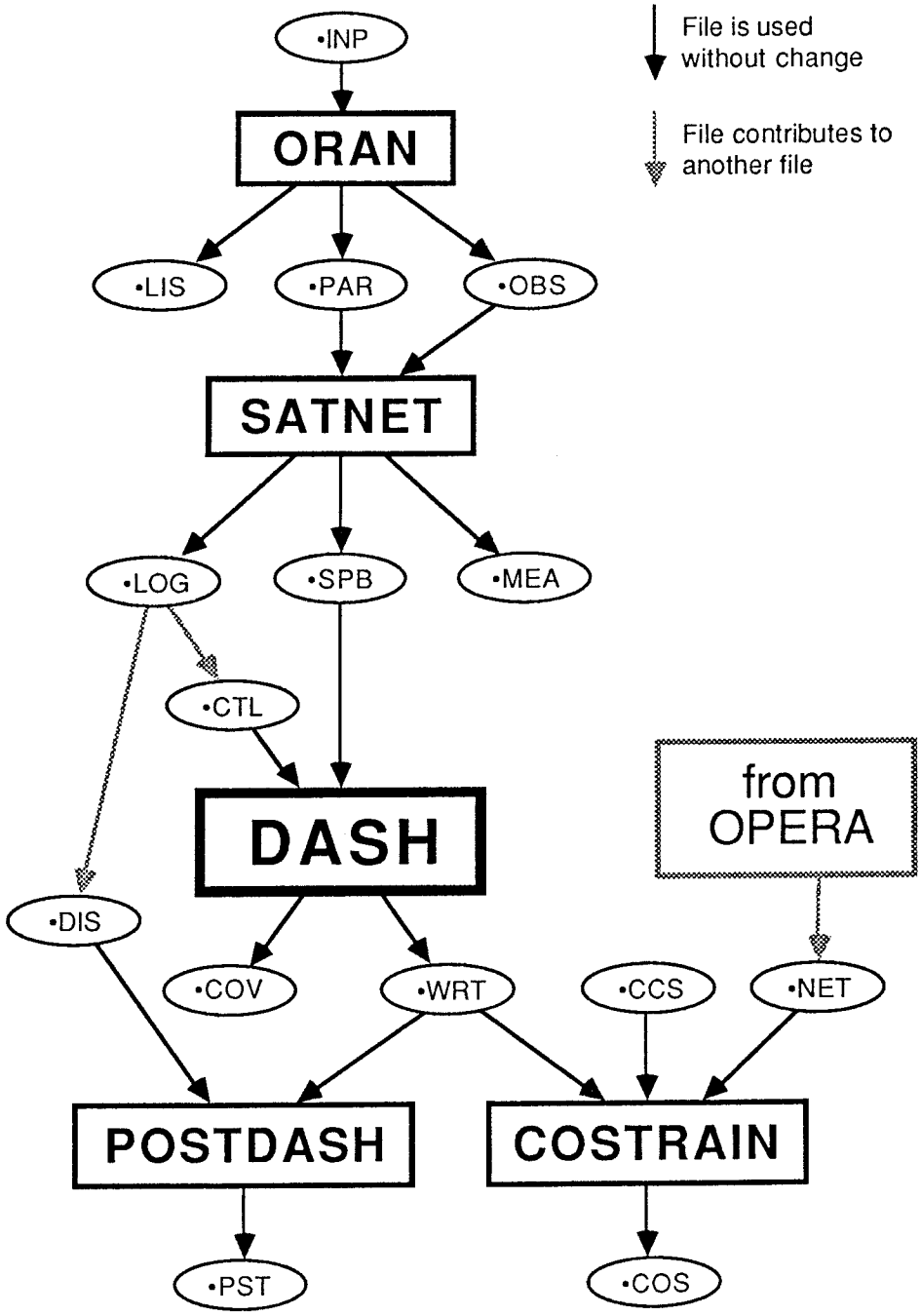

Diagram F.1 Programs and files used for simulation of GPS networks.

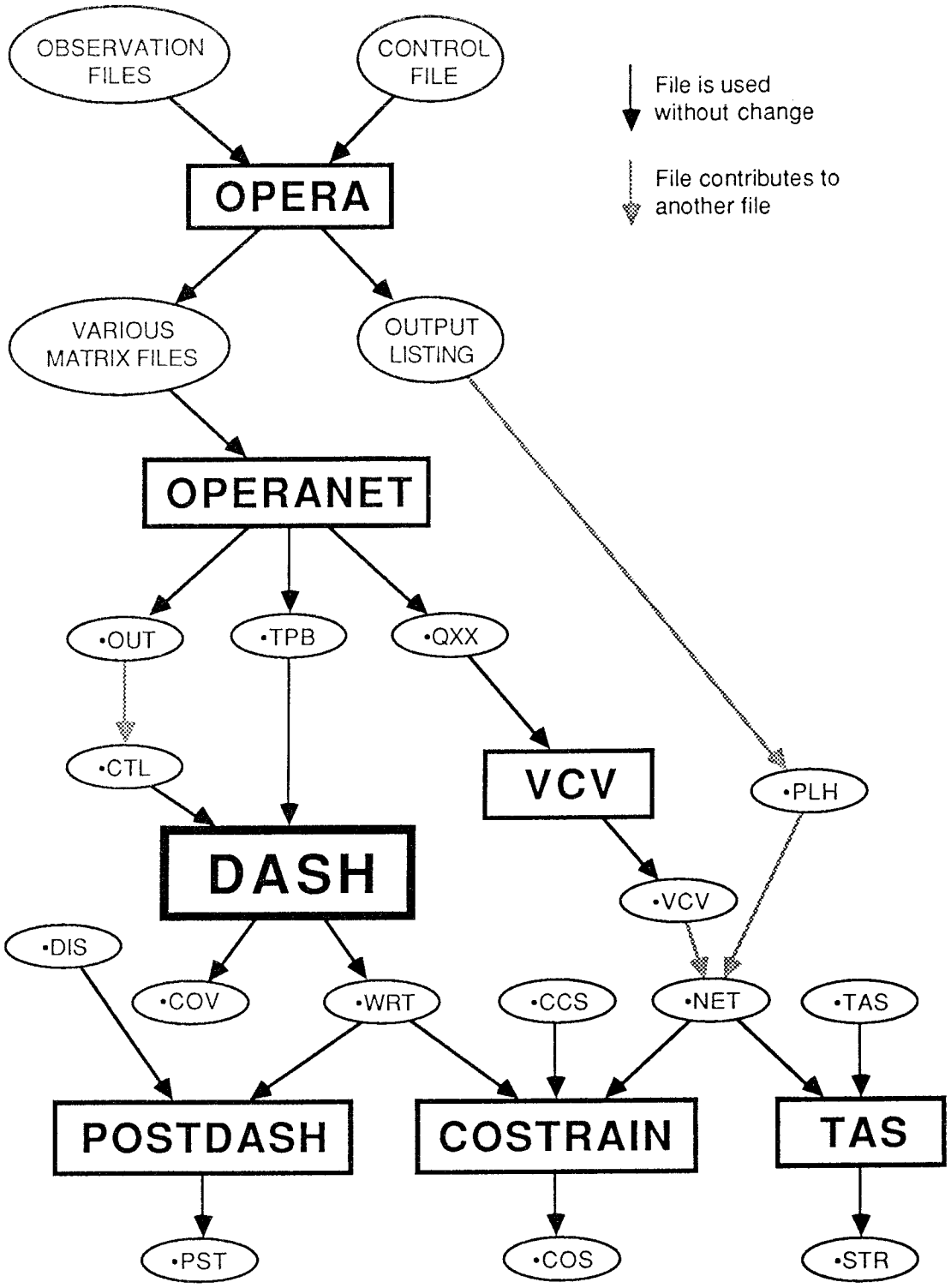

Diagram F.2 Programs and files used for adjustment and simulation of terrestrial networks.

ORAN

This is a covariance analysis programme for orbit adjustment. The mathematical description of the program is given in Hatch & Goad (1973). It allows a wide variety of observations in simulated orbit tracking campaigns but was written before the advent of GPS and its use for GPS creates some difficulties.

(1) The satellite elements are always considered to be adjusted. They could be effectively fixed by assigning small *a priori* variances but then the effect of orbit errors could not be determined.

(2) There is only one bias parameter per observation and thus clock phase errors and ambiguities are not easily included in the model. One possibility is to use the measurement type known as DVLBI which is a double difference observation. The correlations introduced by differencing are not accounted for, as **ORAN** assumes all observations to be independent. Thus the results are not rigorous and depend on the differencing scheme adopted.

(3) As a standard least squares adjustment is simulated, all parameters implicitly have the constant parameter dynamic model. The effect of time dependent systematic errors cannot be easily modelled.

(4) **ORAN** generates the sensitivity matrix and the total perturbation from all considered parameters. Neither of these is particularly convenient. If systematic parameters are considered to be correlated with each other (e.g., the tropospheric zenith delay parameters at adjacent stations) the analysis required after **ORAN** becomes more complex. The perturbation VCV matrix for a group of similar parameters, as generated by **DASH**, is more convenient for analysis.

(5) **ORAN** is a complex program with many options which are not required for this analysis. Modification of the program is not a simple task.

For these reasons **ORAN** has not been used directly for covariance analysis of GPS adjustment. Advantage has been taken of the input structure of **ORAN** which can be used to define a simulated observation scheme, and of the generation of the partial derivatives.

SATNET

This is essentially a reformatting program. The partial derivatives output by **ORAN** are in the •PAR file, and information on the observations is in the •OBS file. These are read by **SATNET**; partial derivatives are generated for

the clock phase parameters and other parameter partials may be generated on request (ionospheric zenith delay, tropospheric mapping functions, cycle slips). Observations may be edited according to receiver number, satellite number, epoch and minimum elevation angle so that the files from one **ORAN** run may be used to create several •SPB files. The information required by **DASH** is written to the •SPB file in a compact form. The •LOG file contains information necessary to create the •CTL control file for **DASH** and the •MEA file is an ASCII file of the observation information contained in the binary file •OBS.

DASH

The heart of the covariance analysis system is **DASH**. The theory of covariance analysis is given in Chapter 5, the Kalman filter algorithm is set out in section 4.3.3 and a description of dynamic models is given in Appendix D. An understanding of the terminology and concepts of these sections is assumed in the following description.

DASH was deliberately designed to be not GPS specific. If fact it is not specific to geodesy and could be used for a wide variety of applications. It accepts a binary file of partial derivatives and observation sigmas (the •SPB file for satellite partials and the •TPB file for terrestrial partials) and processes them in batch mode according to the adjustment model specified in a control file (the •CTL file). The control file consists principally of keywords. The information on parameter numbers, names and *a priori* sigmas is obtained from the **SATNET** •LOG file. The parameter names and *a priori* sigmas may be changed if desired.

The adjustment is based on the Kalman filter algorithm but least squares can also be simulated. If all parameters are assigned the constant dynamic model, the adjustment will be the equivalent of sequential least squares (see Appendix C). If all observations are considered to be in one epoch (as is assumed for the terrestrial observations) the result is a single step least squares adjustment although the equations used for the solution are still those of the Kalman filter.

The parameters in the adjustment are arranged for convenience into groups by means of the control file. Parameters are usually grouped according to behaviour; e.g., the receiver coordinates in one group, orbital elements in

another, tropospheric delay parameters in a third and so on. All parameters in one group have the same characteristics in the adjustment (except for the *a priori* variance which may be different for each parameter). All parameters in a group will be adjusted or unadjusted (considered to be systematic errors). All will have the same dynamic model which may be the constant parameter model, white noise, random walk, 1st order Gauss-Markov process or other second order models not used in this thesis. Parameters in an adjusted group may be eliminated from the solution each epoch by reducing the observation equations as outlined in section 4.3.1. This is used for clock phase errors in GPS adjustment to generate the equivalent of a double difference adjustment. Parameters in a group may be correlated with each other *a priori* but may not be correlated with parameters in other groups. Where parameters in a group are correlated, the correlation matrix is given in the control file. The effect of an incorrect dynamic model may be determined for parameters in an adjusted group as described in section 5.4. The parameters in an unadjusted group may be considered to be known errors (biases) and/or stochastic parameters with known variances and covariances. If the former is specified, perturbations of the adjusted parameter due to the biases are calculated. If the latter is specified, a perturbation VCV matrix is calculated for the whole group. This perturbation VCV may or may not be added into the consider VCV as desired.

The sigmas and perturbation sigmas of adjusted parameters may be output at a specified rate (e.g., every 5 observation epochs) during the adjustment to see how they change with time. After all observation partials have been processed the following information is output.

- computed sigmas of the adjusted parameters. Correlations or variances and covariances are also printed. Printing of off diagonal elements may be suppressed for groups of nuisance parameters if desired.
- Perturbations of the adjusted parameters due to errors in those unadjusted parameters specified as biases.
- perturbation sigmas and off diagonal terms as requested from the perturbation VCV matrix, for each group of unadjusted parameters specified as stochastic variables.
- perturbation sigmas and off diagonal terms as requested from the perturbation VCV, due to the use of an erroneous dynamic model for adjusted parameters.
- perturbation sigmas and off diagonal terms as requested from the total perturbation VCV. This is the sum of perturbation VCV matrices from all

unadjusted groups of stochastic variables that were specified to be included in the total

- sigmas and off diagonal terms as requested for the consider VCV. This is the sum of the computed VCV and the total perturbation VCV together with cross covariance matrices if the option of considering an erroneous dynamic model has been adopted.

On request **DASH** creates a write-out (•WRT) file for specified adjusted parameter groups containing all information required for subsequent specialised analysis This file contains, for the specified adjusted parameters, the computed VCV, the sensitivity matrix , the perturbation VCV matrices of dynamic (non-constant) unadjusted groups, the perturbation VCV and cross covariance matrices for an erroneous dynamic model and the *a priori* VCV matrices of each group of unadjusted parameters. For the analysis in this thesis, this file was created for the adjusted coordinates to allow analysis of baseline errors in **POSTDASH** and propagation of systematic errors through a deformation adjustment using **COSTRAIN**. The •WRT file contains all the information necessary to generate the final **DASH** output and is written in ASCII format to allow easy transfer to other computers and archiving (unlike the files •PAR , •OBS and •SPB files which are written as binary files to minimise storage requirements)

POSTDASH

This program is used to analyse errors in baselines between receiver stations. The VCV matrices are augmented, as described in Appendix G, to include the fixed origin station. Subtotals are formed as requested for the effects of similar groups of errors. The baseline lengths are supplied in the file •DIS and the errors are given in metres and parts per million of the baseline length.

COSTRAIN

The •WRT files of several **DASH** runs may be combined in a simulated deformation adjustment and the systematic errors from **DASH** are propagated through to the deformation parameters. The •NET file contains the coordinates and VCV of the terrestrial net which is assumed to have no systematic errors (the VCV is assumed to be correct) so that the random errors from both epochs and the systematic errors from only one epoch are considered. Systematic errors of the same type from different **DASH** runs may be considered to be either completely correlated or completely uncorrelated.

The •NET file has the same format as input files used for the strain analysis program **TAS** and thus a terrestrial net generated from real data using **OPERA 2.3** may be used. The **COSTRAIN** control file, •CCS , defines the configuration of the deformation adjustment. The output file contains the computed VCV of the adjusted deformation parameters and the perturbation VCVs for each group of systematic errors from the **DASH** runs. The perturbation VCVs due to the combined effect of errors of the same type from different **DASH** runs are calculated together with the total perturbation VCV and the consider VCV.

OPERA 2.3

OPERA 2.3 was developed at the University of the Federal Armed Forces, Munich, and was used for terrestrial network adjustments. This software is described by Hein (1982a, 1982b); Hein & Landau (1983); Eissfeller & Hein (1986) and Landau et al (1987). The features and use in this thesis are described briefly in section 3.4.2. A number of temporary data files are created including those containing the design matrices of partial derivatives and the VCV matrix of the adjusted parameters. This latter matrix is required for strain analysis. The design matrices of partial derivatives may be used to simulate terrestrial adjustment in the same way that the partial derivatives from **ORAN** were used to simulate GPS adjustment.

OPERANET and VCV

OPERANET reads and compacts the **OPERA** files mentioned above. The partial derivatives are written out in the correct format for input to **DASH** and are also written in ASCII so that the order of the parameters in the **OPERA** VCV matrix may be determined. The VCV of the adjusted parameters is also written out in compacted form. This includes the variances and covariances of all adjusted parameters and the program **VCV** is used to extract the VCV of adjusted coordinates (extended to include the origin station) and write this in the format used by the strain analysis program **TAS**. The adjusted coordinates required for strain analysis are extracted from the **OPERA** output file using a text editor. The files of coordinates and VCV may also be used as the terrestrial network in a simulated deformation adjustment using **COSTRAIN**.

TAS

This program and the underlying theory is described in Harvey (1985), The topocentric strain option was used.

APPENDIX G. CONVERSION OF VCV MATRICES

G.1 COORDINATE CONVERSIONS

The receiver coordinate partials generated by ORAN are in terms of local east, north and height axes that are different for each point as noted in section 6.2. This system is not convenient for strain analysis or for the computation of baseline component errors. The conversion of a VCV matrix in (e,n,h) coordinates to (ϕ, λ, h) coordinates is given by

$$VCV_{\phi\lambda h} = \mathbf{J}_a \, VCV_{enh} \, \mathbf{J}_a^T \qquad (G.1.1)$$

where the Jacobian matrix $\mathbf{J}_a$ is

$$\mathbf{J}_a = \begin{pmatrix} 0 & R_M^{-1} & 0 \\ R_L^{-1} & 0 & 0 \\ 0 & 0 & 1 \end{pmatrix} \qquad (G.1.2)$$

where R_M is the radius of curvature in the meridian,

$$R_M = \frac{\nu\,(1 - e^2)}{(1 - e^2 \sin^2\phi)} + h \qquad (G.1.3)$$

R_L is the radius of curvature of a parallel,

$$R_L = (\nu + h)\cos\phi \qquad (G.1.4)$$

and

$$\nu = \frac{a}{\sqrt{1 - e^2 \sin^2\phi}} \qquad (G.1.5)$$

The conversions given by Harvey (1985) may then be used to convert to the (x,y,z) system

$$VCV_{xyz} = \mathbf{J}_b \, VCV_{\phi\lambda h} \, \mathbf{J}_b^T \qquad (G.1.6)$$

where the Jacobian matrix $\mathbf{J}_b$ is

$$\mathbf{J}_b = \begin{pmatrix} \frac{ve^2\cos^2\phi\,\sin\phi\,\cos\lambda}{(1-e^2\sin^2\phi)} - (v+h)\sin\phi\,\cos\lambda & -(v+h)\cos\phi\,\sin\lambda & \cos\phi\,\cos\lambda \\ \frac{ve^2\cos^2\phi\,\sin\phi\,\sin\lambda}{(1-e^2\sin^2\phi)} - (v+h)\sin\phi\,\sin\lambda & (v+h)\cos\phi\,\cos\lambda & \cos\phi\,\sin\lambda \\ \left(\frac{ve^2\sin^2\phi\,\cos\phi}{(1-e^2\sin^2\phi)} + v\cos\phi\right)(1-e^2) + h\cos\phi & 0 & \sin\phi \end{pmatrix} \quad \text{(G.1.7)}$$

and thence to the topocentric east, north, vertical (e,n,v) system described in section 2.2.2.

$$VCV_{env} = \mathbf{J}_c\, VCV_{xyz}\, \mathbf{J}_c^T \quad \text{(G.1.8)}$$

where the Jacobian matrix $\mathbf{J}_c$ is (Harvey, 1985)

$$\mathbf{J}_c = \begin{pmatrix} -\sin\lambda_t & \cos\lambda_t & 0 \\ -\sin\phi_t\cos\lambda_t & -\sin\phi_t\sin\lambda_t & \cos\phi_t \\ \cos\phi_t\cos\lambda_t & \cos\phi_t\sin\lambda_t & \sin\phi_t \end{pmatrix} \quad \text{(G.1.9)}$$

and where ϕ_t , λ_t are the latitude and longitude of the chosen topocentric origin.

The complete conversion from the ORAN / DASH VCV_{enh} to the VCV_{env} used for strain analysis is given by

$$VCV_{env} = \mathbf{J}_c\mathbf{J}_b\mathbf{J}_a\, VCV_{enh}\, \mathbf{J}_a^T\mathbf{J}_b^T\mathbf{J}_c^T \quad \text{(G.1.10)}$$

and for stations close to the topocentric point, the combined Jacobian matrix $\mathbf{J}_c\mathbf{J}_b\mathbf{J}_a$, is close to the identity matrix because the local (e,n,h) axes of the ORAN are close to being parallel to the topocentric (e,n,v) axes. These equations are used to convert computed and perturbation VCV matrices (see Chapter 5) and also, to convert the sensitivity matrix. The sensitivity matrix output by DASH gives perturbations in the same system as the input; i.e., the ORAN (e,n,h) system. From equation 5.2.14,

$$\hat{\mathbf{p}}_{enh} = \mathbf{C}_{enh}\,\delta\mathbf{s} \quad \text{(G.1.11)}$$

and

$$\hat{\mathbf{p}}_{env} = \mathbf{J}_c\mathbf{J}_b\mathbf{J}_a\,\hat{\mathbf{p}}_{enh}$$
$$= \mathbf{J}_c\mathbf{J}_b\mathbf{J}_a\,\mathbf{C}_{enh}\,\delta\mathbf{s} \qquad \text{(G.1.12)}$$

thus

$$\mathbf{C}_{env} = \mathbf{J}_c\mathbf{J}_b\mathbf{J}_a\,\mathbf{C}_{enh} \qquad \text{(G.1.13)}$$

G.2 AUGMENTING THE VCV FOR THE ORIGIN STATION(S)

The VCV and perturbation matrices output by DASH are only for the adjusted parameters, but for an analysis of network baselines or for strain analysis, the coordinates of the origin station(s) which are part of the network are also of interest. It is a simple matter to add rows and columns to the VCV matrices to account for these extra coordinates. As the origin station(s) are held fixed their coordinates have zero variances and covariances.

$$\mathbf{Q}_{aug} = \begin{pmatrix} \mathbf{0} & \mathbf{0} \\ \mathbf{0} & \mathbf{Q} \end{pmatrix} \qquad \text{(G.2.1)}$$

Similarly, these unadjusted parameters have no perturbations and the sensitivity matrix is also augmented

$$\mathbf{C}_{aug} = \begin{pmatrix} \mathbf{0} & \mathbf{C} \end{pmatrix} \qquad \text{(G.2.2)}$$

However there is one important exception to this, namely the perturbation due to an error in the origin station coordinates themselves. In this special case, the perturbation in the origin coordinates is obviously equal to the systematic error in those coordinates and thus the augmented sensitivity matrix is

$$\mathbf{C}_{aug} = \begin{pmatrix} \mathbf{I} & \mathbf{C} \end{pmatrix} \qquad \text{(G.2.3)}$$

From equation G.2.2 and equation 5.2.20, the augmented perturbation VCV for systematic errors other than origin coordinate errors is

$$\mathbf{Q}_{\hat{p}\,aug} = \mathbf{C}_{aug}\mathbf{Q}_s\mathbf{C}^T_{aug}$$

$$= \begin{pmatrix} \mathbf{0} & \mathbf{0} \\ \mathbf{0} & \mathbf{C}\mathbf{Q}_s\mathbf{C}^T \end{pmatrix} \qquad \text{(G.2.4)}$$

The perturbation VCV for errors in the origin coordinates is

$$\mathbf{Q}_{\hat{p}\,aug} = \mathbf{C}_{aug}\mathbf{Q}_s\mathbf{C}^T_{aug}$$

$$= \begin{pmatrix} \mathbf{Q}_s & \mathbf{Q}_s\mathbf{C}^T \\ \mathbf{C}\mathbf{Q}_s & \mathbf{C}\mathbf{Q}_s\mathbf{C}^T \end{pmatrix} \qquad \text{(G.2.5)}$$

Publications from

THE SCHOOL OF SURVEYING, THE UNIVERSITY OF NEW SOUTH WALES.

All prices include postage by surface mail. Air mail rates on application. (Effective April 1990)

To order, write to Publications Officer, School of Surveying, The University of New South Wales, P.O. Box 1, Kensington N.S.W., 2033 AUSTRALIA

NOTE: ALL ORDERS MUST BE PREPAID

UNISURV REPORTS - G SERIES

Price (including postage): $3.50

G14. A. Stolz, "The computation of three dimensional Cartesian coordinates of terrestrial networks by the use of local astronomic vector systems", Unisurv Rep. 18, 47 pp, 1970.

G16. R.S. Mather et al, "Communications from Australia to Section V, International Association of Geodesy, XV General Assembly, International Union of Geodesy and Geophysics, Moscow 1971", Unisurv Rep. 22, 72 pp, 1971.

G17. Papers by R.S. Mather, H.L. Mitchell & A. Stolz on the following topics:- Four-dimensional geodesy, Network adjustment and Sea surface topography, Unisurv G17, 73 pp, 1972.

G18. Papers by L. Berlin, G.J.F. Holden, P.V. Angus-Leppan, H.L. Mitchell & A.H. Campbell on the following topics:- Photogrammetry co-ordinate systems for surveying integration, Geopotential networks and Linear measurement, Unisurv G18, 80 pp, 1972.

G19. R.S. Mather, P.V. Angus-Leppan, A. Stolz & I. Lloyd, "Aspects of four-dimensional geodesy", Unisurv G19, 100 pp, 1973.

G20. Papers by J.S. Allman, R.C. Lister, J.C. Trinder & R.S. Mather on the following topics:- Network adjustments, Photogrammetry, and 4-Dimensional geodesy, Unisurv G20, 133 pp, 1974.

G21. Papers by E. Grafarend, R.S. Mather & P.V. Angus-Leppan on the following topics:- Mathematical geodesy, Coastal geodesy and Refraction, Unisurv G21, 100 pp, 1974.

G22. Papers by R.S. Mather, J.R. Gilliland, F.K. Brunner, J.C. Trinder, K. Bretreger & G. Halsey on the following topics:- Gravity, Levelling, Refraction, ERTS imagery, Tidal effects on satellite orbits and Photogrammetry, Unisurv G22, 96 pp, 1975.

G23. Papers by R.S. Mather, E.G. Anderson, C. Rizos, K. Bretreger, K. Leppert, B.V. Hamon & P.V. Angus-Leppan on the following topics:- Earth tides, Sea surface topography, Atmospheric effects in physical geodesy, Mean sea level and Systematic errors in levelling, Unisurv G23, 96 pp, 1975.

G24. Papers by R.C. Patterson, R.S. Mather, R. Coleman, O.L. Colombo, J.C. Trinder, S.U. Nasca, T.L. Duyet & K. Bretreger on the following topics:- Adjustment theory, Sea surface topography determinations, Applications of LANDSAT imagery, Ocean loading of Earth tides, Physical geodesy, Photogrammetry and Oceanographic applications of satellites, Unisurv G24, 151 pp, 1976.

G25. Papers by S.M. Nakiboglu, B. Ducarme, P. Melchior, R.S. Mather, B.C. Barlow, C. Rizos, B. Hirsch, K. Bretreger, F.K. Brunner & P.V. Angus-Leppan on the following topics:- Hydrostatic equilibrium figures of the Earth, Earth tides, Gravity anomaly data banks for Australia, Recovery of tidal signals from satellite altimetry, Meteorological parameters for modelling terrestrial refraction and Crustal motion studies in Australia, Unisurv G25, 124 pp, 1976.

G26. Papers by R.S. Mather, E.G. Masters, R. Coleman, C. Rizos, B. Hirsch, C.S. Fraser, F.K. Brunner, P.V. Angus-Leppan, A.J. McCarthy & C. Wardrop on the following topics:- Four-dimensional geodesy, GEOS-3 altimetry data analysis, analysis of meteorological measurements for microwave EDM and Meteorological data logging system for geodetic refraction research, Unisurv G26, 113 pp, 1977.

G27. Papers by F.K. Brunner, C.S. Fraser, S.U. Nasca, J.C. Trinder, L. Berlin, R.S. Mather, O.L. Colombo & P.V. Angus-Leppan on the following topics:- Micrometeorology in geodetic refraction, LANDSAT imagery in topographic mapping, adjustment of large systems, GEOS-3 data analysis, Kernel functions and EDM reductions over sea, Unisurv G27, 101 pp, 1977.

G29. Papers by F.L. Clarke, R.S. Mather, D.R. Larden & J.R. Gilliland on the following topics:- Three dimensional network adjustment incorporating ξ , η and N, Geoid determinations with satellite altimetry, Geodynamic information from secular gravity changes and Height and free-air anomaly correlation, Unisurv G29, 87 pp, 1978.

From June 1979 Unisurv G's name was changed to Australian Journal of Geodesy, Photogrammetry and Surveying. These can be ordered from The Managing Editor, Australian Journal of Geodesy, Photogrammetry and Surveying, Institution of Surveyors - Australia , Box 4793 G.P.O., Sydney, N.S.W., 2001, AUSTRALIA.

UNISURV REPORTS - S SERIES

S8 - S19	Price (including postage):		$7.50
S20 onwards	Price (including postage):	Individuals	$18.00
		Institutions	$25.00

S8 A. Stolz, "Three-D Cartesian co-ordinates of part of the Australian geodetic network by the use of local astronomic vector systems", Unisurv Rep. S 8, 182 pp, 1972.

S9 H.L. Mitchell, "Relations between MSL & geodetic levelling in Australia", Unisurv Rep. S 9, 264 pp, 1973.

S10 A.J. Robinson, "Study of zero error & ground swing of the model MRA101 tellurometer", Unisurv Rep. S 10, 200 pp, 1973.

S12. G.J.F. Holden, "An evaluation of orthophotography in an integrated mapping system", Unisurv Rep. S 12, 232 pp, 1974.

S14. Edward G. Anderson, "The Effect of Topography on Solutions of Stokes` Problem", Unisurv Rep. S 14, 252 pp, 1976.

S15. A.H.W. Kearsley, "The Computation of Deflections of the Vertical from Gravity Anomalies", Unisurv Rep. S 15, 181 pp, 1976.

S16. K. Bretreger, "Earth Tide Effects on Geodetic Observations", Unisurv S 16, 173 pp, 1978.

S17. C. Rizos, "The role of the gravity field in sea surface topography studies", Unisurv S 17, 299 pp, 1980.

S18. B.C. Forster, "Some measures of urban residual quality from LANDSAT multi-spectral data", Unisurv S 18, 223 pp, 1981.

S19. Richard Coleman, "A Geodetic Basis for recovering Ocean Dynamic Information from Satellite Altimetry", Unisurv S 19,332 pp, 1981.

S20. Douglas R. Larden, "Monitoring the Earth's Rotation by Lunar Laser Ranging", Unisurv Report S 20, 280 pp, 1982.

S25. Ewan G. Masters, "Applications of Satellite Geodesy to Geodynamics", Unisurv Report S25, 208 pp, 1984.

S27. Bruce R. Harvey, "The Combination of VLBI and Ground Data for Geodesy and Geophysics", Unisurv Report S27, 239 pp, 1985.

S28. Rod Eckels, "Surveying with GPS in Australia", Unisurv S28, 220 pp, 1987.

S29. Gary S. Chisholm, "Integration of GPS into hydrographic survey operations", Unisurv S29, 190 pp, 1987.

S30. Gary Alan Jeffress, "An investigation of Doppler satellite positioning multi-station software", Unisurv S30, 118 pp, 1987.

S31. Jahja Soetandi, "A model for a cadastral land information system for Indonesia", Unisurv S31, 168 pp, 1988.

S32. D. B. Grant, "Combination of terrestrial and GPS data for earth deformation studies" Unisurv S32, 285 pp, 1990.

S33. R. D. Holloway, "The integration of GPS heights into the Australian Height Datum", Unisurv S33, 151 pp.,1988.

S34. Robin C. Mullin, "Data update in a Land Information Network", Unisurv S34, 168 pp. 1988.

S35. Bertrand Merminod, "The use of Kalman filters in GPS Navigation", Unisurv S35, 203 pp., 1989.

S36. Andrew R. Marshall, "Network design and optimisation in close range Photogrammetry", Unisurv S36, 249 pp., 1989.

S37. Wattana Jaroondhampinij, "A model of Computerised parcel-based Land Information System for the Department of Lands, Thailand," Unisurv S37, 281 pp., 1989.

PROCEEDINGS

Prices include postage by surface mail

P1. P.V. Angus-Leppan (Editor), "Proceedings of conference on refraction effects in geodesy & electronic distance measurement", 264 pp., 1968. Price: $6.50

P2. R.S. Mather & P.V. Angus-Leppan (Eds), "Australian Academy of Science/International Association of Geodesy Symposium on Earth`s Gravitational Field & Secular Variations in Position", 740 pp., 1973. Price $12.50

MONOGRAPHS

Prices include postage by surface mail

M1. R.S. Mather, "The theory and geodetic use of some common projections", (2nd edition), 125 pp., 1978. Price $9.00

M2. R.S. Mather, "The analysis of the earth's gravity field", 172 pp., 1971. Price $5.50

M3. G.G. Bennett, "Tables for prediction of daylight stars", 24 pp.,1974. Price $2.00

M4. G.G. Bennett, J.G. Freislich & M. Maughan, "Star prediction tables for the fixing of position", 200 pp., 1974. Price $5.00

M5. M. Maughan, "Survey computations", 98 pp., 1975. Price $8.00

M7. J.M. Rueger, "Introduction to Electronic Distance Measurement", (2nd Edition), 140 pp., 1988. Price $14.00

M8. A.H.W. Kearsley, "Geodetic Surveying". 77pp., 1988. Price $8.00

M10. W. Faig, "Aerial Triangulation and Digital Mapping", 102. pp., 1986. Price $13.00

M11. W.F. Caspary, "Concepts of Network and Deformation Analysis", 183 pp., 1988. Price $22.00

M12. F.K. Brunner, "Atmospheric Effects on Geodetic Space Measurements", 110 pp., 1988. Price $13.00